

UNIVERSITY OF OKLAHOMA
GRADUATE COLLEGE

INVESTIGATION OF METHODOLOGIES FOR MINIMIZING BUILDINGS
ELECTRICITY DEMAND AND COST

A DISSERTATION
SUBMITTED TO THE GRADUATE FACULTY
in partial fulfillment of the requirements for the
Degree of
DOCTOR OF PHILOSOPHY

By
OLUWASEYI TOPE OGUNSOLA
Norman, Oklahoma
2016

INVESTIGATION OF METHODOLOGIES FOR MINIMIZING BUILDINGS
ELECTRICITY DEMAND AND COST

A DISSERTATION APPROVED FOR THE
SCHOOL OF AEROSPACE AND MECHANICAL ENGINEERING

BY

Dr. LI SONG, Chair

Dr. MEIJUN ZHU

Dr. DAVID P. MILLER

Dr. PETER J. ATTAR

Dr. FENG C. LAI

© Copyright by OLUWASEYI TOPE OGUNSOLA 2016
All Rights Reserved.

It's all God.

Acknowledgements

It would have been impossible to complete this dissertation without the support and encouragement of many people.

I like to thank my advisor, Dr. Li Song for accepting me into her research group and mentoring me to become a better researcher. Your mentorship, guidance, and encouragement, has enabled me to finish my PhD with numerous publications, scholarships, and recognitions. I am grateful for your understanding and kindness. It has been a very pleasant experience working with you. I am also very thankful to my committee members, Dr. Meijun Zhu, Dr. Peter J. Attar, Dr. Feng C Lai, and Dr. David P. Miller. Thank you for your time, advice, and constructive feedback through every stage (course plan/advisory conference, general exam, dissertation proposal, and defense) of the PhD. Your support and advice is greatly appreciated. I am also thankful to all AME staff- Kate O'brien Hamoush, Melissa Foster, Rebecca Norris, Danielle Geier, Debra Mattax, and Vicki Pollock. I like to thank my colleagues at the building energy efficiency (BEE) laboratory- Alejandro Rivas, Junke Wang, Shima Shahahmadi, Wesley Thomas, Amber Kapoor, and Gyujin Shim. Thank you all for the moral support. I really appreciate you guys. Special thanks to Dr. Farrokh Mistree and my colleagues at the AME Graduate Student Society for giving me the opportunity to develop networking and leadership skills. I also acknowledge the financial sponsorship received from British Petroleum (BP Fellowship), ASHRAE (Grant-in-aid and Oklahoma City Community Foundation Scholarship), Cleo Cross, Jim and Bee Close, John E. Francis, and OU Graduate College.

I like to thank my friends in Norman, and my church members at the Redeemed Christian Church of God (RCCG) Praise Center. Thank you Olanrewaju Aboaba, Seyi Fadipe, Isaac Taiwo, Oluwatobi Olorunsola, Ojuewa Solaru, Joshua Nnaji, Taiwo Omotoso, Feyi Fakoya, Olalekan Seriki, Uvirkaa Akumaga, and Olalekan Ajayi, to mention a few. Special thanks to my Pastors – Pastor Phillip Ayeni and Dcn. Temitope Rotimi. You have all been my pillar of support. Thank you for believing in me. I also like to thank Rev. Peter Asimi, my father in the Lord. Thank you for your prayers. Special thanks to Dcn. Laniyan for always checking on me. Thank you for your love sir. I would like to thank you all for the emotional and spiritual support, which is overwhelming. You are awesome.

I appreciate my family for their support and prayers throughout the course of this degree. I am thankful for my mother, Mrs. Iyabo Ogunsola for her love, encouragement, and support. You are the best mum in the world. Thank you for supporting and caring for me at all times. Thank you for all the challenges you had to face to make me who I am today. I bless God for your life. I like to also thank my mother-in-law, Mrs. Florence Ogunbiyi for her prayers and continuous support.

To my beautiful wife, Dr. Oyedolapo Ogunbiyi, and our wonderful daughters, Mirabelle and Melinda Ogunsola: You all encouraged me through tough times, gave me the strength to go on, many reasons to smile, and joy that knows no bounds. We did this together! My deepest gratitude is to you all. I am the best man, husband, and father that I can be because I have you all. I love you beyond words.

Finally, ‘except the Lord builds a house, they labor in vain that build it’. I thank God for His faithfulness and love for me throughout this research. To God be the glory.

Table of Contents

Acknowledgements	iv
List of Tables	x
List of Figures.....	xii
Abstract.....	xvii
Chapter 1: Introduction.....	1
1.1 Background.....	1
1.2 Heating, Ventilating, and Air-conditioning (HVAC) Systems	2
1.3 Research Objectives	7
1.4 Research Overview.....	12
1.5 Thesis Contributions.....	14
Chapter 2: Literature Review	16
2.1 State of the Art and Current Challenges.....	16
2.2 Building Load Models	19
2.2.1 Review of Building Load Calculation Methods.....	23
2.2.2 Advances in RC Modeling Approach.....	25
2.3 Cooling Coil Transient Models	27
2.4 Fan-Power Models.....	35
2.5 HVAC System Control and Optimization.....	38
2.5.1 Summary of HVAC Systems Control Methods	42
2.5.2 Strategies for minimizing building demand	46
Chapter 3: HVAC Components Model Description.....	50
3.1 Building Load Model	50

3.2	Fan-Motor Model	56
3.3	Cooling Coil Dynamic Model	59
3.4	Solution Method	66
3.4.1	Time series solution.....	67
3.4.2	Integrated solution method	70
3.5	Stability Analysis.....	72
3.6	Parameter Estimation.....	78
3.7	Summary.....	81
Chapter 4: HVAC Components Model Validation		84
4.1	Building Load Validation	86
4.2	Single Zone Case Study - Thermal Zone F	87
4.2.1	Assumptions	87
4.2.2	Parameter estimation	90
4.2.3	Modeling equations	92
4.2.4	Results	94
4.3	Multiple Zone Case Study	99
4.3.1	Thermal zone A	99
4.3.2	Thermal zone B	102
4.3.3	Thermal zone C	105
4.3.4	Thermal zone D	107
4.3.5	Thermal zone E.....	109
4.3.6	Thermal zone F.....	111
4.3.7	Thermal zone G	114

4.4	Results	116
4.4.1	Summary of cooling load results	125
4.5	Fan-motor model Validation	126
4.5.1	Summary of fan input power predictions	133
4.5.2	Summary of fan speed predictions	133
4.6	Cooling Coil Validation	134
4.6.1	Summary of cooling coil predictions – leaving air temperature	137
4.6.2	Summary of cooling coil predictions – leaving water temperature.....	137
Chapter 5: Development and Validation of Framework for Minimizing Buildings		
	Electricity Demand and Cost.....	138
5.1	Suitability of MPC for HVAC Systems	139
5.2	How the MPC works	141
5.3	MPC with MIMO State Space Models.....	143
5.4	Case Study	149
5.5	Results	150
5.5.1	Cooling demand.....	151
5.5.2	Fan operation	166
5.5.3	Electricity cost	168
Chapter 6: Step by Step Summary of Minimization Framework.....		
6.1	Steps to Thermal Network Modeling of Building Load.....	170
6.2	Steps to Thermal Network Modeling of Cooling Coil	173
6.3	Steps to minimizing building cooling demand.....	174
6.4	Steps to minimizing building electricity cost	176

Chapter 7: Original Contributions to Knowledge/Research.....	177
7.1 Understanding of Stability of R-C thermal network	177
7.2 Understanding of thermal characteristics of building construction.....	180
7.3 Understanding of passive thermal storage capability of building construction	182
7.4 Demonstration of R-C application to cooling coil models.....	188
7.5 Understanding of multiple-zone interactions	191
7.6 Investigation of methods for filling missing gaps in Solar Radiation	195
7.7 Further Applications of Model Predictive Control.....	198
Chapter 8: Conclusions and Future Work	199
8.1 Broader Impact	204
8.2 Limitations.....	206
8.3 Future work	206
References	209
Appendix A: Fan Dynamic Model	218
Appendix B: Fan Static Pressure Reset	222
Appendix C: Results of Time-Series Solution Method.....	223
Appendix D: Alternative MPC Performance Cost	228
Appendix E: Selected Publications	229
Appendix F: Compositions of Floor and Partitions.....	305

List of Tables

Table 2.1a: Comparison of HVAC Systems Control Methods (Hard Control)	43
Table 2.1b: Comparison of HVAC Control Methods (Soft and Hybrid Control).....	44
Table 2.1c: Comparison of HVAC Systems Control Methods (Classical)	44
Table 2.2: Applications of MPC in HVAC System Control	45
Table 3.1: Typical inputs to R-C model	55
Table 3.2: Cooling coil thermal interactions, temperature based approach	65
Table 3.3: Cooling coil thermal interactions, enthalpy based approach.....	66
Table 3.4: Exterior Wall Composition for Heavy Construction.....	80
Table 3.5: Exterior Wall for Medium Construction	80
Table 3.6 Exterior Wall for Light Construction	80
Table 3.7: Solver Characteristics.....	82
Table 3.8: Summary of models utilized in this dissertation	83
Table 4.1: Different estimation scenarios for the R-C parameters	91
Table 4.2: Summary of the nodal and adjacent temperatures.....	94
Table 4.3: Comparison of error indices for Cooling Season Validation	95
Table 4.4: Comparison of error indices for Heating Season Validation	95
Table 4.5: Thermal Zone Grouping and Interactions	99
Table 4.6: State space matrix for Thermal Zone A (Q_{cool} is the cooling load).....	101
Table 4.7: Input matrix for Thermal Zone A.....	102
Table 4.8: State space matrix for Thermal Zone B (Q_{cool} is the cooling load)	104
Table 4.9: Input matrix for Thermal Zone B	104
Table 4.10: State space matrix for Thermal Zone C (Q_{cool} is the cooling load)	106

Table 4.11: Input matrix for Thermal Zone C	106
Table 4.12: State space matrix for Thermal Zone D (Q_{cool} is the cooling load)	108
Table 4.13: Input matrix for Thermal Zone D	108
Table 4.14: State space matrix for Thermal Zone E (Q_{cool} is the cooling load)	110
Table 4.15: Input matrix for Thermal Zone E	111
Table 4.16: Input matrix for Thermal Zone F	111
Table 4.17: State space matrix for Thermal Zone F (Q_{cool} is the cooling load)	113
Table 4.18: State space matrix for Thermal Zone G (Q_{cool} is the cooling load)	115
Table 4.19: Input matrix for Thermal Zone G	115
Table 4.20: Summary of Temperature results for all thermal zones	125
Table 4.21: Summary of fan-power predictions vs measurement	133
Table 4.22: Summary of fan-speed predictions vs measurement	134
Table 4.23: Summary of predicted leaving air temperature vs measurement	137
Table 4.24: Summary of predicted leaving water temperature vs measurement	137
Table 5.1: Summary of MPC Framework	146
Table 5.2: Summary of Optimal Cooling Strategies	163
Table 7.1 : Heating System Downsizing Opportunities in the US	187
Table 7.2: New strategies for minimizing electricity cost in a multi-zone buildings...	195
Table 7.3: Limitations and merits of the SSA, TBA, and SASR methods	196
Table 7.4. Recommended approach for different gap lengths	197

List of Figures

Figure 1.1: Some competing sustainability uses for modern buildings.....	2
Figure 1.2: Schematic of a Central HVAC system (Source: http://energy-models.com/hvac-centrifugal-chillers).....	3
Figure 1.3: Air Handling Unit (Branesky, 2012)	5
Figure 1.4: Some of the thermal interactions in multi-zone buildings.....	6
Figure 1.5: Typical Electricity Index Price for Summer Season.....	8
Figure 1.6: Research flowchart.....	12
Figure 2.1: Input to Thermal Models	20
Figure 2.2: Interpolation techniques for fan-model.....	37
Figure 3.1: R-C Thermal model, showing sol-air temperature and HVAC system input.	52
Figure 3.2a: Office Building with 2 Thermal Zones	57
Figure 3.2b: R-C Model Representation for Building shown in Figure 3.2a	57
Figure 3.3: Summary of Fan Power Model	58
Figure 3.4: Thermal network model for cooling coil, temperature approach	64
Figure 3.5: Thermal network model for cooling coil, enthalpy approach.....	64
Figure 3.6: Simplified thermal model for cooling coil, temperature approach	65
Figure 3.7: Simplified thermal model for cooling coil, enthalpy approach	65
Figure 4.1: Layout of Case Study Building.....	85
Figure 4.2: Case Study Air Handling Unit	85
Figure 4.3: RC model representation of the single zone	88
Figure 4.4: Comparison of building load for the cooling season.	96

Figure 4.5: Comparison of building load for heating season.	97
Figure 4.6: Comparison of zone temperatures for heating season	97
Figure 4.7: Thermal network representation for Zone A	100
Figure 4.8: Thermal network representation for Zone B.....	103
Figure 4.9: Thermal network representation for Zone C.....	105
Figure 4.10: Thermal network representation for Zone D	107
Figure 4.11: Thermal network representation for Zone E.....	109
Figure 4.12: Thermal network representation for Zone F	112
Figure 4.13: Thermal network representation for Zone G	114
Figure 4.14: Room Temperature predictions for Zone A – August 2015	116
Figure 4.15: Room Temperature predictions for Zone A – August 2015	117
Figure 4.16: Room Temperature predictions for Zone A – February 2016	117
Figure 4.17: Room Temperature predictions for Zone B – August 2015	118
Figure 4.18: Room Temperature predictions for Zone C – August 2015	119
Figure 4.19: Room Temperature predictions for Zone D – August 2015	121
Figure 4.20: Room Temperature predictions for Zone D – August 2015	121
Figure 4.21: Room Temperature predictions for Zone D – February 2016	122
Figure 4.22: Room Temperature predictions for Zone E – August 2015.....	122
Figure 4.23: Room Temperature predictions for Zone F – August 2015.....	123
Figure 4.24: Room Temperature predictions for Zone G – August 2015	124
Figure 4.25: Room Temperature predictions for Zone G – February 2016	124
Figure 4.26: Predicted vs Measured Fan Input Power - August 2015.....	127
Figure 4.27: Predicted vs Measured Fan Speed - August 2015	127

Figure 4.28: Predicted vs Measured Fan Input Power - September 2015	128
Figure 4.29: Predicted vs Measured Fan Speed - September 2015	128
Figure 4.30: Predicted vs Measured Fan Input Power - October 2015	129
Figure 4.31: Predicted vs Measured Fan Speed - October 2015	129
Figure 4.32: Predicted vs Measured Fan Input Power - November 2015	130
Figure 4.33: Predicted vs Measured Fan Speed - November 2015	130
Figure 4.34: Predicted vs Measured Fan Input Power - December 2015.....	131
Figure 4.35: Predicted vs Measured Fan Speed - December 2015.....	131
Figure 4.36: Predicted vs Measured Fan Input Power – February 2016	132
Figure 4.37: Predicted vs Measured Fan Speed – February 2016.....	132
Figure 4.38: Supply air temperature vs measurement – August 2015	134
Figure 4.39: Chilled water return temperature vs measurement – August 2015.....	135
Figure 4.40: Supply air temperature vs measurement – September 2015.....	135
Figure 4.41: Chilled water return temperature vs measurement – September 2015	136
Figure 5.1: Components involved in Model Predictive Control (Source: mathworks.com)	141
Figure 5.2: MPC Framework to minimize building electricity cost and demand	147
Figure 5.3: Electricity Tariff for Optimization Period	150
Figure 5.4: Optimized Temperature Trajectory – Thermal Zone A.....	152
Figure 5.5: Optimized Cooling Load Profile – Thermal Zone A	152
Figure 5.6: Optimized Temperature Trajectory – Thermal Zone B	154
Figure 5.7: Optimized Cooling Load Profile – Thermal Zone B	154
Figure 5.8: Optimized Temperature Trajectory – Thermal Zone C	156

Figure 5.9: Optimized Cooling Load Profile – Thermal Zone C	156
Figure 5.10: Optimized Temperature Trajectory – Thermal Zone D	157
Figure 5.11: Optimized Cooling Load Profile – Thermal Zone D	158
Figure 5.12: Optimized Temperature Trajectory – Thermal Zone E	158
Figure 5.13: Optimized Cooling Load Profile – Thermal Zone E	159
Figure 5.14: Optimized Temperature Trajectory – Thermal Zone F.....	161
Figure 5.15: Optimized Cooling Load Profile – Thermal Zone F.....	161
Figure 5.16: Optimized Temperature Trajectory – Thermal Zone G	162
Figure 5.17: Optimized Cooling Load Profile – Thermal Zone G	162
Figure 5.18: Comparison of all zone temperatures	164
Figure 5.19: Optimized Chilled Water Flow Rates	165
Figure 5.20: Optimized Leaving Air Temperature for Cooling Coil	165
Figure 5.21: Optimized Leaving Water Temperature for Cooling Coil.....	166
Figure 5.22: Optimized CFM for entire building	167
Figure 5.23: Optimized Fan Power for the AHU	167
Figure 5.24: Optimized Fan Speed for the AHU.....	168
Figure 5.25: Overview of Electricity Cost	169
Figure 6.1: How to represent building components using the RC model	170
Figure 6.2: Connection of inputs and disturbances to the RC model.....	171
Figure 6.3: Contributions to the cooling load for a typical zone.....	172
Figure 6.4: Thermal network representation for cooling coil.....	173
Figure 6.5: Receding horizon in MPC (Source: www.eng.ox.ac.uk).....	176
Figure 7.1: Thermal Response of Building Construction- Hot-Humid Climate	181

Figure 7.2: Thermal Response of Building Constructions- Cold Climate	182
Figure 7.3: Temperature Float for Thermal Zone 1	184
Figure 7.4: Temperature Float for Thermal Zone 2	184
Figure 7.5: Downsizing Opportunities for Thermal Zone 1 (numbers in %).....	185
Figure 7.6: Downsizing Opportunities for Thermal Zone 2 (numbers in %).....	185
Figure 7.7: Thermal network model for cooling coil, temperature approach	189
Figure 7.8: Thermal network model for cooling coil, enthalpy approach.....	189
Figure 7.9: Integration of Building load and Cooling Coil Models.....	190
Figure 7.10: Optimized Temperature Trajectory – Thermal Zone G.....	193
Figure 7.11: Optimized Cooling Load Profile – Thermal Zone G.....	193
Figure 7.12: Optimized Temperature Trajectory – Thermal Zone C	194
Figure 7.13: Optimized Cooling Load Profile – Thermal Zone C	194
Figure 8.1: Smart Grid Integration	205

Abstract

Heating, ventilating, and air conditioning (HVAC) systems are the largest consumer of electricity in buildings. The HVAC system is complex in terms of components that make them up and their different time scales. The inefficient operation of HVAC system leads to unreasonable electricity consumption during peak periods, which is accompanied by high cost of electricity use. The dynamic changes in building demand, contributions from exogenous inputs such as solar radiation and ambient temperature, and phenomenon such as radiative delays, thermal storage, internal mass etc. are some of the current challenges in buildings systems operation. Due to dynamic and thermal coupling between the conditioned building and HVAC systems components, optimal control is difficult to achieve.

In a multi-zone building, multiple thermal interactions among the different thermal zones and the effects on electricity demand and cost are not well understood, due to lack of fundamental knowledge. The existing strategies for electricity demand and cost control do not consider the dynamics of building construction and multi-zone interactions in their formulation. As a result, existing demand and electricity minimization strategies are not consistent in their conclusions. Meanwhile, multi-zone interactions and building dynamics play a crucial role in the overall electricity demand, cost, and load profiles due to the dependency of states of each individual zone on the thermal characteristics and states of the adjacent zones. The objective of this research is to understand multi-zone and equipment interactions in buildings energy systems, in order to minimize electricity cost. This is the first research to integrate building dynamics into controller formulation and design through the use of a physically

representative thermal model that captures important phenomenon of building load and cooling coil operations.

The intellectual contribution of this research is the understanding of multiple-zone interactions in buildings to aid in effective decision making regarding the operational states of HVAC equipment that minimizes overall electricity cost. Other original contributions are identification of critical thermal zones in a multi-zone building, extension of the R-C thermal network approach for transient modeling of cooling coils, identification of new methods (near constant cooling and temperature recovery/optimal start) for minimizing buildings electricity demand and cost, downsizing of heating system size based on passive thermal storage properties of building construction, and demonstration of the electricity cost savings capabilities in air handling units operations through the use of Model predictive control (MPC) methods. This is the first research to demonstrate predictive control that utilizes building dynamics through the use of models that represent the building physically and captures important phenomenon e.g. radiative delays and thermal storage. Therefore, it provides opportunities to strategically maximize curtailment potentials and human comfort through optimization, and contributes to knowledge through the development of step by step approach to achieve system-wide optimal operation of the air handling unit, based on consideration of time of use electricity tariff. Therefore, the developed framework in this dissertation is useful for smart grid integration, and for building modelers in the areas of fault detection and diagnosis (FDD) and control. As such, the developed framework is very promising for existing and future building automation system (BAS) and emerging technologies in the building sector.

Chapter 1: Introduction

This chapter introduces the overall function of the Heating, Ventilating, and Air-conditioning (HVAC) System and the background information to building load calculations. It also includes the state of the art and current challenges with building energy systems operation and modeling. It concludes with the overview and objectives of this research.

1.1 Background

The United States Green Building Council data (USGBC 2011) shows that buildings account for 65% of electricity consumption in the United States. This trend is observed for most countries of the world, where buildings account for up to 40% of electricity use. A study by Daum and Morel (2010) revealed that commercial buildings are responsible for 18.4% of total primary energy used in the USA. Globally, buildings are responsible for up to 21% of greenhouse gas emissions. The building heating and cooling needs are usually provided by HVAC systems, whose overall function is to compensate for the building load in order to provide thermal comfort.

The primary aim of buildings energy systems is to satisfy thermal comfort requirements, using electricity and energy in the most efficient way. Modern buildings have numerous sustainability requirements. Sustainable building systems operation require energy consumption to be minimized and building services be carried out in the most sustainable way to ensure adequate indoor climate and healthy conditions for occupants. This presents a dilemma due to competing social, economic, and environmental goals (e.g. as shown in Figure 1.1).

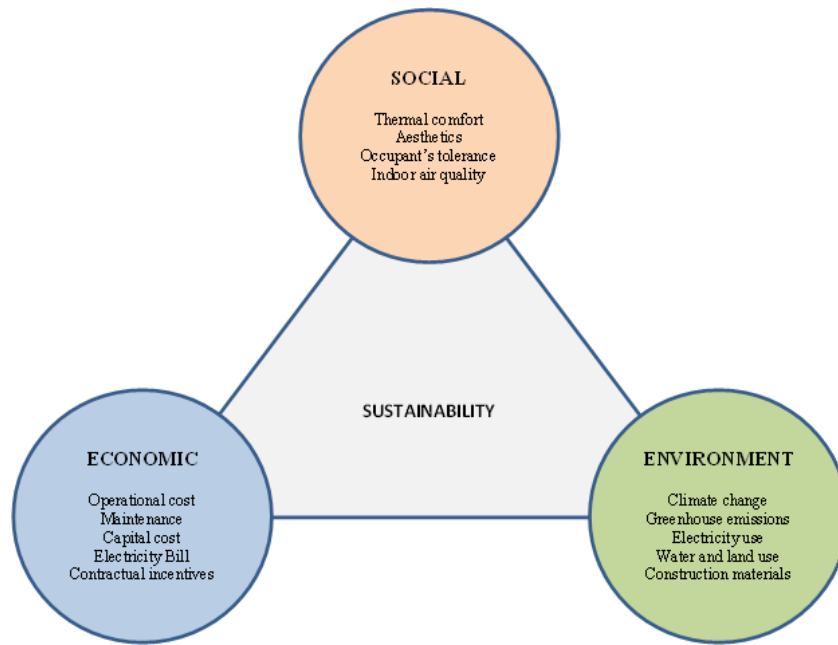


Figure 1.1: Some competing sustainability uses for modern buildings

According to Elton (2010), up to 30% of building energy is used inefficiently or unnecessarily. The reasons for excessive energy consumed in buildings include failure to operate as intended, inappropriate monitoring and control strategy, wrong sizing of the HVAC system, and lack of understanding of dynamic thermal loads and interactions. This has led to the widespread development and implementation of regulations and national policies to encourage or mandate reduced building energy consumption. Meanwhile, the dynamic nature of temperature, weather, internal heat gains, and occupancy schedules, alongside their interactions with the thermal characteristics of building construction continue to provide challenges for optimal operation of HVAC systems.

1.2 Heating, Ventilating, and Air-conditioning (HVAC) Systems

HVAC systems configurations vary considerably based on how they are set up, and the components that make them up. Figure 1.2 shows the schematic of typical

HVAC systems in a central plant. It is an example of a central plant, with one chiller serving multiple air handling units (AHU). Fans, pumps, and compressors are some of the electricity users. The functions of the components are described as follows: Boilers produce hot water or steam for distribution to the working space. The hot water is distributed through hot water pipes to radiators, or passed over heating coils as part of a ventilation system. The cooling equipment provides chilled water for pumping to cooling coils. Through the ventilation system, the treated air is then blown over the cooling coils into the space to be cooled.

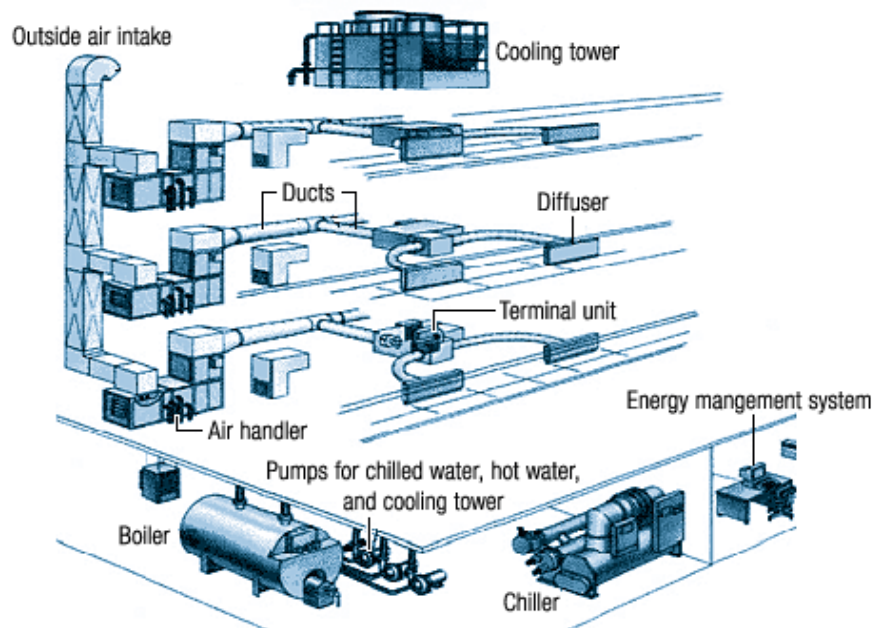


Figure 1.2: Schematic of a Central HVAC system (Source: <http://energy-models.com/hvac-centrifugal-chillers>)

A refrigeration cycle exists in the chiller, and the heat rejection is usually done via a cooling tower or condenser. Pumps are used to circulate the hot and chilled water to the required areas in the building. Fans are used to circulate the conditioned air for distribution to the controlled space. Exhaust fans extract stale air via separate ducts, and expels them outside. Controls in the building set the operational state of equipment (e.g.

on or off) and adjust variables such as the flow rates (air and water), desired temperatures and pressures, to ensure that the components work together in an efficient manner. The dynamic thermal interaction, under the influence of occupant behavior and outdoor climate, between building structure and HVAC system is very difficult to predict. This, in practice, results in non-optimal performance of the building system or malfunctioning of components.

A main component of the HVAC system is the Air handling Unit (AHU), which is shown in Figure 1.3. The AHU provides and delivers conditioned air to the building, in order to maintain the desired temperature and humidity within the building. The main elements of the air handling unit are the coils (heating and cooling) and fans (supply and return). This system is usually applied in buildings with multiplicity of zones such as offices, schools, universities, laboratories, and hospitals. For efficient operation, the HVAC equipment should be suitable for the particular location and application, properly sized, accessible for easy maintenance, and have a simple arrangement, since ductwork and piping make up a significant part of the HVAC system.

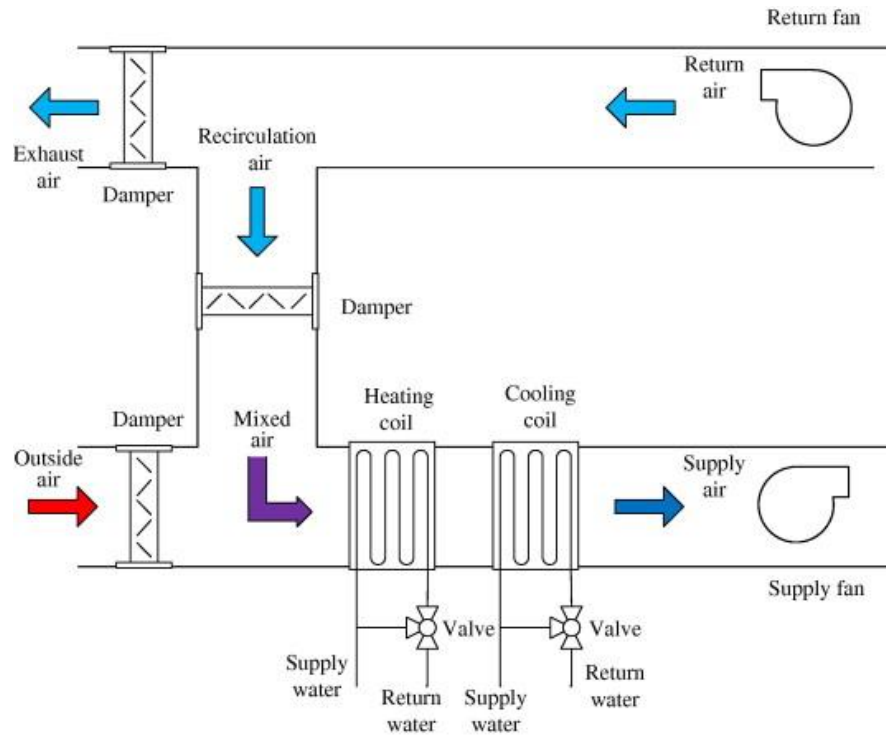


Figure 1.3: Air Handling Unit (Branesky, 2012)

Due to the complexity of HVAC systems, one of the current challenges is how to understand and predict the behavior of the system, given the interdependence and interactions among different components. Figure 1.4 shows some of the thermal interactions in a multiple zone building served by a single Air handling unit. These thermal zones interact with each other but also compete for available cooling/heating from the HVAC system. The thermal zones retain their individual characteristics but also function as part of the integrated building system with multiple coupling and interactions among the different zones and the HVAC equipment.

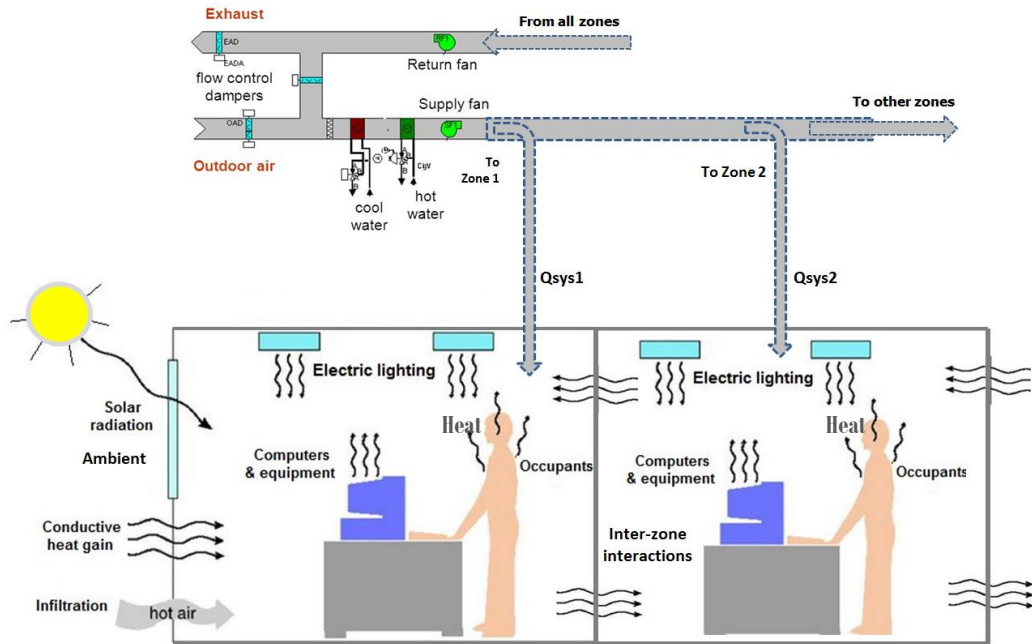


Figure 1.4: Some of the thermal interactions in multi-zone buildings

With increasing number of buildings, thermal zones, and air handling units, effective decision making becomes increasingly difficult due to varying schedules and occupancies, building orientation, multiple interactions, and different thermal response of the thermal zones. These multiple interactions have not been factored into existing strategies for demand control and electricity minimization due to lack of fundamental knowledge. The existing strategies are based on rule of thumb, without consideration for building dynamics and multi-zone interactions in the controller design. For efficient operation of the HVAC system, multi-zone and equipment interactions need to be factored into the HVAC control algorithm for local and supervisory control (determination of zone set points and distribution of cooling/heating for the entire building).

1.3 Research Objectives

The objective of this research is to understand multi-zone and equipment interactions in a multi-zone building, in order to minimize electricity cost. The research integrates concepts from electrical engineering and controls into mechanical engineering to aid in compromised decision making that leads to minimized electricity cost for buildings energy systems.

In recent years, majority of research on optimizing building operation have focused on minimizing total electricity and energy use. However, due to dynamic load changes in building and increasing demand on grid electricity, attention has now shifted from minimizing total electricity consumption to minimizing peak demand and consequently the total cost of electricity. Electricity suppliers have introduced time-of-day pricing such that peak electricity is very expensive to consumers, as a means of controlling demand when the grid is near capacity. A study found that a 1% decline in peak demand would lead to 3.9% monetary savings (Spees and Lave 2007). Figure 1.5 shows typical summer period index price of electricity that was adopted by TXU in 2006 in Dallas TX which reflects the dynamic utility rate. As could be seen, electricity charges during peak hours could be as much as ten (10) times that during off-peak hours.

There are lots of on-going developments on hardware infrastructure for smart grid and integrated smart building design (Edison Foundation, 2012). This has opened more opportunities and increased relevance for research of this nature that is capable of generating grid commands which can be utilized to minimize peak demand.

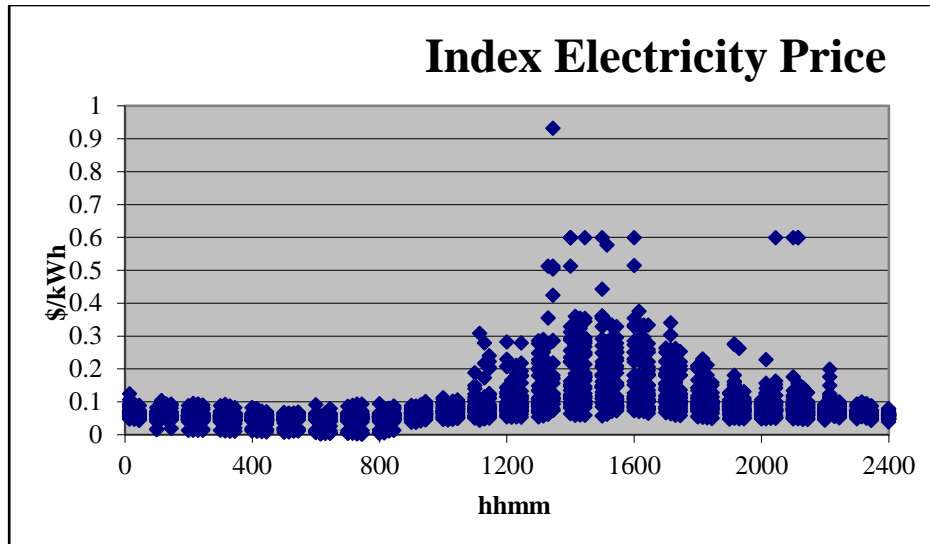


Figure 1.5: Typical Electricity Index Price for Summer Season

Currently, the building sector’s electricity demand targets can be achieved by using today’s and future technologies to significantly reduce the electricity needed by residential and commercial buildings to perform the same services. Current demand response control is primarily focused on curtailment. Curtailment is the response to a utility's contractual incentive that results in a load reduction, either by limiting device demand or by raising room temperature set points. Occupants may experience loss of comfort during the curtailment period. In general, due to the complexity of HVAC systems, the magnitude and duration of the curtailment are estimated by rule of thumb with consideration of occupants’ tolerance. The current state-of-the-art provides opportunities to strategically maximize curtailment potentials and human comfort through optimization. Additionally, there have been very limited studies on curtailment with due consideration to buildings and HVAC systems dynamic response. While there are several common sense and rule of thumb approaches to minimizing building electricity demand and use, most of them are not consistent in their conclusions and

there are no clearly laid out procedures and guidelines for their adoption and application. Such methods have not been feasible thus far due to the lack of fundamental knowledge.

Therefore, there exists lots of methodical, knowledge, and theoretical gaps in the aspect of optimizing operation of building systems. As such, new knowledge and methods are required to understand and determine the operational and optimal configuration and operation of building systems components which will lead to their minimal electricity costs. Currently, there is no model that adequately represents the lag time cooling load and incident solar radiation on wall surfaces. No model that includes both the building and AHU with all of its details. In addition, most of the works are Single Input Single Output (SISO) models, manipulated with PI and other classical controllers. This research expands and extends the application of the lumped thermal network approach to Variable Air Volume (VAV) systems of an AHU in a multi-zone office building. In addition, due to the limitations of current HVAC control and optimization protocols to handle high order differential equation, over-simplified regression-based models have been used. This research contributes to the solution of the optimization problem by using thermal, airflow, and analytical dynamics model that is calibrated and improved using short-period measurement data. The research questions are:

RQ1: How to understand and accurately predict multi-zone interactions in buildings for demand control purposes?

Hypotheses

H1: Zone temperatures for individual zones in a multi-zone building can be treated differently, instead of equally in traditional building operations

New knowledge

- Understanding of thermal interactions among multiple thermal zones in any new or existing buildings
- Understanding of interactions between multiple thermal zones and HVAC equipment to assist in efficient operation of the HVAC equipment

RQ2: How to utilize multi-zone thermal interaction for cost and energy-efficient operation of the HVAC equipment?

Hypotheses

H2: Individual zones in a multi-zone building require different strategies for electricity minimization rather than one strategy applying to all zones as in demand response (DR) literature

New knowledge

- New electricity minimization methods for multiple thermal zones in any new or existing building
- Understanding and determination of near-optima precooling hours for certain thermal zones

While there have been several studies on the minimization of electricity demand and cost in buildings, answers to these questions are not available in today's literature. The academic and research experience of the researcher on control systems, buildings heat transfer, computational fluid dynamics, and thermal model development will be

applied to fill in the identified knowledge gap. The research will focus on the following thrust areas:

T1: Identify suitable thermal models that may be used to carry out fundamental study of building thermal interactions

T2: Identify relevant parameters to accurately model the building load, fans, and cooling coils in air handling units. Create computationally efficient methods to estimate the parameters.

T3: Develop and validate the integrated system model for AHU and building load, as a proof of concept.

T4: Investigate methods for minimizing building electricity cost, using appropriate control methods

T5: Develop framework to study multi-zone interactions and minimize electricity cost

T6: Validate the developed methods using case studies of typical AHU in a multi-zone building.

The above tasks will be carried out through the use of a cyber-physical system (using building dynamics) which serves to integrate physical sensor measurement with thermal and mathematical model for real-time control of HVAC system operation. The model is deduced from fundamental heat transfer and energy conservation laws, and the model parameters were estimated from measured data.

1.4 Research Overview

Figure 1.6 is the research flowchart showing the entire process and interaction between the different objectives.

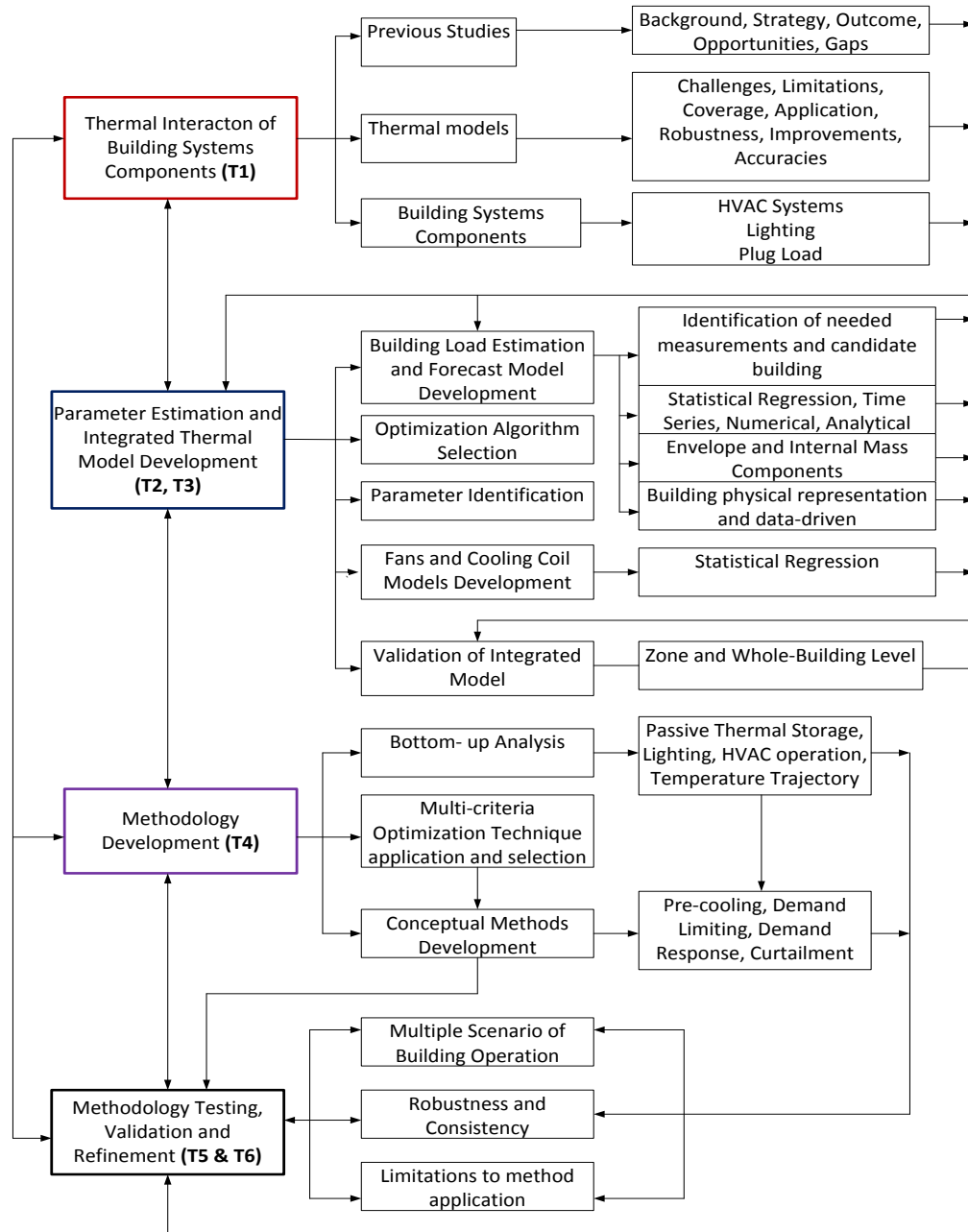


Figure 1.6: Research flowchart

The task in this dissertation will be demonstrated using case study of a typical AHU (with focus on air mixing, fans, cooling coil, and building load operations) serving multiple thermal zones in an office building. For the minimization of building electricity demand and cost, a model predictive approach will be adopted, as it is essential for dynamic load response and control, understanding and optimizing load profiles and distributions, and for climate-responsive design.

The dissertation is laid out in the following order:

Chapter 1: Introduction: This chapter introduces the overall function of the Heating, Ventilating, and Air-conditioning (HVAC) System and the background information to building load calculations. It concludes with research objectives, overview, and summary of the contributions of this dissertation.

Chapter 2: Literature Review: This chapter describes the state of the art and current challenges involved with electricity minimization in multi-zone buildings. It concludes with research gaps identified from critical review of literature.

Chapter 3: HVAC Components Model Development: From the critical review of literature in Chapter 2, existing fan, cooling coil, and building load models were reviewed. This chapter describes the selected thermal and airflow models used in this dissertation as well as the parameter estimation techniques, and solution methods adopted.

Chapter 4: HVAC Components Model Validation: This chapter validates the building load, fan-motor and cooling coil model. The validation was done for a case study multi-zone building, which was used as proof of concept. The validation was

essential to establish that the level of accuracy of these predictive models is appropriate for control purposes.

Chapter 5: Development and Validation of Framework for Minimizing Buildings Electricity Demand and Cost: This chapter described the framework used to investigate methods for minimizing buildings electricity demand and cost. The establishment of accuracy levels of the system predictive models (earlier in Chapter 4) enabled the study of multi-zone interactions and minimization of electricity cost via application of suitable predictive control methods. The demonstration of the framework for a case study multi-zone building reveals some interesting findings and results which are discussed in this chapter.

Chapter 6: Step by Step Summary of Minimization Framework: This chapter summarizes the steps involved in electricity demand and cost minimization, as an overview of the developed framework.

Chapter 7 Original Contributions to knowledge/Research: This chapter highlights the original contributions of this research and the new knowledge generated.

Chapter 8: Conclusions and Future Work

1.5 Thesis Contributions

The intellectual contribution of this research is the understanding of multiple-zone interactions in buildings to aid in effective decision making regarding the operational states of HVAC equipment that minimizes the overall electricity cost. The overall contributions of this research may be summarized as follows

- Understanding of multi-zone thermal interactions in buildings

- Understanding of stability issues involved in thermal modeling of building load and cooling coil
- Investigation of methods for filling missing gaps in solar radiation data
- Study of thermal characteristics of building construction
- Understanding of passive thermal storage capabilities of building construction for appropriate sizing of HVAC equipment
- Extension of the R-C thermal network approach for transient modeling of cooling coils
- Identification of new methods (near constant cooling and temperature recovery/optimal start) for minimizing buildings electricity demand and cost.
- A demonstration of the electricity cost savings capabilities in air handling units operations through the use of Model predictive control (MPC) strategies, integrated with the thermal network models of building load and cooling coil model.
- Scalability and further applications of the developed approaches to smart grid technology.

In the next chapter, the state of the art and current challenges with HVAC system control will be discussed, leading to identification of research gaps.

Chapter 2: Literature Review

Building systems operations are mainly challenged by dynamic load changes, particularly for large commercial buildings. Unlike lighting and plug loads, the HVAC system load is variable. There are different states in which a HVAC system can operate while in heating or cooling mode. These are float, hold, heat, and cool. When floating, the HVAC system is turned off, and the temperature drifts to lower or higher values, depending on the season. In the ‘hold’ state, the system keeps the temperature at a fixed value. Heating/cooling mode implies part-load (for example, running at 2/3rd capacity) or full load, where the system runs at 100% capacity. Inappropriate control strategy and faulty equipment always lead to deficiencies in building systems operation. The dynamic changes in building load also impose additional challenges which make fault detection, diagnosis, and control of HVAC systems difficult.

2.1 State of the Art and Current Challenges

The building geometry and HVAC configuration constitute basic input for building performance simulation. Generally, the calculation of heating and cooling loads in building require the following information about the building envelope:

- Architectural plans
- Building orientation and location
- External/Internal shading, ground reflectance etc.
- Construction materials of walls, roofs, partitions, windows, ceilings, insulating materials and thicknesses
- Amount of glass, type and shading on windows.

Challenges imposed by building information could be particularly huge for buildings with limited or unreliable information about the composition of walls and fenestration. Similarly, Obtaining the most accurate and reliable data within limited time is a challenge often faced by practicing HVAC engineers, since calculated load can only be as accurate as the input data for the simulation.

There have been several studies on minimizing building electricity demand and consumption. Most of these strategies have focused on the HVAC system and lighting for improvements in energy efficiency (Westphalen and Koszalinski 1999; Agarwal et. Al 2011; Delaney et. al 2009; Erickson et. al 2009; Lu et. al, 2010) because they both account for more than 2/3rd of the total electricity use and have the highest potential for operational cost savings. Load-shifting strategies for attenuating the peak load have included natural and mixed mode ventilation, curtailment, pre-cooling, temperature recovery or optimal start, and model based control (Armstrong et. al, 2006, Keeney et. al, 1997, Seem et. al 1989, BCA 2010). Ventilation strategies involve the use of natural ventilation as an important strategy towards reducing energy demand on a building since natural ventilation requires less energy use compared to air-conditioning (BCA 2010). The mixed mode ventilation involves the use of mechanical ventilation only when necessary. It has been found suitable for spaces such as multi-purpose halls, classrooms and even hospital wards. Curtailment is another strategy for reducing building electricity use, particularly in periods of peak demand, which is extremely costly from a grid perspective. Curtailment is the response to a utility contractual incentive that results in a reduction in electrical demand, either by chiller control or by adjusting room temperature set points (Armstrong et. al 2006). Curtailment control is

addressed in a number of papers with focus on incentives but consequences such as indoor conditions are not rigorously studied through methodological approach and building transient thermal response (Haves and Gu 2001; Goldman et. al 2002; Kintner-Meyer et. al 2003; Xing 2004). Temperature recovery refers to the optimal operation of HVAC and other building systems components to restore comfort conditions shortly before the start of occupied periods. In heating mode, starting recovery at the last possible moment leads to the maximum electricity and energy savings. Optimal start requires a transient thermal response model which is not embedded in most HVAC controls where traditionally simplistic models have been used (Seem et. al 1989). More realistic models such as transfer function and step response models (Seem et. al 1989, Armstrong et. al 1992) can lead to more reliable control. A long-recognized way of minimizing building systems energy use is model-based control which measures the important disturbances and estimate their effect on the thermal response of the building (Armstrong et. al 2006). Model-based control helps better regulate temperatures in the presence of disturbances of ambient, solar radiation, and internal heat gains. The most difficult, but potentially most effective, building electricity reduction measure requires control functions that *anticipate* curtailment and increase cooling capacity during this pre-curtailment period (Armstrong et. al 2006). Night pre-cooling has been used for this purpose. A few studies on precooling have used simplified analysis, as well as forward simulation, to show annual savings of up to 50% in mechanical cooling energy input. However, there have been few successful experimental demonstrations of significant pre-cooling and curtailment benefits in real buildings (Keeney and Braun 1997, Braun et. al 2001, Ruud et. al 1990). Likewise, the literature dealing with pre-cooling is rich in

context but it is not consistent in its conclusions because of the uncertainties in building thermal response and the severe thermal capacity and storage limitation constraints (Braun et. al 2001, Ruud et. al 1990, Braun and Chaturvedi 2002). Predictive optimal control offers many advantages, in light of dynamic and thermal coupling between building system components. One of the benefits is substantial energy and electricity savings. However, it is very difficult to achieve optimality because of system complexity.

2.2 Building Load Models

As illustrated in Figure 2.1, the input to thermal models consists of HVAC systems and components, building geometry, internal loads, weather data, operating strategies and schedules, and other parameters. The building load is defined as the rate at which heat must be removed (or added to) to the building to maintain the desired temperature. It is the rate at which heat is instantaneously removed from (or added to) the zone air by convection. Building load calculations are important to determine the appropriate size of HVAC equipment that is necessary to provide needed heating and cooling under normal and extreme weather conditions. There were very few building load calculation methods in the U. S., prior to 1945. Building load calculation methods such as the sol-air temperature, decrement factors, and thermal RC network model were all developed after 1946 (Mao et. al 2013). The first edition of American Society of Heating, Refrigerating, and Air-conditioning Engineers (ASHRAE) handbook was published in 1967, and it adopted the peak load calculation methods in existence at the time. Major advances in building load calculations have since taken place, but their applications have been very limited by available data.

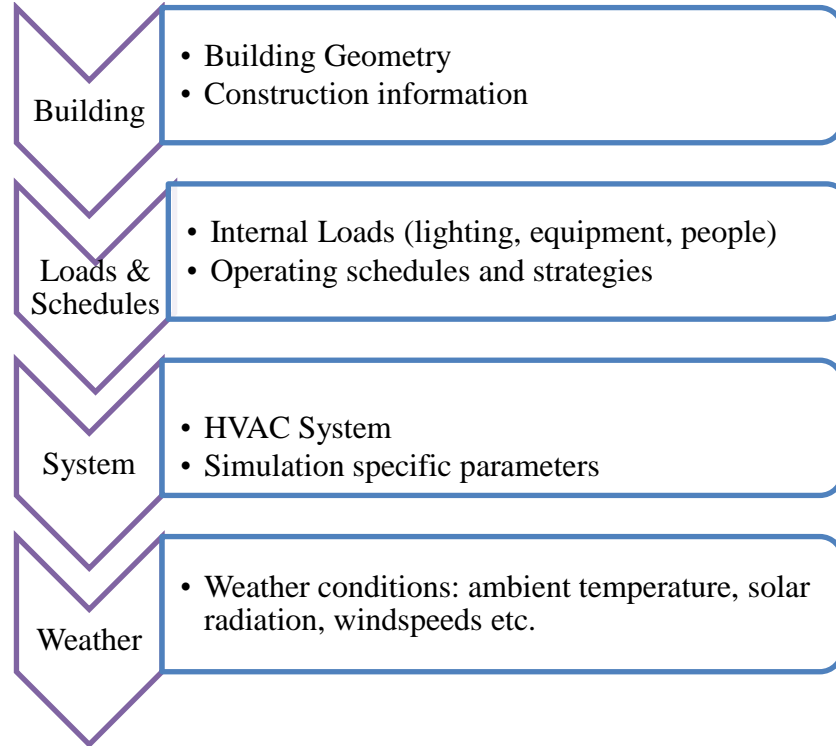


Figure 2.1: Input to Thermal Models

Energy performance simulation programs have been used to predict and study energy performance. Numerous of such tools are available today with differences in their underlying equations, applicability, graphical user interface, and thermodynamic model. All internal heat gains transferred from building envelope and internal heat gains such as occupants, lights and equipment to an indoor environment is converted into cooling load through radiation and convection. The convective portion is added to room air by natural or forced convection, as an instantaneous load, without a time delay. However, the radiative portion is first absorbed by surfaces of the room, and later dissipated over time, with some lag and attenuation effects, which makes cooling load calculations inherently complicated.

Common methods used to measure building energy include use of black box models, or whole building simulation software such as EnergyPlus (DOE 2010), BLAST (Jacobon 1986), or e-Quest (DoE 2010), and through the use of physics based models (Wetter 2006, Goyal et. al 2011). In EnergyPlus Model, the basis for the zone and air system integration is to formulate energy balances for the zone air and solve the resulting ordinary differential equations using a predictor-corrector approach. The formulation of the solution scheme starts with a heat balance on the zone air as shown in Equation (2.1):

$$\begin{aligned}
C_z \frac{dT_z}{dt} = & \sum_{i=1}^{N_{sl}} \dot{Q}_i \\
& + \sum_{i=1}^{N_{surfaces}} h_i A_i (T_{si} - T_z) + \sum_{i=1}^{N_{zones}} m_i C_p (T_{zi} - T_z) + m_{inf} C_p (T_\infty - T_z) \\
& + \dot{Q}_{sys}
\end{aligned} \tag{2.1}$$

Where

$$\sum_{i=1}^{N_{sl}} \dot{Q}_i = \text{sum of convective internal loads}$$

$$\sum_{i=1}^{N_{surfaces}} h_i A_i (T_{si} - T_z) = \text{convective heat transfer from the zone surfaces}$$

$$m_{inf} C_p (T_\infty - T_z) = \text{Heat transfer due to infiltration of outside air}$$

$$\sum_{i=1}^{N_{zones}} m_i C_p (T_{zi} - T_z) = \text{heat transfer due to interzone air mixing}$$

$$\dot{Q}_{sys} = \text{HVAC systems output} = \dot{m}_{sys} C_p (T_{sup} - T_z)$$

$$C_z \frac{dT_z}{dt} = \text{energy stored in zone air}$$

ρ_{air} = zone air density

C_p = zone air specific heat

EnergyPlus uses three solution algorithms (Eulers' method, 3rdOrderBackwardDifference, and integrated solution method) for the zone air heat balance. The load on the zone is used as a starting point to give demand to the air system, such that the simulation of the air system provides the actual supply capability, and the zone temperature is adjusted if necessary. This is referred to as Predictor/Corrector process. EnergyPlus uses the 'Internal Mass' object to describe furniture surface area and thermal mass. Transient heat conduction through building elements such as walls, roofs, floors, etc. is done using conduction transfer functions. The applicability of whole building software (such as EnergyPlus) is very limited since they require detailed information about the construction materials and physical features of the building. In most cases, these details are not available, and the reliability of the simulation results depends heavily on that information. Additionally, whole-building softwares were not designed for control purposes. Black box models are limited by the huge amount of training data needed. Lots of accuracy may be lost when the model is applied for operating conditions that are outside of the training data (Wang and Xu 2006, Xu 2005). Other approaches involve the use of statistical models such as the autoregressive integrated moving average (ARIMA) for modeling building energy consumption (e.g. Javed et. al 2012, and Song et al 2013.). Statistical models are generally the simplest models, and are easy to formulate and interpret. Because they are

purely regression based, they do not physically represent the dynamics and thermal characteristics of the building system.

2.2.1 Review of Building Load Calculation Methods

Lots of researchers have studied building performance and load calculations. There are myriad of methods used for estimation and prediction of cooling and heating loads in buildings. Pang et. al (2012) developed a framework for real-time assessment of building performance. The simulation-based framework allowed the real-time comparison of buildings' actual and expected performance. However, the method is limited by the need to update several factors and variables at every time-step. The updated variables include HVAC operational schedules, weather data, and control set points. Causone et. al (2010) implemented the Heat Balance method and the Radiant Time Series (RTS) method calculation procedure. These procedures are described in ASHRAE handbook of Fundamentals (ASHRAE 2005). The models need lots of data for calibration to accurately predict and reflect system performance. Braga et. al. (2013) proposed a statistical model for estimation of building load and energy consumption profile during a cycle, e.g. one week. The model monitored and controlled energy consumption patterns. Feng et. al (2013) used EnergyPlus for comparison of cooling load differences between radiant and air systems. Factors studied include level of insulation, internal heat gains, solar exposure, and thermal mass effects. Xuemei et. al. (2010) developed a forecast algorithm for cooling load using Support Vector Machine (SVM) model. SVM is a machine learning technique, and the model parameters were determined from measured data. Chen et. al. (2014) likewise accessed the effect of internal heat gains from appliances on real-time and historical buildings energy use.

This was achieved through separate measurements of plug loads, building loads, and lighting loads using energy meters and sensors. Duanmu et. al. (2013) assumed certain linear relationship exists between the cooling load components and important variables (such as temperature difference between room and outdoor air), and applied the Hourly Cooling Load Factor Method (HCLFM), for estimation and forecast of cooling load in buildings. Schiavon et. al (2011) implemented a calculation procedure for cooling loads in underfloor air distribution (UFAD) systems. Regression methods were developed to convert cooling loads of overhead mixing systems to UFAD systems. The method is deemed suitable for design cooling load only.

A major concern in cooling load calculations is the development of a representative model which is suitable to capture the dynamics of the system. The phenomenon of interest includes the thermal delays caused by the building envelope and internal mass effects. In that regard, the thermal network approach has been widely applied. It utilizes resistors and capacitors to represent the conduction and thermal storage effect of building constructions. The thermal network model (also commonly known as Resistances and Capacitances model) is known to provide robust and accurate estimates of building load as compared with measured data. Over the years, there have been several improvements in the thermal network model, but the three resistances and two capacitances (3R2C) representation is widely used for modeling transient heat transfer in building envelopes (Wang and Xu 2015; Mckinley and Alleyne 2008). Other recent versions of the thermal network model include the 3R4C and 4R5C by Fraisse et. al (2011). The thermal network model has been widely applied for modeling of thermal

coupling of building elements, and for comparison of thermal zone aggregated methods (Dobbs and Hency 2012; Dobbs and Hency 2012, Sourbron et. al 2009).

The thermal network model represents the building thermal and internal mass using lumped resistors and capacitors. The envelope Resistance and Capacitance (RC) parameters may be found from properties of building construction, or from measured data. The RC parameters of internal mass are estimated by optimization procedure which minimizes the difference between the actual building load and the model-predicted building load. As such, the optimization procedure avoids the lengthy training and calibration process which is inevitable when using other models. The lumped approach also compensates for errors in the input parameters, since any associated uncertainties are lumped in the RC parameters. The RC parameters have been traditionally estimated by genetic algorithm, and solved numerically using Runge-Kutta or other classical methods (Xu 2005, Ogunsola and Song 2013, Ogunsola et. al, 2014).

2.2.2 Advances in RC Modeling Approach

The thermal network approach has been modified and applied in different forms. Examples include numerical solutions and time series modeling (Ogunsola et. al, 2014). The numerical approach suffers from convergence and stability issues, due to the need for different time steps. In another study, the time series model was deduced from the simplified RC model. The time series model performed superior to pure statistical and autoregressive models, because of improved ability to track abrupt changes in control strategies or set-points. It is also deemed to have less sensitivity to outliers. However, the time series method permits only limited exploration of the thermal network model capabilities. This is because it relies on previous measurements of building load,

weather, and usage of several time-steps to forecast future loads. The needed measurements may be unavailable or unreliable due to sensor malfunction or data quality assurance issues. Most importantly, the time series model becomes increasingly difficult to develop and optimize, with increasing building complexity. There have also been noticeable spikes in the cooling load prediction by the time series (Ogunsola et. al, 2014). The general applicability of the thermal network approach has been limited by the identified issues.

The RC thermal network model has been applied for multiple scenarios and case studies of different building constructions and HVAC systems operation modes. Among several models, The RC model was deemed to be appropriate to capture the dynamics of building construction and HVAC components, with other advantages such as:

- (i) Its ability to physically represent the properties of building construction. This allows fundamental study and investigation of the thermal characteristics of different construction.
- (ii) Its ability to simulate varying schedules of internal loads and HVAC system operation.
- (iii) Its capability to investigate multiple weather and operation scenario across different climates, since it is simulation-based.
- (iv) Its ability to be translated to a state space representation which allows the determination of system stability from model parameters. The state space representation is also ideal for model predictive control. .
- (v) Its capability to optimizing the building heating and cooling demands in response to varying usage and weather conditions (e.g. ambient temperature and solar radiation).

(vi) Its capability for the simulation and representation of internal mass storage effects in buildings, which allows opportunities for harnessing thermal storage effects to the fullest.

(vii) Its ability to simulate floats in space air temperature.

Multiple scenarios of HVAC system operation and strategies with light, medium, and heavy construction of the building envelope have been simulated using thermal network model (Ogunsola et. al, 2014; Ogunsola and Song 2015; Ogunsola et. al 2016). The studies introduced analytical and numerical solution of thermal network model and applied it for the analysis of passive thermal storage opportunities of building construction. This revealed significant opportunities for downsizing of heating system size based on passive thermal storage.

2.3 Cooling Coil Transient Models

This section focusses on transient cooling coil models. The cooling coil is an important component in the air handling unit. Several researchers have developed transient models for the cooling coil. Ye Yao et. al (2013) developed a state space dynamic model for water to air surface heat exchangers. The model was validated by a series of dynamic experiments for exit temperatures and humidities of air and water arising from disturbances in inlet water temperature. The governing equations and assumptions are shown below:

From mass and energy equation for water passing through the coil

$$\dot{m}_{w,E} = \dot{m}_{w,L} = \rho_w u_w A_w \quad (2.1)$$

$$\begin{aligned} \frac{1}{2} \rho_w c_w A_w l \frac{d(t_{w,L} + t_{w,E})}{dt} \\ = \dot{m}_{w,E} c_w (t_{w,E} - t_{w,L}) + a_{gw} A_{gw} \left(t_g - \frac{t_{w,L} + t_{w,E}}{2} \right) \end{aligned} \quad (2.2)$$

$$\dot{m}_{a,E} = \dot{m}_{a,L} = \rho_a u_a A_a \quad (2.3)$$

For dry condition of the coil,

$$\frac{1}{2} \varepsilon_a \rho_a c_a A_a b \frac{d(t_{a,L} + t_{a,E})}{dt} = \dot{m}_{a,E} c_a (t_{a,E} - t_{a,L}) + a_{ga} A_{ga} \left(t_m - \frac{t_{a,L} + t_{a,E}}{2} \right) \quad (2.4)$$

For wet condition of the coil,

$$\begin{aligned} \frac{1}{2} \varepsilon_a \rho_a A_a b \frac{d(W_{a,L} + W_{a,E})}{dt} \\ = \dot{m}_{a,E} (W_{a,E} - W_{a,L}) + \lambda_m A_{ga} \left(W_{gb} - \frac{W_{a,L} + W_{a,E}}{2} \right) \end{aligned} \quad (2.5)$$

$$\begin{aligned} \frac{1}{2} \varepsilon_a \rho_a A_a b \frac{d(h_{a,L} + h_{a,E})}{dt} \\ = \dot{m}_{a,E} (h_{a,E} - h_{a,L}) + \lambda_m A_{ga} q_r \left(W_{gb} - \frac{W_{a,L} + W_{a,E}}{2} \right) \\ + a_{ga} A_{ga} \left(t_m - \frac{t_{a,L} + t_{a,E}}{2} \right) \end{aligned} \quad (2.6)$$

From energy balance for the coil and fins, the following equations apply:

Dry condition:

$$M_g c_g \frac{dt_g}{dt} = a_{gw} A_{gw} \left(\frac{t_{w,L} + t_{w,E}}{2} - t_g \right) + a_{ga} A_{ga} \left(\frac{t_{a,L} + t_{a,E}}{2} - t_m \right) \quad (2.7)$$

Wet condition:

$$M_g c_g \frac{dt_g}{dt} = a_{gw} A_{gw} \left(\frac{t_{w,L} + t_{w,E}}{2} - t_g \right) + a_{ga} A_{ga} \left(\frac{t_{a,L} + t_{a,E}}{2} - t_m \right) + \lambda_m A_{ga} q_r \left(\frac{W_{a,L} + W_{a,E}}{2} - W_{gb} \right) \quad (2.8)$$

Where l =length of coil, a_{ga} =coefficient of heat transfer between the coil and air.

b = length along airflow, A_a = area of windward side, a_{gw} =coefficient of heat transfer between the coil and water, λ_m = coefficient of mass transfer, t_m =surface temperature of fins, M_g = total mass, c_g = mean specific heat of the heat exchanger

The efficiency of sensible heat exchange is given by:

$$\eta_s = \frac{\left(t_m - \frac{t_{a,L} + t_{a,E}}{2} \right)}{\left(t_g - \frac{t_{a,L} + t_{a,E}}{2} \right)} \quad (2.9)$$

To estimate the coil parameters, the following equations were used:

$$NU_w = C_1 Re_w^{n_1} = \frac{a_{gw} R_{d,w}}{\lambda_w}; \quad Re_w = \frac{u_w R_{d,w}}{v_w}; \quad NU_a = C_2 Re_a^{n_2} = \frac{a_{ga} R_{d,a}}{\lambda_a}$$

$$Re_a = \frac{u_a R_{d,a}}{v_a} = \frac{\dot{m}_a R_{d,a}}{v_a \rho_a A_a}; \quad NU_d = C_3 Re_a^{n_3} = \frac{\lambda_m R_{d,a}}{\rho_a D_j}; \quad R_{d,a} = \frac{2(S - 2r_i)(e - \delta_c)}{(S - 2r_i) + (e - \delta_c)}$$

Where The empirical coefficients $C_1, C_2, C_3, n_1, n_2, n_3$ can be determined with experimental data, and δ_c = thickness of fin, e = fin spacing, r_i = inner diameter of the coil.

Three cases were considered (Case I: Start up the chiller; Case II: sudden increase in water flow rate, and case III: stop the chiller). The transient response time was set at 1200s for all cases. The solution method involved linearization of the state space model about typical operating points of water and air temperatures, such that the disturbance values are the input to the system. The state space model predicted the

transient performance within average error of around 15%. However, some of the needed measurements and coil geometric information may not be available.

Jin et. al (2006) extended the cooling coil unit engineering model, and used commissioning information to estimate model parameters by a nonlinear identification method. The model was deemed to capture characteristics of cooling coil unit over a wide range of operating range. The model is simpler than Model 1 above, because it requires less information about the coil geometry. There was no separation into dry and wet regions. The governing equations and assumptions are described in equation (2.10) to (2.20):

The overall thermal resistance of the cooling coil is given by

$$R_{total} = R_a + R_{chw} = \frac{1}{U_{chw}A_{chw}} + \frac{1}{U_aA_a} = \frac{b_{chw}A_{chw}\dot{m}_{chw}^l + b_aA_a\dot{m}_a^l}{b_{chw}A_{chw}\dot{m}_{chw}^l b_aA_a\dot{m}_a^l} \quad (2.10)$$

Where U_{chw} = film coefficient of the chilled water, A_{chw} = heat transfer area of the chilled water side convection, U_a = film coefficient of the air, and A_{chw} = heat transfer area of the air side convection,

$$u_a = \frac{\dot{m}_a}{\rho_a A_a} \quad (2.11)$$

$$u'_{chw} = \frac{l}{\xi} u_{chw} = \frac{l}{\xi} \frac{\dot{m}_{chw}}{\rho_{chw} A_{tube}} \quad (2.12)$$

Where u_a = Velocity of air flow, u'_{chw} = equivalent velocity of cooling water in the counter air flow velocity, l = total length of the tube, and ξ = cooling coil depth.

From energy and mass conservation laws,

$$\rho_{chw} V_{chw} \left(c_{chw} \frac{\partial T_{chw}}{\partial t} + c_{chw} u'_{chw} \frac{\partial T_{chw}}{\partial x} \right) = q \quad (2.13)$$

$$\rho_a V_a \left(\frac{\partial h_a}{\partial t} + u_a \frac{\partial h_a}{\partial x} \right) = -q \quad (2.14)$$

Where V_{chw} and V_a are constants representing the volume of the chilled water and the air element in the mass and heat transfer processes in the respective flow directions.

With assumption of linear variations in T_{chw} and h_a together with assumption $h_a \approx c_{ma} T_a$, the simplified energy and mass equation becomes an ODE which is given by:

$$\frac{dT_{chw}}{dt} + C_1 \dot{m}_{chw} (T_{chw,o} - T_{chw,i}) = \frac{C_2 \dot{m}_a^\ell}{1 + C_3 \left(\frac{\dot{m}_a}{\dot{m}_{chw}} \right)^\ell} (T_a - T_{chw}) \quad (2.15)$$

$$\frac{dT_a}{dt} + C_4 \dot{m}_a (T_{a,o} - T_{a,i}) = - \frac{C_5 \dot{m}_a^\ell}{1 + C_3 \left(\frac{\dot{m}_a}{\dot{m}_{chw}} \right)^\ell} (T_a - T_{chw}) \quad (2.16)$$

Where C_1, C_2, C_3, C_4, C_5 , and ℓ are constants to be determined from manufacturer's data or real time experimental data.

$$C_1 = \frac{l}{\xi} \frac{1}{\rho_{chw} A_{tube}}, C_2 = \frac{b_a A_a}{\rho_{chw} V_{chw} c_{chw}}, C_3 = \frac{b_a A_a}{b_{chw} A_{chw}}, C_4 = \frac{1}{\rho_a A_a}, C_5 = \frac{b_a A_a}{\rho_a V_a c_{ma}}$$

The above equation could be further transformed to a form that requires only the boundary conditions as shown in equation (2.17) to (2.20):

$$\begin{aligned} & \frac{dT_{chw,o}(t)}{dt} + C_1 \dot{m}_{chw}(t) [T_{chw,o}(t) - T_{chw,i}(t - \tau_{chw})] \\ &= \frac{C_2 \dot{m}_a(t)^\ell}{1 + C_3 \left(\frac{\dot{m}_a}{\dot{m}_{chw}} \right)^\ell} [T_{a,o}(t) - T_{chw,o}(t)] \end{aligned} \quad (2.17)$$

$$\begin{aligned} & \frac{dT_{a,o}(t)}{dt} + C_4 \dot{m}_a(t) [T_{a,o}(t) - T_{a,i}(t - \tau_a)] \\ &= - \frac{C_5 \dot{m}_a^\ell}{1 + C_3 \left(\frac{\dot{m}_a}{\dot{m}_{chw}} \right)^\ell} [T_{a,o}(t) - T_{chw,o}(t)] \end{aligned} \quad (2.18)$$

Where:

$$\tau_{chw} = \frac{\xi}{u_{chw}} = \frac{\xi \rho_{chw} A_{tube}}{\dot{m}_{chw}}, \text{ and } \tau_a = \frac{l}{u_a} = \frac{l \rho_a A_a}{\dot{m}_a}$$

τ_{chw} = time interval that the water fluid element takes to transverse from inlet to outlet

τ_a = time interval that the air fluid takes to transverse from inlet to outlet. Some of the coil parameters could be estimated from steady state operation, while others can only be estimated from transient operation.

$$Q = c_{chw} \dot{m}_{chw} (T_{chw,o} - T_{chw,i}) = -c_{ma} \dot{m}_a (T_{a,o} - T_{a,i}) \quad (2.19)$$

$$Q = \frac{C_6 \dot{m}_a^\ell}{1 + C_3 \left(\frac{\dot{m}_a}{\dot{m}_{chw}} \right)^\ell} (T_{a,o} - T_{chw,o}) \quad (2.20)$$

where $C_6 = c_{chw} \frac{C_2}{C_1} = c_{ma} \frac{C_5}{C_4}$; C_6, C_3 and ℓ are estimated from Q in steady state while

the other parameters are estimated under dynamic conditions.

Yao et. al (2004) developed a dynamic cooling coil model and validated it using experiments. The governing equations and assumptions are described in equations (2.21) to (2.25).

Dynamic change in cooling water temperature

$$c_w \frac{\partial T_w}{\partial \tau} - c_w u'_w \frac{\partial T_w}{\partial x} = a_{bn} F_w (T_b - T_w) \quad (2.21)$$

Dynamic change in cooling coil temperature

$$c_m \frac{\partial T_b}{\partial \tau} = a_{bn} F_w (T_w - T_b) + a_{bw} F_a (T_a - T_b) \quad (2.22)$$

Dynamic change in air humidity

$$\frac{\partial d_a}{\partial \tau} + u_a \frac{\partial d_a}{\partial x} = K F_a (d_g - d_a) \quad (2.23)$$

Dynamic change in air enthalpy

$$\frac{\partial h_a}{\partial \tau} + u_a \frac{\partial h_a}{\partial x} = KF_a(h_v - h_a) \quad (2.24)$$

Heat exchange between wet air and cooling coil

$$q = \rho_a u_a A (h_{a,i} - h_{a,o}) \quad (2.25)$$

Where the parameters are as defined in Yao et. al (2004). By linearizing the differential equations about certain operating points, the effect of perturbations of the five important variables (inlet air temperature, inlet air humidity, inlet water temperature, airflow rate, and water flow rate) under different initial conditions were simulated and analyzed.

Zhou and Braun (2007) developed and validated a simplified transient model for cooling and dehumidifying coils. The model was solved using finite element method, and it requires some geometry information of the cooling coil. It utilizes the UA and NTU approach, and requires calculation of fin efficiency, air-side effectiveness, and water-side effectiveness. The model utilized lots of steady state performance indices which enables the simplification. The governing equations are described in equations (2.26) to (2.31):

$$C'_w \frac{\partial T_w}{\partial t} + \dot{C}_w \frac{\partial T_w}{\partial x} + \frac{1}{R'_w} (T_w - T_c) = 0 \quad (2.26)$$

$$C'_c \frac{\partial T_c}{\partial t} + \frac{1}{R'_w} (T_c - T_w) + \frac{1}{R'_a} (T_c - T_{a,su}) = 0 \quad (2.27)$$

In wet case, the energy equation for coil surface is given by:

$$C'_c \frac{\partial T_c}{\partial t} + \frac{1}{R'_w} (T_c - T_w) + \frac{1}{R'_a} (h_{s,c} - h_{a,su}) = 0 \quad (2.28)$$

where C'_w and C'_c are thermal capacitances of the water and coil material per unit length in the water flow direction (i.e., $\rho c_{pA_{cs}}$), respectively. $T_{a,su}$ = Supply air temperature.

$$R'_w = \frac{1}{h_w P}; R'_a = \frac{1}{\varepsilon_a \dot{C}'_a}; R_{a'}^* = \frac{1}{\varepsilon_a^* \dot{M}'_a}; \dot{C}'_a = \frac{\dot{M}_a c_{pa}}{L_c}; \varepsilon_a = 1 - e^{-NTU_a};$$

$$NTU_a = \frac{\eta_a h_a A_a}{\dot{C}'_a}; \varepsilon_a^* = 1 - e^{-NTU_a^*}; \text{and } NTU_a^* = \frac{\eta_a^* h_a A_a}{\dot{C}'_a}$$

\dot{C}'_a is the capacitance rate of the air stream per unit length, P =tube perimeter, ε_a = airside heat transfer effectiveness, R'_w and R'_a are thermal resistances for heat transfer per unit length between the coil material and water and the air and the coil material, $R_{a'}^*$ is air resistance for mass and heat transfer per unit length, η_a is the overall fin efficiency for heat transfer, η_a^* is the overall fin efficiency for both heat and mass transfer. The local exhaust air temperature and humidities are given by:

$$T_{a,ex} = T_{a,su} + \varepsilon_a (T_c - T_{a,su}) \quad (2.29)$$

Wet case:

$$h_{a,ex} = h_{a,su} + \varepsilon_a^* (h_{s,c} - h_{a,su}) \quad (2.30)$$

The most common assumptions for cooling coil models can be summarized as follows:

1. In the process of mass and heat transfer, the thermal properties of wet air, such as specific heat and density are assumed constant. This helps to treat dry air and water vapor as non-reacting ideal gas mixture.
2. Where there is dehumidification, the condensate is removed by gravity from the coil surface immediately.
3. Lewis coefficient is constant during process of heat and mass exchange. This is because the mass and heat exchange between moist air and surface of the coil tubes arrive at a balance.
4. The air and water are well mixed in the cross section normal to their respective flows, such that gradients exist only in the respective flow directions.

5. The humidity of saturated wet air varies in approximately linear relation with the temperature.
6. Coils having more than three tube passes could be modeled as pure counterflow heat exchangers.
7. Within the dry and wet regions, the chilled water temperature and humidity of moist air can be approximated by a linear relation.
8. Air and water flows are steady. The velocities of water and air are uniform along their respective flow directions.
9. There is negligible conduction in the direction of flow for both fluids.
10. There is negligible energy storage within the air (Yao et. al 2013, Jin et. al 2006, Yao et. al 2004, Zhou and Braun 2007).

2.4 Fan-Power Models

There are very few studies on transient modeling of fan-motor power. Steady state models are commonly used, because of the fast transient of fans, which fades out after few seconds. Several steady state models have been proposed in literature (Nassif et. al 2008, Clark 1985, Stein and Hydeman 2004). These models are limited in their applications, by the flexibility in inputs and output variables. The ASHRAE HVAC toolkit fan model (Brandemuehl et. Al 1983) and simplified DOE model (DOE, 1980) used a third order regression model to estimate the fan power as a function of flow rate. The toolkit model is more detailed, as it expresses the fan performance in terms of shaft power and pressure rise. The common limitations to existing models are highlighted below:

HVAC Toolkit simple fan model (Brandemuehl et. Al, 1993, DOE 1980)

It uses a third order regression model of power as a function of airflow rate and involves 4 regression parameters

$$\frac{W_s}{W_d} = C1 + C2 \frac{Q}{Q_d} + C3 \left(\frac{Q}{Q_d}\right)^2 + C4 \left(\frac{Q}{Q_d}\right)^3 \quad (2.31)$$

Where W_d = design fan power and Q_d = design airflow rate. This model requires at least four different operating points and it is based on assumption of constant fan pressure rise and a single system curve. This makes it unsuitable for VAV systems.

HVAC Toolkit detailed fan model (Clark 1985, Brandemuehl et. al, 1983)

It uses a fourth order polynomial regression model of power as a function of a dimensionless coefficient of flow, $\Phi = \frac{Q}{Nd^3}$

$$\psi = A0 + A1\Phi + A2\Phi^2 + A3\Phi^3 + A4\Phi^4 \quad (2.32)$$

$$\eta_f = B0 + B1\Phi + B2\Phi^2 + B3\Phi^3 + B4\Phi^4 \quad (2.33)$$

Where ψ = dimensionless pressure head, and η_f = dimensionless fan power, $\psi =$

$\frac{\Delta P}{\rho N^2 d^2}$ and $\eta_f = \frac{Q\Delta P}{W}$. It involves the identification of 5 regression parameters. The

application of this model is Its application is limited by the assumption of peak fan efficiency for all fan types. Additionally, there is no flexibility in the input variables.

For example, fan power cannot be directly calculated from airflow rate and fan pressure rise.

Nassif et. al 2014 Fan-model

Nassif et. al (2014) used numerical analysis and interpolation techniques based on basic fan laws, as shown in Figure 2.2. Linear or polynomial interpolation could be used to

determine flow, power etc. at any desired operating points, based on measured or manufacturers data.

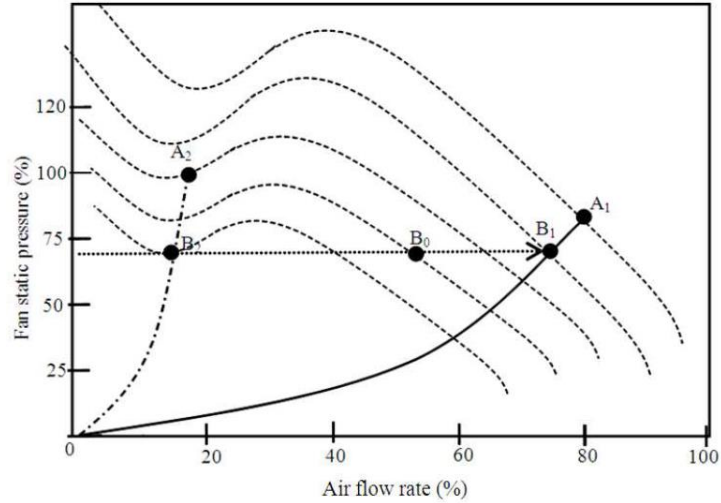


Figure 2.2: Interpolation techniques for fan-model

For example, given fan speed and airflow rate at points A2 and A1, fan speed at point B0, the airflow and fan-power at point B0 could be determined using interpolation as:

$$Q_{B0} = \frac{N_{Bi+1} - N_{B0}}{N_{Bi+1} - N_{Bi}} Q_{Bi} + \frac{N_{B0} - N_{Bi}}{N_{Bi+1} - N_{Bi}} Q_{Bi+1} \quad (2.34)$$

$$W_{B0} = \frac{N_{Bi+1} - N_{B0}}{N_{Bi+1} - N_{Bi}} W_{Bi} + \frac{N_{B0} - N_{Bi}}{N_{Bi+1} - N_{Bi}} W_{Bi+1} \quad (2.35)$$

This model has lots of flexibility in choice of input and output variables. However, only linear interpolation method was demonstrated. However, it may require lot of calibration data to cover wide range of fan's operating points.

Energy plus fan model (DOE 2010)

EnergyPlus fan model uses a fourth order polynomial regression model which expresses fan power as a function of part load airflow ratio.

$$PLR_{cfan} = m_{cfan} / m_{cfan,D}$$

$$f_{pl} = e_0 + e_1 PLR_{cfan} + e_2 PLR_{cfan}^2 + e_3 PLR_{cfan}^3 + e_4 PLR_{cfan}^4 \quad (2.36)$$

$$P_{cfan} = \frac{f_{pl}m_{cfan,D}\Delta P_{cfan}}{1000e_{cfan}\rho_1} \quad (2.37)$$

PLR_{cfan} is the air flow ratio of cooling coil

$m_{cfan,D}$ is the designed flux of cooling coil fan,

f_{pl} is part load factor of cooling coil fan,

e_0, e_1, e_2, e_3, e_4 is the characteristic coefficient of cooling coil fan, P_{cfan} is the power consumption of cooling coil fan, ΔP_{cfan} is the designed power consumption of cooling coil fan, e_{cfan} is the sum efficiency of cooling coil fan, ρ_1 is the air density. This model is limited by its requirement of sum efficiency of fan, which varies with operating points. It also requires lots of training data to determine the coefficients

2.5 HVAC System Control and Optimization

Two important functions of Building Management Control (BMC) systems are local control and supervisory control. The local control loop ensures stability and set-point tracking, taking into account the local process. This is usually done using Proportional Integral Derivative (PID) controls. Supervisory controllers coordinate and supervise several local controllers, and are aimed at global optimal operation of the HVAC system, for determination of optimized set-points.

HVAC systems are typically controlled by Proportional Integral (PI) control laws (Wu et. al, 2007; Bai et. al, 2008). They have time-varying and nonlinear dynamics. The nonlinear control characteristics sometimes cause control performance to vary with operating conditions. In recent years, PID controllers are most commonly used for temperature control and set-points tracking (Huang and Jordan, 2011). The

dynamics of airflow is faster than the thermal zone dynamics. Time lags are introduced by the building envelope (usually of several hours magnitude), cooling and heating coils (usually less than 1 min), ducts and pipes (less than 10s), and by the sensors (usually less than 1 min) (Kulkarni and Hong, 2004). PID controllers actions vary significantly with these operating conditions, and may lead to sluggish and oscillatory behaviors, due to tuning problems.

Moradi et. al (2012) compared the performance of pole-placement and H_∞ controllers for optimal control of an air-handling unit. A nonlinear MIMO model of the AHU was linearized around the operating points, and the state variables estimated via observer and regulator design. The state space equations were solved in Laplace domains, and the performance of the controllers was evaluated by their ability to track desired set-paths. The desired tracking paths in temperature and humidity ratio were achieved by manipulating the supply air and chilled water flow rates. The simple (PID) controller results in high oscillatory behavior of the valve positions for air and water flow rates. However, both PID and H_∞ controllers have not been demonstrated to handle constraints in inputs, state variables, and outputs. Additionally, in optimal control, one of key aims is to optimize the desired set-points or trajectories, such that it results in overall minimal electricity demand and cost.

Huang and Jordan (2011) developed a triple-mode control strategy for year-round temperature control of VAV systems, using bilinear feedback control which achieves robust stability using the principle of invariant and feasible (IF) set. The model does not require online tuning of its parameters. The control strategy was tested using case study of a single zone office, with envelope, radiation, convection, and a central

node temperature model. The triple-mode controller was shown to outperform PID controllers for zone temperature tracking, under different load conditions. However, the triple-mode control is also limited by inability to optimally handle and integrate constraints into the controller design.

Wu et. al (2005) developed a PI controller, coupled with a frequency converter, for airflow control of ventilation units. The dynamic simulations were carried out by integrating an airflow plant model with a PI controller in SIMULINK. The resulting model was tested under two different loading conditions, which correspond to different objectives in thermal comfort. Some important parameters were identified through experiments and analysis of a constant airflow control scheme.

Bai et. al (2008) developed a self-tuning PI controller and applied it for control of HVAC system operation in a test room. The method involves online estimation of the air-conditioning system parameters, and the application of a self-tuning controller to calculate the control signal, based on predicted error and estimated values. Due to delay effects of the air-conditioning process, a smith-predictor algorithm was used for time delay compensation. The predictor-based self-tuning PI controller achieved better performance over adaptive PI controllers in handling effects from load disturbances and set-point variations.

Zaheer-Uddin and Zheng (2000) explored optimal control strategies for HVAC systems operation. They take night-setback, start-up, and energy price discounts into consideration. The algorithm, which was based on gradient search method, was used to solve the multi-stage optimization problem. The model was tested on two environmental zones, with VAV heating (VAVH) system. The resulting zone

temperatures are given based on determined optimal mass flow rates and temperatures for both air and water supply. Results show that implementation of variable set-points will lead to energy savings in buildings.

Kulkarni and Hong (2004) implemented energy optimal control for a residential space with a gas furnace, by modeling sensible heat transfer. A PI controller was developed from a dynamic simulation of the building and control system, and implemented in MATLAB/SIMULINK. The building system was modeled in state space, using a thermal network model. The state space representation facilitates the implementation of an optimal controller (Qi and Deng, 2009). The proportional controller was compared with a two-position control, which is the commonly used control method for residential buildings in the United States. Results show that the optimal proportional control has advantage over the conventional two-position control in terms of thermal comfort. There were no significance differences in energy consumption between the two schemes.

Qi and Deng (2009) developed a multivariable Multi-Input Multi-Output (MIMO) control strategy for simultaneous control of indoor air and humidity. The sensible balance equations of an experimental DX A/C system in a conditioned space, was linearized and written as a state-space representation. The Linear Quadratic Gaussian (LQG) technique was used to design the MIMO controller. The MIMO controller generates two control signals for the compressor and supply fan speed simultaneously. This was shown to have advantage over on-off or SISO control strategy in terms of sensitivity and disturbance rejection.

Ginestet and Marchio (2010) studied the control tuning of a simplified VAV system. They investigated air quality management associated with control of outdoor air flow rates. Several model based control, optimal control, and classical methods were compared in terms of set point and disturbance rejection, their need to be written as a state space model, and previous applications in literature. The chosen model was tested for pollutant rate modeling in a conference room.

Yuan and Perez (2006) developed a model predictive control strategy for temperature control in a single-duct VAV system. The controller's performance was evaluated by conducting simulation-based experiments under four typical weather conditions. The study identified several problems with conventional control, such as the inability to maintain unit level ventilation control due to fluctuating occupancy and cooling loads of multiple zones. Over-ventilation and under-ventilation may occur simultaneously in different zones. The model predictive controller is seen as a multiple zone control method to control temperature and ventilation in real-time. It was shown to be capable of handling limitations in inputs and outputs explicitly, because the constraints are embedded in the control strategy. The MPC is also capable of being tuned intuitively, such that the effect of model parameters can be easily understood (Yuan and Perez, 2006). A single MPC controller can be used for single zone, or multiple zones control.

2.5.1 Summary of HVAC Systems Control Methods

Tables 2.1a, 2.1b, and 2.1c compare the most common methods that have been used for HVAC systems control (modified from Afram and Janabi-Sharifi, 2014). It shows the description of the control method and limitations to current HVAC systems

application. Of all the methods shown in Table 2.1, the model predictive controller (MPC) is a preferred choice for HVAC systems control because it leverages on the use of a predictive model, handles constraints systematically and optimally by embedding the requirements into controller design, and optimizes system operation irrespective of the time scale (slow, medium, or fast dynamics) of the system. The MPC controller is able to control the system at both the supervisory and local control levels. The main limitation of the MPC is the requirement of very accurate predictive dynamic models.

Table 2.1a: Comparison of HVAC Systems Control Methods (Hard Control)

Control Methods	Description	Limitations
Gain Scheduling PID	Different set of gains applied to a nonlinear system divided into piecewise linear regions	Inability to handle time varying constraints and disturbances <i>(Tahersima et. al, 2010; Pal and Mudi 2008)</i>
Nonlinear Control	Uses a control law to drive a nonlinear system toward a stable state	Requires complex mathematical analysis for the identification of stable states <i>(Moradi et. al, 2011; Hodgson 2010)</i>
Robust Control	Designs a controller that works well with time varying disturbances	Require specification of additional parameters which could be impractical to integrate in HVAC systems <i>(Anderson et. al 2008, Al-Assadi et. al 2004, Greensfelder et. al 2011, Dong 2010, Nishiguuchi et. al 2010)</i>
Optimal Control	Solves an optimization problem to minimize a cost function	
Model Predictive Control	Predictive optimal control with disturbance rejection, constraint handling, and slow-moving dynamics integrated into controller design	It requires accurate predictive model. <i>(Elliott 2008, Katipamula 2006).</i>

Table 2.1b: Comparison of HVAC Control Methods (Soft and Hybrid Control)

Control Methods	Examples	Description	Limitations
Soft Control	Fuzzy Logic	Control actions are implemented in the form of if-then statements	Requires extensive knowledge of systems operations and states
	Neural Network	Trained using performance data, to fit a nonlinear mathematical model	It's a completely black box approach. Training data must cover a wide range of operating conditions.
Hybrid Control	Adaptive Fuzzy, Fuzzy PID etc	It's a fusion of hard and soft control	Inherits problems associated with soft and hard control methods, such as requiring large amounts of data, or problems with controller tuning

Table 2.1c: Comparison of HVAC Systems Control Methods (Classical)

Control Methods	Examples	Description	Limitations
Classical Control	ON/OFF	Regulates a given process between upper and lower thresholds	Unable to control time delay due to thermal inertia. Displays large swings in controlled states
	P, PI, PID	Modulates a control variable to achieve control using error dynamics	Controller tuning is cumbersome. Operating conditions should not vary widely from tuning conditions

It is also able to handle varying constraints, which are typical of those in HVAC systems operation where different constraints of temperatures, flow rates, etc. are specified based on occupancy, or time of use. The suitability of MPC for this research is

further discussed in Section 5.1. The different areas where MPC has been applied to HVAC systems control are shown in Table 2.2.

Table 2.2: Applications of MPC in HVAC System Control

Studies	Application	Models used and limitations
<i>He et. al 2005</i>	Temperature control	Fuzzy model. Neglects zone interactions and does not represent building dynamics
<i>Kalogirou 1998, Soteris and Kalogirou 2000</i>	Energy consumption	Artificial neural networks (ANN). Does not represent building dynamics
<i>Jan et. al 2011</i>	Energy savings	Resistance model only. Neglects interzone thermal storage.
<i>Shengwei and Xinqiao 2000</i>	Energy consumption and cost	TRNSYS and genetic algorithm (neglects zone interactions)
<i>Bourhan et. al 2004</i>	Zone temperature	Capacitance model only (assumes similar effect of different wall orientations on the zone temperature. Single zone)
<i>Oldewurtela et. al 2012, Lehmann et. al 2010, Oldewurtela et. al 2010</i>	Zone temperature	RC model. Single zone approach. Identical boundary conditions on partitions, which ignores the influence of neighboring zones. Neglects internal mass effects
<i>Ma et. al 2012</i>	Demand reduction	ARX model (using EnergyPlus with Buildings control virtual testbed (BCVTB) as middle ware)
<i>Karlsson and Hagentoft 2011</i>	Heating supply	Heat balance model. Single zone approach.
<i>Privara et. al 2011</i>	Zone temperature	State space model. No opportunity to observe or understand thermal couplings and interactions
<i>Huang 2011</i>	Zone temperature	Heat balance model. Does not represent building construction physically. Thermal interactions neglected
<i>Yuan and Perez 2006</i>	Zone temperature and ventilation	Heat balance model. Single zone approach. Thermal interactions neglected
<i>Xu and Li 2006</i>	Zone temperature	CARIMA model
<i>Xi et. al 2007</i>	Temperature, fan speed, and chilled water valve	Support Vector Regression. Unable to capture dynamics of building construction and multizone interactions.

None of these studies considered multi-zone interactions and dynamics using a physically representative thermal model of building load and cooling coil in the controller design. Additionally, most of the applications are for zone temperature control

2.5.2 Strategies for minimizing building demand

According to Li and Wang (2012), thermal storage is one of the most promising ways for improving energy storage and energy use in buildings. It can help to balance daily, weekly, and seasonal energy demands (IREA 2013). There are also other claims that passive thermal storage can compensate for extra investment on building insulation (Schnieders and Hermelink 2006). There are active and passive thermal storage strategies. The active strategies involve improvements to the HVAC system operation, while passive strategies involve improving the building envelope, which serves as the interface between the indoor and outdoor environment.

The building envelope helps to moderate and control the fluctuations in the indoor environment, depending on its thermal characteristics, and the outdoor conditions. Fenestration components such as walls, roofs, windows, thermal insulation, and external shading devices make up the building envelope. These high capacity materials are capable of absorbing and progressively releasing radiation. They constitute the thermal mass. The mechanism of absorbing and releasing heat at a later time helps in the control and moderation of the indoor temperature, which is reflected in shift of peak building load (Henze et. al 2005). Diurnal variation in ambient temperature should exceed 10K (18F) for effective utilization of thermal mass.

Other mechanisms for optimal control of building load and electricity profile have been exercised in literature. Morgan and Krarti (2010) developed a simulation environment to implement various control strategies such as predictive optimal control. By allowing the zone temperature to drift during unoccupied periods, the energy use profile of the HVAC system was modeled and compared with actual data.

Henze *et. al* (2005) focused on nighttime pre-cooling as a means for peak load reduction. By utilizing active and passive building storage, constrained by thermal comfort requirements, the study optimized HVAC system operation, and minimized building operation costs. The thermal storage components of the control problem were solved using quasi-Newton method and dynamic programming. The study identified lots of improvement opportunities for thermal storage and peak load reduction potential.

Braun *et. al* (2002) identified potentials for reducing building operating costs as including demand reduction, ventilation with cool nighttime air, pre-cooling, and improved mechanical efficiency. Associated savings are strongly dependent on weather conditions, occupancy schedules, utility rates, and building thermal characteristics.

Snyder and Newell (1990) developed a lumped capacitance model to determine least cooling cost strategies using effective building characteristics for a medium-sized building. The most influential parameters on whole-building cost savings were identified using a fractional factorial analysis (FFA). The four most influential factors on the cost savings were identified as part-load performance, thermal mass level, internal load density, and equipment efficiency. The analysis revealed that thermal characteristics of building construction have a significant impact on the energy use and load profile. Savings of 18% were realized in cooling cost by sub-cooling the thermal

mass before the peak utility rate period, which helps to shift portions of the peak cooling to off-peak period.

Yang and Li (2008) developed a mathematical model to study the effects of night ventilation and thermal mass on the cooling load in buildings. Their model considered the thermal capacity and resistance of building construction and indoor air. In another study (Goyal et. al 2011), additional thermal mass led to energy and cooling cost savings of 18-20% over the base case. These reductions uncover further opportunities for downsizing the HVAC system size, which helps to offset initial investment on additional insulation. Another study involved the use of EnergyPlus for simulation of different building constructions in cold climate. Results show that the distribution and orientation of thermal mass in the building envelope led to negligible savings for high-rise buildings.

From the critical review of literature, the following research gaps have been identified:

- Lack of fundamental understanding and consideration of multi-zone thermal interactions in predictive control of buildings energy systems
- Lack of understanding of interactions between HVAC components and the different zones in a multi-zone building
- Lack of sufficiently accurate (or limited applications) of physics-based transient model that captures important buildings phenomenon such as radiative delays and internal mass effects
- Lack of understanding of applicability/limitations of the thermal network model for buildings heat transfer

- Lack of electricity minimization strategies that utilize buildings dynamics (Existing electricity minimization strategies do not leverage on multi-zone interactions. Also, they are not consistent in their conclusions)

This research seeks to fill the identified gaps through generation of new knowledge and original contributions which include:

- Demonstration of predictive control that utilizes building dynamics, represents the building physically, and captures important phenomenon e.g. multi-zone interactions, radiative delays etc.
- Understanding of thermal interactions among multiple thermal zones in any new or existing buildings
- Understanding of thermal characteristics of building constructions
- Understanding of interactions between multiple thermal zones and HVAC equipment to assist in efficient operation of the HVAC equipment
- Understanding of appropriate electricity minimization strategies for multiple thermal zones in any new or existing building
- Method to determine near -optima precooling hours for certain thermal zones

To achieve the above, accurate thermal models of building load and cooling coil as well as airflow model of fan-power are required. Most of the existing thermal models are not suitable for this research, due to their lack of consideration of building dynamics. The next chapter discusses the selected models in this dissertation, and the solution method adopted.

Chapter 3: HVAC Components Model Description

This chapter describes the thermal and airflow models used for the HVAC components in this dissertation. The models of interest are the building load, fan- motor, and cooling coil models respectively. This chapter also describes the solution and parameter estimation methods adopted. New information presented in this section includes the stability analysis of the thermal network model, and further application of the thermal network approach to transient modeling of cooling coil, using both temperature and enthalpy based methods.

3.1 Building Load Model

Snyder and Newell (1990) and Yang and Li (2008) utilized the thermal network model in their studies. Their models fall under the general class of Resistance-Capacitance (R-C) model, which has been widely used for building performance simulation (Dobbs and Hency 2012, Schmidt and Johannesson 2004, Sourtron et. al 2009, Radecki and Hency 2012, Bueno et. al 2012, Lombard and Mathews 1992, Lombard and Mathews 1999, Xu 2005). This section discusses the dynamics and capabilities of the R-C model for building load and cooling coil modeling.

The R-C model was chosen because of its suitability to capture dynamics of building load, while also representing characteristics of building construction physically. The utilization of physical and thermal characteristics of building construction in the formulation leads to a thermal model which reliably and accurately depicts phenomenon such as internal mass, radiative delays, flexible schedules, multiple scenarios of HVAC system operation etc. In addition, the thermal network representation enables linearization and representation in state space, investigation of

system stability, and integration with other building components such as the cooling coil and fan-motor models. The thermal network model also enables the use of short-term measurements to estimate and optimize model parameters. The state space representation is perfect for predictive optimal control and for exploration of further opportunities related to near-optimal operation of HVAC system components.

With the R-C model, the heat balance equation can be generated from limited information about the physical and thermal characteristics of building construction. Solution methods adopted for the R-C model have included autoregressive, time series, numerical, and, recently, analytical. The important capabilities of R-C model which justifies its suitability for this research could be summarized as follows:

- (i) Capability to physically represent the properties of building construction. This allows for fundamental study and investigation of thermal characteristics of different building components (including windows, walls, roofs, partitions, etc) and constructions (light, medium, and heavy construction).
- (ii) Capability to extend and utilize the R-C representation for other HVAC components such as the cooling coil and fan-motor model, hence enabling seamless integration of air handling unit components.
- (iii) Capability to simulate different HVAC system schedules, set points, and multiple scenarios of HVAC system operation across different climates.
- (iv) Capability to estimate model parameters from limited measurement data, and study the system dynamics from the model parameters.
- (v) Capability to optimize system operation in response to varying weather, ambient temperature, and occupancy schedules.

- (vi) Capability to handle soft and hard constraints due to control and equipment limitations.
- (vii) Capability to provide unit-level information at thermal zones where metering information may not be available due to limited numbers of sensors.
- (iix) Capability to simulate internal mass, thereby harnessing thermal storage capabilities appropriately. This may aid in peak cooling load reduction, which offers significant potential for energy and electricity use in buildings.
- (ix) Capability to simulate floats in space air temperature, when HVAC system is not in operation. This is useful to evaluate worst case conditions due to night setback or other control strategies.

A typical R-C representation for a thermal zone with one exterior wall is shown in Figure 3.1.

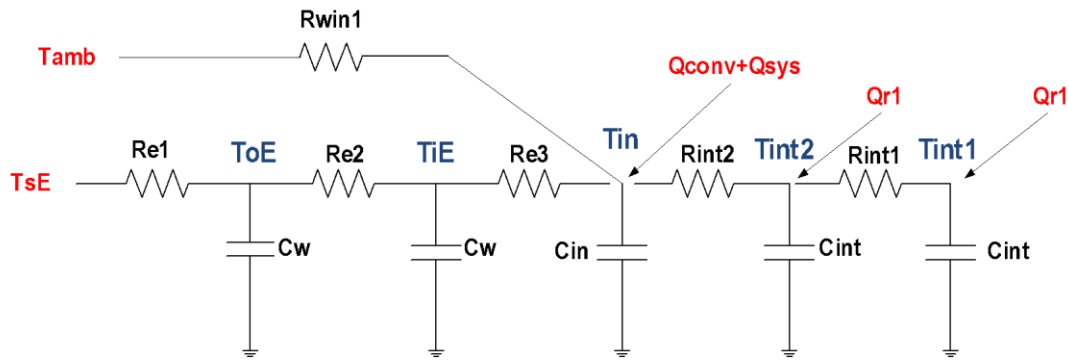


Figure 3.1: R-C Thermal model, showing sol-air temperature and HVAC system input.

The variables are defined as:

T_{sE} = solar air temperature on exterior wall

T_{amb} = ambient temperature

T_{in} = zone temperature

R_{win} = windows thermal resistance

Re_1 , Re_2 , and Re_3 = thermal resistances of exterior wall

R_{int} = thermal resistance of internal mass

C_w = thermal capacitance of exterior wall

C_{in} = thermal capacitance of room air

C_{int} = thermal capacitance of internal mass

Q_{conv} = convective portion of internal heat gains

Q_{sys} = rate at which heat is added to (or extracted from) the system

Q_r = sum of radiative fraction of internal heat gain and transmitted radiation from windows to the zone.

The following simplifying assumptions are commonly made in order to enable the derivation and expression of sensible heat balance equation for the nodal temperatures in the thermal network model:

- Well mixed zone air: The whole indoor circulated air volume is assumed to be at a uniform temperature, which is represented by the zone temperature node.
- Convective heat transfer coefficient: A constant heat transfer coefficient is assumed on wall surfaces, such that the effect of varying wind velocity may be neglected. Likewise, this leads to constant values of convective thermal resistances on exterior and interior surface of walls.
- Positive Pressure: Conditioned spaces are assumed to be adequately pressurized, relative to their surroundings, such that infiltration does not create additional cooling or heating loads in the conditioned space.
- Adiabatic surfaces: Ceilings and floors are considered adiabatic, particularly when they separate thermal zones that are similarly conditioned.

- Other phenomenon: Long wave radiative exchanges between interior surfaces, multiple reflections, and other complex phenomenon are described by the lumped internal thermal mass components of the R-C model.

The above assumptions have been well established in literature, and are frequently made to simplify the thermal network model [Lombard and Mathews (1992); Ogunsola et. al (2014); Ogunsola and Song (2015), Ogunsola and Song (2014), Ogunsola et. al (2016)]. The heat balance equation at each temperature node is given in Equation (3.1)

$$\frac{dT_n}{dt} = -\frac{1}{C_n} \left(\sum_{i=1}^j \frac{1}{R_i} \right) T_n + \frac{1}{C_n} \left(\sum_{i=1, i \neq n}^j \frac{1}{R_i} T_i \right) + \frac{1}{C_n} \sum_{i=1}^p Q_i \quad (3.1)$$

T_n = temperature of the n th node.

C_n = thermal capacitance of node n .

j = total number of connected temperature branches (including ambient, sol-air, and neighbor nodal temperatures) to node n .

T_i = temperature of the i th branch, connected to node n .

p = total number of heat flux branches (such as convection, radiation, and heat extraction or addition rate) impressed on node n .

Q_i = heat flux of the i th branch connected to node n . This term includes internal heat gains such as Q_r and Q_{conv} which are impressed on internal mass and zone temperature nodes respectively. Q_i also includes the heating or cooling rate of a device (Q_{sys}).

Q_{sys} applies to zone temperature nodes only, as shown in Figure 3.1

R_i = resistance of the branch between T_n and T_i .

Typical inputs to the R-C model are as shown in Table 3.1 below:

Table 3.1: Typical inputs to R-C model

Input	Description
Weather	This includes ambient temperature and solar radiation data for the particular location being studied. Where available, actual radiation data is used during simulation. Otherwise, the ASHRAE clear sky model was used to generate solar radiation data.
Occupancy Schedule	Occupancy schedules are the times that occupants are physically present in the thermal zone. This is important because it determines usage and temperature set-points which influences the building load profile. Occupied periods for office building are typically weekdays from 8am – 5pm.
Internal loads	Internal loads are heat generated within the building. They come from lighting, computers, office equipment, and people
HVAC System	The HVAC system operates to maintain thermal comfort within the conditioned space. It compensates for the building heating or cooling loads.
Building Construction Information	The thermal characteristics of building construction determine the temperature fluctuations and thermal delay of radiative heat gains.

Outputs from the R-C building load model may include interior and exterior surface temperature of walls, zone temperatures, heating or cooling loads, and other thermal variables of interest. The R- C model representation may be extended to buildings with

multiple zones, as is typical of office buildings. Figure 3.2a shows a building with two thermal zones. The R-C network representation is shown in Figure 3.2b. Note that some of the nodal temperatures were not shown in the schematic due to space limitations.

3.2 Fan-Motor Model

The modeling of airflow dynamics has not been quite developed in HVAC literature. No comprehensive dynamic model exists for the fan-motor model. The transient response of the fan-motor subsystem is usually in the order of seconds, which is much shorter than the other HVAC components. For example, the transient regimes of building loads may be up to 5000 times that of fan-motor subsystem. Due to this, the use of steady state and regression models for airflow dynamics has been justified. Although fan-motor draws large current during the transient regime, the peak demand is very short-lived, and not reflected in the electricity bill. In addition, most utilities manage load at 5minutes to 1 hour interval and responses at the fast time scale of fan operation are not presently considered. It also happens very fast, that it is not captured by most building automation system (BAS). Therefore, this section focuses on the use of a steady state fan model, which requires very limited fan operation data to simulate fan performance. A description of suitable transient fan model using a state space approach is available in Appendix A. The flowchart shown in Figure 3.3 summarizes the steady state fan model used in this dissertation.

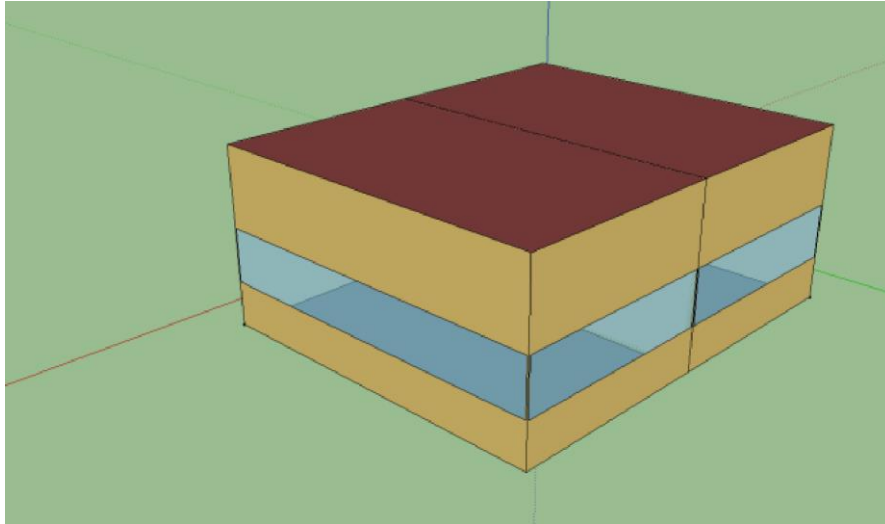


Figure 3.2a: Office Building with 2 Thermal Zones

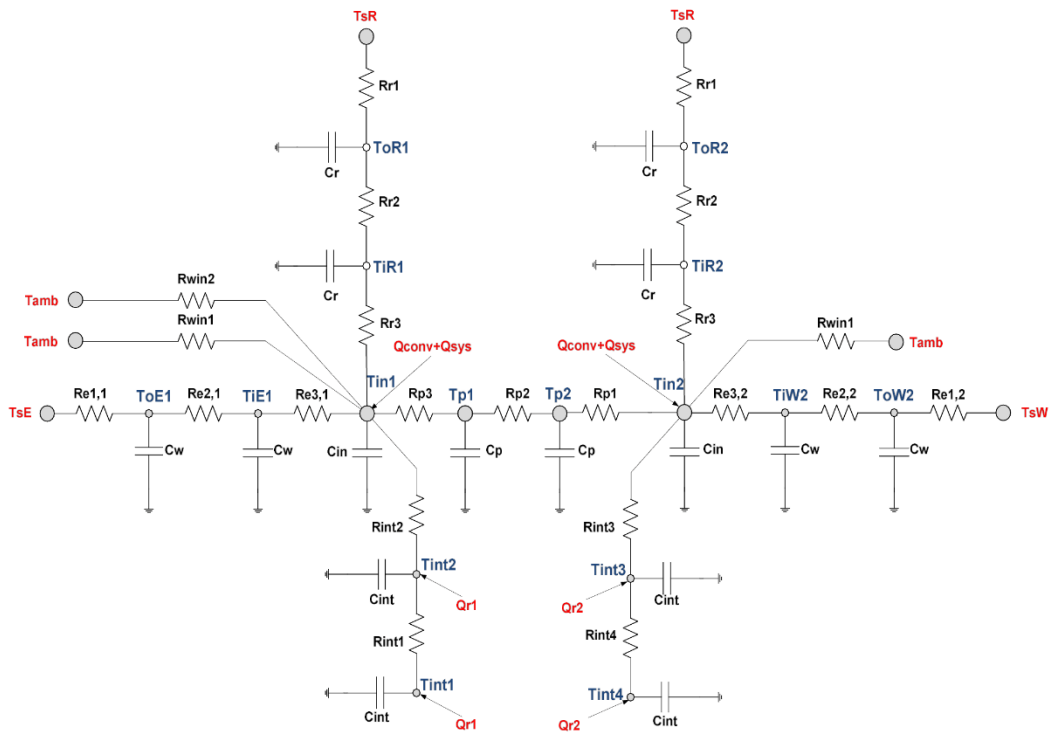


Figure 3.2b: R-C Model Representation for Building shown in Figure 3.2a

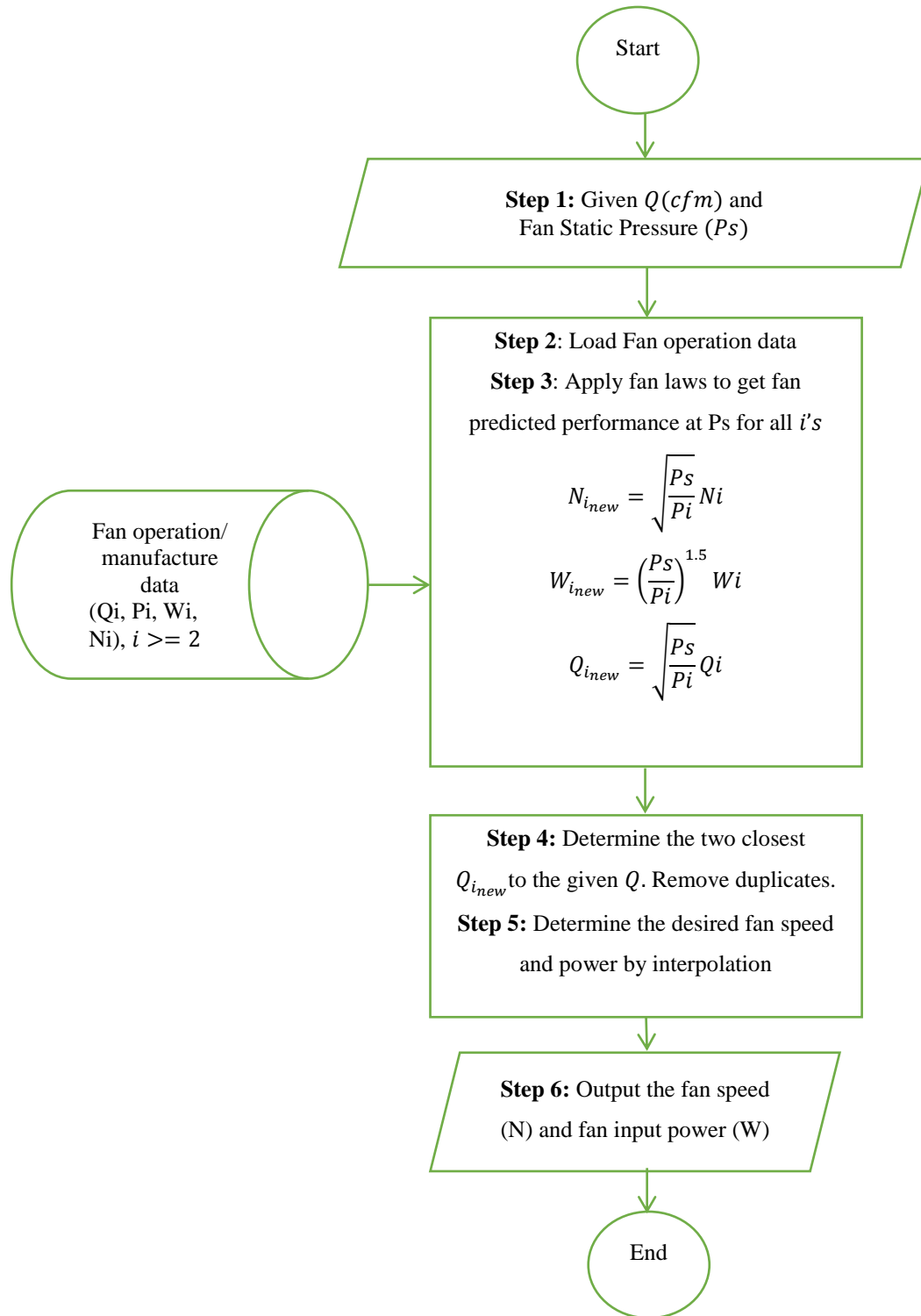


Figure 3.3: Summary of Fan Power Model

Q_i , P_i , W_i , and N_i represent flow (CFM), static pressure, fan input power, and fan speed respectively. The fan's static pressure is reset by total airflow rate, and the calibration results are shown in Appendix B.

3.3 Cooling Coil Dynamic Model

Most of the available cooling coil dynamic models require detailed information about the cooling coil geometry. These details are mostly unavailable.

Additionally, cooling coil manufacturer's data only cover limited range of temperature and flow rates. Lumped models serve such a good purpose of simulating operation of the cooling coil unit with good degrees of accuracy. The cooling coil model in this dissertation was deduced from lumped parameters approach, such that with limited operation data, the cooling coil modeling parameters could be deduced, and the operation predicted with high degrees of accuracy. Depending on the given thermal resistance, the heat transfer from the chilled water to the air may be written as Equation (3.16) or (3.17):

$$q = \frac{T_a - T_{chw}}{R_{total}} \quad (3.16)$$

$$q = \frac{h_a - h_{chw}}{R_{h_{total}}} \quad (3.17)$$

$$\text{where } R_{total} = \frac{1}{(UA)_{chw}} + \frac{1}{(UA)_{air}} \text{ and } R_{h_{total}} = \frac{1}{(UA)_{h_{chw}}} + \frac{1}{(UA)_{h_{air}}}$$

The subscript 'h' denotes enthalpy based thermal resistances of the chilled water and air respectively. According to the Dittus-Boelter correlation, the relationship between the nusselt number and convection coefficient may be represented as Equation (3.18):

$$Nu = \frac{hL}{k} = 0.023Re^{0.8}Pr^n$$

$$= 0.023 \left(\frac{\rho u L}{\mu} \right)^{0.8} \left(\frac{c_p \mu}{k} \right)^n \begin{cases} n = 0.4 \text{ for heating} \\ n = 0.3 \text{ for cooling} \\ \text{valid for } 0.6 \leq Pr \leq 160 \end{cases} \quad (3.18)$$

This correlation is valid for turbulent, internal flows, which is the case for water flow in cooling coil. Additionally, typical range of Prandtl number for water flows are 0.7-1.0 which lies completely in the range of validity of the Dittus-Boelter correlation. As such, the Dittus-Boelter correlation is applicable to water flow in the cooling coil. The UA value for water side of the cooling coil may be expressed as in Equation (3.19):

$$UA \approx hA = \frac{kA}{L} \left[0.023 \left(\frac{\rho u L}{\mu} \right)^{0.8} \left(\frac{c_p \mu}{k} \right)^n \right] = \frac{kA}{L} \left[0.023 \left(\frac{\rho \dot{m} L}{\rho A \mu} \right)^{0.8} \left(\frac{c_p \mu}{k} \right)^n \right] \quad (3.19)$$

where the velocity, u can be expressed as $u = \dot{m} / \rho A$. Inserting this into Equation (3.19) yields:

$$hA = (0.023 L^{-0.2} k^{1-n} c_p^n \mu^{n-1} A^{0.2}) \dot{m}^{0.8} = K \dot{m}^{0.8} \quad (3.20)$$

c_p is the constant-pressure specific heat of the flowing fluid.

k is the conductivity of the flowing fluid.

ρ is density of the flowing fluid.

μ is viscosity of the flowing fluid.

L is a characteristic length of the problem. For pipe flow, $L = D$ where D is the pipe diameter, u is a characteristic velocity of the problem. For pipe flow, $u = \bar{u}$ where \bar{u} is the mean velocity. The expression in bracket could be lumped into the constant K , such that the UA values for water can be represented as shown in Equation (3.21)

$$(UA)_{chw} = K_{chw} \dot{m}_{chw}^{0.8} \quad (3.21)$$

For airflow in the cooling coil, the applicable correlation is Zukauskas correlation for external flow in tube banks with staggered tube elements. This is mostly the case for airflow in HVAC cooling coils. The Zukauskas correlation for external flow in tube banks with staggered geometry is given by:

$$NU_D = FCRe_D^n Pr^m \quad (3.22)$$

Where:

$$n = 0.4 \text{ and } m = 0.36 \text{ for } 10 \leq Re_{Dmax} \leq 500,$$

$$n = 0.6 \text{ and } m = 0.36 \text{ for } 10^3 \leq Re_{Dmax} \leq 2 \times 10^5 \text{ and}$$

$$n = 0.84 \text{ and } m = 0.36 \text{ for } Re_{Dmax} > 2 \times 10^5$$

The airflow rates for the case study cooling coil happened to have Reynolds number in the range $10^3 \leq Re_{Dmax} \leq 2 \times 10^5$ for which the Zukauskas correlation suggests exponent $n = 0.6$. However, when the Zukauskas relation was applied for the cooling coil in this dissertation, it didn't give good prediction. It was also unable to capture any of the fluctuations in the leaving air temperature. Therefore, other approaches were considered. The first approach was to include the exponent n as one of the cooling coil parameters to estimate. To achieve this, the UA value for the air side was assumed to vary with airflow to the power of n , where n was constrained to (0,1). Using that approach, the value of n was estimated based on objective of minimizing the errors in predicted leaving air and water temperature. Using genetic algorithm, the exponent was estimated to be $\cong 0.76$ and it gave a better prediction than the Zukauskas relation. It was also able to capture some trends in the leaving air temperature. However, in quest to improve the model accuracy and develop a cooling coil model with the least possible number of estimated parameters, a second approach was considered. This involved

fixing the value of n and estimating the other coil parameters which are discussed later. Values of n from 0.6 to 0.9 in 0.02 increments were considered. The value of $n = 0.8$ gave similar prediction as $n = 0.76$ for the training data but best prediction for the validation data. This is also consistent with literature where $n = 0.8$ has been used for turbulent flows. Therefore, the UA value of air in this dissertation was assumed to vary with airflow rate by the relation:

$$(UA)_{air} = K_{air} \dot{m}_{air}^{0.8} \quad (3.23)$$

By combining the equations for airside and water side UA values, the expression for thermal resistance becomes:

$$R_{total} = \frac{1}{K_{air} \dot{m}_{air}^{0.8}} + \frac{1}{K_{chw} \dot{m}_{chw}^{0.8}} = \frac{K_{air} \dot{m}_{air}^{0.8} + K_{chw} \dot{m}_{chw}^{0.8}}{K_{air} K_{chw} (\dot{m}_{chw} \dot{m}_{air})^{0.8}} \quad (3.24)$$

From mass and energy conservation, the dynamic change of air and water temperature in an infinitesimal volume can be represented using temperature or enthalpy approach. The temperature based approach is based on the approximation of enthalpy change of air by the specific heat and temperature difference. The assumption has been widely applied in literature. The governing equations are:

Using temperature approach:

$$(\rho VC)_{chw} \frac{\partial T_{chw}}{\partial t} + (\rho VCu)_{chw} \frac{\partial T_{chw}}{\partial x} = \frac{T_a}{R_{total}} - \frac{T_{chw}}{R_{total}} \quad (3.25)$$

$$(\rho VC)_{air} \frac{\partial T_{air}}{\partial t} + (\rho VCu)_{air} \frac{\partial T_{air}}{\partial x} = -\frac{T_a}{R_{total}} + \frac{T_{chw}}{R_{total}} \quad (3.26)$$

Using enthalpy approach for the air, the airside energy balance may be written as:

$$(\rho V)_{air} \frac{\partial h_{air}}{\partial t} + (\rho Vu)_{air} \frac{\partial h_{air}}{\partial x} = -\frac{T_a}{R_{total}} + \frac{T_{chw}}{R_{total}} \quad (3.27)$$

where V_{chw} and V_{air} represent the volume of the chilled water and the air element in the mass and heat transfer processes in their respective flow directions. Approximating T_{chw} , T_{air} , h_{chw} , and h_{air} by a linear equation implies that the instantaneous values of these variables along the coil can be expressed as:

$$T_{chw} = \frac{T_{chw,o} - T_{chw,i}}{l}x + T_{chw,i} \quad (3.28)$$

$$T_{air} = \frac{T_{air,o} - T_{air,i}}{l}x + T_{air,i} \quad (3.29)$$

$$h_{air} = \frac{h_{air,o} - h_{air,i}}{l}x + h_{air,i} \quad (3.30)$$

Taking the first derivations of these equations, we obtain

$$\frac{\partial T_{chw}}{\partial x} = \frac{T_{chw,o} - T_{chw,i}}{l}; \quad \frac{\partial T_{air}}{\partial x} = \frac{T_{air,o} - T_{air,i}}{l}; \quad \frac{\partial h_{air}}{\partial x} = \frac{h_{air,o} - h_{air,i}}{l}$$

Therefore, substituting the above gradients from Equation (3.30) into the mass and energy conservation equations give:

For temperature based approach:

$$(\rho VC)_{chw} \frac{dT_{chw}}{dt} + (\rho VCu)_{chw} \left(\frac{T_{chw,o} - T_{chw,i}}{l} \right) = \frac{T_a}{R_{total}} - \frac{T_{chw}}{R_{total}} \quad (3.31)$$

$$(\rho VC)_{air} \frac{dT_{air}}{dt} + (\rho VCu)_{air} \left(\frac{T_{air,o} - T_{air,i}}{l} \right) = -\frac{T_a}{R_{total}} + \frac{T_{chw}}{R_{total}} \quad (3.32)$$

Which can also be written in terms of temperature differences as:

$$(\rho VC)_{chw} \frac{dT_{chw}}{dt} = - \left(\frac{T_{chw,o} - T_{chw,i}}{l / (\rho VCu)_{chw}} \right) + \frac{T_a - T_{chw}}{R_{total}} \quad (3.33)$$

$$(\rho VC)_{air} \frac{dT_{air}}{dt} = - \left(\frac{T_{air,o} - T_{air,i}}{l / (\rho VCu)_{air}} \right) - \frac{T_a - T_{chw}}{R_{total}} \quad (3.34)$$

For enthalpy based approach, the airside equation is:

$$(\rho V)_{air} \frac{dh_{air}}{\partial t} + (\rho V u)_{air} \left(\frac{h_{air,o} - h_{air,i}}{l} \right) = -\frac{T_a}{R_{total}} + \frac{T_{chw}}{R_{total}} \quad (3.35)$$

Which may also be written in terms of enthalpy differences as:

$$(\rho V)_{chw} \frac{dh_{chw}}{\partial t} = -\left(\frac{h_{chw,o} - h_{chw,i}}{l / (\rho V u)_{chw}} \right) + \frac{h_a - h_{chw}}{R_{total,h}} \quad (3.36)$$

$$(\rho V)_{air} \frac{dh_{air}}{\partial t} = -\left(\frac{h_{air,o} - h_{air,i}}{l / (\rho V u)_{air}} \right) - \frac{h_a - h_{chw}}{R_{total,h}} \quad (3.37)$$

The cooling coil model could then be represented using a two-node thermal network model, as shown in Figures 3.4 to 3.7

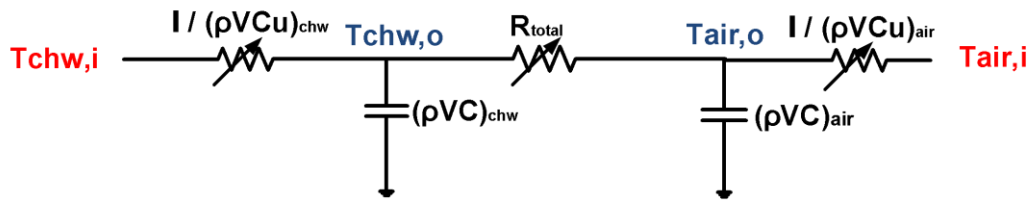


Figure 3.4: Thermal network model for cooling coil, temperature approach

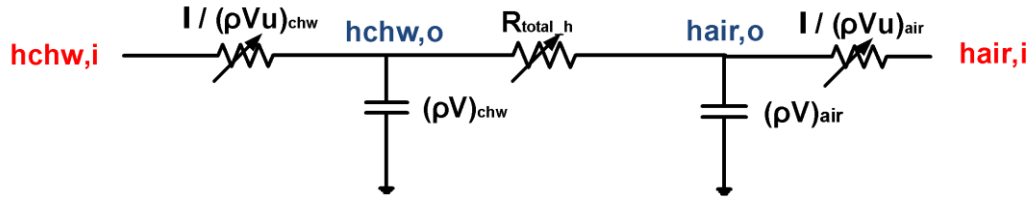


Figure 3.5: Thermal network model for cooling coil, enthalpy approach

This is a three resistance, two capacitance (3R2C) model representation. The resistance values are variable since they are dependent on air and water flow rates. They are, thus, represented using a variable resistor (as indicated by the arrow). The thermal capacitances are constant. The network representation can be further simplified as shown in Figures 3.5 and 3.6:

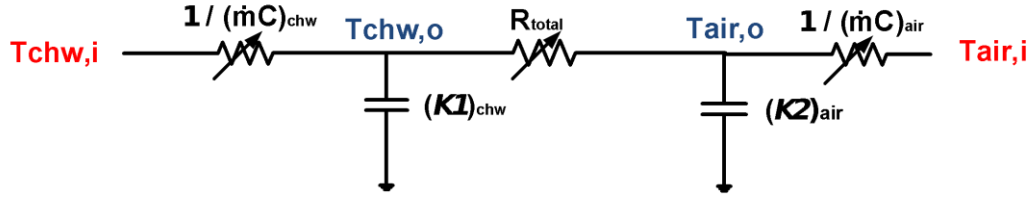


Figure 3.6: Simplified thermal model for cooling coil, temperature approach

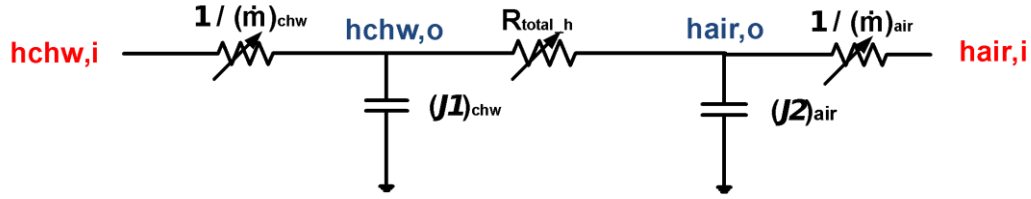


Figure 3.7: Simplified thermal model for cooling coil, enthalpy approach

Where:

$$R_{total} = \frac{1}{K_3 (\dot{m}_{air}^{0.8})} + \frac{1}{K_4 (\dot{m}_{chw}^{0.8})} \quad (3.38)$$

$$R_{total,h} = \frac{1}{J_3 (\dot{m}_{air}^{0.8})} + \frac{1}{J_4 (\dot{m}_{chw}^{0.8})} \quad (3.39)$$

The K 's and J 's are coefficients to be determined from manufacturer or operation data. Only four (4) parameters need to be identified. Tables 3.2 and 3.3 show the thermal interactions among the leaving and entering temperatures.

Table 3.2: Cooling coil thermal interactions, temperature based approach

Variables	$T_{chw,o}$	$T_{air,o}$	$T_{chw,i}$	$T_{air,i}$
$T_{chw,o}$	$-\frac{1}{K_1} (\dot{m}C_{chw} + \frac{1}{R_{total}})$	$\frac{1}{K_1 R_{total}}$	$\frac{\dot{m}C_{chw}}{K_1}$	0
$T_{air,o}$	$\frac{1}{K_2 R_{total}}$	$-\frac{1}{K_2} (\dot{m}C_{air} + \frac{1}{R_{total}})$	0	$\frac{\dot{m}C_{air}}{K_2}$

$$\text{where } R_{total} = \frac{K_3 \dot{m}_{air}^{0.8} + K_4 \dot{m}_{chw}^{0.8}}{K_3 K_4 (\dot{m}_{chw} \dot{m}_{air})^{0.8}}$$

Table 3.3: Cooling coil thermal interactions, enthalpy based approach

Variables	$h_{chw,o}$	$h_{air,o}$	$h_{chw,i}$	$h_{air,i}$
$h_{chw,o}$	$-\frac{1}{J1}(\dot{m}_{chw} + \frac{1}{R_{total_h}})$	$\frac{1}{J1R_{total_h}}$	$\frac{\dot{m}_{chw}}{J1}$	0
$h_{air,o}$	$\frac{1}{J2R_{total}}$	$-\frac{1}{J2}(\dot{m}_{air} + \frac{1}{R_{total_h}})$	0	$\frac{\dot{m}_{air}}{J2}$

$$\text{where } R_{total_h} = \frac{J_3 \dot{m}_{air}^{0.8} + J_4 \dot{m}_{chw}^{0.8}}{J_3 J_4 (\dot{m}_{chw} \dot{m}_{air})^{0.8}}$$

3.4 Solution Method

The thermal network model representation for the building load and cooling coil may be represented as an inhomogeneous system of ordinary differential equations. In state space representation, this can be re-written as:

$$\dot{T} = AT + BU \quad (3.40)$$

where A is the state (or system) matrix and B is the input matrix of dimensions $n \times n$ and $n \times q$, respectively. q is the number of inputs to each model while n represents the number of state variables. Depending on the output of interest, these may be presented as a multiple input multiple output (MIMO) system.

$$A = \begin{pmatrix} a_{11} & \cdots & a_{1n} \\ \vdots & \ddots & \vdots \\ a_{n1} & \cdots & a_{nn} \end{pmatrix} \text{ and } B = \begin{pmatrix} b_{11} & \cdots & b_{1q} \\ \vdots & \ddots & \vdots \\ b_{n1} & \cdots & b_{nq} \end{pmatrix} \quad (3.41)$$

The cooling load, for example, may be represented as:

$$Q_{cool} = CT + DU \quad (3.42)$$

For the building load model, the matrices A and B are time-invariant matrices whose entries are functions of the R-C parameters. For the cooling coil model, the matrices A and B are variable, because their entries are functions of the flow rates. As a first order differential equation, the general solution to Equation (3.40) is given by:

$$T_{t+\delta} = e^{A\delta}T_t + \int_t^{t+\delta} e^{A(t+\delta-\tau)}BU(\tau)d\tau \quad (3.43)$$

where the exponential matrix of $A\delta$ ($e^{A\delta}$) is defined by the power series

$$e^{A\delta} = I + A\delta + \frac{A^2\delta^2}{2!} + \frac{A^3\delta^3}{3!} + \dots + \frac{A^n\delta^n}{n!} + \dots \quad (3.44)$$

δ is the time step, and I is the identity matrix, having the same dimensions as A .

3.4.1 Time series solution

Depending on the distribution of $\mathbf{U}(\tau)$, the computational effort required to evaluate the integral may be minimal or significant. In order to simplify the convolution integral, inputs between time t and $t + \delta$ can be modeled by a piecewise, continuous, linear function as:

$$\mathbf{U}(t) = \mathbf{U}_t + \frac{(\tau - t)}{\delta}(\mathbf{U}_{t+\delta} - \mathbf{U}_t) \quad (3.45)$$

This approach was first utilized by Seem et. al (1985). In their study, the concept was applied to building envelope components only. In other studies, the concept was used to model solar radiation absorbed by vegetation (Knyazikhin et. al). Other functions (such as trigonometry) may be used to model the input between two different time-steps. In this research, the concept of piecewise continuity was extended to include solar radiation, convection, and radiative fraction of internal loads, which are all inputs to the building load model. The ramp function is more appropriate to represent gradually changing variables. It is function of choice to represent ambient temperature, solar radiation, flow rates, and other HVAC variables which have similar behaviors. Plug loads are mostly step functions in reality, but the assumption of piecewise continuity merely substitutes the ramp input in the time step interval where the step change occurs. This is expected to have minimal influence on the model accuracy, and the output of the

time series will not significantly deviate from measured data. The deviation is considered to have a small impact, because it only occurs during the small interval when the plug load is enabled. Substituting Equation (3.45) into Equation (3.43) gives

$$T_{t+\delta} = e^{A_s\delta}T_t + \int_t^{t+\delta} e^{A_s(t+\delta-\tau)}B_s \left[\mathbf{U}_t + \frac{(\tau-t)}{\delta}(\mathbf{U}_{t+\delta} - \mathbf{U}_t) \right] d\tau \quad (3.46)$$

By changing variable $\alpha = \tau - t$, the equation can be rewritten as

$$\begin{aligned} T_{t+\delta} = e^{A_s\delta}T_t + & \left[\int_0^\delta e^{A_s(\delta-\alpha)} d\alpha \right] B_s \mathbf{U}_t \\ & + \left[\int_0^\delta \alpha e^{A_s(\delta-\alpha)} d\alpha \right] \left[\frac{B}{\delta} (\mathbf{U}_{t+\delta} - \mathbf{U}_t) \right] \end{aligned} \quad (3.47)$$

Seem et al. (1985) described the steps for integrating the two integrals. The solution to the first integral is

$$\left[\int_0^\delta e^{A_s(\delta-\alpha)} d\alpha \right] = A_s^{-1}(e^{A_s\delta} - I) \quad (3.48)$$

and the solution to the second integral is

$$\left[\int_0^\delta \alpha e^{A_s(\delta-\alpha)} d\alpha \right] = A_s^{-1}A_s^{-1}(e^{A_s\delta} - I) - A_s^{-1}\delta \quad (3.49)$$

Substituting these into Equation (3.47) yields

$$T_{t+\delta} = \varphi T_t + (\Gamma_1 - \Gamma_2)\mathbf{U}_t + \Gamma_2\mathbf{U}_{t+\delta} \quad (3.50)$$

where

$$\varphi = e^{A_s\delta}; \quad \Gamma_1 = A_s^{-1}(e^{A_s\delta} - I)B = A_s^{-1}(\varphi - I)B; \quad \Gamma_2 = A_s^{-1}\left(\frac{\Gamma_1}{\delta} - B\right)$$

Equation (3.52) relates the state at time $t + \delta$ to the state at time, t , and the inputs at the times t , and $t + \delta$. Using the forward shift operator, defined by $FT_t = T_{t+\delta}$ to relate the states to previous input, Equation (3.50) can be written as

$$(FI - \varphi)T_t = (F\Gamma_2 + \Gamma_1 - \Gamma_2)\mathbf{U}_t \quad (3.51)$$

$$T_t = (FI - \varphi)^{-1}(F\Gamma_2 + \Gamma_1 - \Gamma_2)\mathbf{U}_t \quad (3.52)$$

Substituting Equation (3.52) into Equation (3.42) yields

$$Q_{cool,t} = [C(FI - \varphi)^{-1}(F\Gamma_2 + \Gamma_1 - \Gamma_2)\mathbf{U}_t + D\mathbf{U}_t] \quad (3.53)$$

Equation (3.53) then relates the output from the system to the inputs, and the intermediate nodal temperatures are already lumped into the formulation. The expression $(FI - \varphi)^{-1}$ could be simplified further, based on the definition of a matrix inverse, as shown in Equation (3.54).

$$(FI - \varphi)^{-1} = \frac{R_o F^{n-1} + R_1 F^{n-2} + \dots + R_{n-2} F + R_{n-1}}{F^n + e_1 F^{n-1} + \dots + e_{n-1} F + e_n} \quad (3.54)$$

With further simplification and manipulation, the expression for the cooling load reduces to:

$$Q_{cool,t} = \sum_{j=0}^n (S_j \mathbf{U}_{t-j\delta}) - \sum_{j=1}^n (e_j y_{t-j\delta}) \quad (3.55)$$

where

$$\begin{aligned} S_o &= CR_o\Gamma_2 + D; S_j = C[R_{j-1}(\Gamma_1 - \Gamma_2) + R_j\Gamma_2] + e_j D \text{ for } 1 \leq j \leq n-1; S_n \\ &= CR_{n-1}(\Gamma_1 - \Gamma_2) + e_n D \end{aligned} \quad (3.56)$$

Equation (3.56) relates current outputs to time series of current and past inputs and time series of past outputs. The value of n , which determines the required number of past values, is equal to the smaller of the number of nodal temperatures in the thermal network and the rank of matrix A_s . With multiple (or increased number of) zones, the number of states increase linearly, and so is the required number of past values. Therefore, the time series solution is limited by the computational effort required and by

unavailability of sufficient past values of inputs and outputs. Case study results of time-series solution are shown in Appendix C.

3.4.2 Integrated solution method

At any instant, the stability of the system depends on the eigenvalues of the system matrix, A . This is applicable to both building load and cooling coil models. The building load model is unique, in that, $q \geq p$, that is, the input matrix must include the heat flux sources in addition to ambient and sol-air temperature inputs. To derive an integrated solution method to the state variables in the thermal network model, reconsider Equation (3.46): $T_{t+\delta} = e^{A\delta}T_t + \int_t^{t+\delta} e^{A(t+\delta-\tau)}B \left[\mathbf{U}_t + \frac{(\tau-t)}{\delta}(\mathbf{U}_{t+\delta} - \mathbf{U}_t) \right] d\tau$.

The expression is valid for any initial condition, t . If the initial conditions at time $t=0$ are known, then the solution becomes

$$T_\delta = e^{A\delta}T_o + \int_0^\delta e^{A(\delta-\tau)}B \left[\mathbf{U}_o + \frac{(\tau)}{\delta}(\mathbf{U}_\delta - \mathbf{U}_o) \right] d\tau \quad (3.57)$$

To obtain the integrated solution, the exponential matrix $e^{A\delta}$ and the convolution integral $\int_0^\delta e^{A(\delta-\tau)}B \left[\mathbf{U}_o + \frac{(\tau)}{\delta}(\mathbf{U}_\delta - \mathbf{U}_o) \right] d\tau$ need to be evaluated. According to Cleve and Loan (2003), common approaches used to evaluate the exponential matrix include Taylor series, Laplace, ordinary differential equation, and matrix decomposition. The matrix decomposition method utilizes the asymptotic stability property (which is necessary for the convergence of the matrix exponential) to evaluate the exponential matrix. It is based on similarity transformation (which uses the eigenvectors of the matrix) of the form:

$$A = VDV^{-1} \quad (3.58)$$

Note that this does not diagonalize the matrix A ; instead it represents it as products of a diagonal matrix D of eigenvalues and a full matrix V whose columns are the corresponding eigenvectors (from $AV = VD$). By substituting Equation (3.58), the power series definition of e^{At} simplifies to:

$$e^{At} = Ve^{Dt}V^{-1} \quad (3.59)$$

Where the eigenvectors of A form the columns of V , i.e.,

$$V = [v_1 | \dots | v_n] \text{ and } Av_j = \lambda_j v_j, \quad j = 1, \dots, n \quad (3.60)$$

$$e^{Dt} = \text{diagonal matrix}(e^{\lambda_1 t}, \dots, e^{\lambda_n t}) \quad (3.61)$$

provided that V is nonsingular, the exponential matrix of At may be expressed as

$$e^{At} = V(\text{diag}(e^{\lambda_1 t}, \dots, e^{\lambda_n t}))V^{-1} \quad (3.62)$$

This expresses the exponential matrix of A as explicit function of the eigenvectors and eigenvalues. Substituting Equation (3.62) into (3.57) yields:

$$T_\delta = e^{A\delta}T_o + \int_0^\delta V(\text{diag}(e^{\lambda_1(\delta-\tau)}, \dots, e^{\lambda_n(\delta-\tau)}))V^{-1}B \left[\mathbf{U}_o + \frac{(\tau)}{\delta}(\mathbf{U}_\delta - \mathbf{U}_o) \right] d\tau \quad (3.63)$$

Which is explicit relationship between the states (temperatures) of the different thermal zones in a building and the eigenvalues of the R-C state matrix, as well as inputs such as heating/cooling rates, ambient, solar radiation, internal heat gains etc. The integrated solution method (for building load model) has been applied in Ogunsola and Song (2014, 2015, 2016) for investigation of building passive thermal storage, and for prediction of building load in multi-zone buildings. It requires only the initial conditions of temperatures and values of the current inputs. This is advantageous over numerical solution, time series, and other approaches. For example, the heat extraction

or addition rate of a device may be determined as a function of desired zone temperature and the heat gains or loss within the building.

3.5 Stability Analysis

In the solution methods described above, one of the concerns is the feasible region of model parameters that assure asymptotic stability of the state matrix for all time steps. The time series and numerical solution methods are more prone to erroneous results if unreasonable time steps are used. For the integrated solution, stability analysis is crucial in order to understand the limitations and applicability. For the integrated solution method to be suitable,

- i. The full matrix of eigenvectors of A must be non-singular, and
- ii. The exponential matrix must converge, i.e. A must be asymptotically stable (since $e^{At} = V(\text{diag}(e^{\lambda_1 t}, \dots, e^{\lambda_n t}))V^{-1}$).

In this section, it is desirable to investigate the stability of the R-C thermal network and ascertain conditions under which the matrix inversion approach will be suitable. For the building load and cooling coil model, a careful analysis of the differential equation, $\frac{dT_n}{dt} = -\frac{1}{C_n} \left(\sum_{i=1}^j \frac{1}{R_i} \right) T_n + \frac{1}{C_n} \left(\sum_{i=1, i \neq n}^j \frac{1}{R_i} T_i \right) + \frac{1}{C_n} \sum_{i=1}^p Q_i$, reveals some important properties of the generalized R-C state matrix. It is:

- (i) A square matrix with negative diagonal entries (from the diagonal terms

$$-\frac{1}{C_n} \left(\sum_{i=1}^j \frac{1}{R_i} \right) T_n), \text{ and}$$

- (ii) The sum of each row ≤ 0

To illustrate, consider an example R-C state matrix of dimensions $n \times n$

$$A = \begin{bmatrix} a_{1,1} & a_{1,2} & \cdots & a_{1,n} \\ a_{2,1} & a_{2,2} & \cdots & a_{2,n} \\ \vdots & \vdots & \cdots & \vdots \\ a_{n,1} & a_{n,2} & \cdots & a_{n,n} \end{bmatrix}$$

The identified features of the R-C state matrix imply that:

- (i) $a_{i,i} < 0, \quad \forall i \in (1:n)$
- (ii) $\sum_{i,j=1}^{i,j=n} a_{i,j} \leq 0, \quad \forall i \in (1:n)$

The identified features hold for all feasible, finite R-C parameter set ($R > 0, C > 0$).

These identified features of the R-C state matrix correspond to diagonal dominance, defined as follows: A square matrix of order n with entries a_{ij} which are real or complex is said to be diagonally dominant if:

$$|a_{ii}| \geq \sum_{j=1, j \neq i}^n |a_{ij}| \quad \forall i \in (1:n)$$

i.e., if for every row of the matrix, the magnitude of the diagonal entry in a row is larger than or equal to the sum of the magnitudes of all the other (non-diagonal) entries in that row. If the equality holds for at least one row of the matrix, the matrix is said to be *weakly* diagonally dominant. A matrix is said to be *strictly* diagonally dominant if:

$$|a_{ii}| > \sum_{j=1, j \neq i}^n |a_{ij}| \quad \forall i \in (1:n)$$

i.e., if for every row of the matrix, the magnitude of the diagonal entry in a row is larger than the sum of the magnitudes of all the other (non-diagonal) entries in that row. If an irreducible matrix is weakly diagonally dominant, but is strictly diagonally dominant in at least one row (or column), then the matrix is irreducibly diagonally dominant (Poole, 2014).

The index(es) at which the inequality row-sum (i.e. $\sum_{i,j=1}^{i,j=n} a_{i,j} < 0$) occurs correspond to exterior nodes with resistor connections to ambient or solar-air temperature in the thermal network model of building load. For the cooling coil model, this corresponds to the leaving chilled water and leaving air temperature nodes respectively.

Case 1: Internal Zones with adiabatic assumptions

If there are no ambient or external temperature connections in the building under study (e.g. internal zones or group of internal zones with adiabatic assumptions), the R-C state matrix has only two (2) features

$$(i) \ a_{i,i} < 0, \quad \forall i \in (1:n)$$

$$(ii) \ \sum_{i,j=1}^{i,j=n} a_{i,j} = 0, \quad \forall i \in (1:n)$$

In that case, the R-C state matrix is singular (since sum of each row =0), and the system may be unstable or marginally stable. The implication is that modeling of internal thermal zones with such assumptions may lead to instability, and the matrix inversion solution method will not be suitable. Temperatures may not converge, or lead to unreasonable values.

Case 2: Exterior Zones

With connections to ambient or solar-air temperature, $\sum_{i,j=1}^{i,j=n} a_{i,j} < 0$ holds for at least one value of i , where $i \in (1:n)$.

With connection to ambient or solar-air temperature on all nodes, $\sum_{i,j=1}^{i,j=n} a_{i,j} < 0$ holds for all values of i , where $i \in (1:n)$.

Case 3: Cooling Coil

The cooling coil temperature nodes have resistor connections to entering water and air temperatures. Therefore, $\sum_{i,j=1}^{i,j=n} a_{i,j} < 0$ holds for all values of i , where $i \in (1:n)$.

The Gershgorin circle and the Levy-Desplanques theorems apply to diagonally dominant matrices as follows:

(i) A strictly diagonally dominant matrix (or an irreducibly diagonally dominant matrix) is non-singular (Horn and Johnson 1999; Mackiw, 1995; Horn and Johnson, 1985). That an $n \times n$ strictly diagonally dominant matrix is nonsingular could be traced back to Levy (1881) and Des-planques (1887). This theorem is equivalent to Gerschgorin's Theorem which is similarly the case that any $n \times n$ irreducibly diagonally dominant matrix being nonsingular is equivalent to Taussky's Theorem (Varga and Gillis, 1963).

Proof:

Suppose the matrix A is singular. Then, there exists a non-zero vector $\mathbf{x} = (x_1, \dots, x_n)$ such that $A\mathbf{x} = \mathbf{0}$. Let x_k be the element of \mathbf{x} such that $|x_k| \geq |x_i|$ for all i . $x_k \neq 0$ since \mathbf{x} is a nonzero vector by definition. Then,

$$\sum_i A_{ki}x_i = 0, i.e. \quad A_{ki}x_i = -\sum_{i \neq k} A_{ki}x_i$$

Thus, by the triangle inequality:

$$|A_{kk}||x_k| \leq \sum_{i \neq k} |A_{ki}||x_i| \leq \sum_{i \neq k} |A_{ki}||x_k|$$

Since x_k is non-zero, dividing by $|x_k|$ gives:

$$|A_{kk}| \leq \sum_{i \neq k} |A_{ki}|$$

Which contradicts the strict diagonal dominance definition above. This is a proof by contradiction.

(ii) *Every eigenvalue of matrix A_{nn} satisfies:*

$$|\lambda - A_{ii}| \leq \sum_{j \neq i} |A_{ij}| \quad i \in \{1, 2, \dots, n\}$$

Proof:

Suppose that λ is an eigenvalue of the matrix A . Then $\lambda I - A$ is singular. The matrix $\lambda I - A$ is strictly diagonally dominant if $|\lambda - A_{ii}| > \sum_{j \neq i} |A_{ij}|$ for every i . If $\lambda I - A$ is strictly diagonally dominant, then it is non-singular, and as a result, λ is not an eigenvalue. If λ is an eigenvalue, then $|\lambda - A_{ii}| \leq \sum_{j \neq i} |A_{ij}|$ must hold. This shows that every eigenvalue of the matrix A must be within a distance d of A_{ii} for some i . As a result of this and other Gershgorin's theorems, ranges for eigenvalues can be found (Brakken-thal, 2007). They lead to the following theorems:

(iii) *If a matrix is strictly diagonally dominant and all its diagonal elements are positive, then the real parts of its eigenvalues are positive (positive definitiveness). If all its diagonal elements are negative, then the real parts of its eigenvalues are negative (negative definitiveness) (Mckenzie 1960, Argyros and Szidarovszky, 1993, Varga, 2009; and Cvetković and Nedović, 2009).*

Implication:

(i) If all temperature nodes are connected to ambient or sol-air temperature, then the R-C state matrix is *strictly* diagonally dominant and asymptotically stable.

(ii) For the R-C thermal network of building load, if there is at least one internal node, then the R-C state matrix is *weakly* diagonally dominant. It is much more challenging to prove that a *weakly* diagonally dominant R-C state matrix is irreducible. However, the stability could be assured by introducing a dummy resistance and dummy ambient into the thermal network at internal nodes. The dummy ambient is set to zero vector, so that it has no influence on the forced response, while the dummy resistance is lumped into the estimation process, or assigned a value that is several orders of magnitudes larger than the estimated R values. This implies that the introduced R has little or no influence on the natural response (due to insignificant contribution, i.e. $1/(RC)$). Additionally, the impact of the dummy resistance fades off with time step (from e^{At}). The introductions of the dummy variables make the R-C state matrix strictly diagonal, hence, non-singular and asymptotically stable. In such instance, the R-C parameter domain could be unconstrained, and the integrated solution will converge for any time-steps.

(iii) The R-C thermal model of cooling coil is *strictly* diagonally dominant; hence, it is asymptotically stable.

These are all as a direct consequence of the Gershgorin circle and the Levy-Desplanques theorems.

Since the integrated solution method involves computation of the eigenvalues and eigenvectors, it provides additional information about the dynamics of the system. For example, it enables the investigation of system stability without solving the governing differential equations. The dependence of the solution on matrix inverse, eigenvector, and matrix exponential reveals further information about the transient

behavior of the system. Asymptotic stability implies that all eigenvalues of the state matrix must lie in the open left hand plane for the system to eventually be driven by forcing inputs, rather than by initial conditions. This also implies observability and controllability of the system, and the existence of unique eigenvectors and matrix inverse. From assumption of piecewise continuity (Eq. 3.45) and the evaluation of the matrix exponential (Eq. 3.61), an explicit solution of all nodal temperatures is obtainable. Using the state transition matrix and the input matrix, the solution at a current (or future) time step is dependent on the value from a previous time step, inputs from the previous and current steps, and the elapsed time between the two time steps. The building load is expressed as the HVAC system output required to achieve the measured temperature for the period of investigation.

3.6 Parameter Estimation

Accuracy of the RC thermal model depends largely on accurate estimation of the model parameters. For the building load model, the model parameters are broadly classified as envelope and internal mass components. Estimating the value of these parameters require a nonlinear optimization process. These parameters have been estimated in several ways. The envelope RC parameters may be estimated directly from the construction material, or from the thermal characteristics of the building construction in frequency domain. The internal mass parameters are more challenging to estimate, since the physical properties of components such as carpets, furniture, and other radiation absorbing surfaces within the indoor environment are not readily available.

The parameter search region of RC values and the training data used have significant effects on the performance of the thermal network model in post-training or calibration period. Effective and adequate estimation of the RC parameters require fundamental understanding of the physical limitations and thermal characteristics of building construction. For example, generalized unconstrained optimization search of RC parameters using near-constant zone temperatures or thermal loads tend to detect local or global optimas at high C values. Physically, this corresponds to envelope construction with extremely high density and/or specific heat, and/or thicknesses. In reality, such building constructions are not feasible due to cost, comfort, and materials constraints. Extremely high C values imply large time constants such that the effect of ambient temperature on zone temperature is filtered out, almost completely. In that case, the swings in indoor temperature are severely regulated. Additional consequences are that the zone temperature becomes less sensitive to the internal loads and HVAC cooling rate, because the absorbed radiations by the high thermal capacitance get released very slowly. Similarly, the high C values perform poorly for winter validation, where temperature fluctuations are not captured by the model, due to the high C values. Similarly, extremely low C values lead to significant fluctuations in temperature and building loads, due to almost direct coupling between ambient and room temperature. Therefore, the optimized values determined by unconstrained search may not be feasible in reality. The approach adopted in this dissertation is to limit the parameter search range of R-C values based on physical properties of typical light, medium, and heavy construction. The due consideration for physical constraints and limitations of building construction is one of the advantages of the R-C approach, in

that the building construction and properties are physically represented. The typical properties of light, medium, and heavy construction materials are shown in Tables 3.4 to 3.6 below.

Table 3.4: Exterior Wall Composition for Heavy Construction

	$L(\text{mm})$	k (W/mK)	ρ (kg/m ³)	C_p (J/KgK)	Resistance (m ² .K/W)
M01 100mm brick	101.6	0.89	1920	790	
M15 200mm heavyweight concrete	203.2	1.95	2240	900	
I02 50mm insulation	50.8	0.03	43	1210	
F04 Wall air space	-	-	-	-	0.15
G01a 19mm gypsum	19	0.16	800	43	

Table 3.5: Exterior Wall for Medium Construction

	$L(\text{mm})$	$k(\text{W/mK})$	$\rho(\text{kg/m}^3)$	$C_p(\text{J/KgK})$
M01 100mm brick	101.6	0.89	1920	790
I02 50mm insulation	50.8	0.03	43	1210
G01a 19mm gypsum	19	0.16	800	43

Table 3.6 Exterior Wall for Light Construction

	$L(\text{mm})$	$k(\text{W/mK})$	$\rho(\text{kg/m}^3)$	$C_p(\text{J/KgK})$
Wood Siding-1	9	0.14	530	900
Fiberglass quilt	66	0.04	12	840
Plasterboard-1	12	0.16	950	840

The common parameter estimation methods (such as sequential quadratic programming, conjugate gradient, and conventional nonlinear least square minimization) require the user to specify initial guesses, and in most cases, this determines the convergence speed. Additionally, most of these solvers tend to find local minimas near the starting point X_0 . There are several optimization solvers, with different characteristics. The most common solvers and their characteristics are shown in Table 3.7 below: The applicability and reliability of the optimized values depend on the desired solution and the nature of objectives and constraints.

In this dissertation, a genetic algorithm (combined with pattern search) was mostly used, because it doesn't require initial guesses to jump start the parameter estimation. It could be used when the task does not require an absolute minimum, and it may be combined with other optimization methods such as pattern search. For the cooling coil model, the parameters were estimated using a combination of genetic algorithm and particle swarm optimization. Genetic algorithm has been used for estimation of internal mass parameters for office buildings with light, medium, and heavy construction of the building envelope (Ogunsola and Song 2014, 2015). Results from genetic algorithm may then be used as initial guess into the solvers which have proof of convergence. The parameters are estimated by minimizing the difference between the models predicted outputs, and the measured output (e.g. cooling loads or exit temperature of cooling coil).



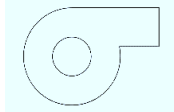
3.7 Summary

The various models utilized in this dissertation are summarized in Table 3.8

Table 3.7: Solver Characteristics

Solver	Nature of Convergence	No gradients required	Stochastic start points	Deterministic start points	User-supplied start points	Deterministic iterates	Stochastic iterates	Population based	Can run in parallel	Unbounded constraints
GlobalSearch	Fast convergence to local optima for smooth problems.		√			√				
MultiStart	Fast convergence to local optima for smooth problems.		√	√	√	√	√			
Patternsearch	Proven convergence to local optimum, slower than gradient-based solvers.	√		√	√					
Particleswarm	No convergence proof.	√	√	√	√		√	√	√	
Genetic Algorithm	No convergence proof.	√	√	√	√		√	√	√	√
Simul anneal bnd	Proven to converge to global optimum for bounded problems with very slow cooling schedule.	√			√		√			
fmincon, fminunc, fseminf, lsqcurvefit, lsqnonlin	Proven quadratic convergence to local optima for smooth problems			√	√					
fminsearch	No convergence proof	√		√	√					√

Table 3.8: Summary of models utilized in this dissertation

Schematic & Description	Approach	Parameters	Contributions
 Dynamic Building load model	Thermal network approach. Based on fundamental heat transfer.	Estimated using optimization techniques. Determined from actual measurements. The parameters are constrained, based on physical characteristic of building constructions.	Stability analysis. Parameter domain estimation. Solution approach. Extended application of thermal network model
 Cooling coil transient model	Thermal network approach (with variable R's and C's). Based on energy balance.	The parameters are flow dependent. They are estimated from actual measurements. They represent heat capacities of cooled air and chilled water respectively.	New thermal network approach to transient cooling coil modeling. Use of flow dependent resistances and capacitances (RC)
 Fan-motor model	Steady state model, based on fan laws. Assumption of similar fan power consumption under similar operating flow and static pressure conditions. Actual fan power determined by interpolation.	Parameters not explicitly defined, because similarity laws are used.	Using measured fan data to predict fan-power and speed with good accuracy.

Chapter 4: HVAC Components Model Validation

This chapter validates the component models described in Chapter 3. As a proof of concept, a multi-zone building which is a section of the Engineering Laboratory (EL) building at the University of Oklahoma was used as a case study. The validation is essential to understand the level of accuracy of the different models of building load, cooling coil, and fan-power for both cooling and heating season operation, and their suitability for predictive control in multi-zone buildings. The validation also gauged the level of accuracy of the variable R-C cooling coil model, which was newly developed in this study. Figure 4.1 shows the layout of the EL- building. It is made up of seven (7) thermal zones, and served by a single duct, variable air volume (VAV), air handling unit (AHU). The colors indicate how the different thermal zones are grouped. The case study air handling unit and some of its associated sensors are shown in Figure 4.2.

The building load, cooling coil, and fan-power modeling procedures described in the preceding chapter are tested and validated in this section. The building load model is validated at both single and multiple thermal zones level. For the single zone case study, the purpose was to capture the dynamics and variations at the zone level. Reasonably high model accuracy at the zone level could then easily be extended to the case of buildings with multiple thermal zones. To evaluate the accuracy of the different models, the Mean Error (ME), Mean Absolute Error (MAE), Mean Biased Error (MBE), and Coefficient of Variance of the Root Mean Square Error (CVRMSE) are used. MBE and CVRMSE are most commonly used to validate forecast models (Ramanathan 1995).

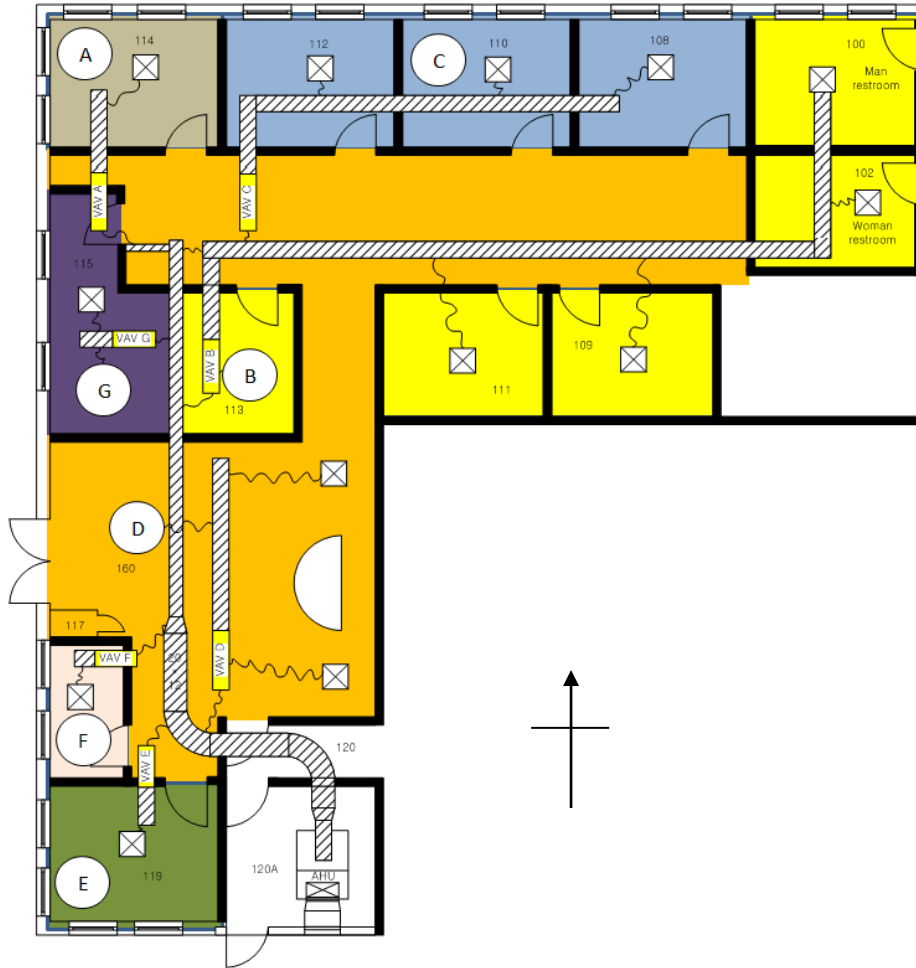


Figure 4.1: Layout of Case Study Building

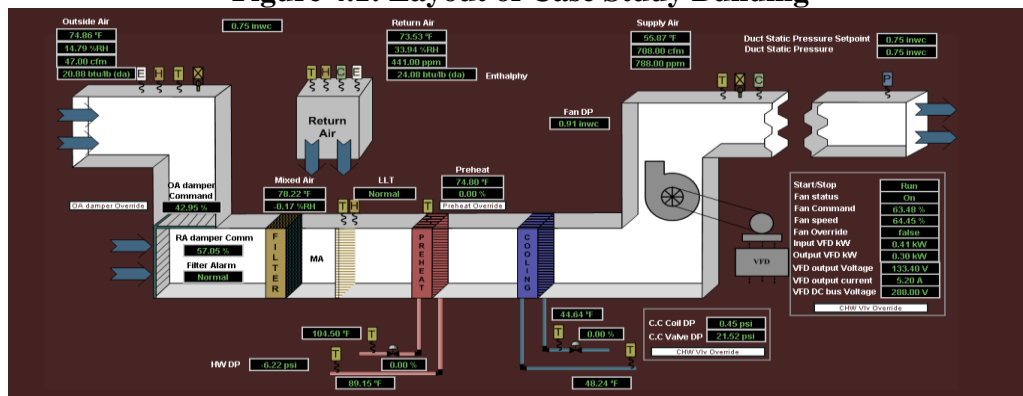


Figure 4.2: Case Study Air Handling Unit

Any single error indices provide only one projection of the model errors, and therefore only emphasize a certain aspect of the accuracy. In this dissertation, a combination of

error indices was used to evaluate the performance of the models, to adequate comparison of performance. This practice is highly recommended in literature (Chai and Draxler 2014). The formulas for the different errors are given in Equations (4.1) to (4.3):

$$ME = \frac{\sum_{i=1}^n (y_i^{est} - y_i)}{n} \quad (4.1)$$

$$CVRMSE(\%) = \frac{\sqrt{\frac{\sum_{i=1}^n (y_i^{est} - y_i)^2}{n}}}{(\sum_{i=1}^n y_i)/n} \times 100 \quad (4.2)$$

$$MBE(\%) = \frac{\sum_{i=1}^n (y_i^{est} - y_i)}{\sum_{i=1}^n y_i} \times 100 \quad (4.3)$$

$MAE = \frac{\sum_{i=1}^n |y_i^{est} - y_i|}{n}$, where y_i^{est} is the estimated value by the model, y_i is the measured (or actual) value, and n is the number of data points. Typical acceptable calibration tolerances for simulations are MBE values of $\leq 10\%$ and CVRMSE values of $\leq 30\%$ (DoE 2008).

4.1 Building Load Validation

The building load model was validated for cases of single thermal zone, and multiple zones in a VAV system. The single zone case study (Section 4.2) simulates the cooling load and heat extraction (or addition) rate required to maintain a given temperature. While the multiple zone case study (Section 4.3) simulates the room temperature, given a heat extraction or addition rate. The predicted room temperatures and cooling loads are compared with measurement in terms of the error indices (ME, MAE, MBE, and CVRMSE)

4.2 Single Zone Case Study - Thermal Zone F

The first case study is that of a single thermal zone. Thermal Zone F, in Figure 4.1 was used. It has adjacent rooms on both sides, and exposure to ambient temperature on the west facing wall. The selected zone is a good candidate because it has its individual thermostat and sensors, which can measure all the variables needed for building load estimation. The needed measurements are outside air temperature, solar radiation, zone temperature, and the cooling (or heating rate) from the HVAC system. The zone temperature and heat extraction rate (or addition rate, as the case may be) are obtained from the Building Automation System (BAS). The sensors are deemed to be reasonably accurate, without any data integrity issues. For the single zone case study, time steps of 1 hour were used for the building load simulation.

4.2.1 Assumptions

Though the simulated zone is part of a larger building, it was assumed that adjacent spaces are similarly conditioned, such that the single zone could be treated as a stand-alone room with negligible thermal interaction with adjacent thermal zones. The assumption is expected to have insignificant influence on the building load predictions, since the adjacent zones have similar occupancy schedules and set points. Only heat transfer through the west exposed wall was considered. All other surfaces were within the single zone were treated as adiabatic. The RC model representation of the single zone is shown in Fig. 4.3.

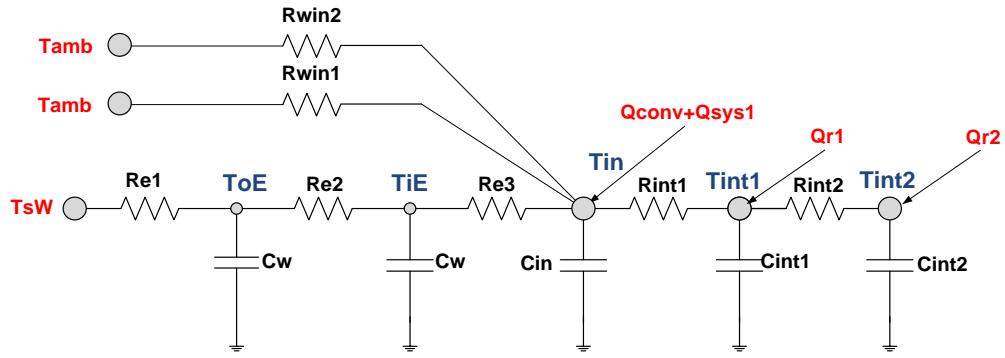


Figure 4.3: RC model representation of the single zone

The inputs to the model include envelope and internal load components, which have been shown to have significant influence on the temperature and building load. The windows are treated as pure thermal resistances, since they have negligible storage capabilities as compared with walls and other envelope components. The transmitted solar radiation through the windows directly reaches two virtual internal nodes. The additional thermal mass within the building, such as the floor/ceiling, furniture, carpets etc. is considered by lumping them into the 2R2C model, with the capacitances (C_{int} 's) and resistances (R_{int} 's) trained and determined using physical characteristic of the construction (See Ogunsola and Song 2012). The RC parameters and variables shown in Figure 4.3 are categorized as follows:

R-C Parameters

- Rwin - the windows thermal resistance
- Cw- thermal capacitance of wall
- Rint- thermal resistance of internal mass
- Cint – thermal capacitance of internal mass
- Cin- indoor air thermal capacitance

Variables

The input to the model include T_{sW} , T_{amb} , Q_{conv} , Q_{sys1} , Q_{r1} , and Q_{r2} . A brief description of key variables is given below:

T_{oE} and T_{iE} :	Outside and inside surface temperature of the building envelope
T_{int1} and T_{int2} :	Virtual temperatures of internal mass nodes
T_{in} :	Zone Temperature
T_{sW} :	Solar-air temperature on west-facing wall
T_{amb} :	Ambient temperature
Q_{sys1} :	System input (+ve for heating, and –ve for cooling). It is 100% convective.
$Q_{r1} = Q_{r2} = Q_r$:	This is the total solar radiation incident on the internal mass node. It is made up of transmitted solar radiation from windows and radiative part of the internal heat gains.
Q_{conv} :	This is the convective part of the internal load. For the single zone case study, the internal loads were assumed to split equally into convection and radiation heat gains. This implies that 50% of the internal heat gain becomes cooling load instantaneously, while the remaining 50% is radiated, to be released at a later time. The internal load (equipment and people) density of 25 W/m^2 was assumed for occupied hours. An internal load density of 5 W/m^2 was assumed for unoccupied hours. ASHRAE/IES 90.1-2010 standards recommend $16.15\text{--}32.3 \text{ W/m}^2$ for offices and institutional buildings. The assumed values are within this range.

As shown in Figure 4.3, the thermal network representation of the single zone involves 6 resistances and 5 capacitances. Training (measurement) data are needed to determine the R-C parameters that minimize the error between temperature and building

load predicted by the model, and the actual values. The number of parameters to estimate depends on available information. Since the volume of the room is known, the indoor capacitance, C_{in} which is derived from the air mass within the occupied space, is a known parameter. Typical medium construction materials for windows in a medium type office were assumed. The assumed compositions of partitions and floor are shown in Appendix.

The R-C properties of other supporting structural components are assumed to be lumped into the estimated RC parameters. The thermal capacitances of envelope and internal mass nodes are generally assumed to be equal (i.e. $C_{int1} = C_{int2}$). The above simplifying assumptions reduce the number of parameters to be estimated to 7, i.e. 5 resistances (R_{e1} , R_{e2} , R_{e3} , R_{int1} , and R_{int2}) and 2 capacitances (C_w and $C_{int1}=C_{int2}$). Typical meteorological year weather data (version 3) was used in this study. As a model calibration process however, the weather data was modified by replacing the ambient temperature, solar radiation, and wind speeds with actual measured data for Norman, Oklahoma, obtained from Mesonet. The material of building construction is a required input in EnergyPlus, a whole building simulation software. A medium construction, according to ASHRAE classification, was assumed for the office building. The RC thermal model accuracy was evaluated by comparing the temperature and building load results with EnergyPlus and measured data.

4.2.2 *Parameter estimation*

To estimate the parameters, there are several possible approaches. Some of the estimation approaches are shown in Table 4.1.

Table 4.1: Different estimation scenarios for the R-C parameters

	Scenario	Parameters Fixed	Parameters estimated	Assumed Values
1	5R2C	None	$(R_{e1}, R_{e2}, R_{e3}, R_{int1}, R_{int2}, C_w \text{ and } C_{int})$	-
2	4R2C	R_{e3}	$(R_{e1}, R_{e2}, R_{int1}, R_{int2}, C_w \text{ and } C_{int})$	Given outside air convection coefficient
3	3R2C	R_{e1} and R_{e3}	$(R_{e2}, R_{int1}, R_{int2}, C_w \text{ and } C_{int})$	Given outside and inside convection coefficient
4	2R2C	$R_{e1}, R_{e3},$ and R_{e2}	$(R_{int1}, R_{int2}, C_w \text{ and } C_{int})$	Given outside and inside convection coefficient, and medium construction

The first scenario involves estimation of all 7 R-C parameters. The other scenarios involve further assumptions about convection coefficients, and construction information. Flexibility in choice of estimation scenario, and possibility to deduce the model parameters from building usage information is one of the limitations of whole building software like EnergyPlus. From limited information and measured data, feasible R-C parameters can be deduced for all the scenarios indicated in Table 4.1.

For this case study, 3 days of measurement data were used for the training period (summer: July 1-3, 2013 and winter: January 1-3, 2013). The model was validated using 10 days in both summer and winter seasons (summer: July 22-31, 2013 and winter: January 21-30, 2013). Since both summer and winter data were used for training period, two solution options are possible:

- (i) Estimation of R-C parameters of Table 4.1 from cooling season data. This is followed by validation of the model performance (in terms of zone temperature and building load prediction accuracies) for both cooling and heating season.
- (ii) Estimation of R-C parameters of Table 4.1 from heating season data. This is followed by validation of the model performance (in terms of zone temperature and building load prediction accuracies) for both cooling and heating season.

Estimation of the R-C parameters using both cooling and heating season data is critical to ensure the selection of most accurate, robust, and representative R-C values for the thermal zone. The training periods were selected to be those corresponding to typical building operation in cooling and heating seasons respectively. The R-C parameter combination with the best model accuracy (in terms of error indices and coefficients of fit) was chosen.

4.2.3 Modeling equations

The differential equations for the thermal network model shown in Figure 4.3 could be written as shown in Equations 4.4 to 4.8:

Outside surface temperature node

$$\frac{dT_{oE}}{dt} = -\frac{1}{C_w} \left(\frac{1}{R_{e1}} + \frac{1}{R_{e2}} \right) T_{oE} + \frac{1}{C_w} \left(\frac{1}{R_{e1}} T_{sw} + \frac{1}{R_{e2}} T_{iE} \right) \quad (4.4)$$

Inside surface temperature node

$$\frac{dT_{iE}}{dt} = -\frac{1}{C_w} \left(\frac{1}{R_{e2}} + \frac{1}{R_{e3}} \right) T_{iE} + \frac{1}{C_w} \left(\frac{1}{R_{e2}} T_{oE} + \frac{1}{R_{e3}} T_{in} \right) \quad (4.5)$$

Zone temperature node

$$\begin{aligned}
\frac{dT_{in}}{dt} = & -\frac{1}{C_{in}} \left(\frac{1}{R_{e3}} + \frac{1}{R_{int1}} + \frac{1}{R_{win1}} + \frac{1}{R_{win2}} \right) T_{in} \\
& + \frac{1}{C_{in}} \left(\frac{1}{R_{e1}} T_{iE} + \frac{1}{R_{int1}} T_{int1} + \frac{1}{R_{win1}} T_{amb} + \frac{1}{R_{win2}} T_{amb} + Q_{conv} \right. \\
& \left. + Q_{sys1} \right)
\end{aligned} \tag{4.6}$$

Internal mass nodes

$$\begin{aligned}
\frac{dT_{int1}}{dt} = & -\frac{1}{C_{int1}} \left(\frac{1}{R_{int1}} + \frac{1}{R_{int2}} \right) T_{int1} \\
& + \frac{1}{C_{int1}} \left(\frac{1}{R_{int1}} T_{in} + \frac{1}{R_{int2}} T_{int2} + Q_{r1} \right)
\end{aligned} \tag{4.7}$$

$$\frac{dT_{int2}}{dt} = -\frac{1}{C_{int2}} \left(\frac{1}{R_{int2}} \right) T_{int2} + \frac{1}{C_{int2}} \left(\frac{1}{R_{int2}} T_{int1} + Q_{r2} \right) \tag{4.8}$$

The set of differential equations could be represented in state space as shown in Equation 4.9.

$$\dot{T} = AT + BU \tag{4.9}$$

The states are the temperatures (2 wall temperatures, 2 virtual temperatures to account for internal mass, and 1 room temperature), the inputs are ambient, solar-air temperature, radiation, and system heating or cooling rate. A is a 5×5 matrix of constant coefficients. T is a matrix of dimension 5×1 , since there are 5 temperature nodes. B is of dimension 5×5 , and U is a 5×1 matrix, since there are 5 inputs. A summary of the nodal and adjacent temperatures is presented in Table 4.2

Table 4.2: Summary of the nodal and adjacent temperatures

Type	Nodal Temperature	Adjacent Temperature Branches	Thermal Capacitance	Heat Flux Branches
Room Temperature	T_{in}	T_{iE} , T_{int1} , and T_{amb}	C_{in}	Q_{conv} , Q_{sys}
External Wall	T_{oE}	T_{sW} , T_{iE}	C_w	
	T_{iE}	T_{oE} , T_{in}		
Internal Mass	T_{int1}	T_{int2} , T_{in}	C_{int1}	Q_{r1}
	T_{int2}	T_{int1}	C_{int2}	Q_{r2}

4.2.4 Results

The temperature and building load results of the thermal network model is compared with EnergyPlus predictions and measured data in this section. The results for cooling season and heating season validation are shown in Tables 4.3 and 4.4 respectively. The four cases shown in Tables 4.3 and 4.4 correspond to

- (i) RC parameters estimated using cooling season training data and validated for another period in the cooling season (Table 4.3).
- (ii) RC parameters estimated using heating season training data and validated for the cooling season (Table 4.3).
- (iii) RC parameters estimated using cooling season training data and validated for the heating season (Table 4.4).
- (iv) RC parameters estimated using heating season training data and validated for another period in the heating season (Table 4.4).

Tables 4.3 and 4.4 compare the accuracy of the RC model and EnergyPlus with measured values in terms of well-established error indices. The values asterisked in Tables 4.3 and 4.4 are those with least error and highest correlation to the measured

cooling load. The comparison of performance across different training and validation seasons aid in selection of most appropriate RC scenario for year-round prediction of building load, based on acceptable calibration tolerances.

Table 4.3: Comparison of error indices for Cooling Season Validation

Training Season	Scenario	ME (W)	MBE (%)	CVRM SE (%)	ME (W)	MBE (%)	CVRMSE (%)
Cooling	5R2C	6.02	4.984	36.33	23.73	-0.86*	58.36
	4R2C	4.54	4.854	36.93			
	3R2C	3.79	3.447	28.94			
	2R2C	-3.33*	4.137	17.27*			
Heating	5R2C	6.5	6.752	41.61			
	4R2C	11.08	8.501	47.99			
	3R2C	37.08	1.469	43.98			
	2R2C	16.06	4.023	43.89			

Table 4.4: Comparison of error indices for Heating Season Validation

Training Season	Scenario	ME (W)	MBE (%)	CVRM SE (%)	ME (W)	MBE (%)	CVRMSE (%)
Cooling	5R2C	65.57	73.67	-149.27	97.95	111.46	-232.17
	4R2C	67.51	75.03	-155.38			
	3R2C	35.63	38.45	-115.96			
	2R2C	8.17*	6.67*	-95.88*			
Heating	5R2C	29.37	-33.28	322.73			
	4R2C	40.75	-70.63	345.13			
	3R2C	66.05	-145.10	346.16			
	2R2C	8.86	-40.97	313.64			

As could be seen in Table 4.3, cooling season training data generally gives better accuracies for building load prediction than heating season training data. This may partly be due to the near-constant zone temperatures recorded in the cooling season, because this is favorable for simulation and parameter estimation purposes. Among the different RC estimation methods, the 2R2C parameters estimated using cooling season data perform superior to the other scenarios for both the cooling and

heating seasons. Overall, most of the RC parameters scenario demonstrated better accuracy as compared with EnergyPlus. EnergyPlus has been validated for different scenarios (DoE 2010), and it is not the intention to re-validate the software. However, as could be seen in Tables 4.3 and 4.4, due to lack of parameter estimation methods, EnergyPlus results may be unreliable when building construction information is limited or not available. The 2R2C scenario is seen to pass both validation criteria of $MBE < 10\%$ and $CVRMSE < 30\%$ for the cooling season. However, all of the other RC scenarios and EnergyPlus did not meet these criteria. This implies that the RC model is more suitable for cooling season than the heating season, for the case study. Overall, the 2R2C was selected as the appropriate RC scenario to represent the studied thermal zone.

The 2R2C scenario was then used to test the overall effectiveness through comparison with EnergyPlus and measured data from the 2012 summer season and the 2014 winter season. The periods of testing are deliberately selected to be disjointed in order to ascertain the robustness of the 2R2C. Figures 4.4 to 4.6 show results of the building loads and zone as they compare with measurements and EnergyPlus.

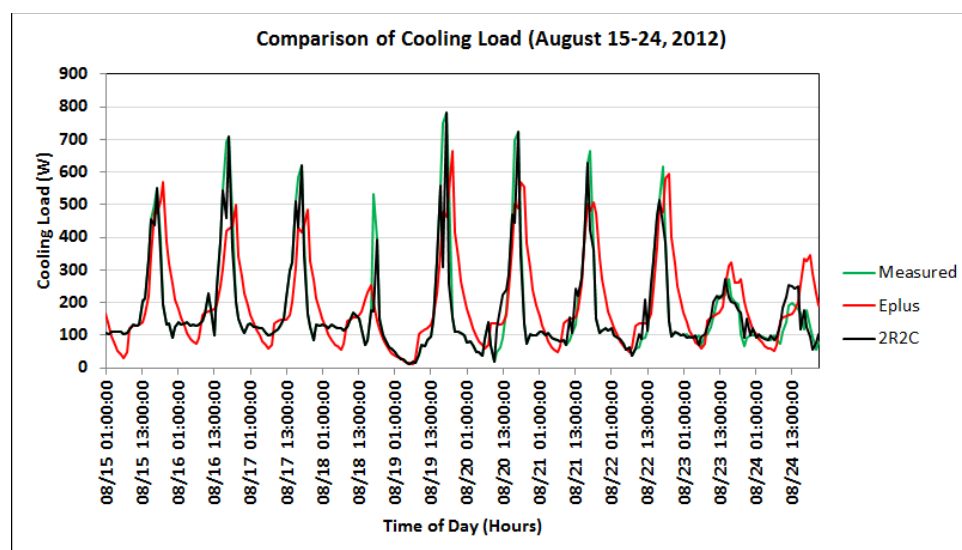


Figure 4.4: Comparison of building load for the cooling season.

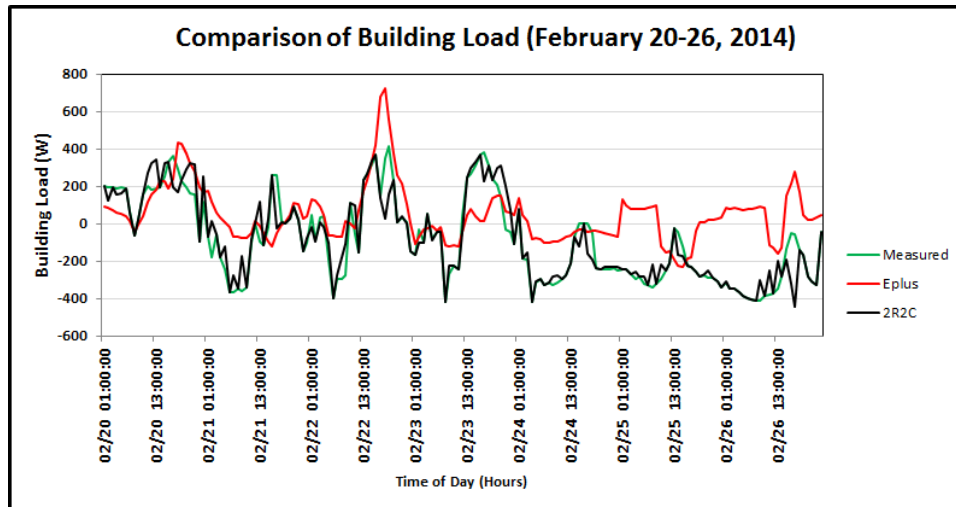


Figure 4.5: Comparison of building load for heating season.

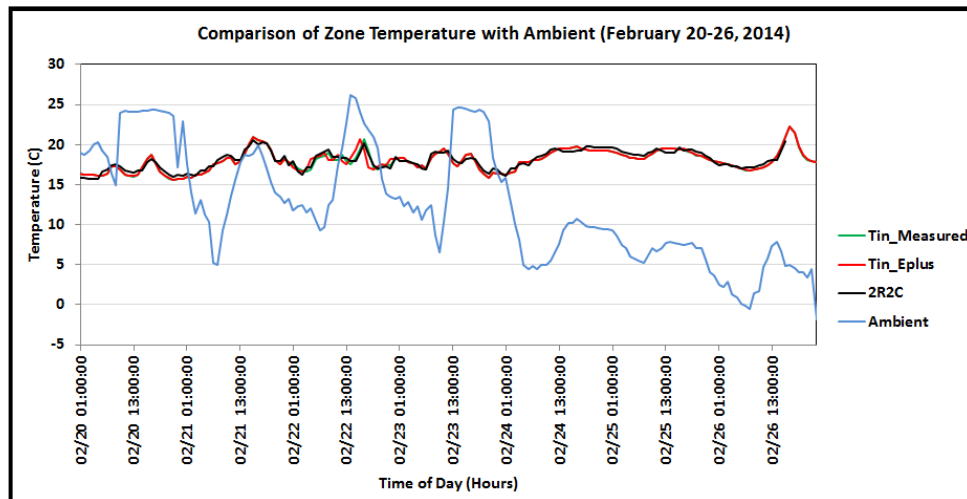


Figure 4.6: Comparison of zone temperatures for heating season

As shown in Figure 4.4, both the EnergyPlus and 2R2C models are observed to trend the cooling load, but there are occasional under-predictions. Meanwhile, the 2R2C captured many fluctuations in the cooling load which were not captured by EnergyPlus. With only 3 days training data, an accurate building load forecast was made for 10 days in the cooling season. The temperature trajectory for both 2R2C and EnergyPlus shows satisfaction of zone temperature within errors of less than ± 0.05 °C and is therefore not presented here. The integrated solution has eliminated the issues of noticeable and

unwanted spikes that were observed after using the time series model (Ogunsola et. al 2014). The RC model is also seen to consistently track the cooling load for both occupied and unoccupied hours. Comparison of the building load for the heating season is shown in Figure. 4.5. The validation period both heating and cooling modes, as indicated by the positive and negative values on the building load axis. The RC model is seen to generally track the building load patterns even where there is switch from heating to cooling, and vice versa. With only 3 days of training data, reasonably accurate building load estimation was made for up to 10 days in this heating season. Occasional spikes are noted in the 2R2C model predictions as noted in Figure 4.5, but they die out gradually. EnergyPlus simulation of the building load is also shown in Figure 4.5. Figure 4.6 shows the measured room temperature, RC predicted zone temperature, EnergyPlus predicted zone temperature, and ambient temperature. Figure 4.6 explains the reason for the switch from heating to cooling, which is consistent with the ambient temperature crossing below and above the room temperature, respectively. It also shows how the RC and EnergyPlus predicted temperature trends well with the measured room temperature. The computational expense of the RC model is mainly due to the parameter estimation, which is done mostly using Genetic Algorithm, particle swarm optimization, or global search. On a desktop computer with core i3, 1.7 GHz processor, 4 GB RAM, and 500 GB hard disk drive, the parameter estimation takes between 45 minutes and 1hr depending on convergence tolerances. Once the RC parameters are estimated, the simulation requires little computational effort. Hourly simulation of building load for a 1-week period takes less than 1minute to complete on a desktop computer with above configuration. This is quite large when compared with

EnergyPlus (which uses $<0.9s$). However, the RC computation time for each time-step is within reasonable range of value that is appropriate for control purposes.

4.3 Multiple Zone Case Study

For the multiple zone case, the Engineering laboratory building at the University of Oklahoma was used. As shown in Figure 4.1, there are seven thermal zones. Similar modeling assumptions made for the single zone case (Section 4.2.1) are also applicable. However, for the multi-zone case study, the thermal interactions of adjacent zones are considered during the estimation of the R-C parameters. The following sections discuss the thermal model representation and interactions between the different temperature nodes. For the multiple zone case, time steps of 1 minute were used for the simulation. Table 4.5 shows how the thermal zones are grouped, the exposures, and their interactions with adjacent zones.

Table 4.5: Thermal Zone Grouping and Interactions

Thermal Zone	Rooms	Exposures to ambient	Adjacent Zones (interactions)
A	114	North, West	C and D
B	100, 102, 109, 111, 113	North	C , D, and G
C	108, 110, 112	North	A, B, and D
D	Corridor	West	A, B, C, E, F, G
E	119	South, West	D and F
F	118	West	D and E
G	115	West	B and D

4.3.1 Thermal zone A

The thermal interactions between the zone temperature node, envelope, and internal mass are shown in Figure 4.7 and Tables 4.6 to 4.7. For clarity, the partitions' RC parameters are not fully shown in the representation

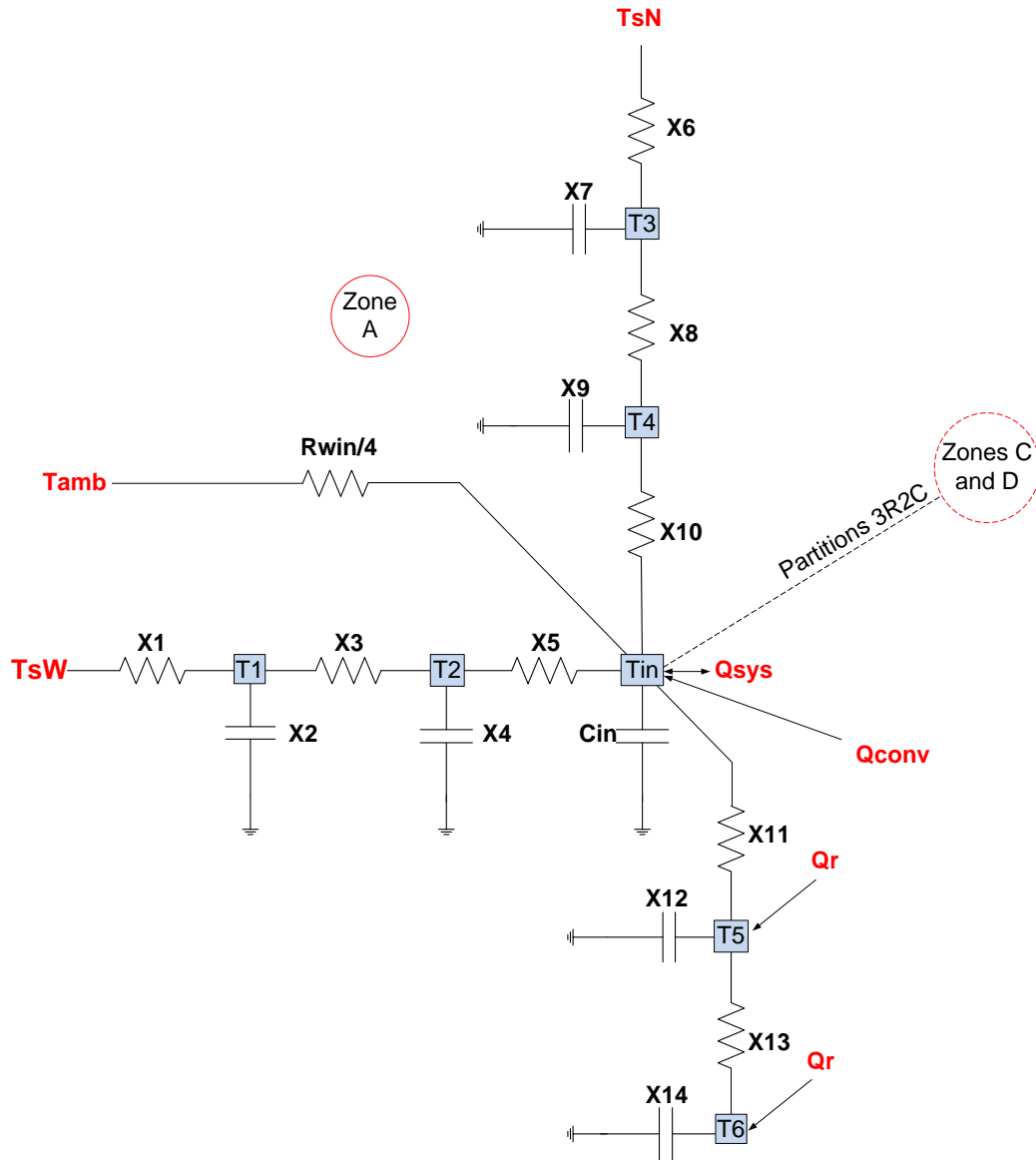


Figure 4.7: Thermal network representation for Zone A

Table 4.6: State space matrix for Thermal Zone A (Q_{cool} is the cooling load)

	$T1$	$T2$	$T3$	$T4$	$T5$	$T6$	T_{in}
$T1$	$-\frac{1}{X2}(\frac{1}{X1} + \frac{1}{X3})$	$\frac{1}{X2X3}$	0	0	0	0	0
$T2$	$\frac{1}{X4X3}$	$-\frac{1}{X4}(\frac{1}{X3} + \frac{1}{X5})$	0	0	0	0	$\frac{1}{X4X5}$
$T3$	0	0	$-\frac{1}{X7}(\frac{1}{X6} + \frac{1}{X8})$	$\frac{1}{X7X8}$	0	0	0
$T4$	0	0	$\frac{1}{X9X8}$	$-\frac{1}{X9}(\frac{1}{X8} + \frac{1}{X10})$	0	0	$\frac{1}{X9X10}$
$T5$	0	0	0	0	$-\frac{1}{X12}(\frac{1}{X11} + \frac{1}{X13})$	$\frac{1}{X12X13}$	$\frac{1}{X12X11}$
$T6$	0	0	0	0	$\frac{1}{X14X13}$	$-\frac{1}{X14X13}$	0
T_{in}	0	$\frac{1}{C_{in}X5}$	0	$\frac{1}{C_{in}X10}$	$\frac{1}{C_{in}X11}$	0	$-\frac{1}{C_{in}}(\frac{1}{X5} + \frac{1}{X10} + \frac{1}{X11} + \frac{4}{R_{win}}) + partitions$
Q_{cool}	0	$\frac{1}{X5}$	0	$\frac{1}{X10}$	$\frac{1}{X11}$	0	$-\left(\frac{1}{X5} + \frac{1}{X10} + \frac{1}{X11} + \frac{4}{R_{win}} + partitions\right)$

Table 4.7: Input matrix for Thermal Zone A

	T_{amb}	T_{sN}	T_{sW}	Q_{conv}	Q_{sys}	Q_r
$T1$	0	0	$\frac{1}{X2X1}$	0	0	0
$T2$	0	0	0	0	0	0
$T3$	0	$\frac{1}{X7X6}$	0	0	0	0
$T4$	0	0	0	0	0	0
$T5$	0	0	0	0		$\frac{1}{X12}$
$T6$	0	0	0	0	0	$\frac{1}{X14}$
T_{in}	$\frac{4}{CinRwin}$	0	0	$\frac{1}{Cin}$	$-\frac{1}{Cin}$	0
Q_{cool}	$\frac{4}{Rwin}$	0	0	1	0	0

Note: X values are the R-C parameters. Partitions involve sets of 3R2C

4.3.2 Thermal zone B

The thermal interactions between the zone temperature node, envelope, and internal mass are shown in Figure 4.8 and Tables 4.8 to 4.9. For clarity, the partitions' RC parameters are not fully shown in the representation.

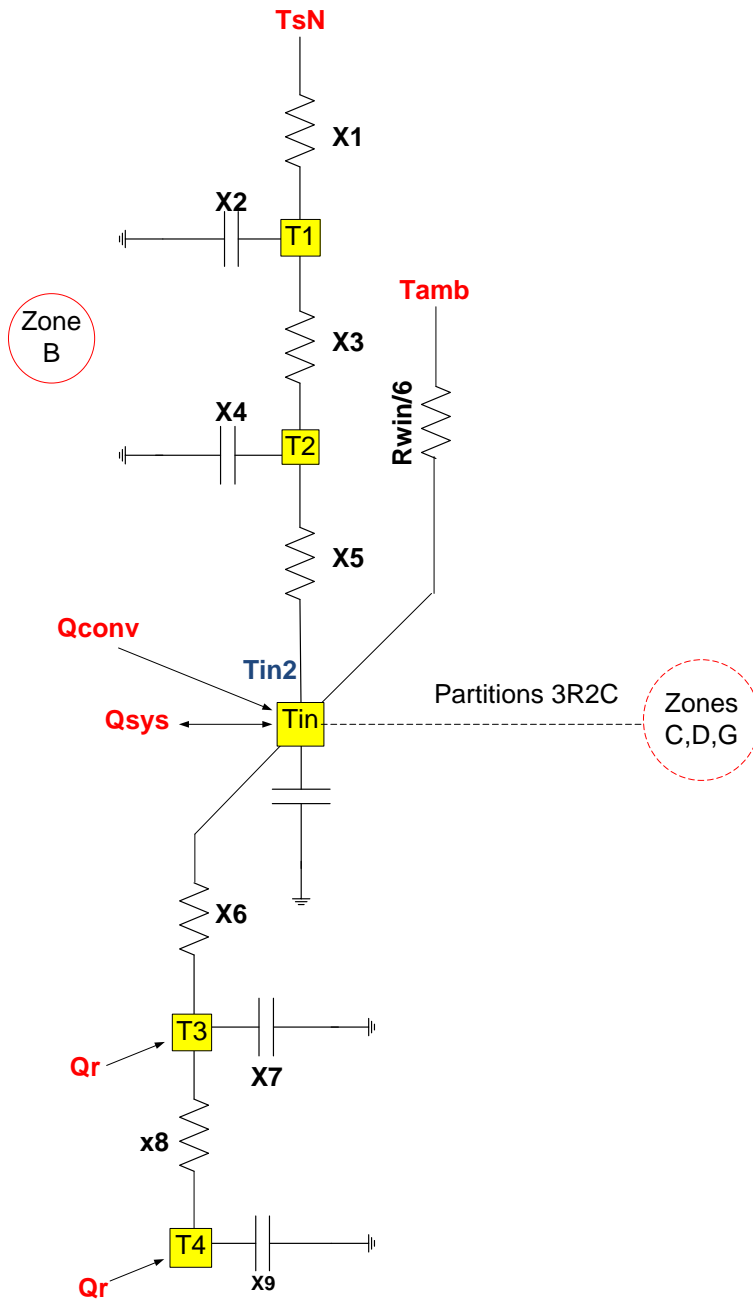


Figure 4.8: Thermal network representation for Zone B

Table 4.8: State space matrix for Thermal Zone B (Q_{cool} is the cooling load)

Zone B	T1	T2	T3	T4	Tin
T1	$-\frac{1}{X2}(\frac{1}{X1} + \frac{1}{X3})$	$\frac{1}{X2X3}$			
T2	$\frac{1}{X4X3}$	$-\frac{1}{X4}(\frac{1}{X3} + \frac{1}{X5})$			$\frac{1}{X4X5}$
T3			$-\frac{1}{X7}(\frac{1}{X6} + \frac{1}{X8})$	$\frac{1}{X7X8}$	$\frac{1}{X7X6}$
T4			$\frac{1}{X9X8}$	$-\frac{1}{X9X8}$	
Tin		$\frac{1}{CinX5}$	$\frac{1}{CinX6}$		$-\frac{1}{Cin}(\frac{1}{X5} + \frac{1}{X6} + \frac{2}{Rwin} + partitions)$
Qcool	0	$\frac{1}{X5}$	$\frac{1}{X6}$	0	$-(\frac{1}{X5} + \frac{1}{X6} + \frac{2}{Rwin} + partitions)$

Table 4.9: Input matrix for Thermal Zone B

Zone B	Tamb	TsN	Qconv	Qsys	Qr
T1	0	$\frac{1}{X2X1}$			
T2	0	0	0	0	0
T3	0	0	0	0	$\frac{1}{X7}$
T4	0	0	0	0	$\frac{1}{X9}$
Tin	$\frac{2}{CinRwin}$	0	$\frac{1}{Cin}$	$-\frac{1}{Cin}$	0
Qcool	$\frac{2}{Rwin}$	0	1	0	0

Note: X values are the R-C parameters. Partitions involve sets of 3R2C for each adjacent thermal zone.

4.3.3 Thermal zone C

The thermal interactions between the zone temperature node, envelope, and internal mass are shown in Figure 4.9 and Tables 4.10 to 4.11. For clarity, the partitions' RC parameters are not fully shown in the representation.

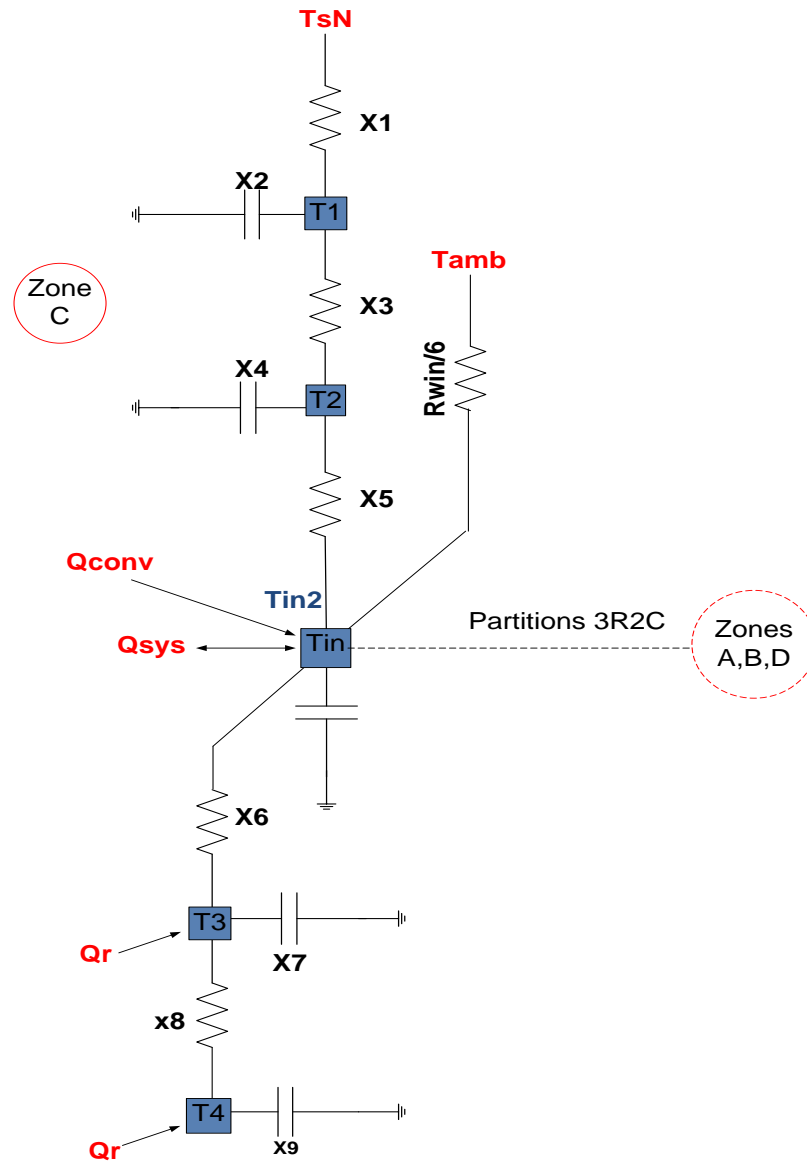


Figure 4.9: Thermal network representation for Zone C

Table 4.10: State space matrix for Thermal Zone C (Q_{cool} is the cooling load)

Zone C	T1	T2	T3	T4	Tin
T1	$-\frac{1}{X2}(\frac{1}{X1} + \frac{1}{X3})$	$\frac{1}{X2X3}$	0	0	0
T2	$\frac{1}{X4X3}$	$-\frac{1}{X4}(\frac{1}{X3} + \frac{1}{X5})$	0	0	$\frac{1}{X4X5}$
T3	0	0	$-\frac{1}{X7}(\frac{1}{X6} + \frac{1}{X8})$	$\frac{1}{X7X8}$	$\frac{1}{X7X6}$
T4	0	0	$\frac{1}{X9X8}$	$-\frac{1}{X9X8}$	0
Tin	0	$\frac{1}{CinX5}$	$\frac{1}{CinX6}$	0	$-\frac{1}{Cin}(\frac{1}{X5} + \frac{1}{X6} + \frac{6}{Rwin})$
Qcool	0	$\frac{1}{X5}$	$\frac{1}{X6}$	0	$-(\frac{1}{X5} + \frac{1}{X6} + \frac{6}{Rwin} + partitions)$

Table 4.11: Input matrix for Thermal Zone C

Zone C	Tamb	TsN	Qconv	Qsys	Qr
T1	0	$\frac{1}{X2X1}$	0	0	0
T2	0	0	0	0	0
T3	0	0	0	0	$\frac{1}{X7}$
T4	0	0	0	0	$\frac{1}{X9}$
Tin	$\frac{6}{CinRwin}$	0	$\frac{1}{Cin}$	$-\frac{1}{Cin}$	0
Qcool	$\frac{6}{Rwin}$	0	1	0	0

Note: X values are the R-C parameters. Partitions involve sets of 3R2C for each adjacent thermal zone.

4.3.4 Thermal zone D

The thermal interactions between the zone temperature node, envelope, and internal mass are shown in Figure 4.10 and Tables 4.12 to 4.13. For clarity, the partitions' RC parameters are not fully shown in the representation.

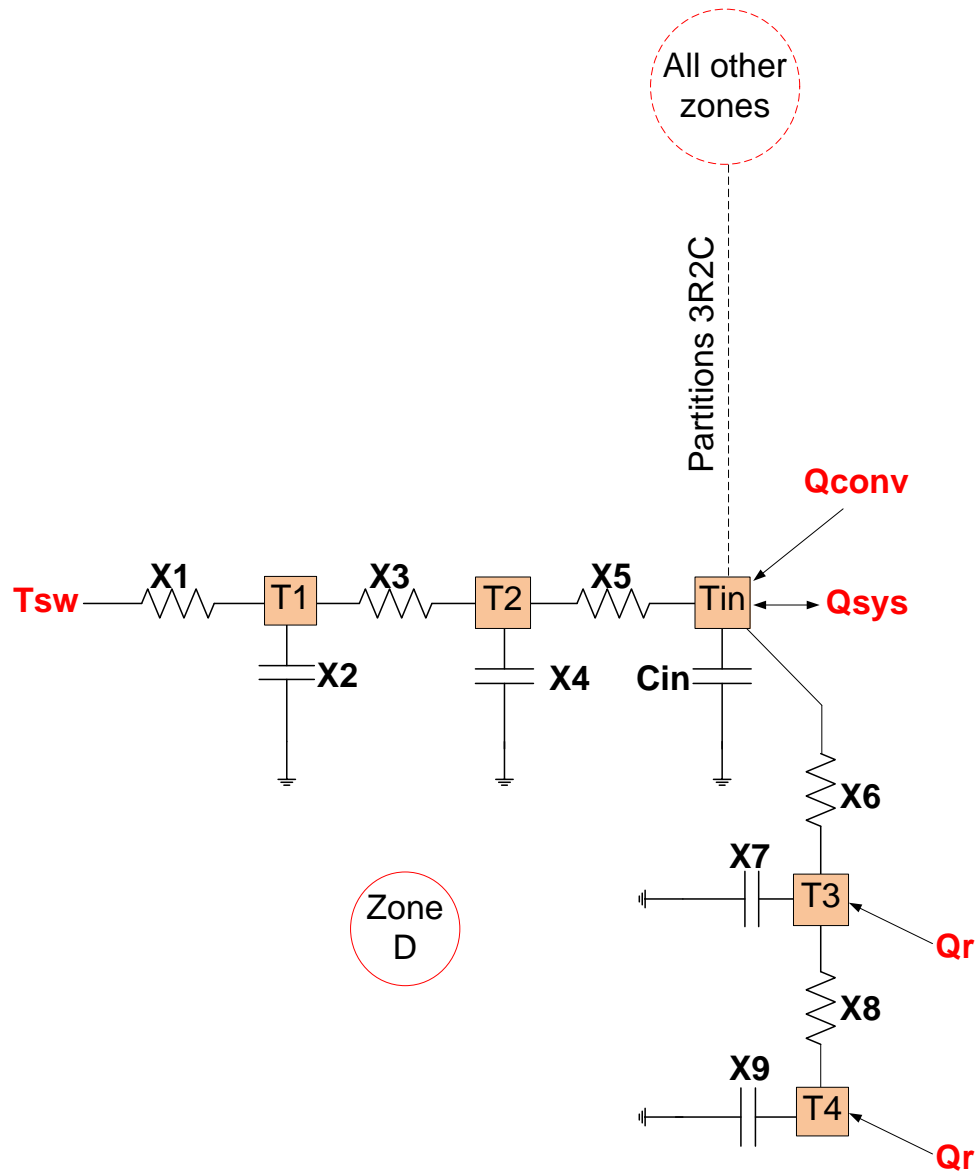


Figure 4.10: Thermal network representation for Zone D

Table 4.12: State space matrix for Thermal Zone D (Q_{cool} is the cooling load)

Zone D	T1	T2	T3	T4	Tin
T1	$-\frac{1}{X2}(\frac{1}{X1} + \frac{1}{X3})$	$\frac{1}{X2X3}$	0	0	0
T2	$\frac{1}{X4X3}$	$-\frac{1}{X4}(\frac{1}{X3} + \frac{1}{X5})$	0	0	$\frac{1}{X4X5}$
T3	0	0	$-\frac{1}{X7}(\frac{1}{X6} + \frac{1}{X8})$	$\frac{1}{X7X8}$	$\frac{1}{X7X6}$
T4	0	0	$\frac{1}{X9X8}$	$-\frac{1}{X9X8}$	
Tin	0	$\frac{1}{CinX5}$	$\frac{1}{CinX6}$	0	$-\frac{1}{Cin}(\frac{1}{X5} + \frac{1}{X6} + partitions)$
Qcool	0	$\frac{1}{X5}$	$\frac{1}{X6}$	0	$-(\frac{1}{X5} + \frac{1}{X6} + partitions)$

Table 4.13: Input matrix for Thermal Zone D

Zone D	TsW	Qconv	Qsys	Qr
T1	$\frac{1}{X2X1}$	0	0	0
T2	0	0	0	0
T3	0	0	0	$\frac{1}{X7}$
T4	0	0	0	$\frac{1}{X9}$
Tin	0	$\frac{1}{Cin}$	$-\frac{1}{Cin}$	0
Qcool	0	1	0	0

Note: X values are the R-C parameters. Partitions involve sets of 3R2C for each adjacent thermal zone.

4.3.5 Thermal zone E

The thermal interactions between the zone temperature node, envelope, and internal mass are shown in Figure 4.11 and Tables 4.14 to 4.15. For clarity, the partitions' RC parameters are not fully shown in the representation.

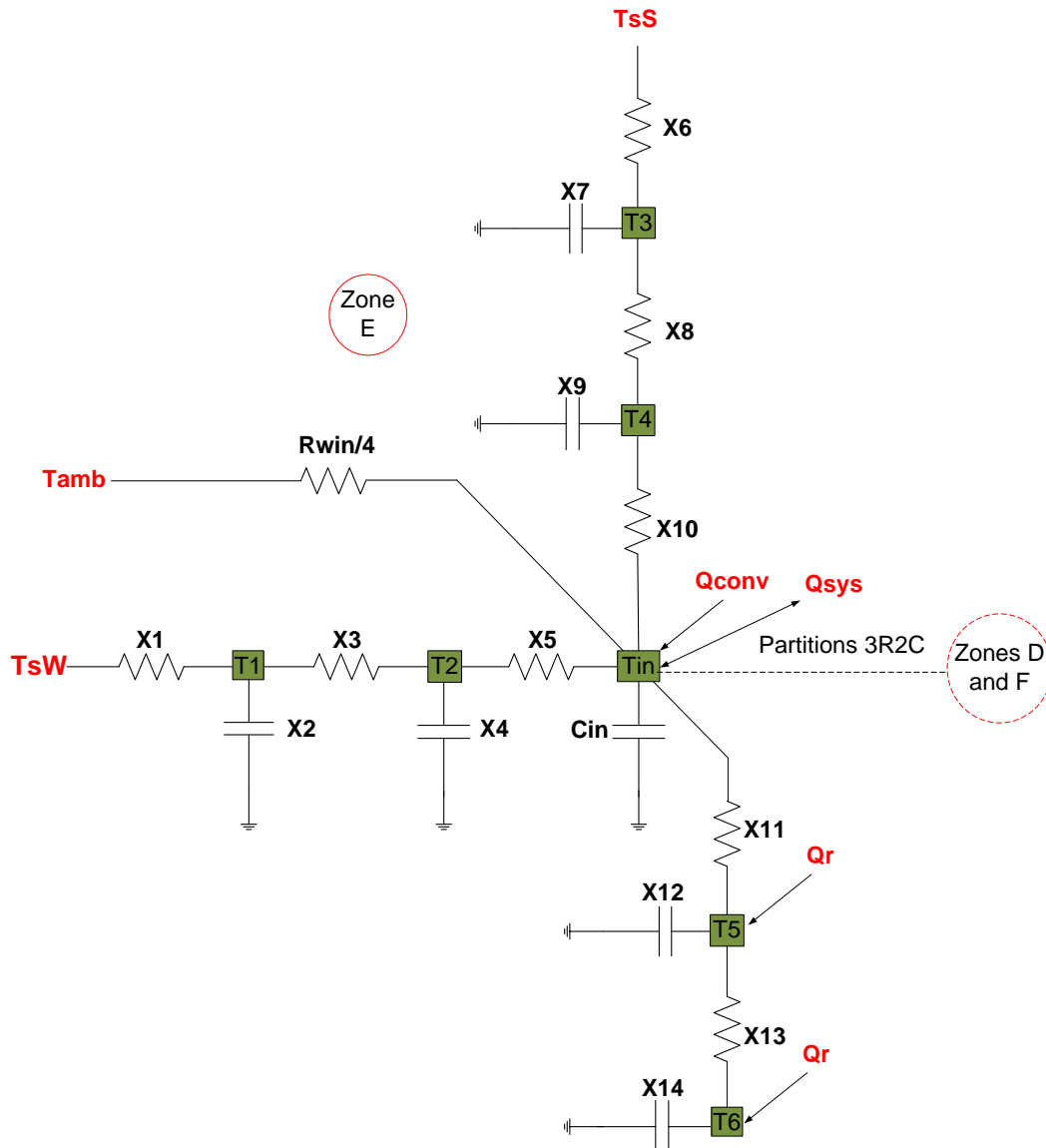


Figure 4.11: Thermal network representation for Zone E

Table 4.14: State space matrix for Thermal Zone E (Q_{cool} is the cooling load)

Zone E	T1	T2	T3	T4	T5	T6	Tin
T1	$-\frac{1}{X2}(\frac{1}{X1} + \frac{1}{X3})$	$\frac{1}{X2X3}$	0	0	0	0	0
T2	$\frac{1}{X4X3}$	$-\frac{1}{X4}(\frac{1}{X3} + \frac{1}{X5})$	0	0	0	0	$\frac{1}{X4X5}$
T3	0	0	$-\frac{1}{X7}(\frac{1}{X6} + \frac{1}{X8})$	$\frac{1}{X7X8}$	0	0	0
T4	0	0	$\frac{1}{X9X8}$	$-\frac{1}{X9}(\frac{1}{X8} + \frac{1}{X10})$	0	0	$\frac{1}{X9X10}$
T5	0	0	0	0	$-\frac{1}{X12}(\frac{1}{X11} + \frac{1}{X13})$	$\frac{1}{X12X13}$	$\frac{1}{X12X11}$
T6	0	0	0	0	$\frac{1}{X14X13}$	$-\frac{1}{X14X13}$	0
Tin	0	$\frac{1}{CinX5}$	0	$\frac{1}{CinX10}$	$\frac{1}{CinX11}$	0	$-\frac{1}{Cin}(\frac{1}{X5} + \frac{1}{X10} + \frac{1}{X11} + \frac{1}{4} + \frac{1}{Rwin} + partitions)$
Qcool	0	$\frac{1}{X5}$	0	$\frac{1}{X10}$	$\frac{1}{X11}$	0	$-\left(\frac{1}{X5} + \frac{1}{X10} + \frac{1}{X11} + \frac{1}{4} + \frac{1}{Rwin} + partitions\right)$

Table 4.15: Input matrix for Thermal Zone E

Zone E	T_{amb}	T_{sS}	T_{sW}	Q_{conv}	Q_{sys}	Q_r
T1	0	0	$\frac{1}{X2X1}$	0	0	0
T2	0	0	0	0	0	0
T3	0	$\frac{1}{X7X6}$	0	0	0	0
T4	0	0	0	0	0	0
T5	0	0	0	0		$\frac{1}{X12}$
T6	0	0	0	0	0	$\frac{1}{X14}$
Tin	$\frac{4}{CinRwin}$		0	$\frac{1}{Cin}$	$-\frac{1}{Cin}$	0
Qcool	$\frac{4}{Rwin}$	0	0	1	0	0

Note: X values are the R-C parameters. Partitions involve sets of 3R2C for each adjacent thermal zone.

4.3.6 Thermal zone F

The thermal interactions between the zone temperature node, envelope, and internal mass are shown in Figure 4.12 and Tables 4.16 to 4.17. For clarity, the partitions' RC parameters are not fully shown in the representation.

Table 4.16: Input matrix for Thermal Zone F

Zone F	T_{amb}	T_{sW}	Q_{conv}	Q_{sys}	Q_r
T1	0	$\frac{1}{X2X1}$	0	0	0
T2	0	0	0	0	0
T3	0	0	0	0	$\frac{1}{X7}$
T4	0	0	0	0	$\frac{1}{X9}$
Tin	$\frac{2}{CinRwin}$	0	$\frac{1}{Cin}$	$-\frac{1}{Cin}$	0
Qcool	$\frac{2}{Rwin}$	0	1	0	0

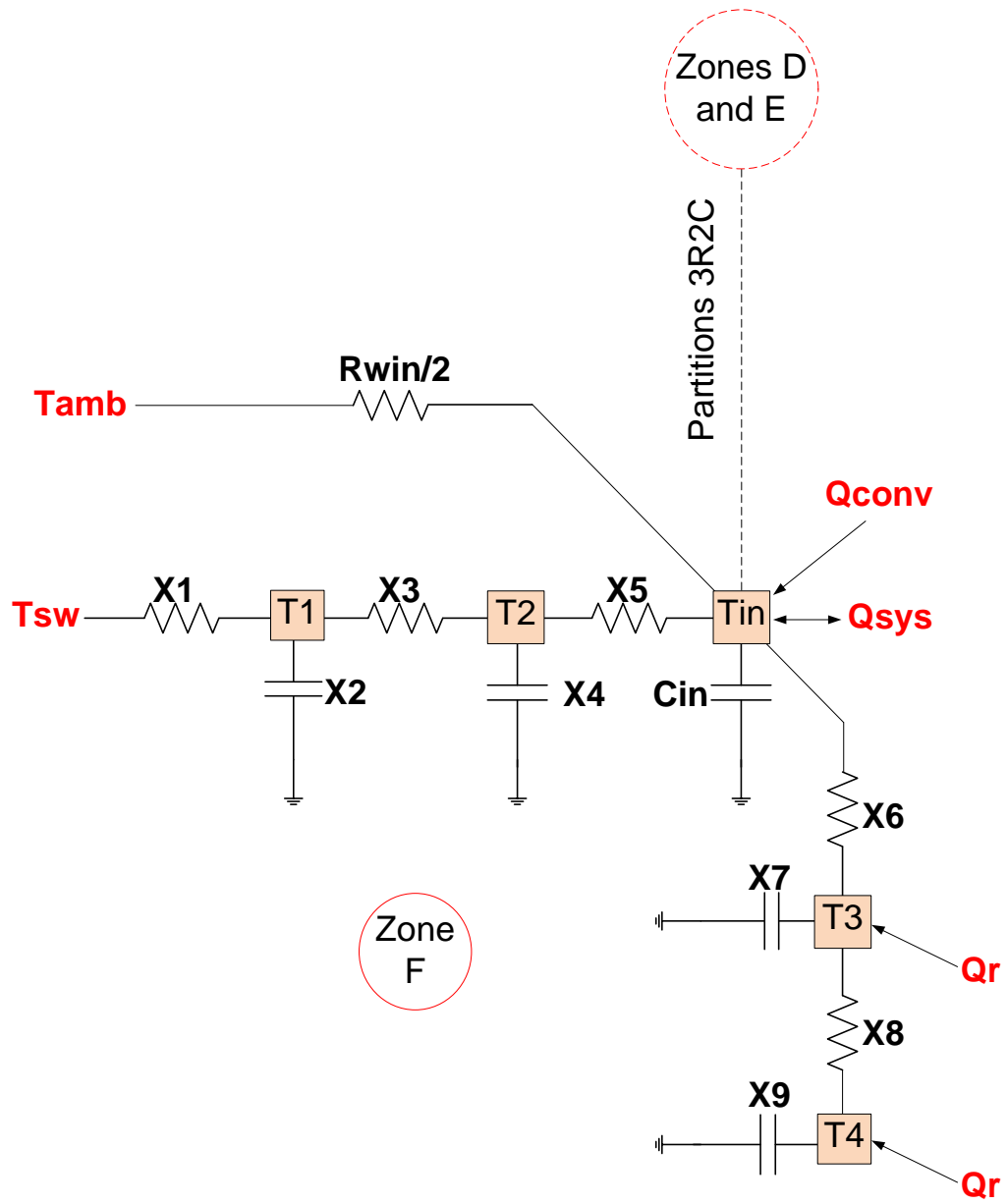


Figure 4.12: Thermal network representation for Zone F

Table 4.17: State space matrix for Thermal Zone F (Q_{cool} is the cooling load)

Zone	$T1$	$T2$	$T3$	$T4$	T_{in}
F8					
T1	$-\frac{1}{X2}(\frac{1}{X1} + \frac{1}{X3})$	$\frac{1}{X2X3}$	0	0	0
T2	$\frac{1}{X4X3}$	$-\frac{1}{X4}(\frac{1}{X3} + \frac{1}{X5})$	0	0	$\frac{1}{X4X5}$
T3	0	0	$-\frac{1}{X7}(\frac{1}{X6} + \frac{1}{X8})$	$\frac{1}{X7X8}$	$\frac{1}{X7X6}$
T4	0	0	$\frac{1}{X9X8}$	$-\frac{1}{X9X8}$	0
T_{in}	0	$\frac{1}{CinX5}$	$\frac{1}{CinX6}$	0	$-\frac{1}{Cin}(\frac{1}{X5} + \frac{1}{X6} + \frac{2}{Rwin} + partitions)$
Q_{cool}	0	$\frac{1}{X5}$	$\frac{1}{X6}$	0	$-(\frac{1}{X5} + \frac{1}{X6} + \frac{2}{Rwin} + partitions)$

Note: X values are the R-C parameters. Partitions involve sets of 3R2C for each adjacent thermal zone.

4.3.7 Thermal zone G

The thermal interactions between the zone temperature node, envelope, and internal mass are shown in Figure 4.13 and Tables 4.18 to 4.19. For clarity, the partitions' RC parameters are not fully shown in the representation.

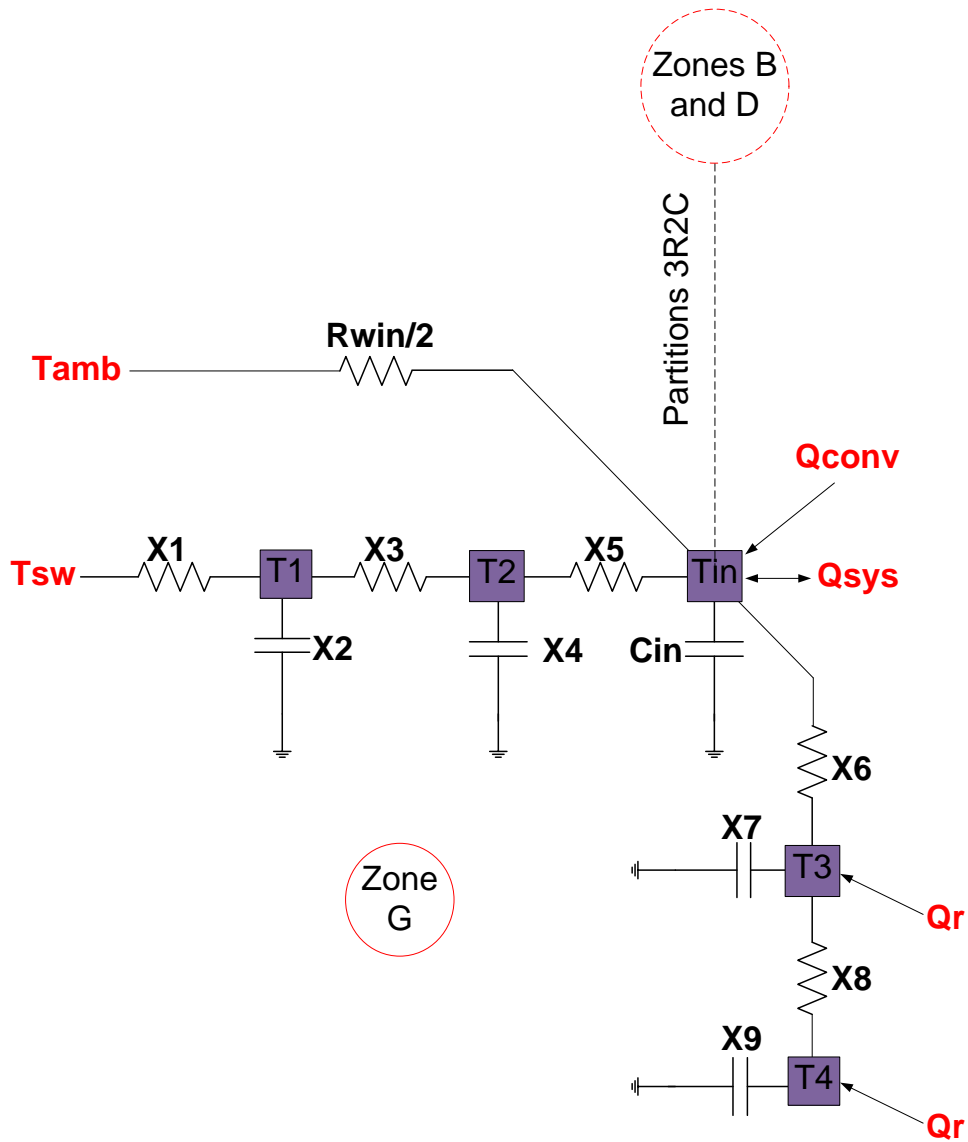


Figure 4.13: Thermal network representation for Zone G

Table 4.18: State space matrix for Thermal Zone G (Q_{cool} is the cooling load)

Zone G	T1	T2	T3	T4	Tin
T1	$-\frac{1}{X2}(\frac{1}{X1} + \frac{1}{X3})$	$\frac{1}{X2X3}$	0	0	0
T2	$\frac{1}{X4X3}$	$-\frac{1}{X4}(\frac{1}{X3} + \frac{1}{X5})$	0	0	$\frac{1}{X4X5}$
T3	0	0	$-\frac{1}{X7}(\frac{1}{X6} + \frac{1}{X8})$	$\frac{1}{X7X8}$	$\frac{1}{X7X6}$
T4	0	0	$\frac{1}{X9X8}$	$-\frac{1}{X9X8}$	0
Tin	0	$\frac{1}{CinX5}$	$\frac{1}{CinX5}$		$-\frac{1}{Cin}(\frac{1}{X5} + \frac{1}{X6} + \frac{2}{Rwin} + partitions)$
Qcool	0	$\frac{1}{X5}$	$\frac{1}{X6}$		$-\left(\frac{1}{X5} + \frac{1}{X6} + \frac{2}{Rwin} + partitions\right)$

Table 4.19: Input matrix for Thermal Zone G

Zone G	Tamb	TsW	Qconv	Qsys	Qr
T1	0	$\frac{1}{X2X1}$	0	0	0
T2	0	0	0	0	0
T3	0	0	0	0	$\frac{1}{X7}$
T4	0	0	0	0	$\frac{1}{X9}$
Tin	$\frac{2}{CinRwin}$	0	$\frac{1}{Cin}$	$-\frac{1}{Cin}$	0
Qcool	$\frac{2}{Rwin}$	0	1	0	0

Note: X values are the R-C parameters. Partitions involve sets of 3R2C for each adjacent thermal zone.

4.4 Results

This section presents results of the thermal network prediction of zone temperature as compared with measurements. The measurement periods were randomly selected to cover summer (August and September) operations. The building load model was also validated for winter operation, and the results are presented below.

Figures 4.14, 4.15 and 4.16 shows predicted zone temperature for thermal Zone A for August 2015, September 2015, and February 2016 respectively. It could be seen that the predicted room temperature agrees and trends well with the measured value (MBE and CVRMSE both less than 3.5%), despite the fluctuations in ambient temperature. Particularly, the fluctuations in zone temperature were well captured by the thermal model for both summer and winter cases.

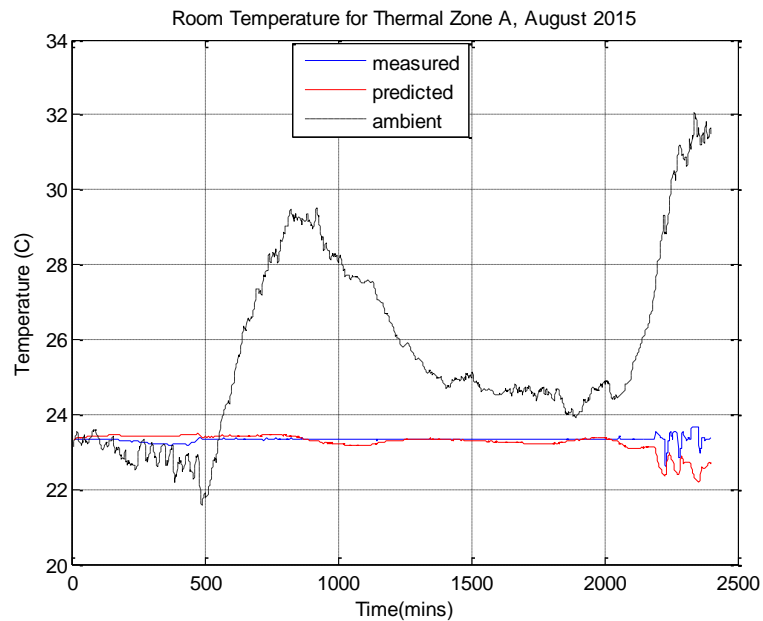


Figure 4.14: Room Temperature predictions for Zone A – August 2015

(ME = -0.0664°C , MAE = 0.1554°C , MBE = -0.2845% , CVRMSE = 1.1516%)

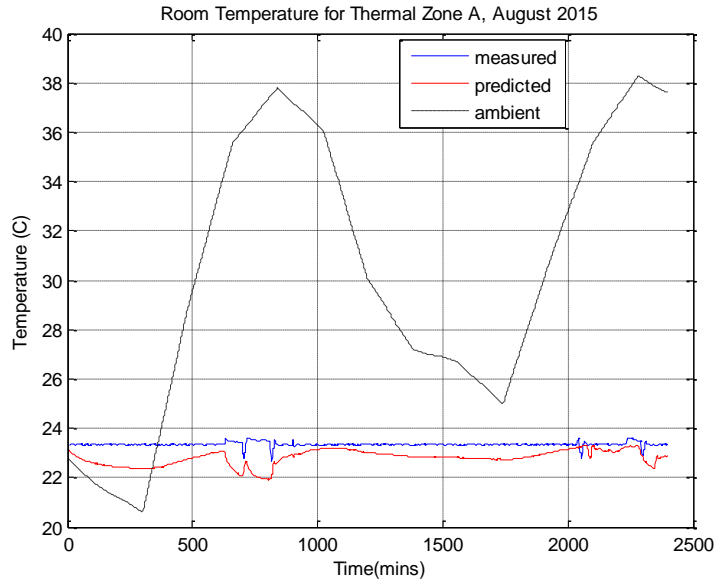


Figure 4.15: Room Temperature predictions for Zone A – August 2015

(ME = -0.5395°C , MAE = 0.5424°C , MBE= -2.3107% , CVRMSE = 2.6848%)

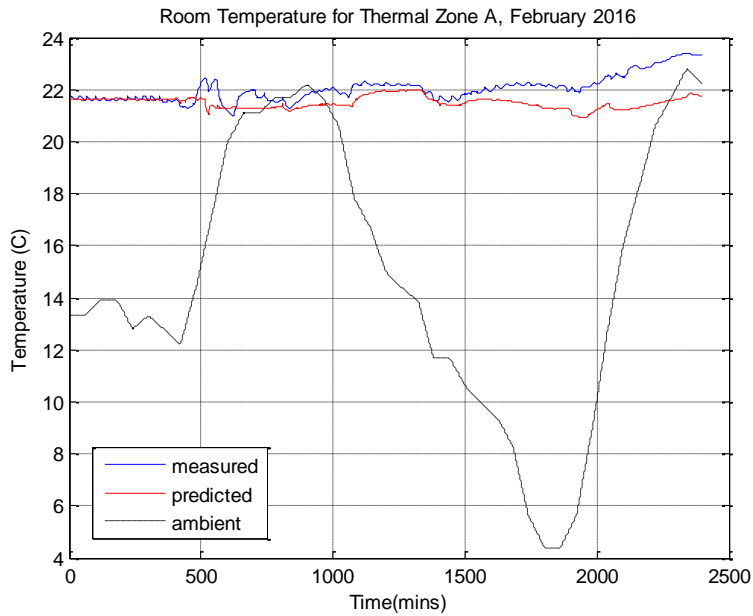


Figure 4.16: Room Temperature predictions for Zone A – February 2016

(ME = -0.5362°C , MAE = 0.5645°C , MBE= -2.4337% , CVRMSE= 3.3993)

However, the model accuracy is much higher for cooling periods (August and September 2015) than for the winter period (February 2016), as could be seen in Figure

4.16. This observation is in agreement with previous results for a single thermal zone which was presented in Section 4.2.4.

Figure 4.17 shows the predicted room temperature of thermal Zone B for August 2015. The room temperature predicted by the model trends well with the measured value, but the error was slightly higher (CVRMSE=4.1%) than the values for Thermal Zone A.

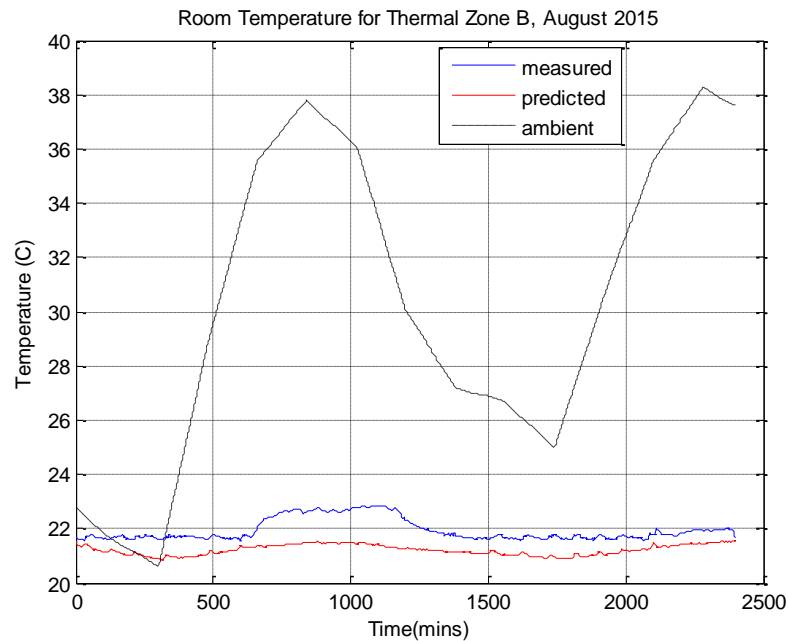


Figure 4.17: Room Temperature predictions for Zone B – August 2015

(ME = -0.7353°C, MAE = 0.7353°C, MBE= -3.3508%, CVRMSE = 4.1193%)

The increased deviation could be attributed to the way Thermal Zone B was grouped together during the simulation. Unlike the other thermal zones, Thermal Zone B is made up of rooms that are not physically adjacent to one another. In grouping the rooms and treating them as a single zone, it is assumed that they all have a uniform temperature. The predicted temperature was only compared with the measured temperature at the room where the sensor is located. In reality, the actual temperature in the different

rooms that make up Zone B may differ by a few degrees, based on their thermal interactions with adjacent thermal zones. Despite the issues above, the thermal network model predicted the temperature with less than 4.2% MBE and CVRMSE. This is very acceptable for minute-by-minute simulation. Figure 4.18 show the predicted room temperature of thermal Zone C for August 2015.

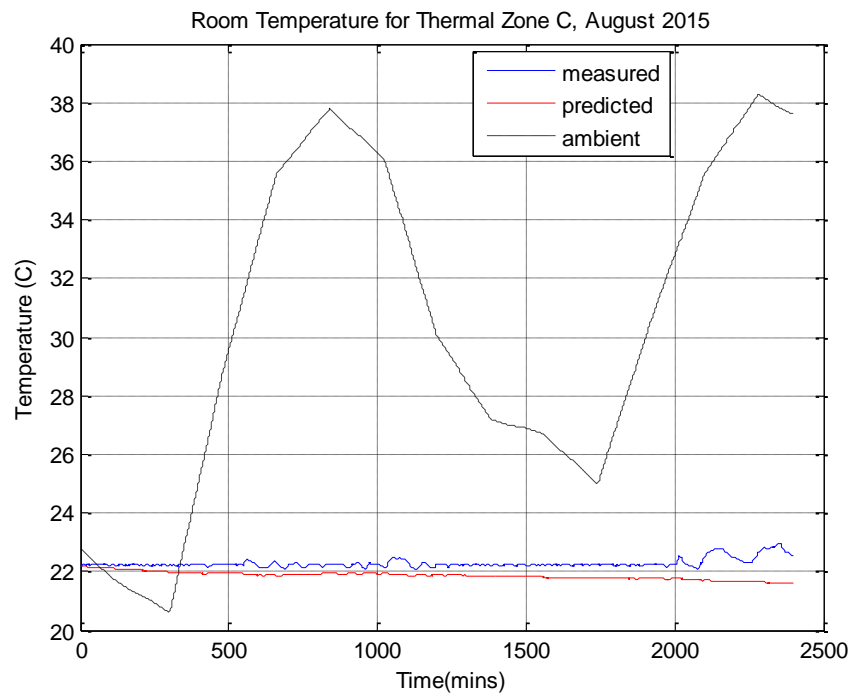


Figure 4.18: Room Temperature predictions for Zone C – August 2015

(ME = -0.4296°C, MAE = 0.4296°C, MBE = -1.9281%, CVRMSE= 3.0054%)

The room temperature predicted by the model trends well with the measured value. For this particular zone, the slight fluctuations in the room temperature were not captured in the predicted values. The thermal network model consistently under-predicted the measured room temperature by around 0.43°C, as could be seen in the values of Mean Error (ME) and Mean Absolute Error (MAE). The assumed occupancy patterns and

internal loads may have contributed to the consistent under-prediction. If a slightly higher internal load density was assumed, the predicted temperature would be higher.

Figures 4.19, 4.20 and 4.21 show predicted zone temperature of thermal Zone D for August 2015, September 2015, and February 2016 respectively. The thermal network model demonstrated very good predictions and accuracy for Thermal Zone D. Both summer and winter validations show MBE and CVRMSE of less than 2.6%. It is interesting to see that the temperature predictions for February 2016 capture all the fluctuations in zone temperature for the entire simulation period. This demonstrates that the thermal network model could also have very good accuracy for winter period. The difference between this thermal zone and others is its lack of direct coupling to ambient through windows. Figure 4.22 show predicted zone temperature of thermal Zone E for August 2015. As shown in Figure 4.22, the thermal network model predictions are near-perfect for the entire simulation period, with MBE of $< 1\%$. Figure 4.23 shows predicted zone temperature of thermal Zone F for August 2015. As shown in Figure 4.23, the thermal network model temperature predictions are within 2.3% CVRMSE as compared with the measured room temperature. Thermal Zone F was the single zone case study of Section 4.2, where the cooling load CVRMSE was about 14%.

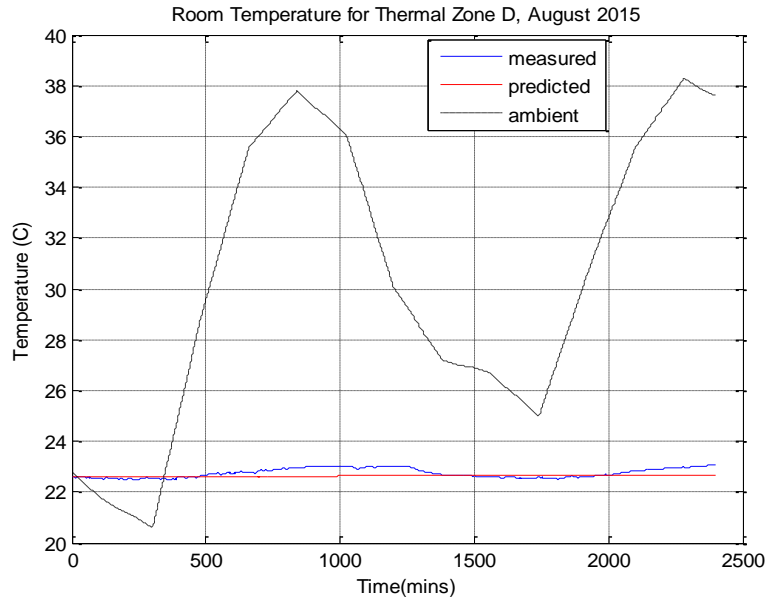


Figure 4.19: Room Temperature predictions for Zone D – August 2015

(ME = -0.1279°C , MAE = 0.1788°C , MBE= -0.5623% , CVRMSE = 2.2789%)

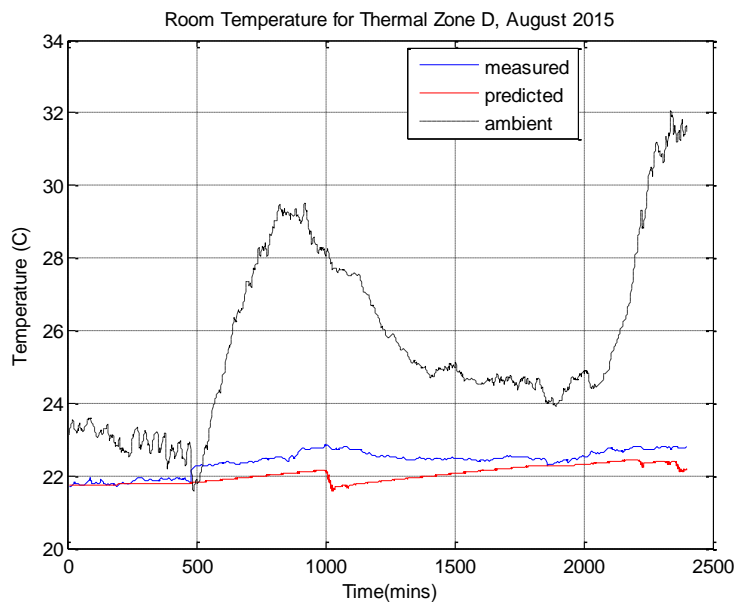


Figure 4.20: Room Temperature predictions for Zone D – August 2015

(ME = -0.3843°C , MAE = 0.3855°C , MBE= -1.7152% , CVRMSE = 2.8902%)

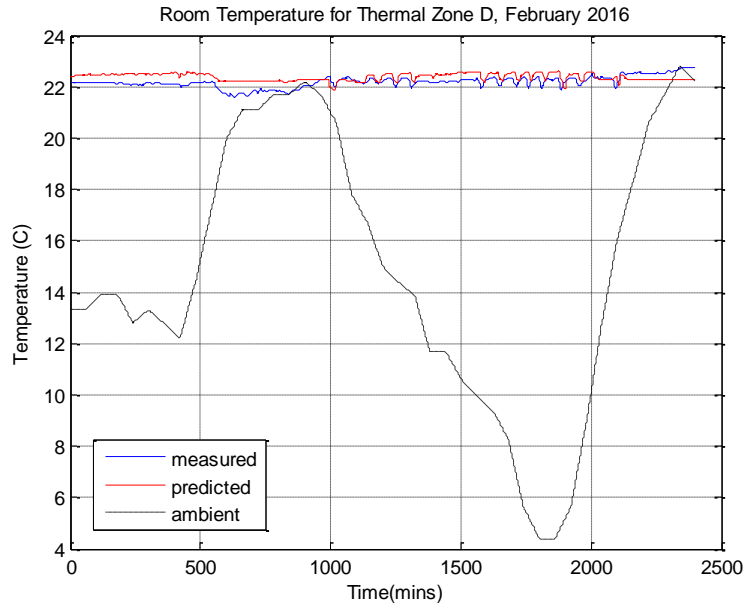


Figure 4.21: Room Temperature predictions for Zone D – February 2016

(ME = 0.1853°C, MAE = 0.2873°C, MBE = 0.8355%, CVRMSE = 2.5207%)

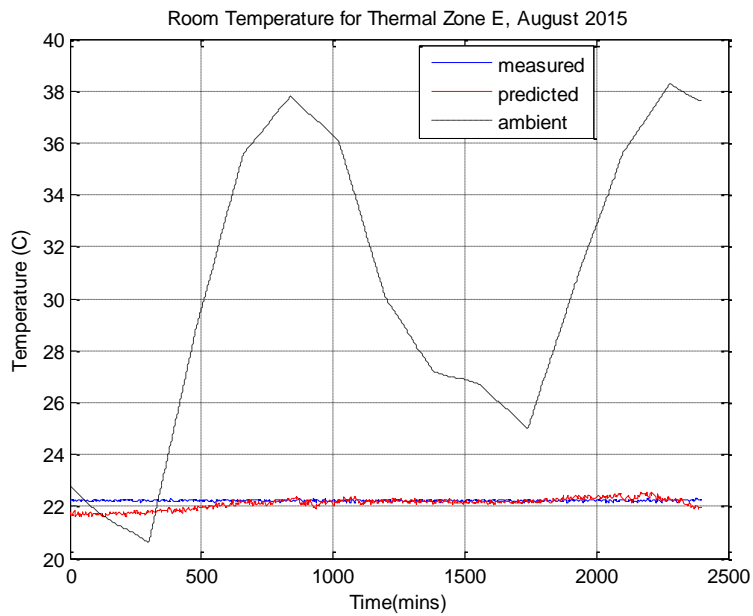


Figure 4.22: Room Temperature predictions for Zone E – August 2015

(ME = -0.1219°C, MAE = 0.1818°C, MBE = -0.5483%, CVRMSE = 2.3161%)

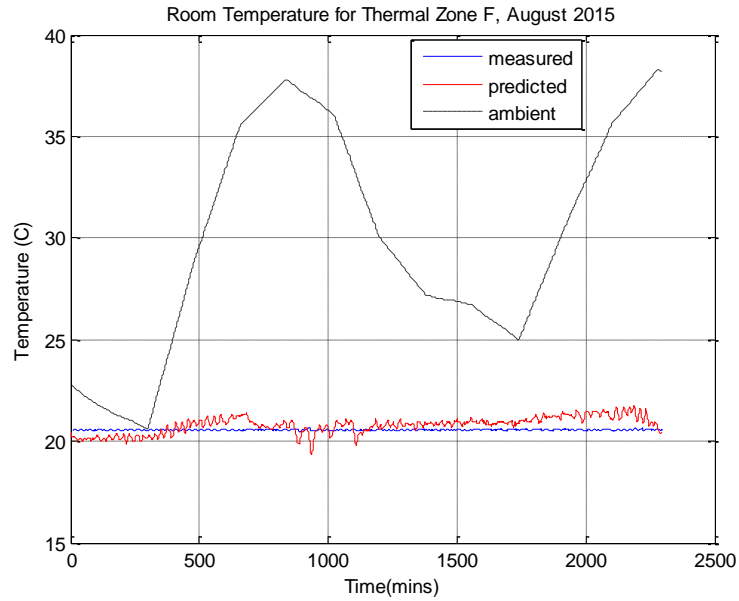


Figure 4.23: Room Temperature predictions for Zone F – August 2015

(ME =0.2336°C, MAE =0.4070°C, MBE =1.1362%, CVRMSE = 2.2974%)

Unlike the single zone case study which only considered heat transfer on the west-exposed wall, the multiple zone case shown in Figure 4.23 considered thermal interactions with adjacent zones and heat transfer in all directions (except roof and ground).

Figures 4.24 and 4.25 show predicted zone temperature of thermal Zone G for August 2015 and February 2016 respectively. The thermal network model demonstrated very good predictions and accuracy for this thermal zone, as seen by its ability to track very minor fluctuations in room temperature. As shown in Figure 4.25, the winter season predicted temperature trends well with the measured value, particularly where there are fluctuations in the room temperature.

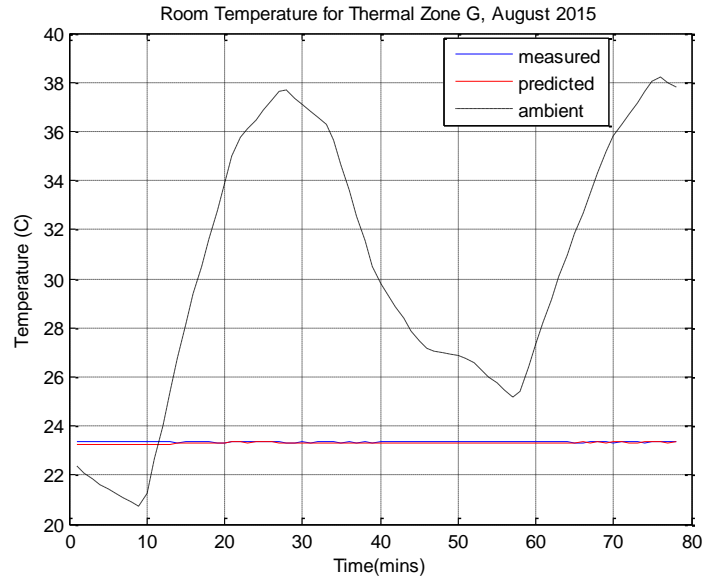


Figure 4.24: Room Temperature predictions for Zone G – August 2015

(ME = -0.0417°C, MAE = 0.0452°C, MBE = -0.1788%, CVRMSE = 0.2268%)

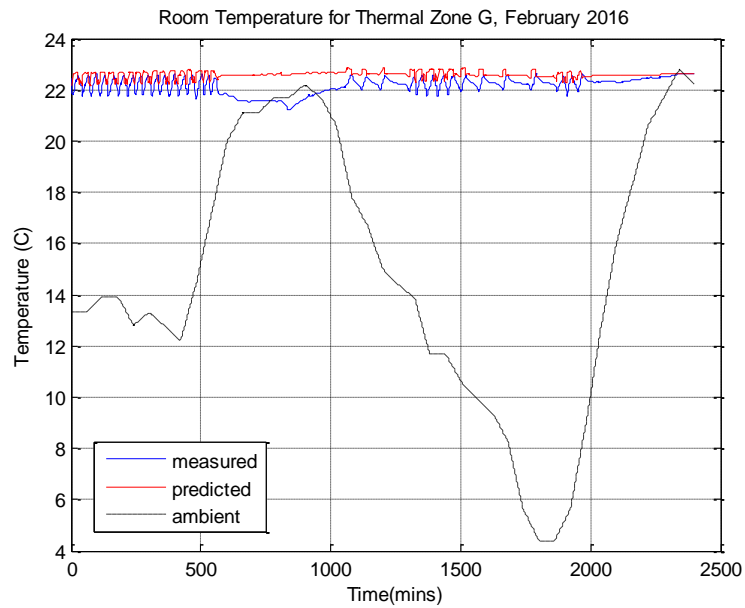


Figure 4.25: Room Temperature predictions for Zone G – February 2016

(ME = 0.4219°C, MAE = 0.4550°C, MBE = 1.9036%, CVRMSE = 3.2431%)

The largest model errors were recorded around the hour of the day where peak ambient temperature occurs. The observation is similar to that of thermal zones D, E,

and F. However, the CVRMSE was less than 3.3% for both summer (August 2015) and winter (February 2016) validation.

4.4.1 Summary of cooling load results

Table 4.20 shows summary of the temperature results for the different thermal zones and cases considered. As could be seen, the temperature is predicted accurately within a consistent error of less than 4.2% for both summer and winter cases. The few winter cases were used as a proof of concept to see how the thermal network model performs for winter season. This study focuses on the summer operation.

Table 4.20: Summary of Temperature results for all thermal zones

<i>Thermal Zones</i>	Summer - August 2015				Winter - February 2016			
	ME (°C)	MAE (°C)	MBE (%)	CV RMSE (%)	ME (°C)	MAE (°C)	MBE (%)	CV RMSE (%)
A	-0.066	0.155	-0.285	1.15	-0.536	0.565	-2.434	3.400
B	-0.735	0.735	-3.351	4.12	-	-	-	-
C	-0.430	0.430	-1.928	3.01	-	-	-	-
D	-0.128	0.179	-0.562	2.28	0.185	0.287	0.836	2.521
E	-0.035	0.200	-0.158	2.33	-	-	-	-
F	-0.403	0.439	-1.958	3.395	-	-	-	-
G	-0.231	0.231	-0.989	2.269	0.422	0.455	1.904	3.243

Overall, the thermal model predictions are generally more accurate for summer period operation. Similarly, the thermal model performed better for unoccupied period temperature and cooling load simulations, due to near accurate assumption of internal load profiles and occupancy. Therefore, a common source of model error could be in the assumed occupancy schedules and internal loads. Though typical office schedule was assumed, and the internal load density was selected based on ASHRAE recommendations for office and institutional buildings, the actual occupancy and internal load profiles may differ from the assumed values. This may have contributed to

the slight under-prediction of temperature which was observed for most thermal zones, particularly during peak periods.

4.5 Fan-motor model Validation

This section presents the results of fan power and speed predicted by the chosen fan model, as compared with actual measurement. The case study fan is a 3HP forward curved fan. The inputs to the steady state fan model are the airflow and fan static head. The fan static pressure is reset based on total flow rate. The comparison of model predicted static pressure, and the measured value is shown in Appendix B. The training period data included random fan power, airflow, speed, and fan static head for June to July 2015. The data covered different ranges of operation of airflow and static heads. The validation period covered operating periods from August 2015 to February 2016. The results are shown in Figures 4.26 to 4.37. The predicted fan input power and speed trends well with the measured values, although there are occasional spikes in the predicted values. The fan input power profile varied greatly between months, as shown in Figures 4.26 to 4.37.

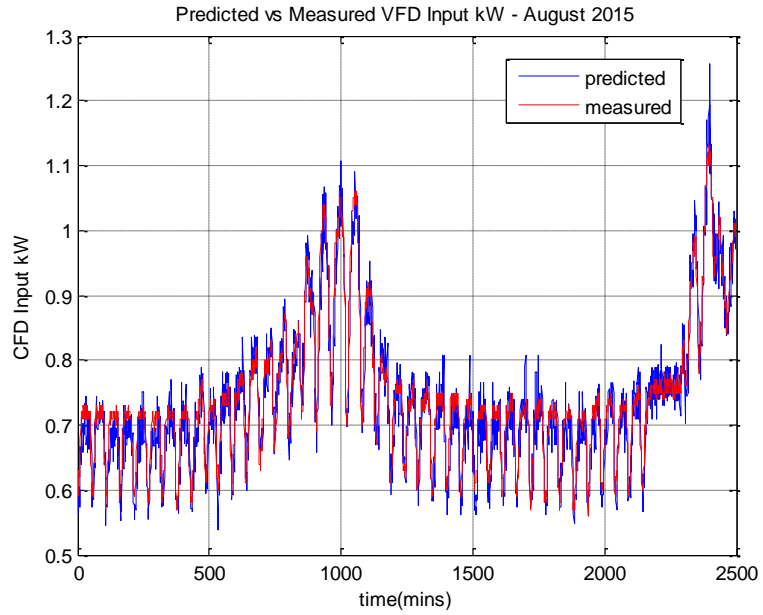


Figure 4.26: Predicted vs Measured Fan Input Power - August 2015

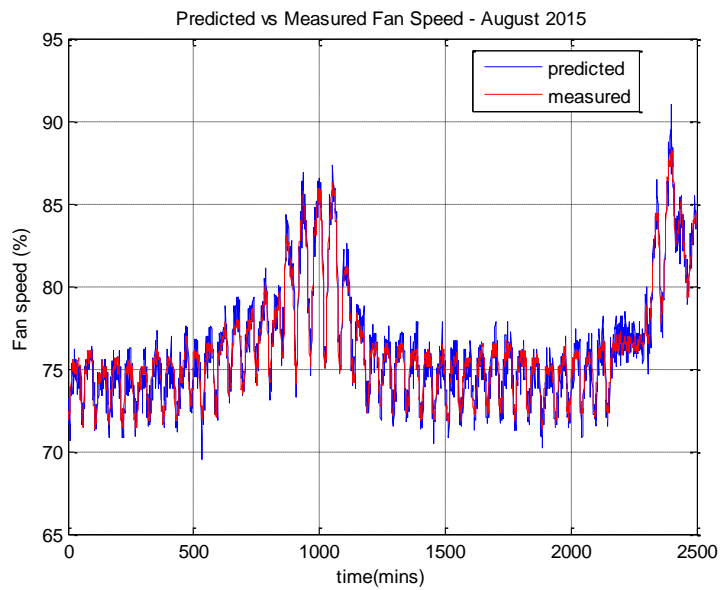


Figure 4.27: Predicted vs Measured Fan Speed - August 2015

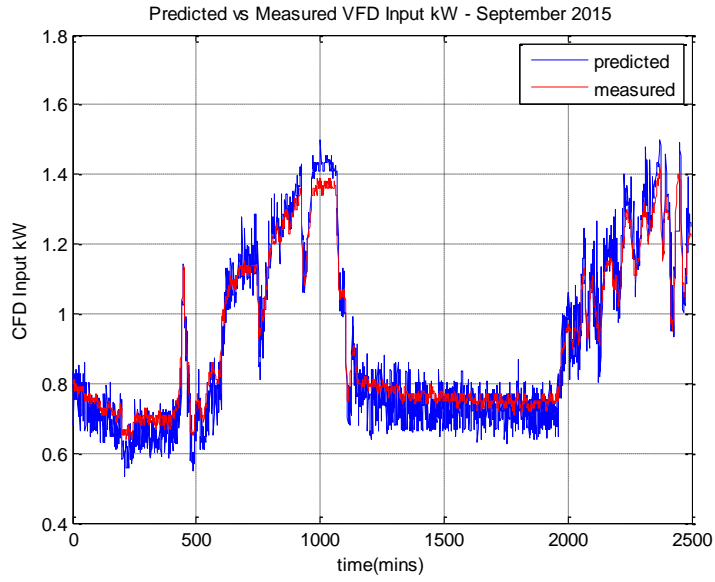


Figure 4.28: Predicted vs Measured Fan Input Power - September 2015

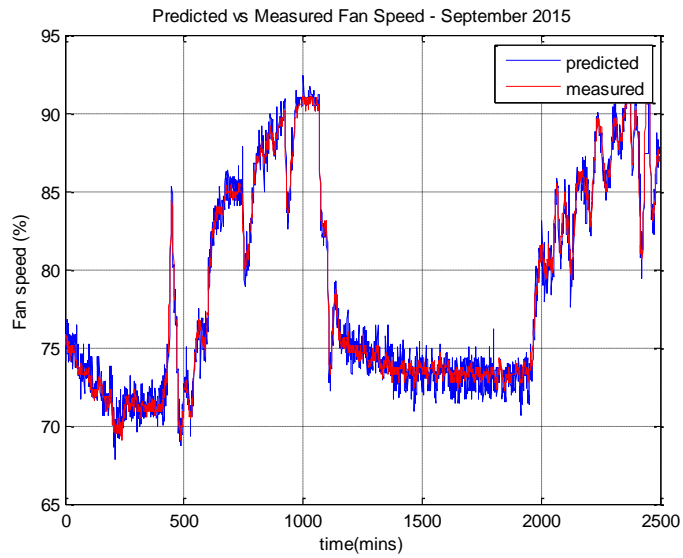


Figure 4.29: Predicted vs Measured Fan Speed - September 2015

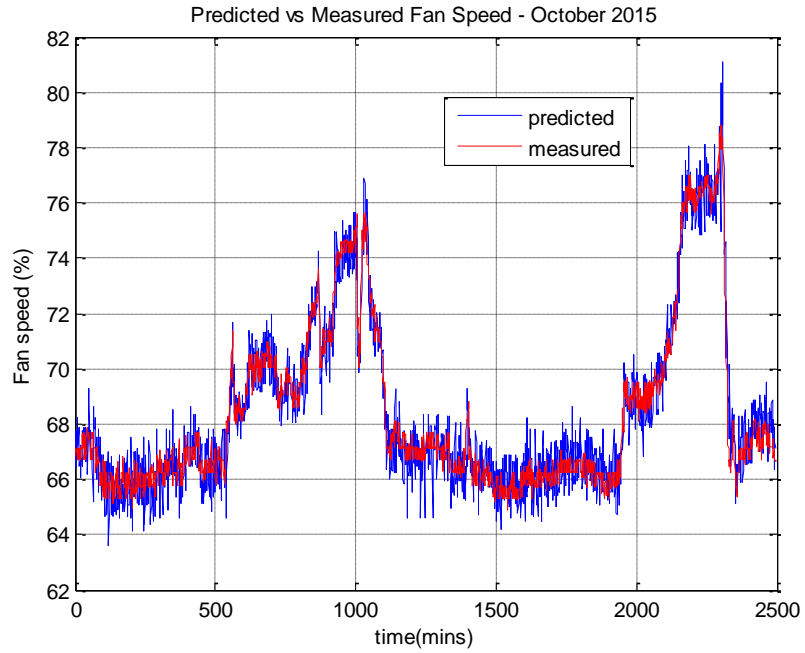


Figure 4.30: Predicted vs Measured Fan Input Power - October 2015

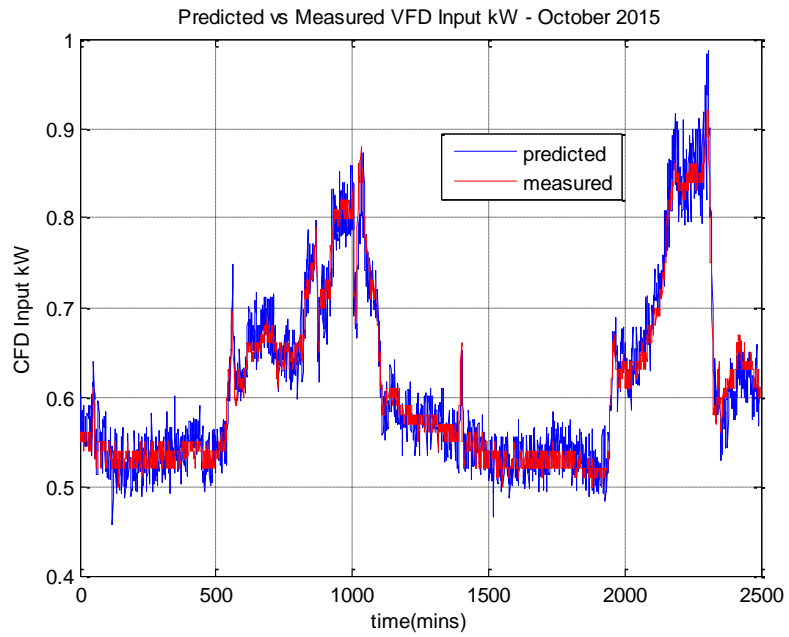


Figure 4.31: Predicted vs Measured Fan Speed - October 2015

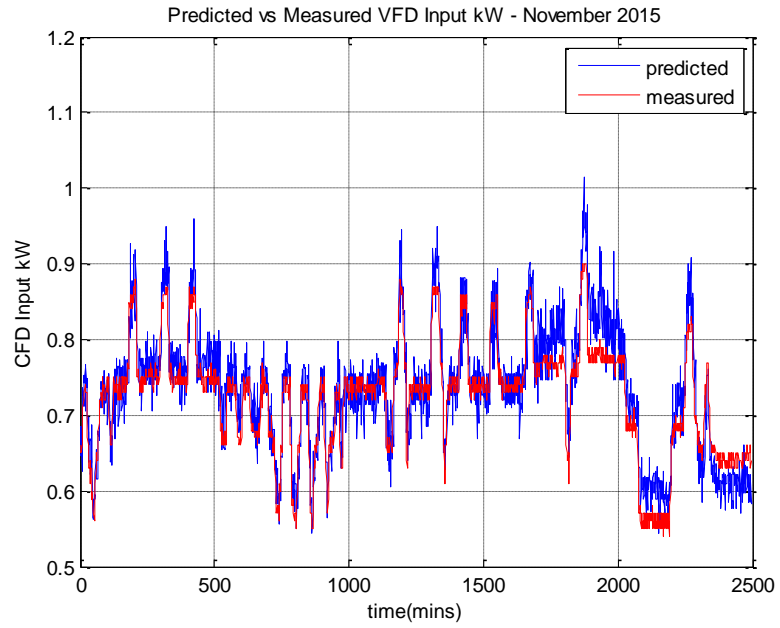


Figure 4.32: Predicted vs Measured Fan Input Power - November 2015

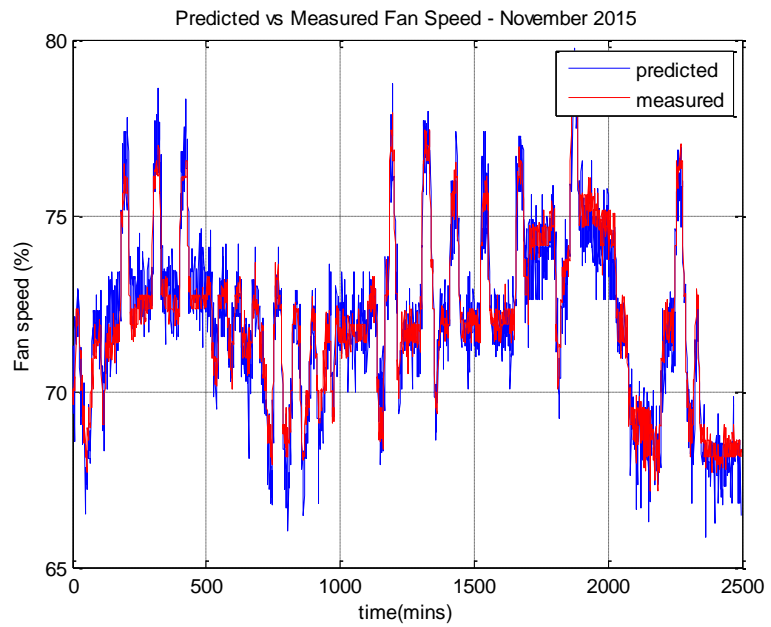


Figure 4.33: Predicted vs Measured Fan Speed - November 2015

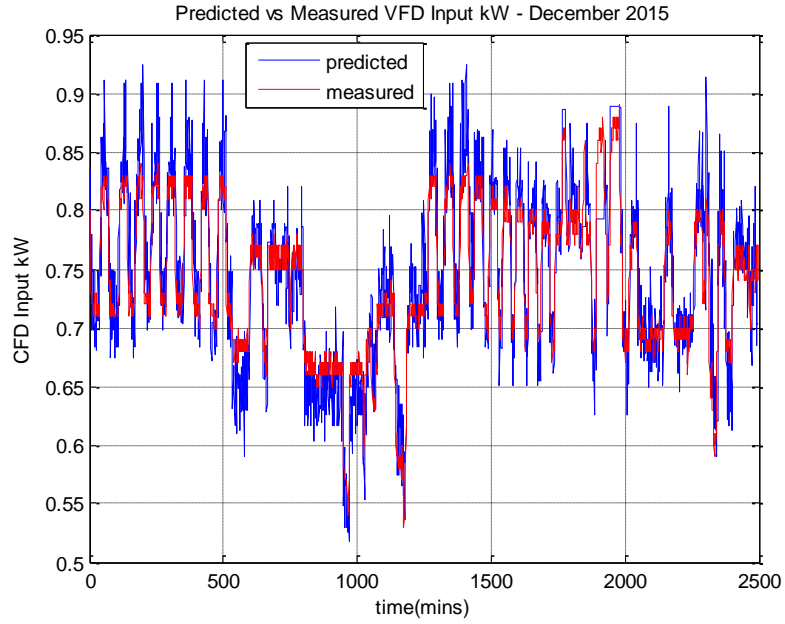


Figure 4.34: Predicted vs Measured Fan Input Power - December 2015

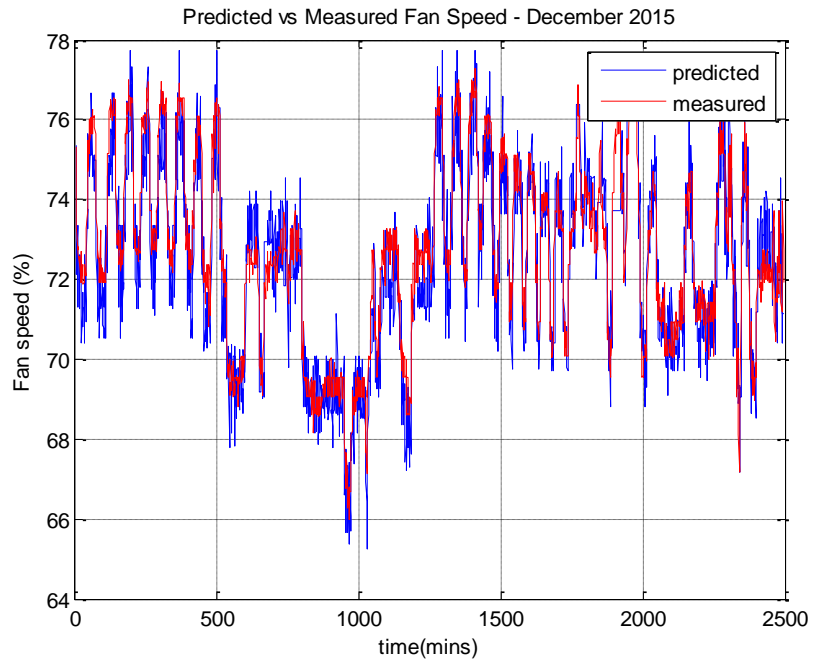


Figure 4.35: Predicted vs Measured Fan Speed - December 2015

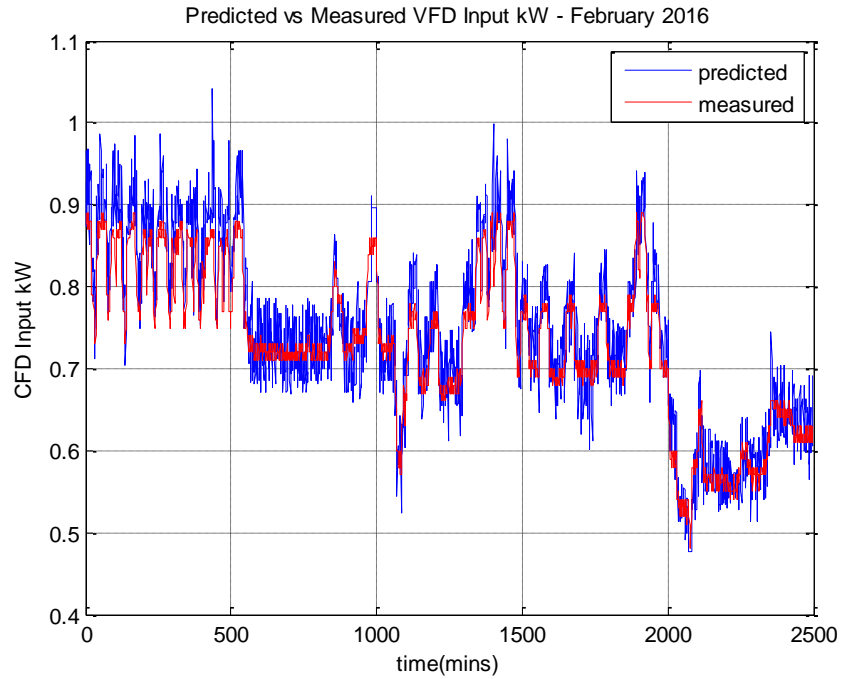


Figure 4.36: Predicted vs Measured Fan Input Power – February 2016

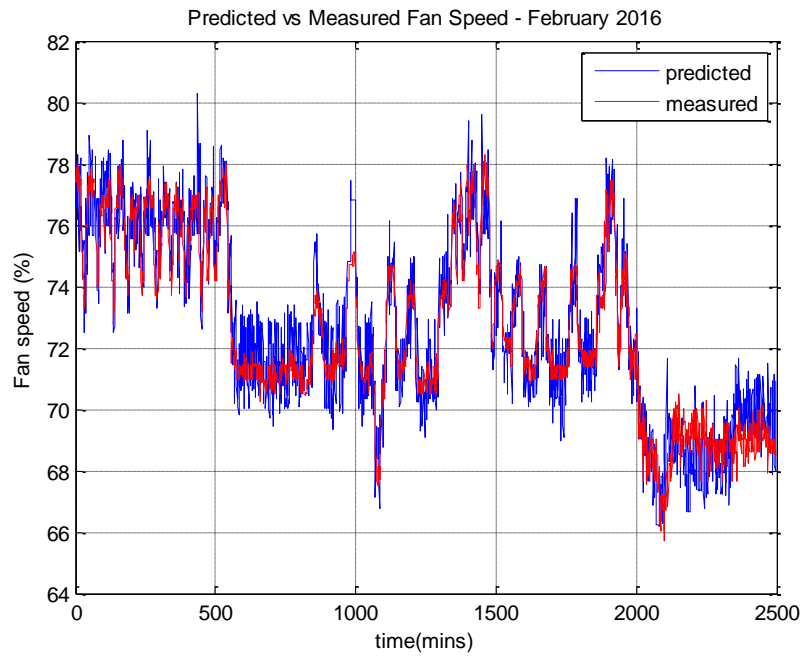


Figure 4.37: Predicted vs Measured Fan Speed – February 2016

4.5.1 Summary of fan input power predictions

Table 4.21 shows summary of the fan power predictions for the different month. As shown in Table 4.21, the steady state fan model was able to accurately estimate the fan input power to within 2.5% MBE. The cubic relationship between fan power and airflow implies that errors in the airflow calculation would get magnified. The highest error was observed for September prediction when the fan operated with the highest input power and at higher fan speeds as compared to the other months.

Table 4.21: Summary of fan-power predictions vs measurement

Validation month	ME (kW)	MAE(kW)	MBE (%)	CVRMSE (%)
August 2015	-0.007	0.024	0.890	3.976
September 2015	-0.009	0.047	0.979	6.344
October 2015	0.002	0.019	0.350	3.888
November 2015	0.012	0.028	1.649	4.765
December 2015	0.006	0.025	0.760	4.411
February 2016	0.018	0.032	2.432	5.371

4.5.2 Summary of fan speed predictions

The steady state fan model estimated the fan speed to within 1.4% CVRMSE. The high accuracy was very consistent across the different months simulated. The high accuracy in the fan speed predictions is due to direct correlation between airflow and speed.

Table 4.22: Summary of fan-speed predictions vs measurement

Validation month	ME (%)	MAE (%)	MBE (%)	CVRMSE (%)
August 2015	0.013	0.669	0.017	1.096
September 2015	-0.008	0.647	0.010	1.075
October 2015	0.043	0.600	0.063	1.110
November 2015	-0.072	0.648	0.100	1.143
December 2015	-0.219	0.746	-0.301	1.276
February 2016	0.075	0.810	0.103	1.403

4.6 Cooling Coil Validation

Figures 4.38 to 4.41 show the predicted leaving water and air temperatures vs measured values for Summer of 2015 (August and September).

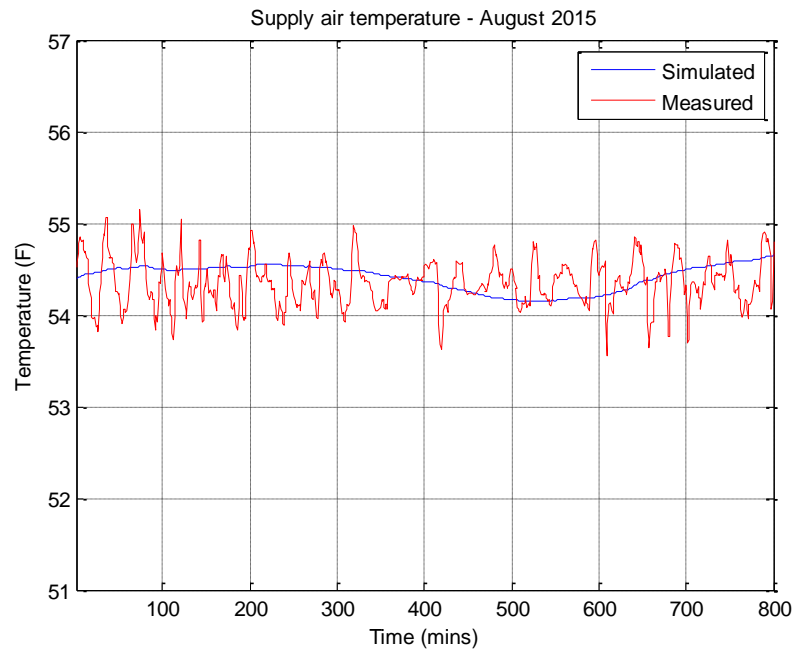


Figure 4.38: Supply air temperature vs measurement – August 2015

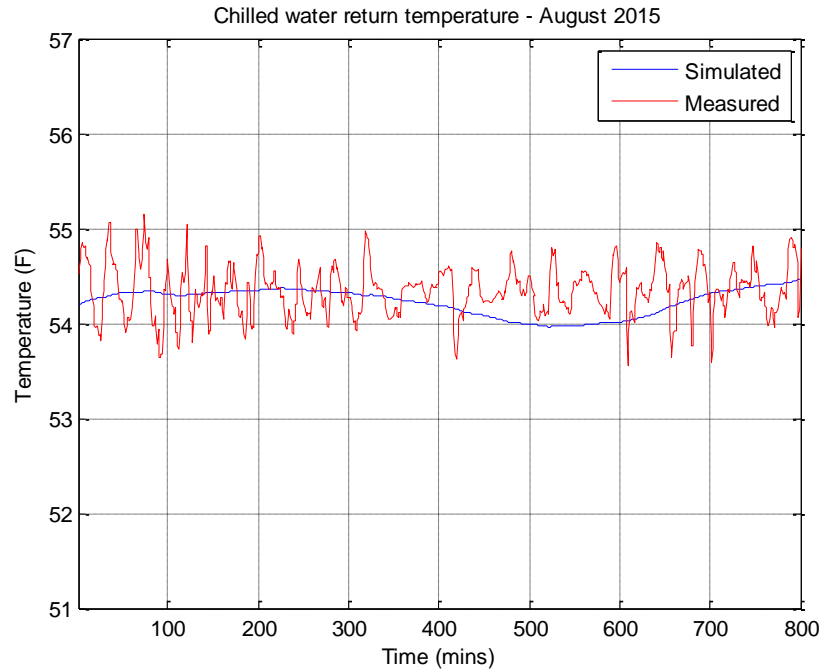


Figure 4.39: Chilled water return temperature vs measurement – August 2015

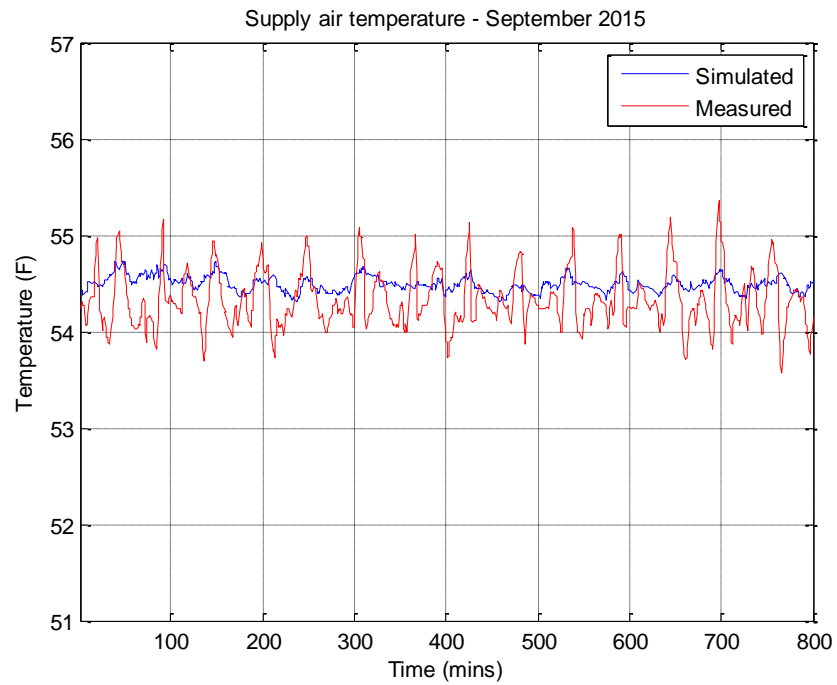


Figure 4.40: Supply air temperature vs measurement – September 2015

As shown in Figures 4.38 and 4.40, the cooling coil model is more accurate in predicting the leaving air temperature than the leaving water temperature. The model was unable to capture the fluctuations in the leaving air temperature, but the predicted values were within 0.4F relative to the measured value for the entire validation season. The fluctuations might be caused by oscillations due to PID controller actions.

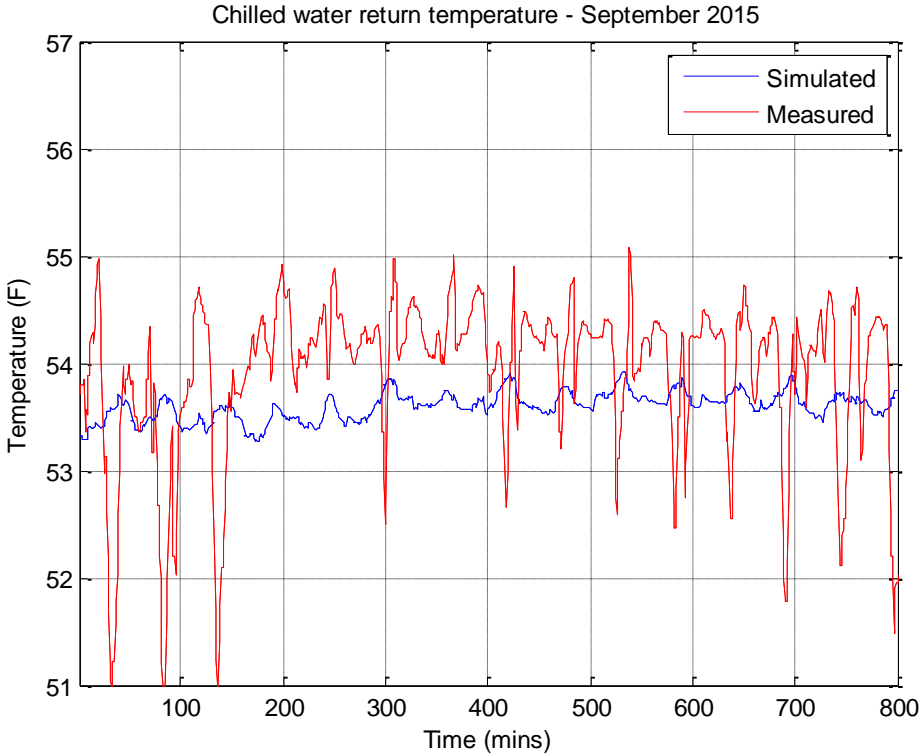


Figure 4.41: Chilled water return temperature vs measurement – September 2015

As shown in Figure 4.41, the model could not trend with the spikes in leaving water temperature for the September 2015 validation case. The fluctuations might be similarly caused by oscillations due to PID controller actions. However, the overall mean absolute error is less than 1F, and that degree of accuracy is sufficient for the purpose of this study.

4.6.1 Summary of cooling coil predictions – leaving air temperature

Table 4.23 shows summary of the leaving air temperature results for August and September 2015. As could be seen, the leaving air temperature was predicted accurately within 0.4F mean absolute error.

Table 4.23: Summary of predicted leaving air temperature vs measurement

Validation month	ME (F)	MAE (F)	MBE (%)	CVRMSE (%)
August 2015	0.011	0.402	0.020	1.062
September 2015	0.043	0.323	0.080	0.743

4.6.2 Summary of cooling coil predictions – leaving water temperature

Table 4.24 shows summary of the leaving water temperature results for August and September 2015. As could be seen, the leaving water temperature was predicted within 0.9F mean absolute error.

Table 4.24: Summary of predicted leaving water temperature vs measurement

Validation month	ME (F)	MAE (F)	MBE (%)	CVRMSE (%)
August 2015	0.359	0.791	0.666	2.412
September 2015	0.124	0.896	0.233	2.222

Chapter 5: Development and Validation of Framework for Minimizing Buildings Electricity Demand and Cost

Having established the level of accuracy of the air handling unit components in Chapter 4, this chapter describes the framework for integrating the component models together, in order to minimize electricity demand and cost. To achieve this, a crucial requirement is a model-based predictive control (MPC) framework which seamlessly integrates with the dynamic model and utilizes limited sensor information to make informed decision about optimal control sequence. MPC is relatively new, but has been adopted and applied in the HVAC field. Some of the areas of application include but is not limited to weather predictions and indoor climate control (Oldewurtel et. al 2010), temperature control (Wallace et. al, 2012), ventilation control (Yuan and Perez, 2006), air quality (Ginestet and Marchio, 2010), energy (Parisio et. al, 2014). MPC has received particular attention, since it naturally accounts for the factors of weather and occupancy, constraints on thermal comfort, and embedded uncertainties, while achieving systemic integration of the many variables and factors involved. MPC adopts performance indices that are similar to linear quadratic regulator (LQR) strategies. Optimizations with classical control and H-1 or H-infinity norms are complex in their implementation, and they do not embed the constraints into their formulation.

There has been very limited (or no) application of MPC for study of multi-zone interactions and minimization of electricity cost in a multi-zone variable air volume system. This is due to unavailability of accurate predictive system models. This study is the first to utilize the integrated building load and cooling coil thermal network model in a MPC framework to aid understanding of multi-zone interactions and minimize

electricity cost. The thermal network models used in this study have capability to capture fluctuations in zone temperatures due to variations in solar radiation, ambient, internal equipment, schedules, occupancies etc. Application of the thermal network model for building load and cooling coil modeling, and establishment of the accuracy level of the thermal network model enabled the utilization of MPC in this study. New information presented in this chapter includes a flowchart showing how the MPC framework will be used to minimize building electricity demand and cost, identification of critical zones for a case study multi-zone building, study of zone interactions, and new methods for minimizing buildings electricity demand and cost in a multi-zone building.

5.1 Suitability of MPC for HVAC Systems

MPC strategies can be applied to complex systems with many control variables, as it provides a systemic way of handling states and inputs constraints. These constraints are often encountered in different engineering applications in forms of valve limitations, physical constraints, plants or process operation limits, and safety constraints. MPC accounts for constraints via the solution to a constrained optimization problem which determines the predicted input optimally. The basic components of a model predictive controller are prediction, optimization, and receding horizon.

There are certain characteristics of HVAC systems that make MPC the ideal candidate for minimizing building electricity demand and cost. Some of the characteristics are highlighted below:

- Narrow range of operation, constrained by thermal comfort requirements (e.g. temperature and humidity control, etc).
- Limitations on equipment (airflow rates (CFM), water flow rates (Gallons per minute, GPM), fan speeds, valve commands) etc. in form of hard constraints.
- Presence of some uncontrollable inputs (weather, ambient, occupancy, changing schedules, etc).
- Presence of some unmeasured states (e.g. internal and external surface temperature of walls)
- Varying dynamics responses and timescales of different components (e.g. medium transient from cooling coils, and slow transient from building load)
- Radiative heat transfer delays and dynamic time of use electricity pricing, which implies that reducing overall electricity use does not necessarily imply lower cost of electricity
- Multivariable dynamic and thermal interactions among multiple zones
- Variable constraints for certain time-steps (e.g. different temperature limits for occupied and unoccupied hours)
- Unavailability of building construction information, which calls for model parameter estimation techniques. Limited or unreliable data about previous building usage necessitate the use of reduced order models
- MPC provides a consistent approach that will be applicable to both existing and new buildings
- MPC does not require a control law
- MPC can be used for both local and supervisory control

5.2 How the MPC works

Some of the components of a model predictive controller are the prediction, receding horizon, modeling, performance index, degrees of freedom, constraints handling, and multi-variable. The general overview of the components involved in the MPC framework is shown in Figure 5.1

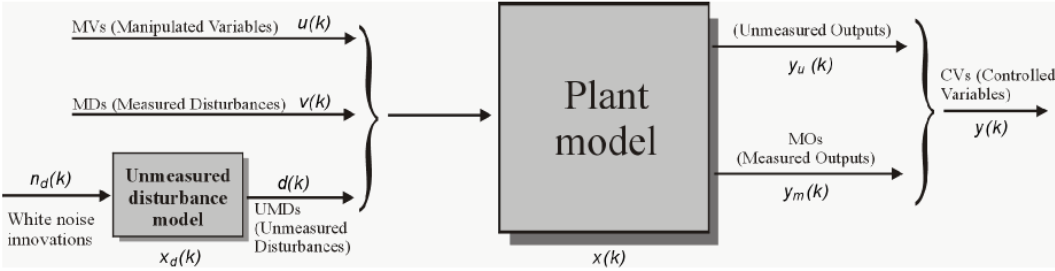


Figure 5.1: Components involved in Model Predictive Control (Source: mathworks.com)

Prediction involves the forecast of future response of the controlled plant using a dynamic model. For any given predicted input sequence, forward simulation of the dynamic model over a given prediction horizon generates the corresponding state predictions. Prediction is necessary for ensuring that the output does not deviate from the desirable trajectory. Prediction horizon should be beyond the key dynamics of the process. MPC embeds constraints into its algorithm from the controller formulation. This systematic handling of constraints ensures that the input strategies are optimized. MPC is able to handle multi-variable interactions, for example, between flowrates, temperature, pressure, etc, where changes in one input affects all of the output. PID, lead, lag compensators are good for SISO. They become quite difficult to implement for a MIMO system. MPC automatically takes the multivariable interactions into account.

Optimization of the dynamic system require the definition of a performance cost, which most often, is a function of the states and inputs. The model predictive controller determines a feedback law to minimize the predicted performance cost over the chosen horizon. The generalized performance cost is quadratic in nature, and has the following form:

$$J(k) = \sum_{i=0}^N x^T(k+1|k)Qx(k+1|k) + u^T(k+1|k)Ru(k+1|k) \quad (5.1)$$

Where Q and R are positive definite matrices. Obviously, $J(k)$ is a function of the manipulated vector $\mathbf{u}(k)$. Alternative performance cost is shown in Appendix D. The optimal input sequence required to minimize $J(k)$ is denoted as $\mathbf{u}^*(k)$. The constraints on input and states could be included in the optimization problem, as appropriate constraints on $\mathbf{u}(k)$. For linear systems, the MPC strategy reduces to the minimization of a quadratic objective, subject to linear input and state constraints.

Receding horizon involves the input of only the first element of the optimal predicted input to the plant ($u(k) = u^*(k|k)$). At each sampling instant, the process of computing the optimal predicted sequence and implementing the first element is repeated. As such, the prediction horizon remains the same, despite future optimization. This approach is referred to as the receding horizon strategy. The dependence of the state prediction and optimal input sequence \mathbf{u}^* on the current state measurement $x(k)$ introduces feedback into the model predictive control strategy. This provides some degree of robustness to model uncertainty and errors. Additionally, with proper design of cost and constraints, the receding horizon strategy ensures that the performance of the closed-loop system is very similar to that of the optimal prediction.

Decision making requires processing time, and therefore, cannot always be instantaneous. Likewise, common predictive control laws are implemented in discrete time. Therefore, the ideal model for MPC must have a discrete representation. The appropriate sample rate must be chosen, in order to avoid unnecessary increase in the number of decision variables. The ideal recommendation is to use 10 samples within the settling time of the system. The model should give good long range prediction, and decision has to be based upon the most recent measurements. The most common models where the MPC has been applied are listed below:

1. Discrete state-space models

$$x_{k+1} = Ax_k + Bu_k \quad (5.2)$$

$$y_k = Cx_k + Du_k + d_k \quad (5.3)$$

Where d_k =disturbance estimate

2. CARIMA models

$$a(z)y_k = b(z)u_k + T(z) \frac{\zeta_k}{\Delta} \quad (5.4)$$

Where ζ_k is a zero mean random variable, and

3. Step response models

$$y_k = H(z)\Delta u_k + d_k; \quad \Delta u_k = u_k - u_{k-1} \quad (5.5)$$

5.3 MPC with MIMO State Space Models

Discrete MIMO state space models are one-step ahead predictive model of the form in Equation (5.2) and (5.6):

$$y_{k+1} = Cx_{k+1} + Du_{k+1} + d_{k+1} = C(Ax_k + Bu_k) + Du_{k+1} + d_{k+1} \quad (5.6)$$

The one-step ahead prediction can be used for n-steps ahead by solving the model recursively, i.e. by using x_{k+1} to find x_{k+2} etc. The pattern is shown in Equations (5.7) and (5.8)

$$x_{k+n} = A^n x_k + A^{n-1} B u_k + A^{n-2} B u_{k+1} + \dots + A B u_{k+n-1} + B u_{k+n-1} \quad (5.7)$$

$$y_{k+n} = C x_{k+n} + D u_{k+n} + d_{k+n} \quad (5.8)$$

Where for simplicity, it is assumed that $d_{k+n} = d_k$

For the expressions in Equation (5.7) and (5.8), it is important to note the sample at which prediction is being made. A double subscript is commonly used for notation e.g.

$x_{k+4|k}$ implies a 4-step ahead prediction ($k + 4$), with prediction made at k

$x_{k+6|k+2}$ also implies a 4-step prediction, but with prediction made at $k + 2$

We can rewrite equations (5.7) and (5.8) as

$$x_{k+n|k} = A^n x_k + A^{n-1} B u_{k|k} + \dots + A B u_{k+n-1|k} + B u_{k+n-1|k} \quad (5.9)$$

$$y_{k+n|k} = C x_{k+n|k} + D u_{k+n|k} + d_{k|k} \quad (5.10)$$

And the prediction can be split into known and a decision part

$$\begin{aligned} y_{k+n|k} &= [C A^n x_k + d_k] \\ &+ [C (A^{n-1} B u_{k|k} + A^{n-2} B u_{k+1|k} + \dots + A B u_{k+n-1|k} + B u_{k+n-1|k}) \\ &+ D u_{k+n|k}] \end{aligned} \quad (5.11)$$

Where the first term of Equation (5.11) represents the known part, and the second term is the decision. A vector of vectors representation is commonly used to simplify and capture the vector of future predictions as shown below:

$$\begin{bmatrix} x_{k+1|k} \\ x_{k+2|k} \\ \vdots \\ x_{k+n|k} \end{bmatrix} = x_{\rightarrow k+1}, \quad \begin{bmatrix} y_{k+1|k} \\ y_{k+2|k} \\ \vdots \\ y_{k+n|k} \end{bmatrix} = y_{\rightarrow k+1}$$

The arrow implies that this is a vector of vectors. x_{k+1} indicates the first value. Arrow pointing to the right implies that this is a prediction. The vector of all predictions from x_{k+1} could then be represented as:

$$x_{\rightarrow k+1} = \begin{bmatrix} Ax_k \\ A^2x_k \\ \vdots \\ A^n x_k \end{bmatrix} + \begin{bmatrix} Bu_{k|k} \\ ABu_{k|k} + Bu_{k+1|k} \\ \vdots \\ A^{n-1}Bu_{k|k} + \dots + Bu_{k+n-1|k} \end{bmatrix} \quad (5.12)$$

$$x_{\rightarrow k+1} = \begin{bmatrix} A \\ A^2 \\ \vdots \\ A^n \end{bmatrix} x_k + \begin{bmatrix} B & 0 & \dots & 0 \\ AB & B & \dots & \vdots \\ \vdots & \vdots & \vdots & \vdots \\ A^{n-1}B & A^{n-2}B & \dots & B \end{bmatrix} \begin{bmatrix} u_{k|k} \\ \vdots \\ \vdots \\ u_{k+n-1|k} \end{bmatrix} \quad (5.13)$$

Which may be represented as:

$$x_{\rightarrow k+1} = P_x x_k + H_x u_{\rightarrow k} \quad (5.14)$$

Where $P_x = \begin{bmatrix} A \\ A^2 \\ \vdots \\ A^n \end{bmatrix}$ and $H_x = \begin{bmatrix} B & 0 & \dots & 0 \\ AB & B & \dots & \vdots \\ \vdots & \vdots & \vdots & \vdots \\ A^{n-1}B & A^{n-2}B & \dots & B \end{bmatrix}$ depend solely on the model

parameters and matrices. The output $y_{\rightarrow k+1}$ could be represented as (for the case where $D = 0$)

$$y_{\rightarrow k+1} = \begin{bmatrix} CA \\ CA^2 \\ \vdots \\ CA^n \end{bmatrix} x_k + \begin{bmatrix} d_k \\ d_k \\ \vdots \\ d_k \end{bmatrix} + \begin{bmatrix} CB & 0 & \dots & 0 \\ CAB & CB & \dots & \vdots \\ \vdots & \vdots & \vdots & \vdots \\ CA^{n-1}B & CA^{n-2}B & \dots & CB \end{bmatrix} \begin{bmatrix} u_{k|k} \\ \vdots \\ \vdots \\ u_{k+n-1|k} \end{bmatrix} \quad (5.15)$$

Which can be simplified as Equation (5.16)

$$y_{\rightarrow k+1} = [P x_k + L d_k] + H u_{\rightarrow k} \quad (5.16)$$

With $P = \begin{bmatrix} CA \\ CA^2 \\ \vdots \\ CA^n \end{bmatrix}$, $L d_k = \begin{bmatrix} d_k \\ d_k \\ \vdots \\ d_k \end{bmatrix}$ and $H = \begin{bmatrix} CB & 0 & \dots & 0 \\ CAB & CB & \dots & \vdots \\ \vdots & \vdots & \vdots & \vdots \\ CA^{n-1}B & CA^{n-2}B & \dots & CB \end{bmatrix}$

The advantage of above representation is that it is a compact form of the prediction for all horizons. The predictions separate into a known part and a part which can be selected and optimized. MPC framework may be summarized as shown in Table 5.1. In this study, the MPC is geared directly to the building dynamic model and cooling coil model respectively. It helps to determine sequence of control actions that minimize cooling demand from the building and chilled water flow simultaneously. The MPC does not directly solve the fan model used in this study, since it is based on a steady state model (which has been justified because of inability to capture fan’s fast transients). However, the minimized building demand is compensated for by the flow (and pressure) supplied by the fan. The optimization is to be considered alongside static pressure reset strategies that significantly save fan power.

Table 5.1: Summary of MPC Framework

	Steps	Description
1	Prediction	Predicts performance using dynamic plant model. Lots of flexibility is afforded in plant model types, e.g. multivariable, linear, nonlinear, discrete, or continuous model.
2	Optimization	Minimize performance cost by optimizing future control sequences, based on current states. The approach is computationally more efficient than optimizing using feedback control laws.
3	Receding Horizon	Implement first control sequence, then move one step ahead, and repeat optimization. This invariably embeds feedback into the implementation, which reduces effect of uncertainty and modeling errors.
4	Constraints handling	Systematic handling of constraints by embedding it in the optimization. Constraints are handled optimally.

Figure 5.2 is a flowchart showing how the MPC framework will be used to minimize building electricity demand and cost.

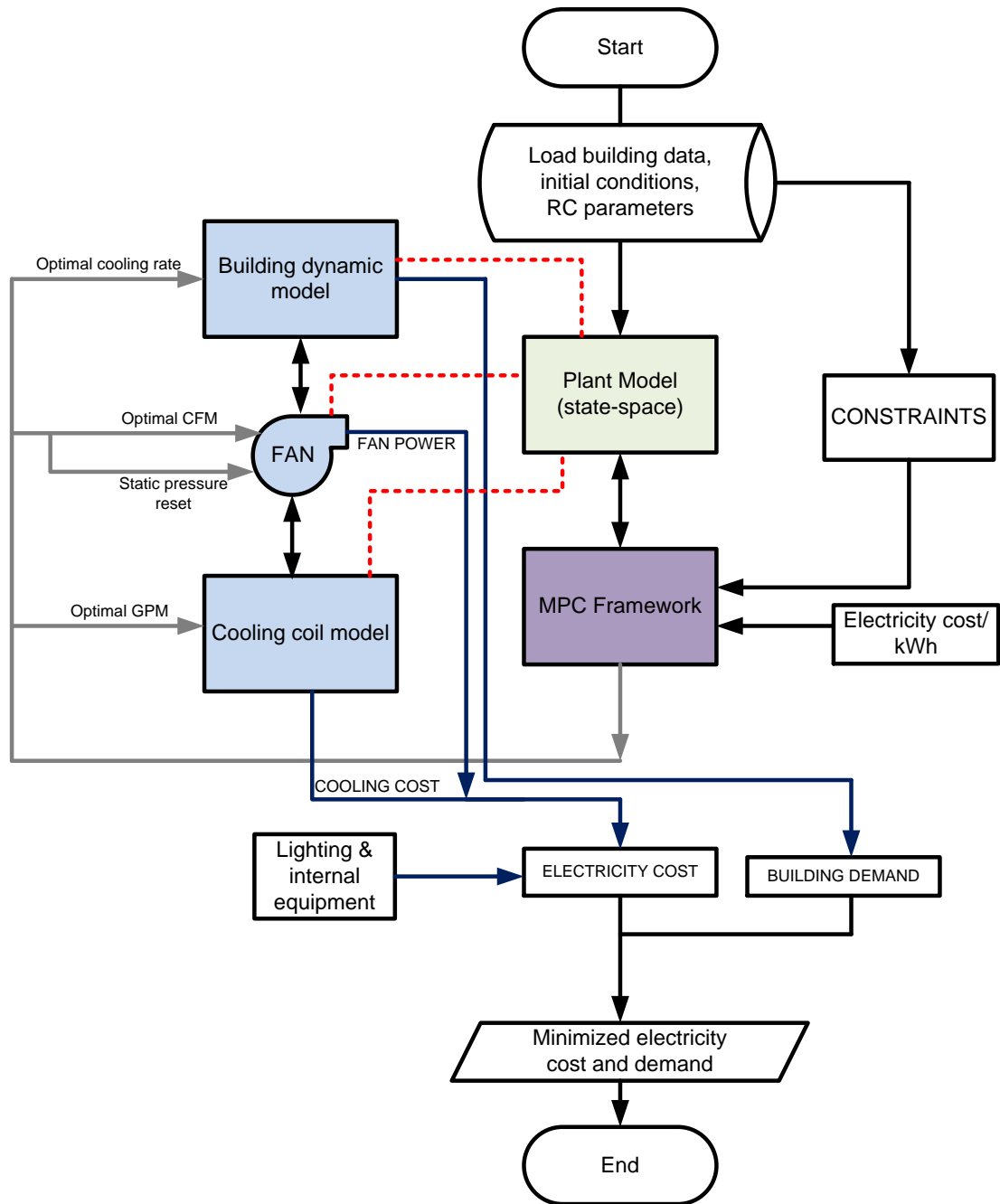


Figure 5.2: MPC Framework to minimize building electricity cost and demand

The MPC integrates with the plant model (which is made up of buildings dynamic model, cooling coil model, and the fan-power model), and determines sequence of control actions (building cooling rate, and cooling coil flow rates) to minimize building electricity demand and cost over a given horizon, while satisfying the constraints. The methodology was applied for minimization of building electricity demand and cost (multiple zone case study). Results are presented and discussed in next section. The dotted red line in Figure 5.2 indicates that the plant model is integration of the building dynamic model, fan model, and the cooling coil model. The MPC utilizes the plant model, constraints, and electricity cost function to determine the optimal water flow rate for the cooling coil, optimal cooling rate for the building load, and optimal CFM and static pressure for the fan, based on overall goal of minimizing the electricity cost and demand over a specified horizon.

To minimize building electricity cost, the objective function is written as a quadratic function in the water flow rate (GPM) and cooling rate, subject to constraints on temperatures (for thermal comfort and safety), the cooling rate, and the GPM (equipment limitation), with electricity tariff w_k (for the given time-step) applied as a weight factor, as shown in Equation (5.17).

Minimize:

$$J(k) = \sum_{i=0}^{N-1} w_k^2 x^T(k+1|k) Q x(k+1|k) + w_k^2 u^T(k+1|k) R u(k+1|k) \quad (5.17)$$

Subject to: $A_c \mathbf{x} \leq \mathbf{x}_c$

$$A_u \mathbf{u} \leq \mathbf{u}_c$$

Where A_c is constraints matrix for the states, x_c is the constraints on the states (e.g. for thermal comfort), A_u is constraints matrix for the manipulated variable (u), and u_c is the constraint on the cooling rate and GPM (from equipment limitation). Q is deduced from the cooling load function (shown in Tables 5.6 to 5.19, Chapter 5) for each thermal zone, and R is a specified positive definite matrix. The control sequence (GPM and cooling rates) which minimize the objective function (Equation 5.17) over the given horizon could then be determined using quadratic programming or any other efficient optimization method. The step by step approach for the optimization is summarized in Chapter 7.

5.4 Case Study

To demonstrate the electricity minimization procedure developed in this study, it was applied to a section of the Engineering Laboratory building at the University of Oklahoma, for a period of 24hours in summer (August 2015). The electricity tariff profile used is as shown in Figure 5.3. It involves an off peak period (9pm – 7am), medium peak period (8am – 12pm, and 5pm -9pm), and peak period (12pm-5am). The tariff was deduced from U.S Energy Information Agency range of electricity data for commercial buildings in the state of Oklahoma. For the building load model, the constraints on zone temperatures are:

- $15^{\circ}\text{C} (59F) \leq T_{zone} \leq 25^{\circ}\text{C}(78.8F)$ for 5pm – 8am (unoccupied period)
- $21.1^{\circ}\text{C} (70F) \leq T_{zone} \leq 24^{\circ}\text{C}(75.2F)$ for 8am – 5pm (occupied period)

For the cooling coil, the constraints on leaving water and air temperatures are:

- $11.1^{\circ}\text{C} (52F) \leq T_{air_exit} \leq 13.8^{\circ}\text{C} (57F)$ and
- $11.1^{\circ}\text{C}(52F) \leq T_{water_exit} \leq 13.8^{\circ}\text{C} (57F)$

The constraints on water flow (GPM) and air flow rates (CFM) were specified as:

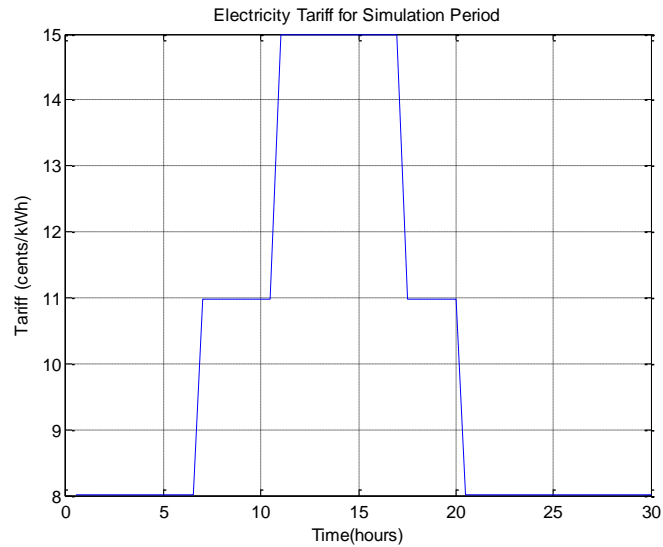


Figure 5.3: Electricity Tariff for Optimization Period

(Deduced from https://www.eia.gov/electricity/monthly/current_year/august2015.pdf)

- $0 \leq \text{Supply air flow rate (CFM)} \leq 2500$ and
- $0 \leq \text{Water flow rate (GPM)} \leq 50$

To perform the minimization, the prediction time step was specified as 1minute, while the control time-step was chosen to be 5 minutes. It was assumed that the price of electricity is known 3 hours ahead. This was deemed a suitable timeframe for the control system to adjust the operation of the system based on anticipated changes in electricity price.

5.5 Results

This section presents the results of minimization of cooling demand, fan power, cooling coil water flow rate, and electricity cost using the MPC framework. The results

enable the study of multi-zone interactions, and aid in identification of new methods for minimizing electricity cost in a multi-zone building.

5.5.1 Cooling demand

Figures 5.4 and 5.5 show the comparison of temperature trajectory and cooling demand for Thermal Zone A.

As shown, the optimized cooling rate suggests more cooling for the first ten hours of the day, which leads to a lower temperature compared to the original temperature. As shown in Figure 5.5, precooling this thermal zone leads to significantly lesser cooling demand during the peak hours, as compared to the original cooling profile. The original operation suggests that the air conditioning system has little or no intelligence to anticipate the peak ambient temperature and solar radiation. The sudden peak demand in cooling (during peak hours when electricity is most expensive) contributes to higher cost of electricity. With the optimized profile, the cooling demand was nearly flat throughout the day, fluctuating by approximately 200W, while the original operation mode fluctuates by nearly 1kW. Based on the new cooling profile, the reduction in peak cooling demand is more than 100%. For Thermal Zone A, the strategy suggested by the optimized MPC is very similar to pre-cooling strategies, where the building is pre-cooled, to reduce the cooling demand at a later time. Since zone A thermally interacts with Zones C and D, it could be seen that the temperature profile of Zone C (Figures 5.8 and 5.9) has influence on the minimization strategy of Zone A.

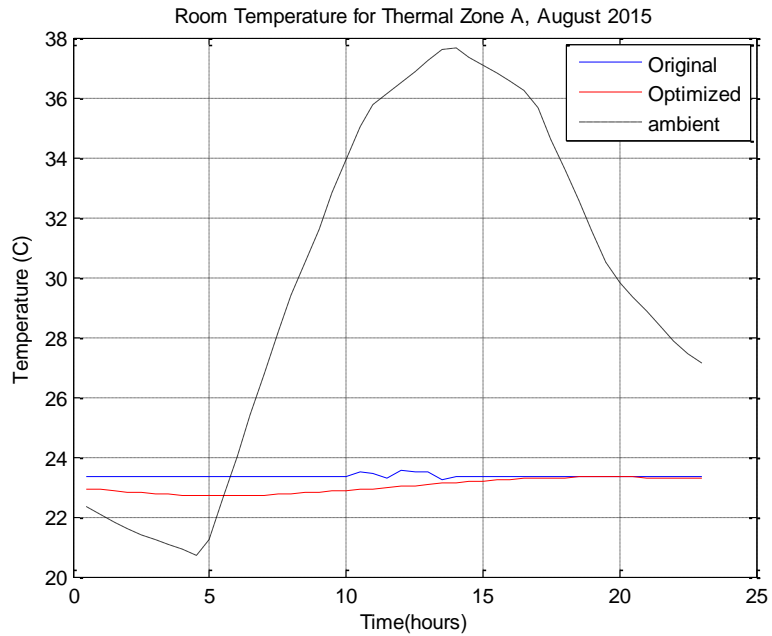


Figure 5.4: Optimized Temperature Trajectory – Thermal Zone A

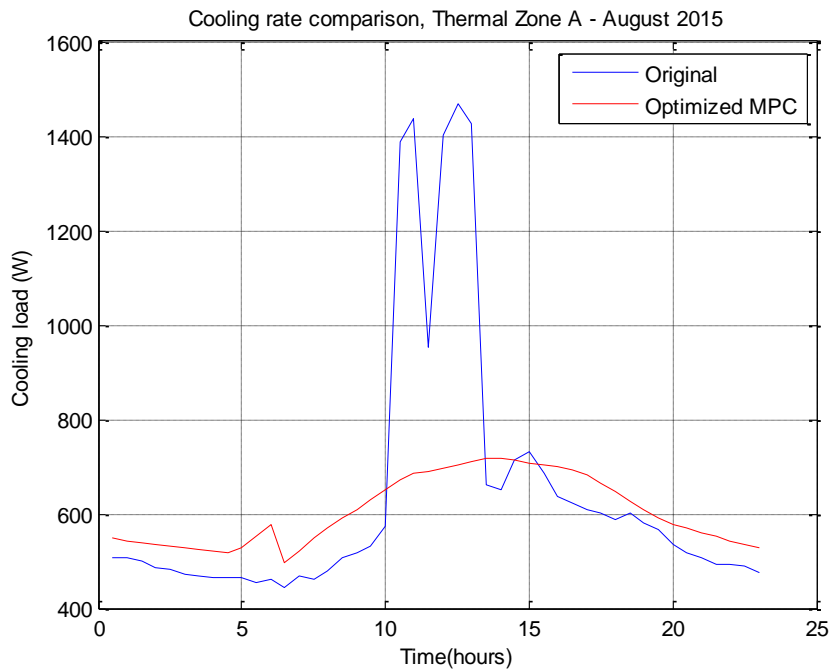


Figure 5.5: Optimized Cooling Load Profile – Thermal Zone A

Precooling is generally carried out by rule of thumb, with one of the challenges being the optimization of pre-cooling hours, i.e., how many hours of pre-cooling is near

optimal. In this study, the MPC demonstrated an advantage due to the determination of near-optimal amount of cooling, temperature profile, and precooling duration that leads to minimization of daily electricity cost.

Figures 5.6 and 5.7 show the comparison of temperature trajectory and cooling demand for Thermal Zone B. As shown, the optimized cooling rate suggests a near constant (but reduced) cooling for 24 hours, which leads to slightly higher zone temperature compared to the original temperature. As shown in Figure 5.6 and 5.7, allowing the temperature to increase slightly throughout the day leads to significantly less cooling demand during the peak hours. With the optimized profile, the cooling demand was nearly flat throughout the day, fluctuating by approximately 100W, while the original operation mode fluctuates by nearly 1kW. Based on the optimized cooling profile, the reduction in peak cooling demand is more than 100%. For Thermal Zone B, the strategy suggested by the optimized MPC is near-constant cooling for every hour of the day. This strategy is very similar to temperature set-point adjustment, where the zone temperature is set at the upper limit of comfort. While Zone B thermally interacts with zones C, D, and G, it is seen that Zone C has more thermal influence on Zone B. The thermal interactions between Zones B and C come into play, as the temperature of Zone B did not reach the upper comfort limit, despite the reduced cooling.

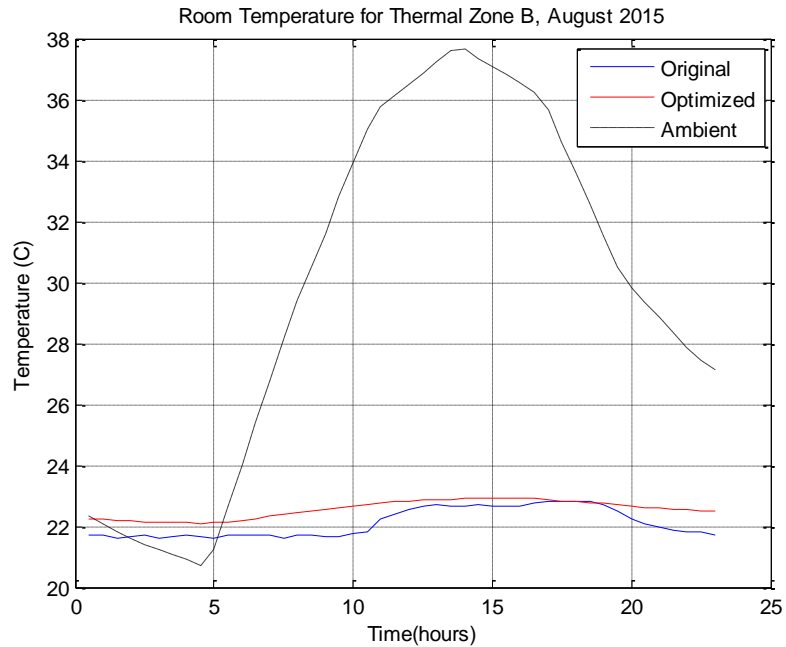


Figure 5.6: Optimized Temperature Trajectory – Thermal Zone B

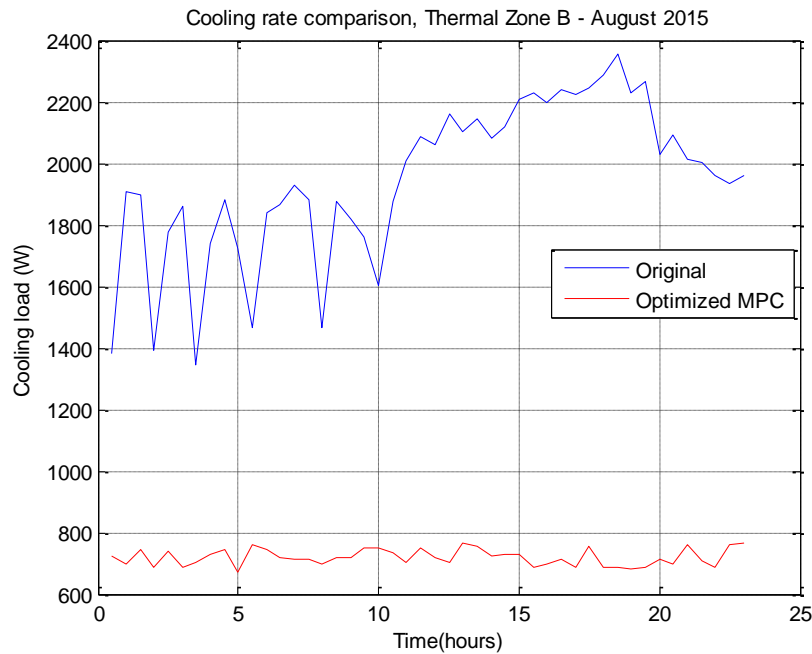


Figure 5.7: Optimized Cooling Load Profile – Thermal Zone B

Figures 5.8 and 5.9 show the comparison of temperature trajectory and cooling demand for Thermal Zone C. As shown, the optimized cooling rate suggested by the

MPC is precooling during the first 9 hours of the day, which leads to a lower temperature compared to the original temperature. As shown in Figure 5.8, precooling this thermal zone leads to lower temperature as compared to the original operation. It also leads to significantly lower cooling demand during the peak hours, as shown in Figure 5.9. Among all the zones, Zone C has the lowest temperature during occupied hours. It is seen to be a critical zone for this multi-zone building. Maintaining its temperature near the lower limit of comfort enables its surrounding zones (A, B, and D) to keep their temperature within the limits of comfort. The original cooling profile fluctuates a lot, as shown in Figure 5.9, with changes of more than 1.5kW around 9am. With the optimized profile, the cooling demand was nearly flat throughout the day, fluctuating by approximately 200W, while the original operation mode fluctuates by approximately 1.7kW. Based on the optimized cooling profile, the reduction in peak cooling demand is more than 100%.

The strategy suggested for thermal zone C is very similar to pre-cooling strategies, and the associated challenges have been described earlier. However, Zone C was maintained at the lower limit of comfort during peak hours, contrary to existing strategies. This zone serves as heat sink for the other thermal zones. In this study, the MPC determined the optimized pre-cooling duration for Thermal Zone C, for which the daily electricity cost in the entire building is minimized.

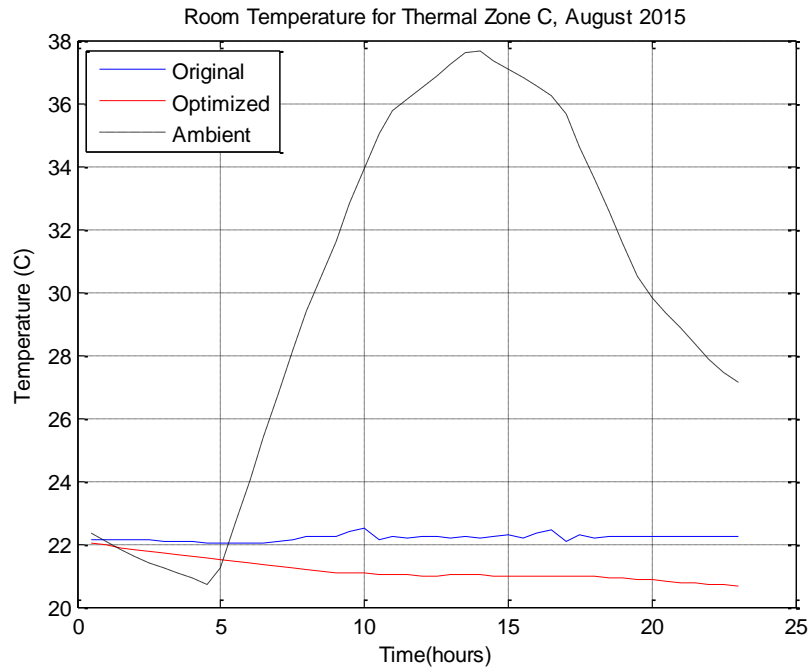


Figure 5.8: Optimized Temperature Trajectory – Thermal Zone C

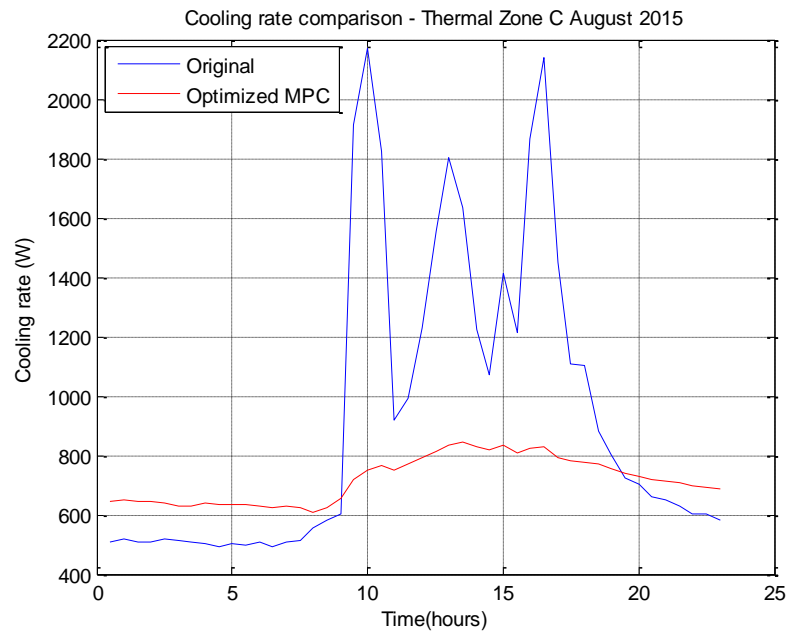


Figure 5.9: Optimized Cooling Load Profile – Thermal Zone C

Figures 5.10 and 5.11 show the comparison of temperature trajectory and cooling demand for Thermal Zone D (which is the corridor). This zone interacts with all

other thermal zones. As shown, the MPC determined that no cooling is necessary for this thermal zone. The optimized temperature and cooling are very similar to the original values. Figures 5.12 and 5.13 show the comparison of temperature trajectory and cooling demand for Thermal Zone E. This thermal zone interacts with Zones D and F.

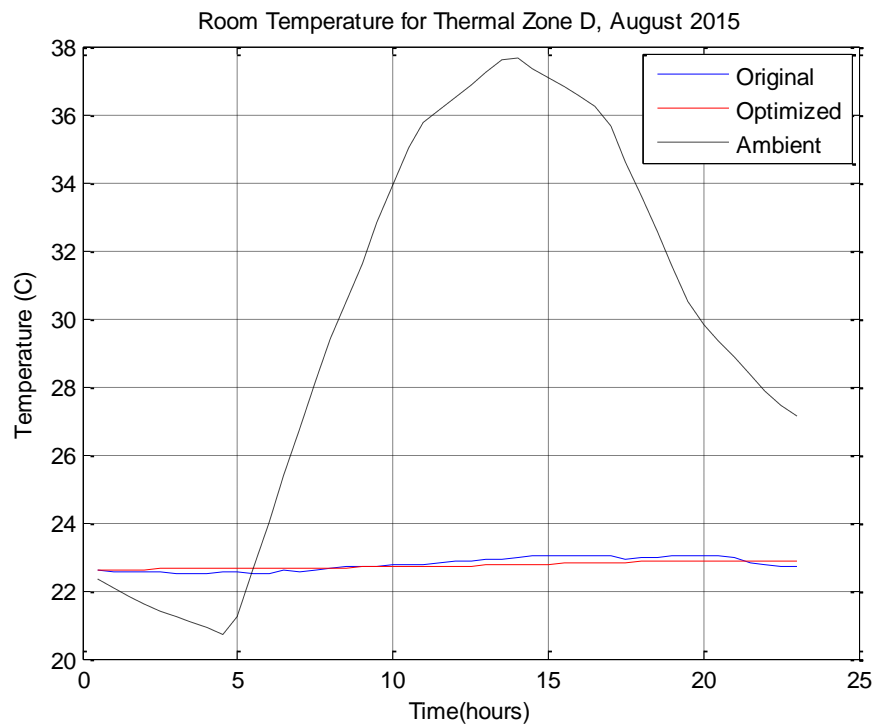


Figure 5.10: Optimized Temperature Trajectory – Thermal Zone D

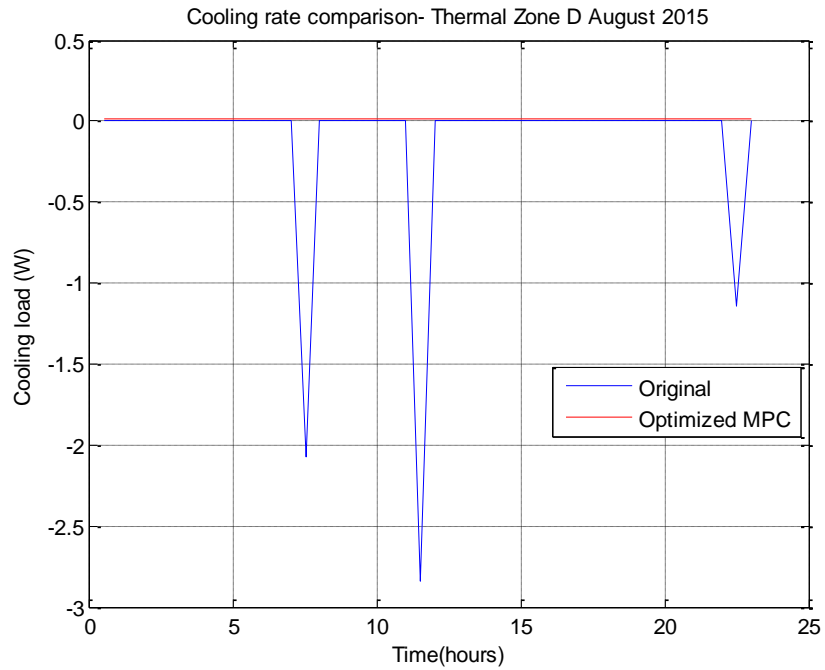


Figure 5.11: Optimized Cooling Load Profile – Thermal Zone D

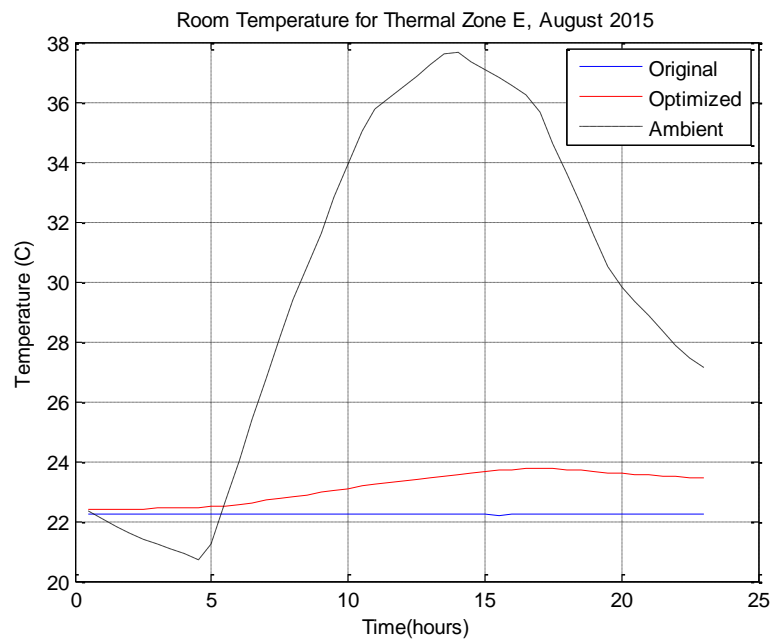


Figure 5.12: Optimized Temperature Trajectory – Thermal Zone E

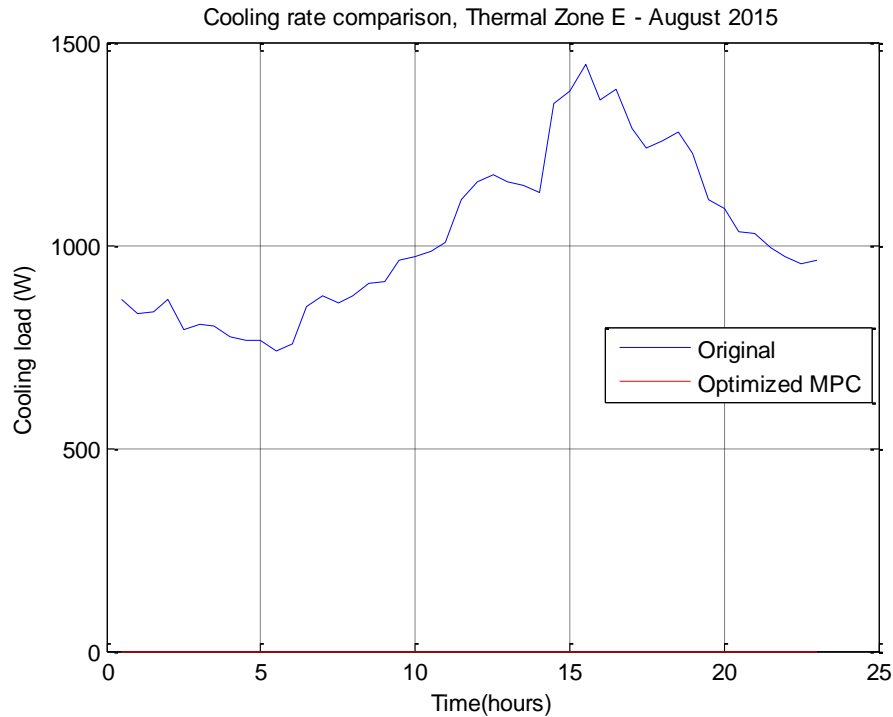


Figure 5.13: Optimized Cooling Load Profile – Thermal Zone E

As shown in Figure 5.13, the MPC determined that no cooling is necessary for thermal Zone E. The temperature is seen to float by around 2°C due to this. By allowing the temperature to float, the entire cooling cost for this thermal zone could be saved, while maintaining the zone temperature within comfort limits. It could be seen that the peak zone temperature is slightly shifted from the ambient temperature, due to thermal mass effects. Temperature floats are predominantly controlled by thermal characteristics of building construction. So, the temperature float strategy suggested by MPC for this thermal zone allowed the observation of passive thermal storage effects. The observed phenomenon is advantageous for heating system design.

Figures 5.14 and 5.15 show the comparison of temperature trajectory and cooling demand for Thermal Zone F. As shown in Figure 5.15, the MPC determined that no cooling is necessary for thermal Zone F. Instead of maintaining the zone

temperature as constant like the original operation, the optimized strategy involves both temperature float and set-point adjustment. The set-point adjustment is based on the lower band of 21°C (70F) which was specified as a constraint for the occupied hours. The temperature floated between 21°C and 23°C. The strategy is very similar to that applied to thermal zone E, which allowed for observation of passive thermal storage effects.

Figures 5.16 and 5.17 show the comparison of temperature trajectory and cooling demand for Thermal Zone G. As shown in Figure 5.17, the MPC determined that no cooling is necessary for thermal Zone G during unoccupied hours. Therefore, the temperature is allowed to float during unoccupied hours. For occupied hours, the temperature is maintained at the upper limit, while the cooling rate is ramped up. Despite that, the optimized cooling rate is approximately 50% of the original. This is contrary to existing strategies which involves pre-cooling the building when electricity is cheaper and allowing temperature float during peak hours. Zone G and Zone C are critical zones, having temperatures maintained at the upper and lower limits of comforts respectively during occupied periods. All other zones have their temperature floating within comfort limits during occupied hours.

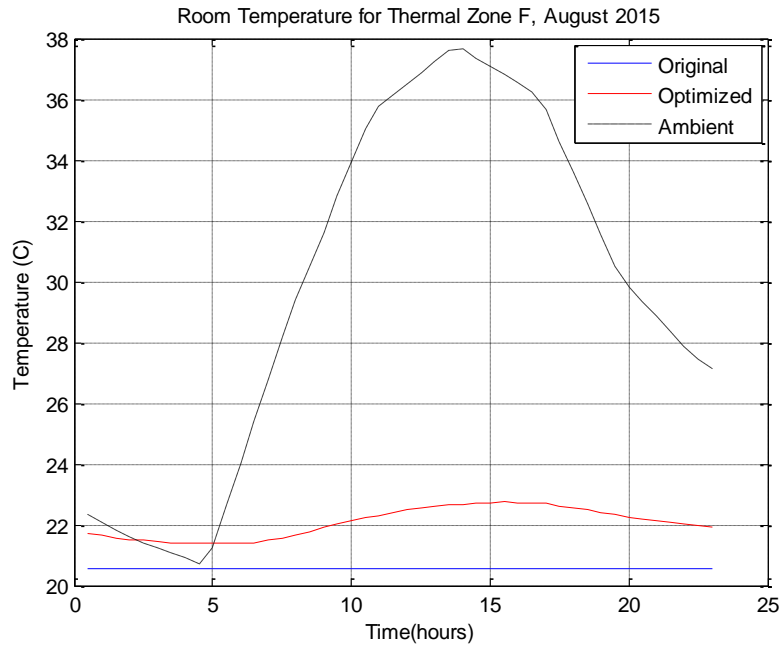


Figure 5.14: Optimized Temperature Trajectory – Thermal Zone F

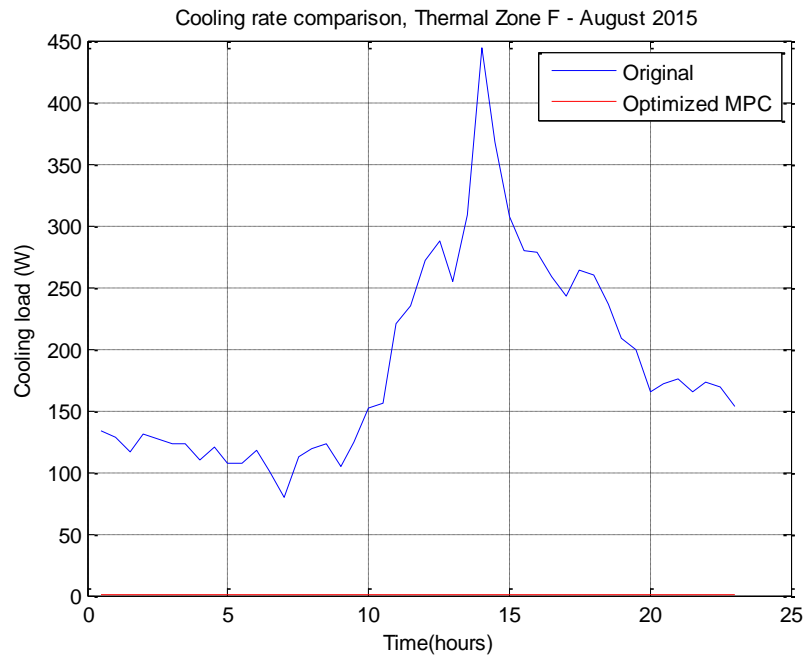


Figure 5.15: Optimized Cooling Load Profile – Thermal Zone F

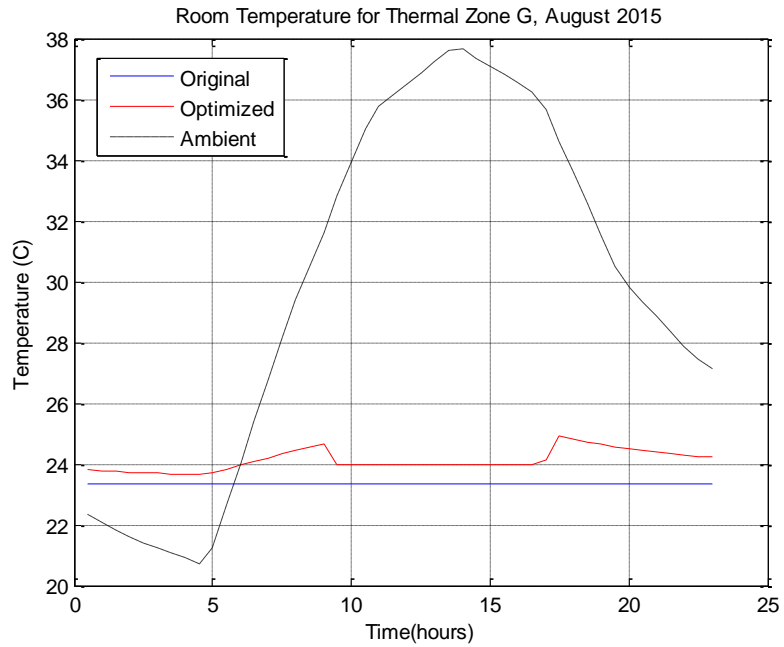


Figure 5.16: Optimized Temperature Trajectory – Thermal Zone G

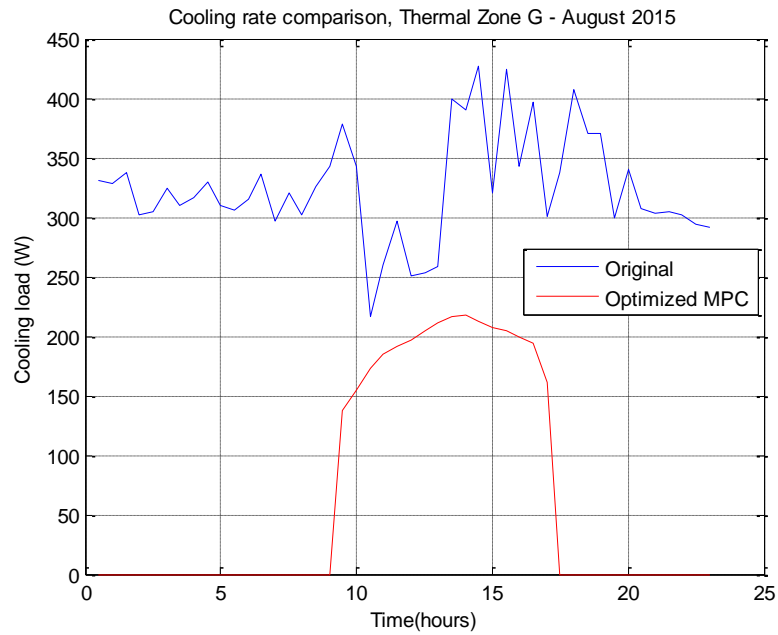


Figure 5.17: Optimized Cooling Load Profile – Thermal Zone G

A summary of the methods for each thermal zone is given in Table 5.2

Table 5.2: Summary of Optimal Cooling Strategies

Zone	Strategy	Overview
A	Optimal precooling	Optimally cool more when electricity is less expensive, and cool less during peak hours
B	Near-constant cooling	Apply a near-constant cooling that reduces total electricity cost and peak demand
C (critical zone)	Optimal precooling to lower limit of temperature	Optimally cool more when electricity is less expensive, and cool to maintain zone temperature at lower limit of comfort during peak hours
D	Temperature float	Allow zone temperature to float within comfort limits, while cooling system is turned off
E		
F	Temperature float + set-point adjustment	Adjust base temperature set-point (in this case, the lower limit) and allow zone temperature to float within comfort limits
G (critical zone)	Temperature float + optimal start	Allow temperature float during off peak hours. Recover temperature at start of occupied hours and maintain upper limit of temperature during peak hours.

Figure 5.18 shows the zone temperature for all the thermal zones. It could be seen that temperature of other zones during peak hours lie between the limits of those of zones C and G, which have been identified as the two critical zones.

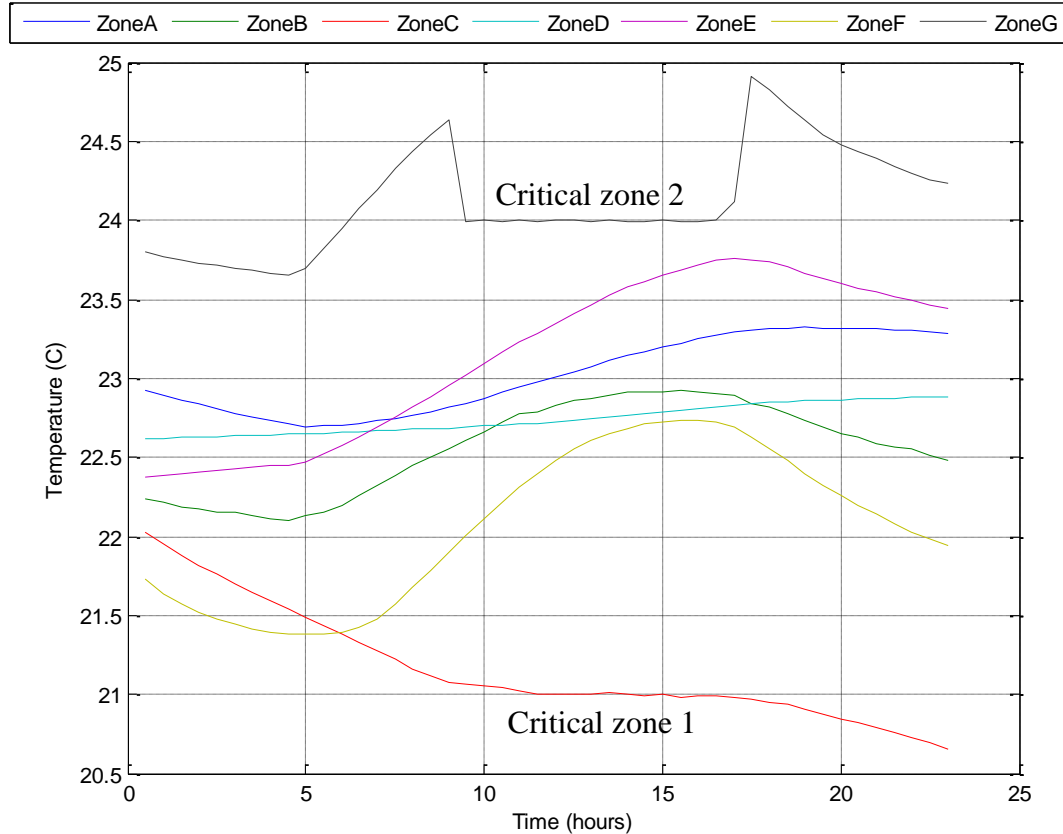


Figure 5.18: Comparison of all zone temperatures

Figure 5.19 shows comparison of the optimized water flow rate and the original values. As shown, the optimized profile indicates more water flow during unoccupied hours and less during peak periods where electricity is expensive. The profile shown (with crests during unoccupied period and valley during occupied period) is preferred for the minimization of cooling demand and electricity cost. Figure 5.19 shows significant savings in water flow as the peak optimized GPM is less than the least GPM from the original operation. The corresponding exit air and water temperatures are shown in Figures 5.20 and 5.21.

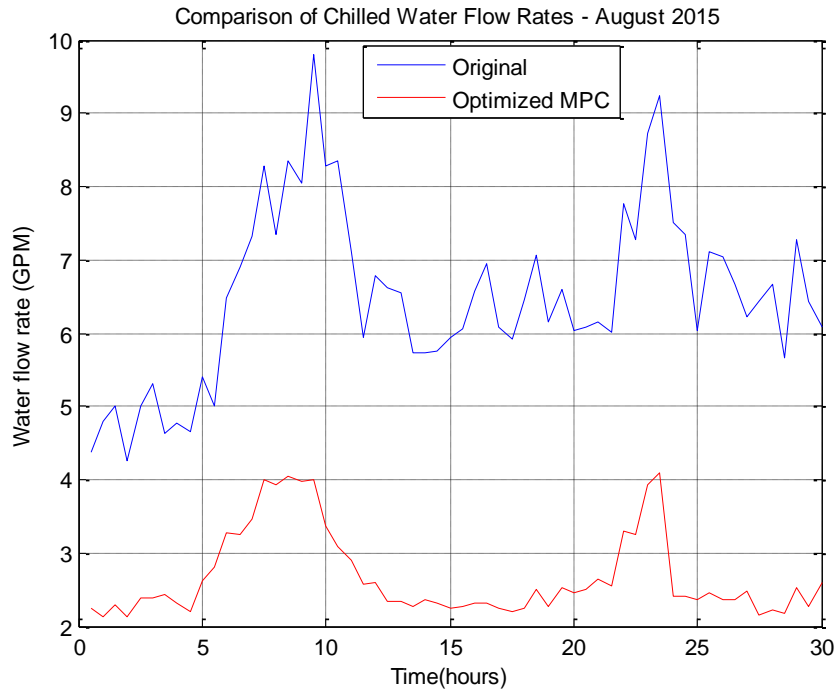


Figure 5.19: Optimized Chilled Water Flow Rates

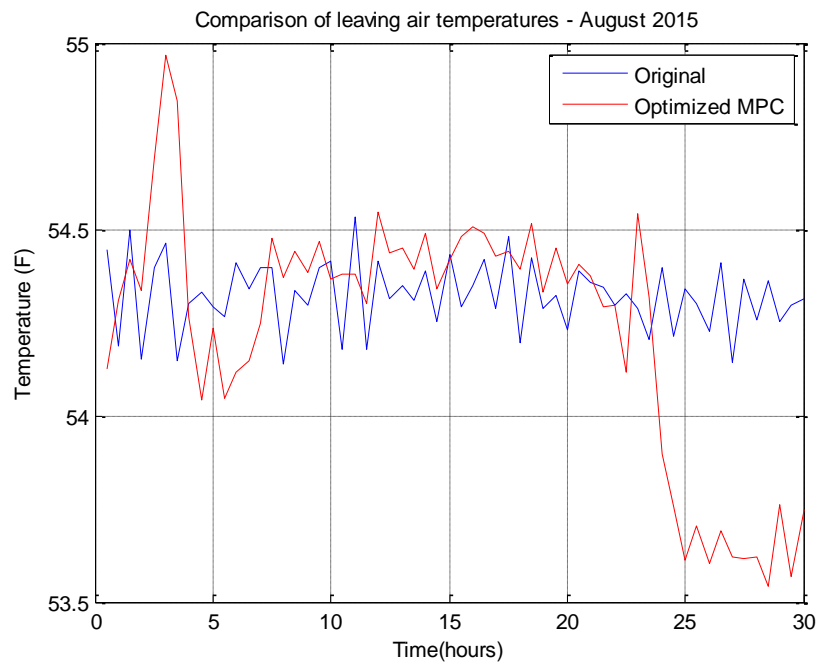


Figure 5.20: Optimized Leaving Air Temperature for Cooling Coil

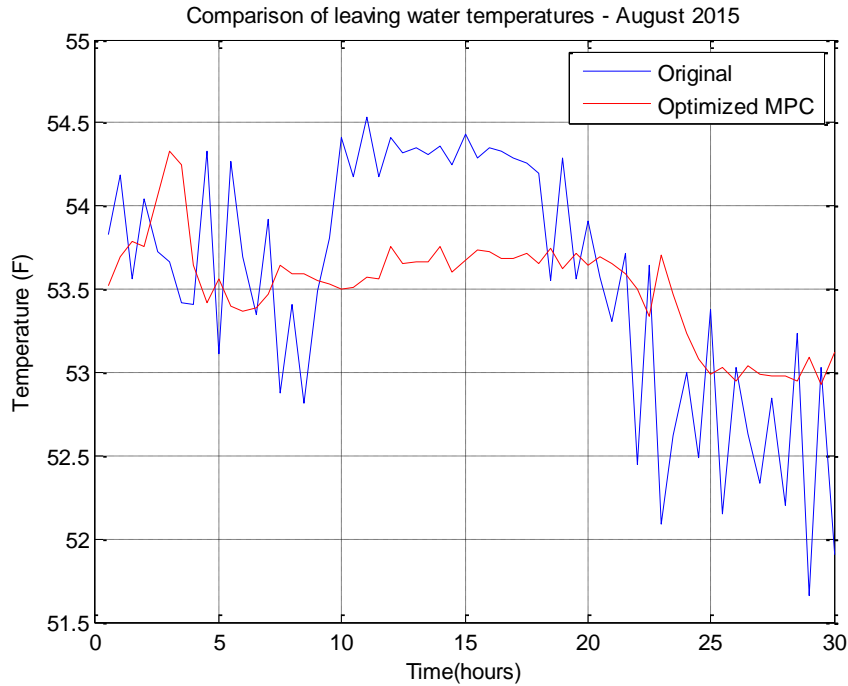


Figure 5.21: Optimized Leaving Water Temperature for Cooling Coil

It could be seen that the temperatures lie within the specified limits.

5.5.2 Fan operation

Figure 5.22 shows the optimized air flow rate for the entire building. As shown, the air flow rate is reduced by more than 50%. Additionally, there are very few fluctuations in the optimized air flow rate compared with the original, as seen in the nearly flat airflow profile shown in Figure 5.22. Figures 5.23 and 5.24 show the optimized fan power and fan speed respectively. As shown, the savings in fan power is significant, particularly during occupied hours. The overall savings in fan power is more than 50%.

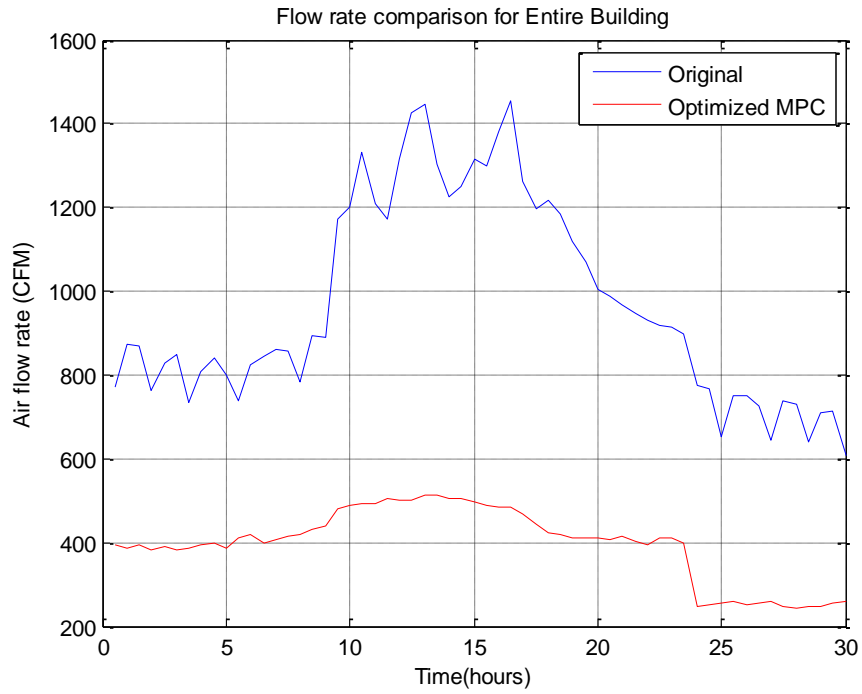


Figure 5.22: Optimized CFM for entire building

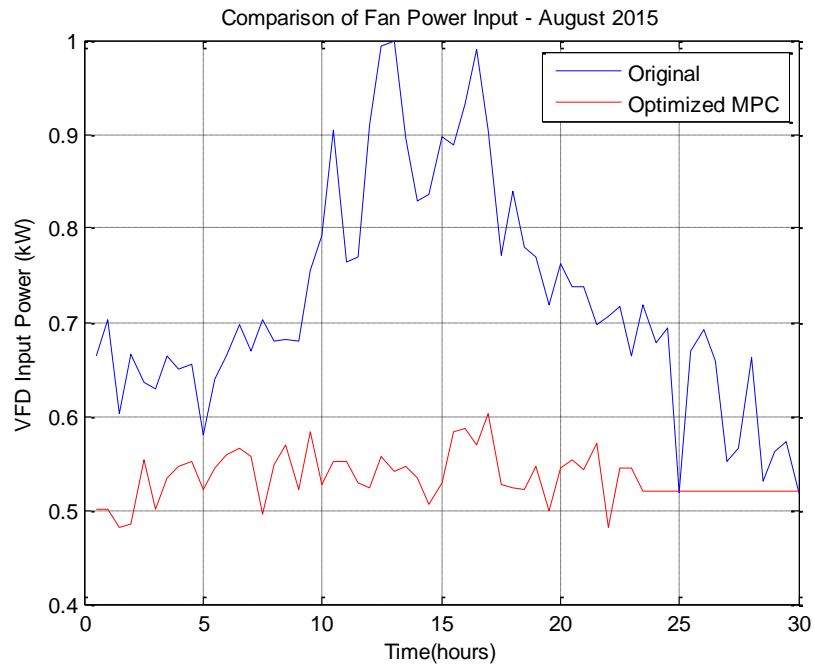


Figure 5.23: Optimized Fan Power for the AHU

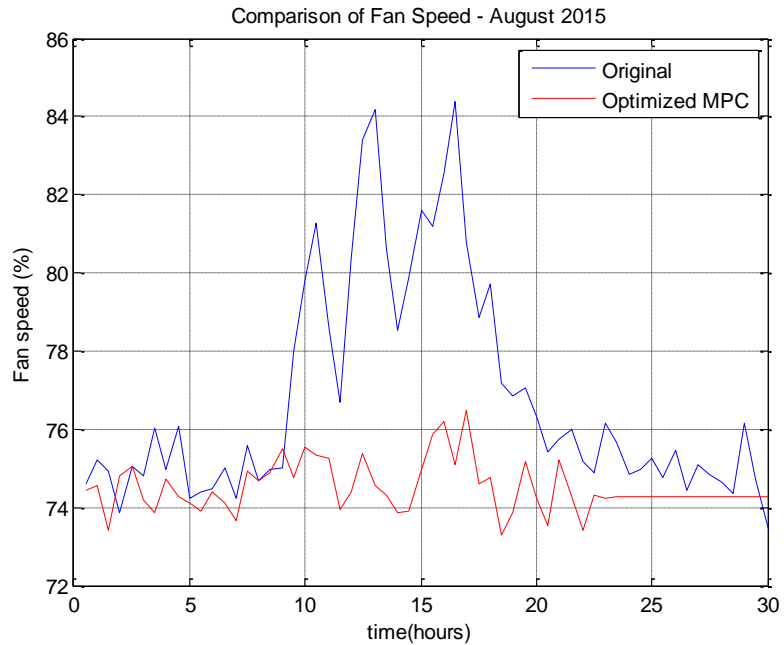


Figure 5.24: Optimized Fan Speed for the AHU

Additionally, as shown in Figure 5.24, the optimized fan operation suggests a narrow range of fan speed, as compared with the original. The optimized fan speed is between 73% and 76% of full speed.

5.5.3 Electricity cost

Figure 5.25 shows the summary of electricity cost which includes cooling cost, fan operating cost, and cost of lighting. The cooling cost was determined based on assumed chiller efficiency of 0.75kW/ton. As shown, the total electricity cost through optimal operation is significantly lower than the original cost of operation.

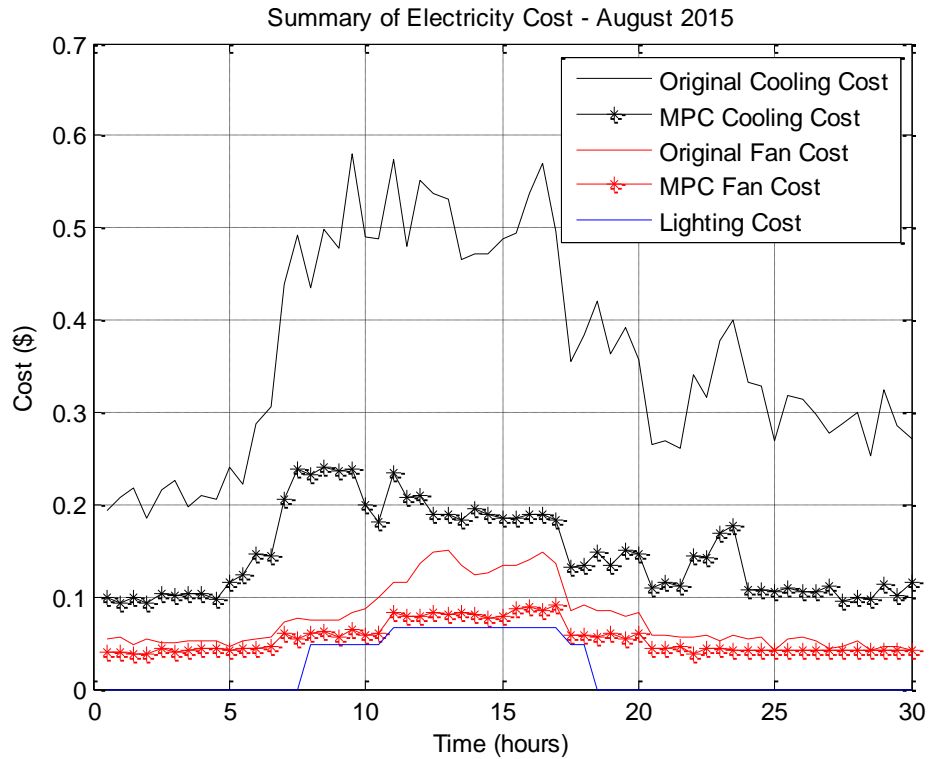


Figure 5.25: Overview of Electricity Cost

For the case study building, the savings in electricity cost is realized at every hour of the day, as the optimized cooling cost is consistently less than $\frac{1}{2}$ of the original cost. Analysis of the daily electricity cost shown in Figure 5.25 reveals total savings of up to \$13/day in electricity cost. Further savings could be achieved through lighting system operation, but that was not considered in this study.

Chapter 6: Step by Step Summary of Minimization Framework

Following the successful demonstration of model predictive control for minimizing electricity demand and cost in Chapter 5, this chapter describes the steps involved in the minimization framework. New information includes summary steps to cooling coil modeling using the R-C thermal network model, and stability check for the R-C state matrix.

6.1 Steps to Thermal Network Modeling of Building Load

- Identify case study building and internal loads
- Gather information about equipment limitations (e.g. temperatures, flow rates, pressure, speeds, etc.)
- Understand building layout (dimensions of walls, roof, windows, etc)
- Gather building construction materials information (if available)
- From building layout, sketch the thermal network representation (e.g. Figure 6.1):

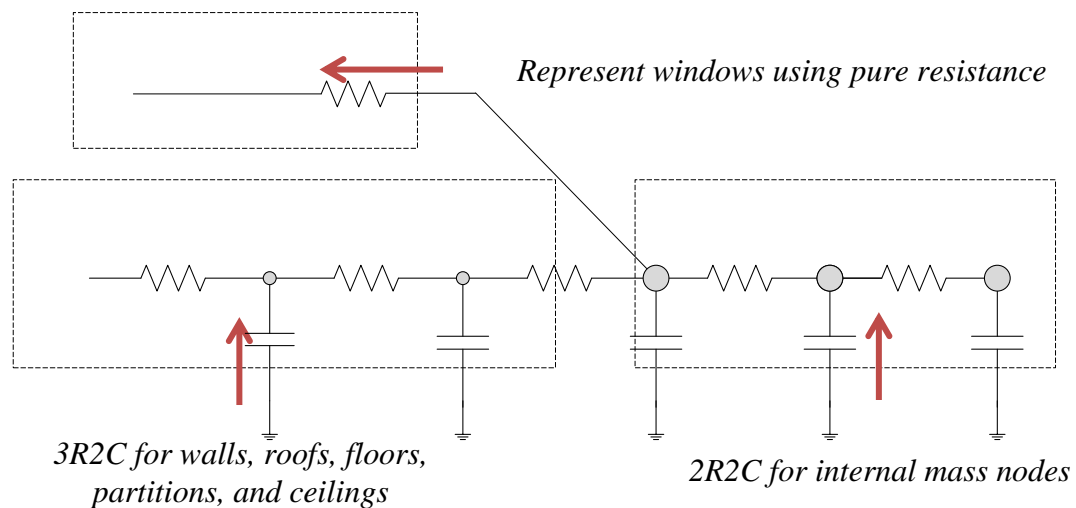


Figure 6.1: How to represent building components using the RC model

- Use 3R2C for walls, roofs, and ceilings; 2R2C for internal mass; 3R2C for partitions; and R for windows.
- Connect ambient, solar-air temperature, convection input, and solar-radiation inputs to their respective nodes as shown in Figure 6.2. (Convection input and cooling/heating rates connect directly to the zone temperature node while solar radiation connects to internal mass nodes. Ambient connects directly to windows, and solar-air temperature connects to exterior surfaces of walls, roofs, etc).

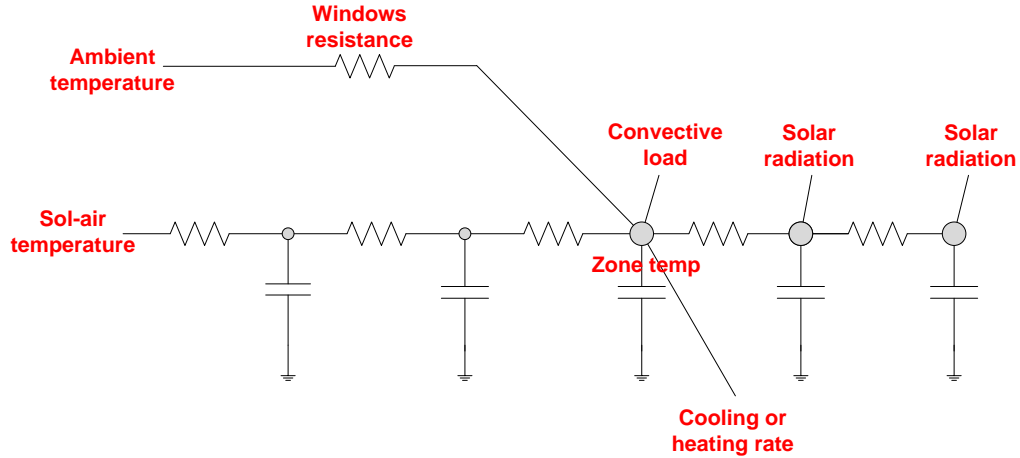


Figure 6.2: Connection of inputs and disturbances to the RC model

- To assure asymptotic stability of the R-C thermal network for the building load, connect a dummy ambient and dummy resistance to internal nodes
- Write the heat transfer equations for every nodal temperature, and express the total cooling load as the output in the state space equation.

$$\frac{dT_n}{dt} = -\frac{1}{C_n} \left(\sum_{i=1}^j \frac{1}{R_i} \right) T_n + \frac{1}{C_n} \left(\sum_{i=1, i \neq n}^j \frac{1}{R_i} T_i \right) + \frac{1}{C_n} \sum_{i=1}^p Q_i \quad (6.1)$$

$$Q_{cool} = -\left(\sum_{iz=1}^{m1} \frac{1}{R_i}\right)T_n + \left(\sum_{iz=1, iz \neq n}^{j1} \frac{1}{R_i}T_i\right) + \sum_{i=1}^{p1} Q_{iz} \quad (6.2)$$

Q_{iz} represent convection and cooling/heating rates connected to thermal zone iz , $m1$ is total number of thermal zones, and $j1$ is total number of temperature nodes connected to zone iz . The other variables are as previously defined. The contributions to the zone temperature node depicted by Equation (6.2) are as shown in Figure 6.3

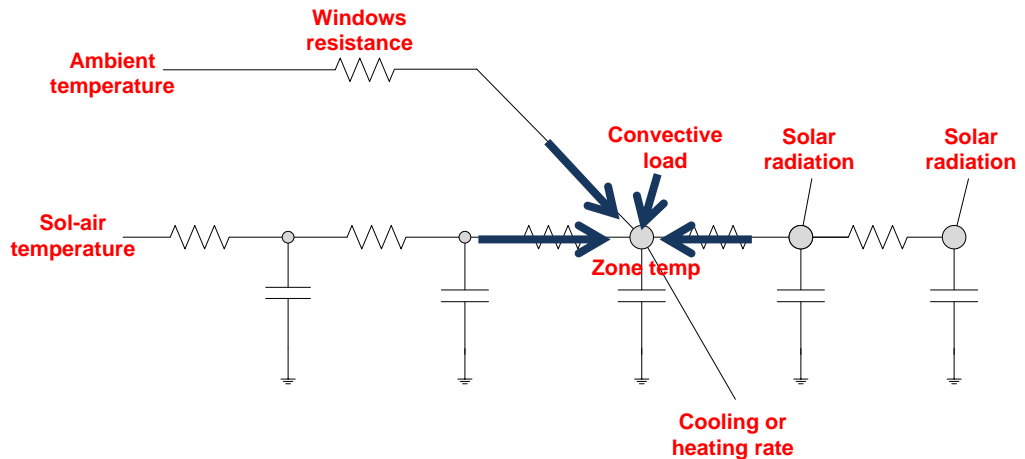


Figure 6.3: Contributions to the cooling load for a typical zone

- Check for stability, based on the requirement that the R-C state matrix is strictly diagonally dominant (i.e. sum of each row is <0 , and diagonal elements are <0)
- Gather needed data about variables such as ambient and solar radiation.
- Gather measurement data (Building usage information for cooling or heating season. Cooling rate, temperature set-points, flow rates (air and water). Time steps may be as small as 1minute.

- Identify optimized RC parameter set using genetic algorithm, particle swarm optimization, or combined with any other solver. Constraints on envelope RC parameters may be based on limits set by typical light and heavy weight construction. The internal mass capacitances and resistances could be an order of magnitude higher. Some of the R's could be assumed based on given (or assumed) heat transfer coefficient on interior or exterior wall surface.
- Validate model for another cooling or heating season by comparing predicted loads and temperatures with actual measurements.

6.2 Steps to Thermal Network Modeling of Cooling Coil

- Identify case study cooling coil
- Gather dynamic information: entry and leaving chilled water temperatures, chilled water flow rate, entry and leaving air temperatures (or enthalpies), air flow rate, etc. Time steps should be 1minute or smaller.
- Sketch the thermal network representation (using variable 3R2C for the coil), as shown in Figure 6.4

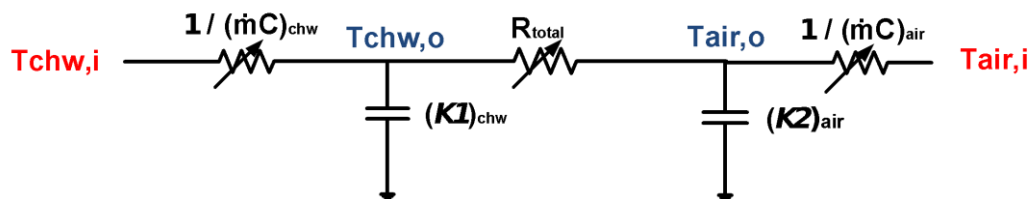


Figure 6.4: Thermal network representation for cooling coil

- Write the heat transfer equations for the chilled water outlet temperature (**Tchw, o**) and leaving air temperature (**Tair, o**). Since this is an R-C thermal network, the dynamic equations are similar to Equation 6.1 for the building load model.

- Identify the optimized parameters ($K1, K2, K3,$ and $K4$) using genetic algorithm, particle swarm optimization, or any other solver.
- Validate the model by comparing predicted exit temperatures with actual measurements, for given dynamic fluctuations in air and water flow rates.
- The R-C state matrix for the 3R-2C cooling coil model is strictly diagonally dominant, and does not require use of dummy variables to ensure stability.

6.3 Steps to minimizing building cooling demand

- After the thermal network model is developed and validated for the building load and cooling coil models, develop an integrated dynamic state space model, with state space matrices ($A_c, B_c, C_c,$ and D_c), where the subscript c implies that this is a continuous model.
- Convert the continuous state-space model to discrete model for a given sampling time, and extract the new matrices ($A_d, B_d, C_d,$ and D_d). Here, the subscript d refers to ‘discrete’

$$x_{k+1} = A_d x_k + B_d u_k \quad (6.3)$$

$$y_k = C_d x_k + D_d u_k \quad (6.4)$$

- Identify suitable time-steps and horizons (n) for which the cooling demand will be minimized ahead.
- From the time-steps and optimization horizon, generate the MPC model matrices which relate subsequent control actions, states, and outputs, to the current state and controls, as described by Equations (6.5) and (6.6)

$$x_{\rightarrow k+1} = P_x x_k + H_x u_{\rightarrow k} \quad (6.5)$$

$$\text{Where } P_x = \begin{bmatrix} A_d \\ A_d^2 \\ \vdots \\ A_d^n \end{bmatrix} \text{ and } H_x = \begin{bmatrix} B_d & 0 & \cdots & 0 \\ A_d B_d & B_d & \cdots & \vdots \\ \vdots & \vdots & \ddots & \vdots \\ A_d^{n-1} B & A_d^{n-2} B_d & \cdots & B_d \end{bmatrix}$$

$$y_{\rightarrow k+1} = \begin{bmatrix} C_d A_d \\ C_d A_d^2 \\ \vdots \\ C_d A_d^n \end{bmatrix} x_k + \begin{bmatrix} C_d B_d & 0 & \cdots & 0 \\ C_d A_d B_d & C_d B_d & \cdots & \vdots \\ \vdots & \vdots & \ddots & \vdots \\ C_d A_d^{n-1} B_d & C A^{n-2} B & \cdots & C_d B_d \end{bmatrix} \begin{bmatrix} u_{k|k} \\ \vdots \\ \vdots \\ u_{k+n-1|k} \end{bmatrix} \quad (6.6)$$

- Write the objective function as the minimization of a quadratic function in the water flow rate (GPM) and cooling rate, subject to constraints on temperatures (for thermal comfort and safety), the cooling rate, and the GPM (equipment limitation).

Minimize:

$$J(k) = \sum_{i=0}^{N-1} x^T(k+1|k) Q x(k+1|k) + u^T(k+1|k) R u(k+1|k) \quad (6.7)$$

Subject to: $A_c \mathbf{x} \leq x_c$

$$A_u \mathbf{u} \leq u_c$$

Where A_c is constraints matrix for the states, x_c is the constraints on the states (e.g. for thermal comfort), A_u is constraints matrix for the manipulated variable (u), and u_c is the constraint on the cooling rate and GPM (from equipment limitation). Q is deduced from the cooling load function (shown in Tables 5.6 to 5.19) for each thermal zone, and R is a specified positive definite matrix.

- Using quadratic programming or any other efficient solver, determine the control actions (GPM and cooling rates) which minimize the objective function (Equation 6.7) over the given horizon.

- Apply only the first control action ($u_{k+1|k}$) to the discretized system, and determine the new state x_{k+1} and output y_{k+1}
- Repeat the above procedure with the prediction and control horizon shifted ahead one-step at a time (known as receding horizon), until the entire optimization period is covered, as shown in Figure 6.5.

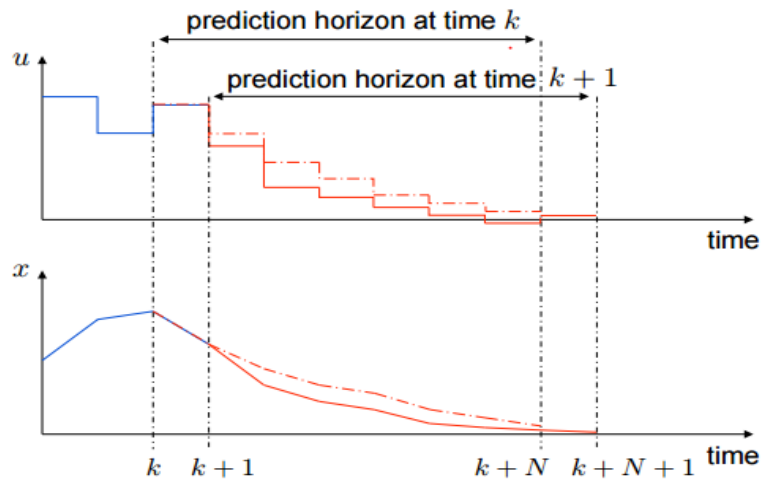


Figure 6.5: Receding horizon in MPC (Source: www.eng.ox.ac.uk)

6.4 Steps to minimizing building electricity cost

Electricity cost minimization requires the consideration of electricity tariff over the given period. To minimize the cost of electricity, the procedure is similar to cooling demand optimization, but with electricity tariff w_k (for the given time-step) applied as a weight on the objective function as shown in Equation (6.8).

$$J(k) = \sum_{i=0}^{N-1} w_k^2 x^T(k+1|k) Q x(k+1|k) + w_k^2 u^T(k+1|k) R u(k+1|k) \quad (6.8)$$

Subject to: $A_c \mathbf{x} \leq \mathbf{x}_c$

$$A_u \mathbf{u} \leq \mathbf{u}_c$$

Chapter 7: Original Contributions to Knowledge/Research

This chapter highlights the original contributions to knowledge/research based on results shown in Chapters 3 through 6. This dissertation has helped to bridge some of the knowledge gap in buildings energy systems operations and helped to further understanding of important phenomenon which are described in Sections 6.1 to 6.7 below.

7.1 Understanding of Stability of R-C thermal network

Published in: Ogunsola, O.T. and Song, L., 2015. Application of a simplified thermal network model for real-time thermal load estimation. Energy and Buildings, 96, pp.309-318.

The R-C thermal network approach has been widely applied for modeling of building load, but the stability of the R-C thermal network has not been investigated. The stability issues are important to understand the applicability (and limitations) of the thermal network approach and for identification of feasible R-C parameter domains.

The generalized equation for temperature nodes in a R-C thermal network is given by:

$$\frac{dT_n}{dt} = -\frac{1}{C_n} \left(\sum_{i=1}^j \frac{1}{R_i} \right) T_n + \frac{1}{C_n} \left(\sum_{i=1, i \neq n}^j \frac{1}{R_i} T_i \right) + \frac{1}{C_n} \sum_{i=1}^p Q_i \quad (7.1)$$

where

T_n = temperature of the nth node.

C_n = thermal capacitance of node n.

j = total number of connected temperature branches (including ambient, sol-air, and neighbor nodal temperatures) to node n.

T_i = temperature of the ith branch, connected to node n.

p = total number of heat flux branches (such as convection, radiation, and heat extraction or addition rate) impressed on node n .

Q_i = heat flux of the i th branch connected to node n . This term includes internal heat gains such as Q_r and Q_{conv} which are impressed on internal mass and zone temperature nodes respectively. Q_i also includes the heating or cooling rate of a device (Q_{sys}).

Q_{sys} applies to zone temperature nodes only

The first two terms of Equation (7.1) form the R-C state matrix. In understanding the behavior of the system, the R-C state matrix is instrumental to the study of building construction characteristics. It also determines the stability of the system. It could be observed that all diagonal entries of the R-C state matrix are negative. This is an important feature of stable systems, with stabilizing eigenvalues. As part of the original contributions of this study, certain features of the R-C state matrix were identified.

These are:

- i. The sum of each row corresponding to internal nodes are $=0$. For internal nodes, the heat balance equation is analogous to Kirchoff's current law, where the algebraic sum of currents at a node $= 0$.
- ii. The sum of each row with connections to ambient (or sol-air) temperature are <0 ; Therefore, the number of connections to ambient is equal to the number of rows having their sums <0 .
- iii. Without any connections to ambient or sol-air temperature, the R-C model will be, at best, marginally stable. This follows from (i) and (ii), because all rows in the R-C state matrix sums to zero in that case. This does not require additional proof.

- iv. With R-C parameters trained using actual buildings measurements; the R-C state matrix may not be symmetric.

The identified features hold for generalized R-C network model with envelope and internal mass components. The new findings enable the understanding of the stability of the R-C thermal network, and are summarized as follows:

- Internal zones modeled using the R-C network will be unstable or marginally stable. This is because the sum of each row in the R-C state matrix $=0$
- The generalized R-C model with a mix of exterior and interior nodes has R-C state matrix which is weakly diagonally dominant. The R-C state matrix must be irreducible for it to be non-singular and asymptotically stable. This is much more difficult to prove. The stability could be assured through the addition of dummy resistances and dummy ambient to all internal nodes. The dummy ambient is set to zero vector, so that it has no impact on the forced response. The dummy resistance is lumped into the estimation process, or given several orders of magnitude above the estimated R-values. The introduction of the dummy variables enable the R-C state matrix to be strictly diagonally dominant, for which the Gershgorin circle and the Levy-Desplanques theorems apply.
- The generalized R-C model with connections to ambient (and/or sol-air) in all temperature nodes has R-C state matrix which is *strictly* diagonally dominant. According to Gershgorin circle and the Levy-Desplanques theorems, the R-C state matrix will be non-singular, and the system is asymptotically stable. Unconstrained parameter search methods could be used to identify the R-C values.

- The 3R-2C model of cooling coil is strictly diagonally dominant, with negative diagonal elements. Hence, it is asymptotically stable.

Significance: The above findings are important, because they identify the stability issues of the thermal network model, which have never been investigated. The identified features of the R-C thermal network enable a quick check on the R-C state matrix for complex buildings with several nodes and branch connections. They also imply that the modeling of interior zones (without the introduction of dummy ambients) would lead to a R-C network model, which is, best case, neutrally stable. In such situations, the matrix inversion solution method would not be suitable.

7.2 Understanding of thermal characteristics of building construction

Published in: Ogunsola, O. and Song, L., 2014, November. Investigation of Building Passive Thermal Storage for Optimal Heating System Design. In ASME 2014 International Mechanical Engineering Congress and Exposition (pp. V08AT10A040-V08AT10A040). American Society of Mechanical Engineers.

The R-C parameters determine the category and classification of building construction (e.g. as light, medium, or heavy construction) and time scales of the building or cooling coil transient response. In this thesis, the R-C model was applied to further understanding of building construction characteristics by comparing the thermal response of light, medium, and heavy construction materials. The investigations include temperature floats study (i.e. temperature response in the absence of HVAC) as well as the thermal response of the building construction when HVAC system is in operation, for different climate classifications in the United States. Thermal responses of the different construction for two climate zones (Hot-humid and Cold) in the United States

are shown in Figures 7.1 and 7.2. The temperature responses depicted in the Figures offer insightful information to the behavior of the different construction. Some of the new findings are that:

- For cold and very cold climates, the HVAC system should not be turned off for more than two hours to avoid the risk of zone temperature dropping below the comfort limit.
- The heating system must be operating at full load shortly before and at the time of occurrence of minimum daily temperature.
- By factoring the passive thermal storage of building construction into the design of heating system, the heating system could be downsized by up to 33% for heavy construction, 23% for medium construction, and 22% for light construction in a Hot-humid climate while savings of up to 18%, 12%, and 9% are possible for heavy, medium, and light construction respectively in a cold climate.

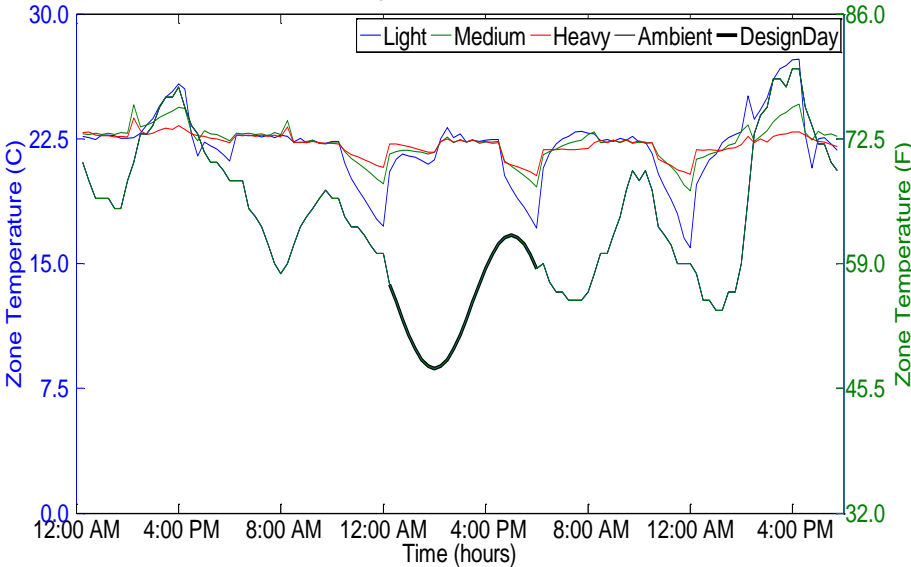


Figure 7.1: Thermal Response of Building Construction- Hot-Humid Climate

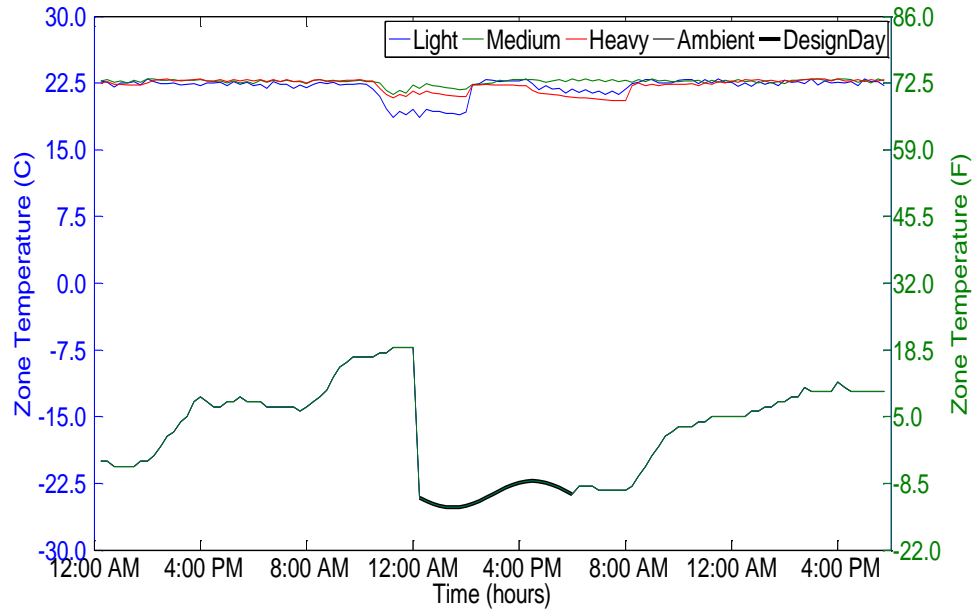


Figure 7.2: Thermal Response of Building Constructions- Cold Climate

Significance: The understanding of these behaviors is important for climate-responsive building envelope design which is essential to appropriately size HVAC equipment and minimize buildings cooling or heating needs. On a global scale, these findings help in making appropriate choice of construction types for different climate categories. The construction materials used have influence on material wastes, and sustainable use of resources (for example, in the use of light or medium construction materials instead of heavy construction).

7.3 Understanding of passive thermal storage capability of building construction

Published in: Ogunsola, O., Song, L. and Wang, Y., 2016. Analysis of passive thermal storage opportunities for heating system design. Science and Technology for the Built Environment.

The ASHRAE recommended heating load calculation model is most commonly used for heating load calculations. It adopts a simplified approach by considering only

steady-state conductive heat transfer. However, due to thermal storage effect, heat generated in daytime may still be stored in buildings and released at a later time. Such assumption leads to significantly over-sized heating systems which are usually accompanied by high initial cost and higher cost of energy use. The above simplified approach has been justified because it evaluates worst case conditions that can reasonably occur during a heating season, when diurnal temperature variations are considered small enough to ignore. By allowing space air to drift to reasonably lower values, buildings need to be warmed up before being occupied in the morning. The worst case conditions might happen during warm-up or beginning of occupied hours. Due to thermal and internal mass effects, heat gains in buildings during daytime may still be stored in the walls and radiation absorbing surfaces within the building. Heat absorbed by the thermal mass during occupied hours could be released during unoccupied hours. The heat released by the thermal mass may partially (or totally) compensate for the space heating needs during unoccupied periods without temperature dropping below the set minimum. Some of the investigations carried out in this study include temperature float study and heating system downsizing through consideration of passive thermal storage characteristics of building construction. A heavy wall construction was used for the building envelope. The temperature trajectory during floating period is mostly influenced by the envelope thermal mass, internal mass, and the incident outdoor conditions. As shown in Figures 7.3 and 7.4, there are varying behaviors across different climate classifications. For the thermal zone 1, very cold regions will achieve the night setback temperature within 5 h after the heating system was turned off. Meanwhile, hot-dry climates and marine regions will not reach the

setback temperature before the heat gains of the next day kicks in. By the start of occupancy period of the following day, typical office buildings in hot-dry climates have only experienced about 3.5C(6.3F) drop in zone temperature. The heat gains of the following day are sufficient to take the temperature to within 2.5C(4.5F) of desired conditions for comfort.

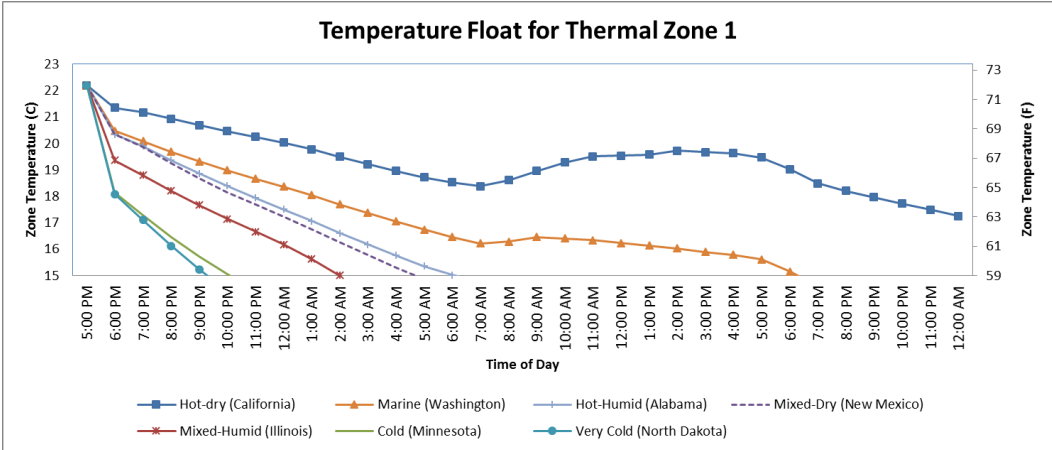


Figure 7.3: Temperature Float for Thermal Zone 1 (Zone 1 has north and east facing windows)

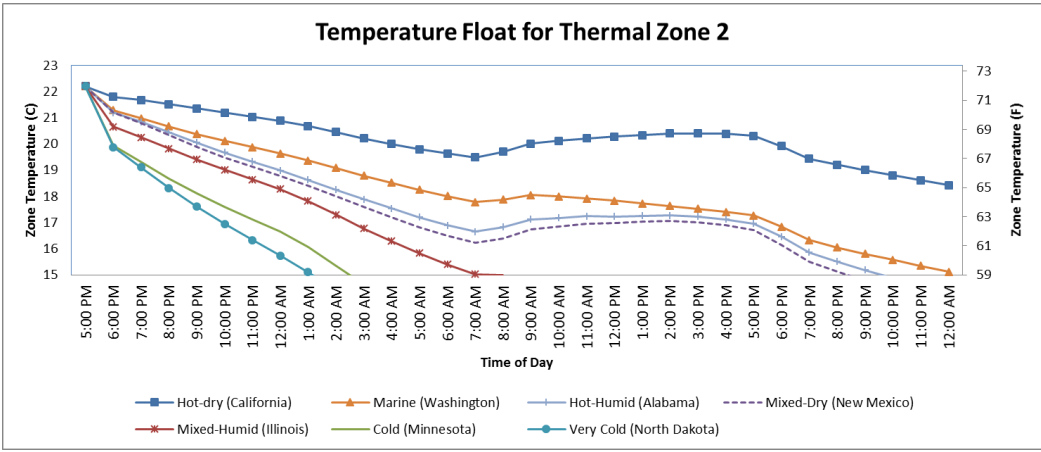


Figure 7.4: Temperature Float for Thermal Zone 2 (Zone 2 has only north-facing windows)

As could be deduced from Figures 7.5 and 7.6, downsizing opportunities vary widely across the U.S. but generally seem to decrease from southern states to northern states.

North-eastern states of the U.S. have the least savings. The largest savings is noted in California (54%), and the least was observed for Maine (14%).

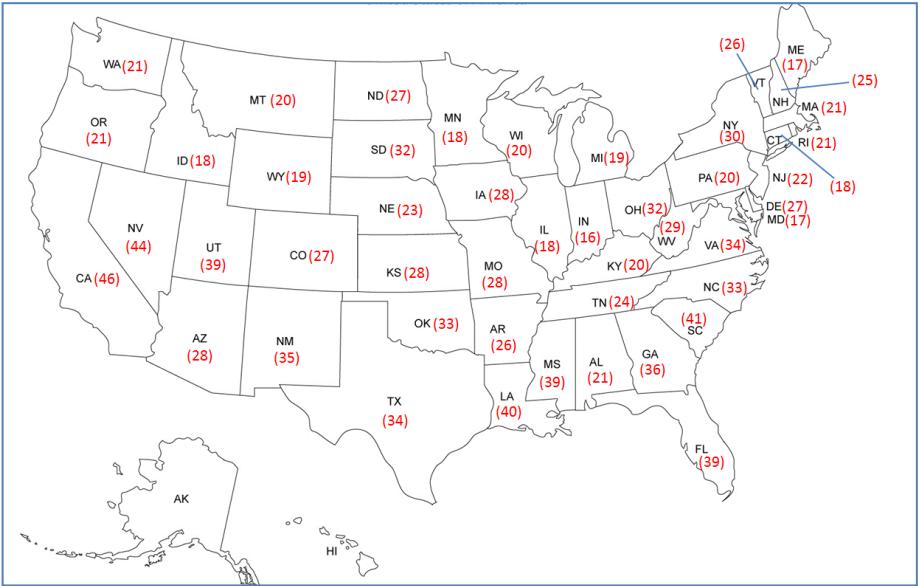


Figure 7.5: Downsizing Opportunities for Thermal Zone 1 (numbers in %)

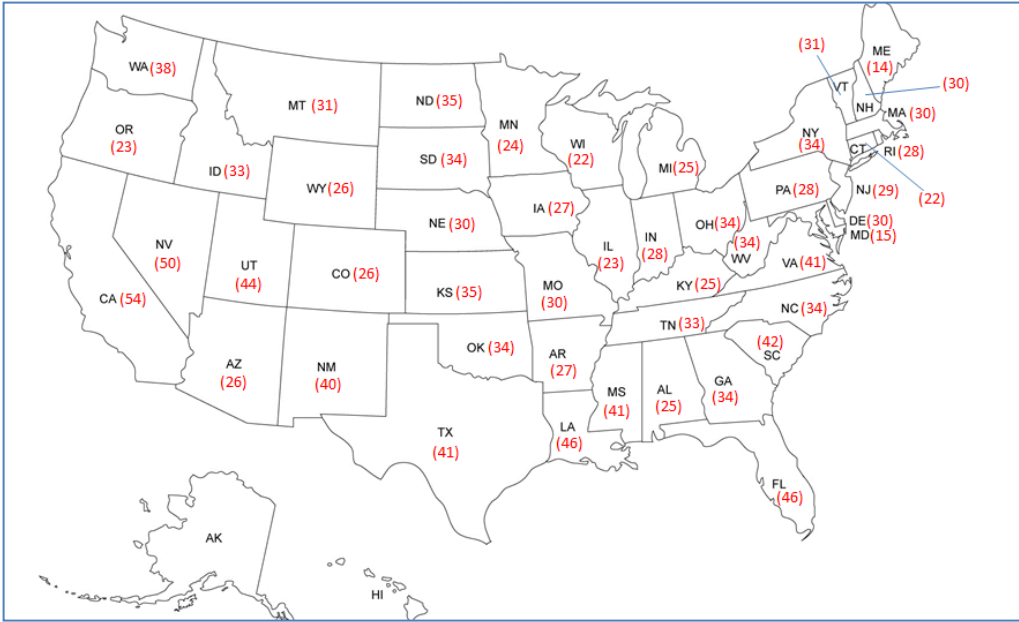


Figure 7.6: Downsizing Opportunities for Thermal Zone 2 (numbers in %)

Overall, hotter regions are seen to have larger downsizing opportunities, as compared with colder regions. This implies that using the ASHRAE method for hot regions such

as Florida and California may lead to significantly oversized system with the margin greater than 40%. The ASHRAE approximation is thus seen to be more suitable for colder regions, where the percentage of oversize is often less than 20%. Some of the new findings in this study include:

- i. The potential for equipment downsizing and energy savings in heating system operation is seen to increase according to climate type: Very cold region < Cold region < Mixed-Humid < Mixed- Dry < Hot-Humid < Marine < Hot-Dry Regions.
- ii. By analyzing the thermal response of the building construction for the heating design days, results show varying downsizing opportunities, ranging from 14% to 54% across the US.
- iii. For all the locations studied, there are savings on heating system size by considering passive thermal storage.
- iv. This study also offers insight into climate regions for which the ASHRAE approximation is most suitable.
- v. Additionally, reduction in heating system size implies corresponding reductions in electricity users such as fans and pumps. With HVAC systems accounting for 65% of electricity used in the United States, the overall contribution is in sustainable energy/electricity use through efficient sizing of equipment, and reduction of greenhouse gases due to electricity generation. Table 7.1 gives overview of the climate types and the downsizing opportunities.

Table 7.1 : Heating System Downsizing Opportunities in the US

Location Information		Climate Description			Downsizing (%)	
Station ID	State	Classification	Climate Type	ASHRAE	Zone 1	Zone 2
722230	Alabama	Class I	Hot-Humid	2A	21.0	25.0
722740	Arizona	Class I	Hot-dry	2B	28.0	26.0
723418	Arkansas	Class II	Hot-Humid	2A	26.0	27.0
722950	California	Class I	Hot-dry	2B	46.0	54.0
724769	Colorado	Class II	Cold	5B	27.0	26.0
725040	Connecticut	Class I	Cold	5A	18.0	22.0
724088	Delaware	Class II	Mixed-Humid	4A	27.0	30.0
722030	Florida	Class II	Hot-Humid	2A	39.0	46.0
747810	Georgia	Class II	Hot-Humid	2A	36.0	34.0
726813	Idaho	Class III	Cold		18.0	33.0
725314	Illinois	Class II	Mixed-Humid	4A	18.0	23.0
724320	Indiana	Class I	Mixed-Humid	4A	16.0	28.0
725460	Iowa	Class I	Cold	5A	28.0	27.0
724504	Kansas	Class III	Mixed-Humid	4A	28.0	35.0
724354	Kentucky	Class III	Mixed-Humid	4A	20.0	25.0
722405	Louisiana	Class II	Hot-Humid	2A	40.0	46.0
726060	Maine	Class I	Cold	6A	18.0	14.0
745940	Maryland	Class II	Mixed-Humid	4A	17.0	15.0
725067	Massachusetts	Class II	Cold	5A	21.0	30.0
725375	Michigan	Class I	Cold	5A	19.0	25.0
726575	Minnesota	Class II	Cold	6A	18.0	24.0
747686	Mississippi	Class II	Mixed-Humid	4A	39.0	41.0
723489	Missouri	Class II	Mixed-Humid	4A	28.0	30.0
727730	Montana	Class I	Cold	6B	18.0	31.0
725540	Nebraska	Class II	Cold	5A	23.0	30.0
723860	Nevada	Class I	Hot-Dry	2B	44.0	50.0
726055	New Hampshire	Class II	Cold	5A	25.0	30.0
725020	New Jersey	Class I	Mixed-Humid	4A	22.0	29.0

723650	New Mexico	Class I	Mixed-Dry	4B	35.0	40.0
744860	New York	Class I	Mixed-Humid	4A	30.0	34.0
723013	North Carolina	Class I	Hot-Humid	2A	33.0	34.0
727676	North Dakota	Class I	Very Cold	7	27.0	35.0
724288	Ohio	Class II	Cold	5A	32.0	34.0
723575	Oklahoma	Class II	Mixed-Humid	4A	33.0	34.0
726959	Oregon	Class III	Marine	5A	21.0	23.0
724080	Pennsylvania	Class I	Mixed-Humid	4A	20.0	28.0
725070	Rhode Island	Class I	Cold	5A	21.0	28.0
722080	South Carolina	Class I	Hot-Humid	2A	41.0	42.0
726625	South Dakota	Class II	Cold	5A	32.0	34.0
723340	Tennessee	Class I	Mixed-Humid	4A	24.0	33.0
722598	Texas	Class II	Hot-Humid	2A	34.0	41.0
724754	Utah	Class II	Hot-Dry	2B	39.0	44.0
726170	Vermont	Class I	Cold	6A	26.0	31.0
724050	Virginia	Class I	Mixed-Humid	4A	34.0	41.0
727938	Washington	Class II	Marine	4C	21.0	38.0
724140	West Virginia	Class I	Mixed-Humid	4A	29.0	34.0
726400	Wisconsin	Class I	Cold	6A	20.0	22.0
725640	Wyoming	Class I	Cold	6B	19.0	26.0

Significance: Results of this study suggests that the current heating device standard results in significantly oversized system for hot humid and hot dry regions of the U.S. These results are significant; with the potential of establishing a new heating device design standard for certain climate classifications.

7.4 Demonstration of R-C application to cooling coil models

(New results: To be submitted to ASHRAE Journal of Science and Technology for the Built Environment)

The cooling coil is an important component of the air handling unit. Most available cooling coil model require detailed information about the coil geometry, which is not available. Sometimes, available information is not reliable due to aging and other changes in the cooling coil due to use. This study extended the application of the R-C network model for transient modeling of cooling coil, through the use of flow-variable resistances and capacitances. The application of the R-C network to transient cooling coil model was illustrated using both temperature and enthalpy-based approaches.

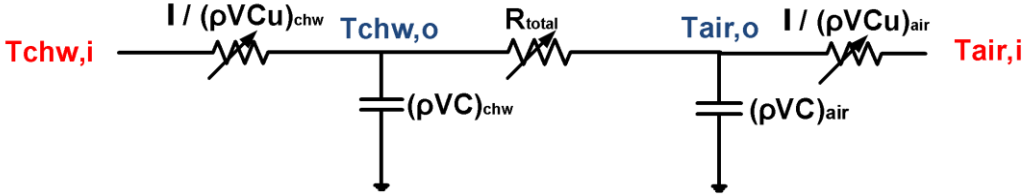


Figure 7.7: Thermal network model for cooling coil, temperature approach

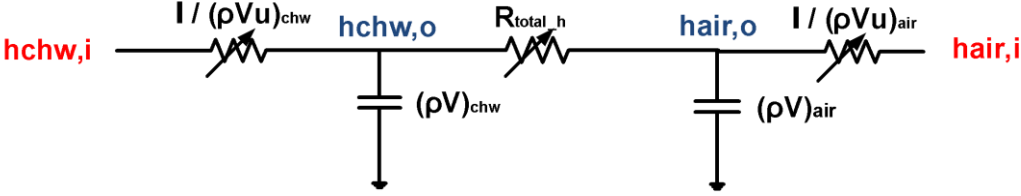


Figure 7.8: Thermal network model for cooling coil, enthalpy approach

The R-C representation enables the investigation of the time scale (e.g. time constants) as well as thermal capacities of the cooling coil unit, from short-term usage data. The demonstration of a flow-variable R-C network model for the cooling coil enhances compatibility with (and enables seamless integration of) the building load model, the chiller model, and the cooling coil model (as shown in Figure 7.9)

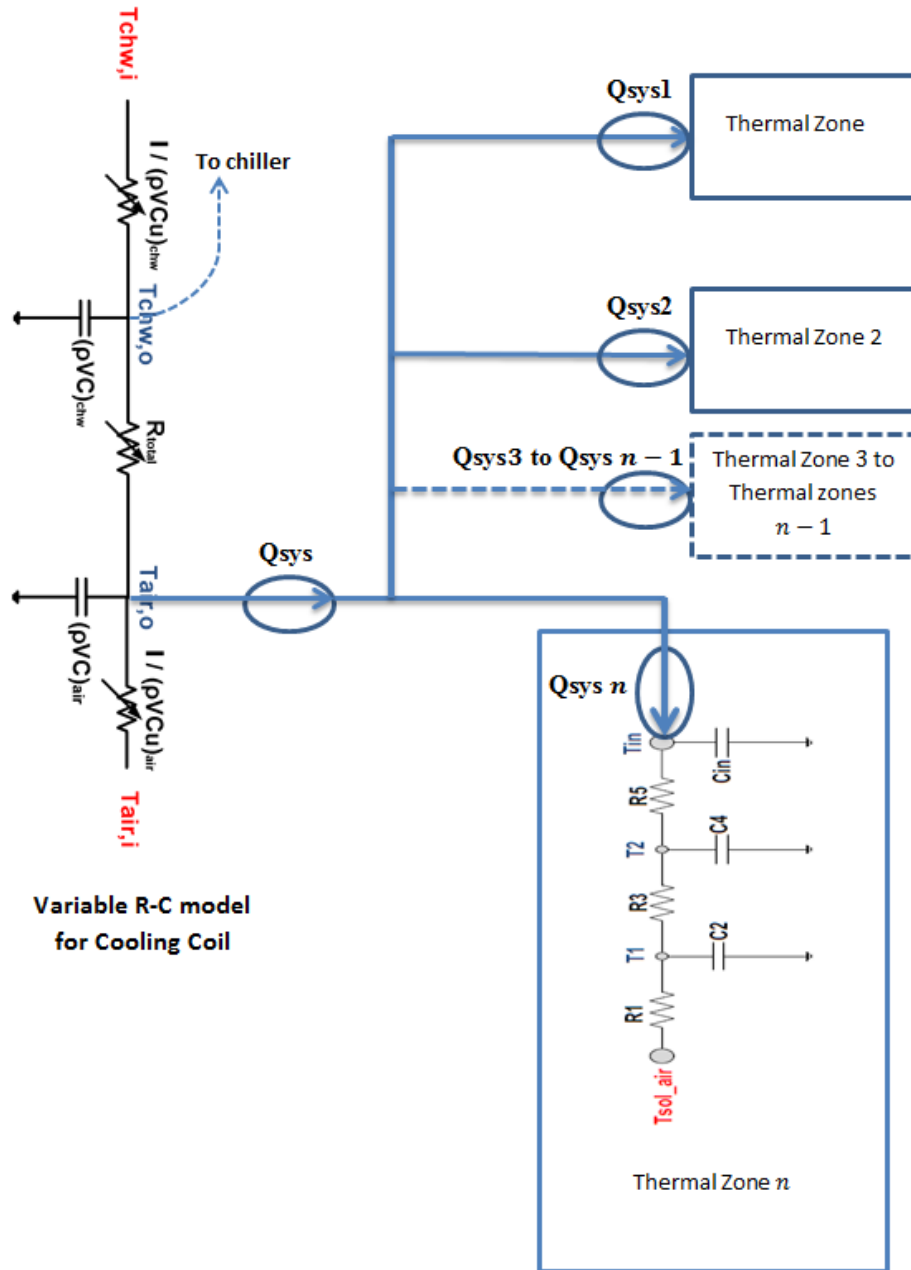


Figure 7.9: Integration of Building load and Cooling Coil Models

As such, existing control methods could be used for control and minimization of overall electricity cost, energy use, and other objectives as set by the researcher.

Significance: The integration of the building load and cooling coil model helped to simultaneously study the thermal responses of building and cooling coil, despite the differences in their time scales. This has helped to overcome some of the difficulties in

integration of the building load with the cooling coil model. One of the new findings is that the R-C state matrix for the 3R-2C cooling coil model is strictly diagonally dominant, and does not require use of dummy variables to ensure stability.

7.5 Understanding of multiple-zone interactions

(New results: To be submitted to ASHRAE Journal of Science and Technology for the Built Environment)

The purpose of thermal zoning in buildings is to group rooms that have similar loads and usage profiles, for the purposes of control. Such areas or zones could therefore be controlled by a single thermostat. Multiple zone interactions imply that cooling/heating needs in a particular zone is dependent on the states of the other zones. In a multi-zone building, the individual zones retain their thermal characteristics, but thermally interact with one another and compete for the available cooling/heating from the HVAC system. Therefore, the use of single zone modeling ignores important interactions among multiple thermal zones. The diversity of schedules, set-points, occupancy, usage, building orientation, and construction materials among multiple zones make the near-optima distribution of available cooling challenging. The study and understanding of multi-zone thermal interactions play a crucial role in efficient and intelligent operation of the HVAC equipment.

To study and understand multi-zone interactions, a multi-zone building with a variable air volume air handling unit was used as a case study. The case study building was also used as proof of concept that the R-C thermal model accurately predicts zone temperatures to between 0.16C (0.29F) and 0.7C (1.26F) mean absolute error (using

1min time-steps). The simulation results are shown in Chapter 5. The R-C thermal model requires short term data of actual building measurement to accurately predict temperatures and loads. No additional sensors are required, beyond the standard. The overall accuracy means that it could be adapted and applied for multiple control purposes (e.g. temperature and building load control) and fault diagnosis in any type of building.

Fundamental understanding of thermal zone interactions is critical to the minimization of overall electricity use in buildings, which is critical to achieving sustainable energy future. Integration of the plant model of building load, fans, and cooling coil enabled the study and understanding of different zone interactions. The approach is extendable to any type of system with producer-consumer relationship (such as multiple AHUs in a building, multiple buildings in a plant, or multiple buildings in a grid-network). Going by current state of knowledge, similar minimization strategies are generically applied to multiple thermal zones in a building. This study has led to interesting findings which have not been depicted in literature. Some of the new findings are:

- i. In a multiple zone building, individual zones require different minimization strategies, based on their thermal characteristics, orientation/exposure to ambient, and their inter-relationship with other zones. Therefore, the generic application of existing minimization strategies to all zones in a multiple zone building may not be effective.
- ii. In a multi-zone building, some of the thermal zones may serve as heat sink (as shown in Figures 7.10 to 7.13), and require cooling during on-peak hours, in order to achieve overall minimized electricity cost of entire building, due to their

thermal interaction with other zones. In the example study of 7 thermal zones, 2 of the zones were determined to be critical zones which required the above strategy.

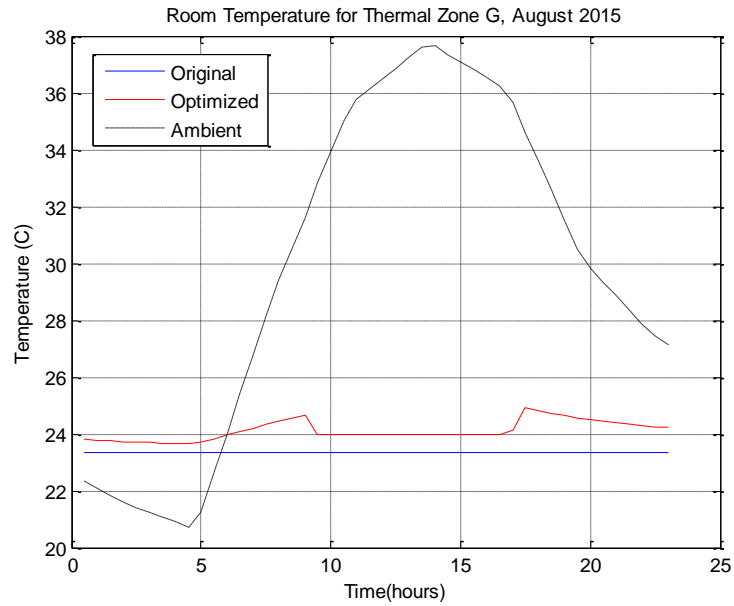


Figure 7.10: Optimized Temperature Trajectory – Thermal Zone G

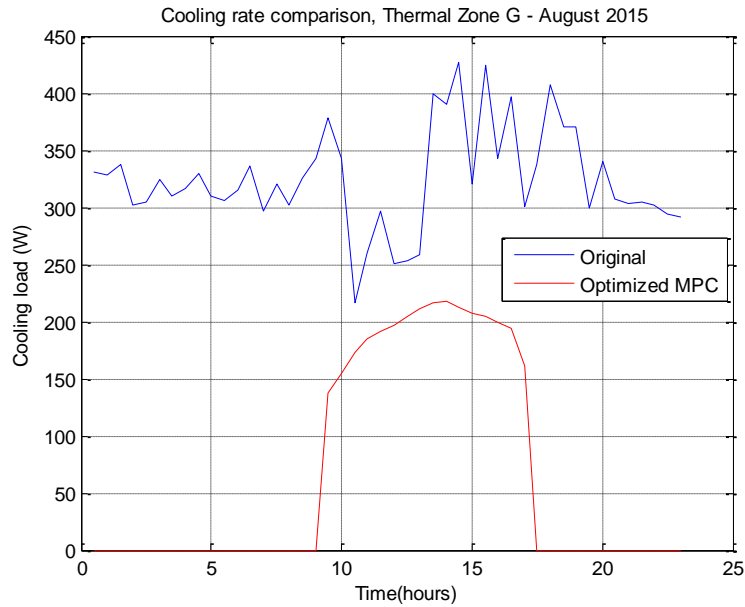


Figure 7.11: Optimized Cooling Load Profile – Thermal Zone G

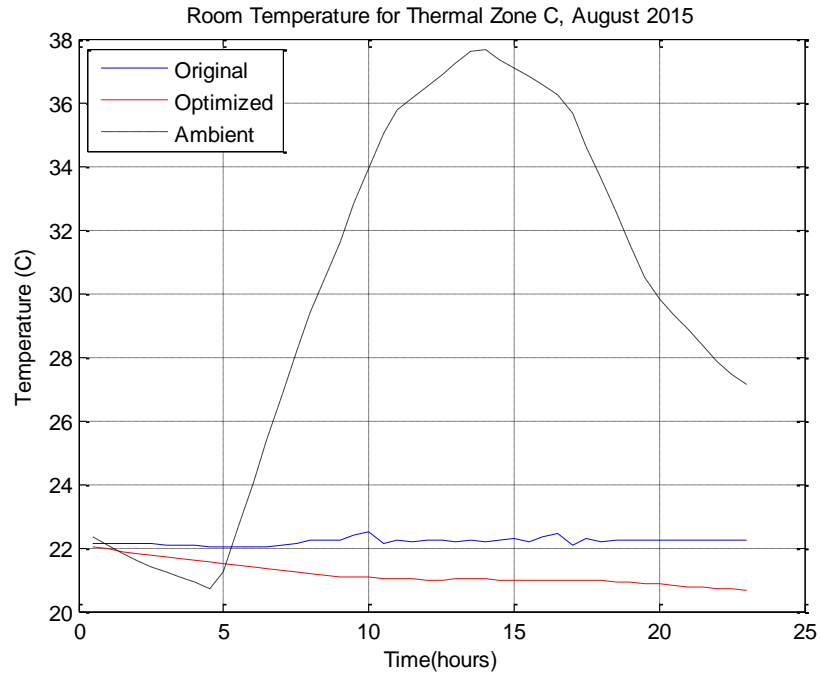


Figure 7.12: Optimized Temperature Trajectory – Thermal Zone C

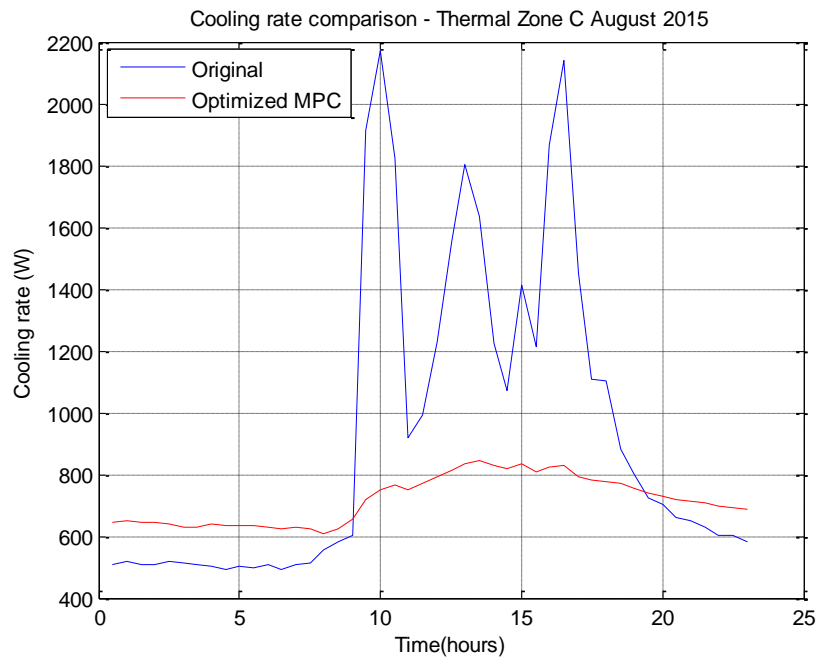


Figure 7.13: Optimized Cooling Load Profile – Thermal Zone C

- iii. Near –optimal determination of pre-cooling hours: precooling hours are generally determined by rule of thumb. The integration of the building load,

fans, and cooling coil model enabled use of control algorithms to determine near-optima precooling hours for thermal zones requiring such strategies.

- iv. This study identified some new strategies for minimizing electricity cost in a multiple zone building as shown in Table 7.2:

Table 7.2: New strategies for minimizing electricity cost in a multi-zone buildings

Strategy	Description
Near-constant cooling	Apply a near-constant cooling that reduces total electricity cost and peak demand
Temperature float + optimal start	Allow temperature float during off peak hours. Recover temperature at start of occupied hours and maintain upper limit.
Optimal precooling to lower limit of temperature	Optimally cool more when electricity is less expensive, and cool to maintain zone temperature at lower limit of comfort during peak hours

- v. The consideration of multi-zone interactions will lead to near-optima distribution of loads among complex network of interacting thermal zones served by one or more air handling units

7.6 Investigation of methods for filling missing gaps in Solar Radiation

Published in: Ogunsola, O. T., & Song, L. (2014). Restoration of long-term missing gaps in solar radiation. Energy and Buildings, 82, 580-591.

Solar radiation is an important climatic variable and widely used in building performance monitoring and analysis. However, due to sensor malfunction, data transmission problems, and quality assurance issues, there are often short-term or long-term missing data on solar radiation. These gaps are challenging for building performance monitoring and control. This study examined and compared three different

approaches, namely, singular spectrum analysis (SSA), statistically adjusted solar radiation (SASR), and the temperature-based approach (TBA), for restoring missing gaps (of up to 30 days) in solar radiation data. The limitations and merits of each method are summarized in the Tables 7.3 and 7.4.

Table 7.3: Limitations and merits of the SSA, TBA, and SASR methods

Method	Limitations	Merits
SSA	<ul style="list-style-type: none"> -Needs sufficient data points (10 days data in this study), to capture trend and oscillatory components. No existing method to determine the required number of data points -Accuracy dependent on proper choice of window length. Window length is often selected randomly or by rule of thumb. No generally acceptable rule for window length -In reconstructing missing gaps, the number of Eigen components to retain is often selected randomly, in order to filter out noise components 	<ul style="list-style-type: none"> -Independent of other climate variables -Able to identify trends, oscillations, and noise -Has highest accuracy for smaller gap lengths -There is no need to perform any time shift -There is no need to decompose daily solar radiation into hourly values -With proper choice of parameters, could be applied directly to fill missing data in total daily radiation as well
TBA	<ul style="list-style-type: none"> -Dependent on dry-bulb temperature -Time shift has to be performed when information about sunrise and sunset time is available -There is risk of losing some accuracy through decomposition of daily total radiation into hourly values -The length of existing data (dry-bulb temperature) required is equal to the number of days of missing data 	<ul style="list-style-type: none"> -Has very consistent level of accuracy for every gap length -Has highest accuracy for gap lengths greater than 10 days -Useful where solar radiation is reported as daily summations
SASR	<ul style="list-style-type: none"> -Dependent on dry-bulb temperature -Because of the statistical adjustment, there is risk of overcompensation during clear sky months -There is no procedure to determine the number of sufficient data to determine the statistical relationship between the ASHRAE clear sky model and the degree of over-prediction -Accuracy is generally lower for non-clear sky locations -The length of existing data (dry-bulb temperature) required is equal to the number of days of missing data -Not robust, therefore gives inconsistent results for different climate 	<ul style="list-style-type: none"> -SASR is model-based and statistically derived from the ACSM -There is no need to perform time shift -There is no need to decompose daily solar radiation into hourly values -It is the only method (among the three approaches) that is suitable for decomposing the total radiation into diffuse and direct components

Table 7.4: Recommended approach for different gap lengths.

Climate type	Gap length				
	1–2 days	2–5 days	5–15 days	10–25 days	>25 days
Mixed-humid	SSA		SSA, TBA	TBA	
Dry	SSA	SSA, TBA, SASR	TBA, SASR		

The approach could be extended to other climate types in continental US states. TBA method relies on the use of dry bulb temperature to estimate missing gaps in daily radiation. The SASR method was developed as one of the standard procedures of the ASHRAE 1413 research project (Hu et. al, 2014). This study introduced the use of SSA for filling missing gaps in solar radiation. SSA incorporates elements from a wide range of mathematical fields including classical time series analysis, multivariate statistics and geometry, dynamical systems, as well as signal processing. The study concluded by recommending appropriate methods for different gap lengths in solar radiation data, using case studies of two climates (mixed-humid, and dry).

Some of the findings are:

- SSA is the most suitable for shorter gap lengths of 5 days and smaller.
- TBA is the most suitable for larger gap lengths.
- SASR is seen to have very good agreement for locations with lots of clear sky days.
- The accuracy of SSA decreases with increasing gap length, but accuracies of TBA and SASR are less sensitive to gap length, since they are model-based.

- The appropriate method depends on other factors such as length of existing data, availability of reliable dry bulb temperature data and climate of the location.

7.7 Further Applications of Model Predictive Control

There has been very limited (or no) application of MPC for study of multi-zone interactions and minimization of electricity cost in a multi-zone variable air volume system, using the thermal network model. This is due to gaps in knowledge of important building phenomenon such as radiative delays and dynamic load changes due to solar radiation, ambient and internal load fluctuations. The unavailability of sufficiently accurate dynamic predictive model for building load and HVAC systems components have also limited the use of MPC. Most researchers use over-simplified regression models in form of ARIMA or time-series, without considering the dynamics of the building and HVAC components. The use of the accurate thermal network model in this study enabled the utilization of building dynamics in the MPC to achieve minimization objectives of choice, as determined by the researcher. Establishment of the accuracy level of the thermal network model enabled the utilization of MPC. Integration of the plant model of building load, fans, and cooling coil with the MPC opened up opportunities to study different zone interactions. This is the first research to demonstrate predictive control that utilizes building dynamics through the use of models that represent the building physically and captures important phenomenon e.g. radiative delays, thermal storage, multi-zone interactions etc.

Chapter 8: Conclusions and Future Work

The intellectual contribution of this dissertation is the understanding of multi-zone thermal interactions in buildings through the application of thermal models of building load and cooling coil (Sections 3.1, 3.2, 3.3, 5.5 and 7.5). This led to development and validation of methods for minimizing buildings electricity demand and cost at the air handling unit level (Section 5.1 – 5.3). It involved the development and validation of accurate and integrated dynamic thermal and airflow models for real-time building load prediction, cooling coil performance, and fan system operation, all of which are essential for the minimization of building electricity use at the air handling unit level. The developed models are part of a cyber-physical system (since they are physical based and deduced from fundamental study of building dynamics) which serves to integrate physical sensor measurement with thermal and mathematical model for real-time optimization and control of HVAC system operation. Further, all the developed models have been validated for actual air handling units components, with mean percentage errors generally <3% (Section 4.4, 4.5, and 4.6).

Through this research, the applicability of the thermal network approach of heat transfer has been expanded significantly, in areas such as the sizing of heating system (Section 7.3, and Ogunsola et. al, 2016), real-time forecast of cooling load (Section 4.3 - 4.4; Ogunsola et. al 2014, Ogunsola and Song 2015), understanding of fundamental characteristics of building construction from thermal modeling (Section 7.2; Ogunsola and Song 2015), application of variable R-C network for cooling coil model (Section 3.3, 4.6, and 7.4), study of passive thermal storage (Section 7.3 and Ogunsola et. al 2016), parameter estimation and identification for thermal model (Section 3.6;

Ogunsola and Song, 2014; Ogunsola and Song, 2013), identification of stability criteria for the thermal network model (Section 3.5 and 7.1; Ogunsola and Song, 2014), understanding of multi-zone thermal interactions (Section 5.5 and 7.5), and identification of multiple methods for minimization of electricity cost in a multi-zone building (Section 5.5 and 7.5).

This dissertation introduced the formulation, integrated solution, and validation of the simplified thermal network model of building load and cooling coil, using case study of multiple zones in a variable air volume system (Section 3.3 and 3.4). This research also identified certain features of the state matrix for building load and cooling coil, and conditions under which their thermal network models will be asymptotically stable (Section 3.5). The thermal network of cooling coil is asymptotically stable, since it is strictly diagonally dominant, with negative diagonal elements. The understanding of the stability issues assured the observability and controllability of the system while also eliminating concerns about invertibility of the state matrices for the thermal model, which is a necessary condition for all nodal temperatures and heat flux to remain bounded.

This research also contributes to knowledge in the development of step by step approach that may be followed to achieve system-wide optimal operation of the air handling unit, based on consideration of time of use electricity tariff (Section 6.1 to 6.4). Limited sensors information was utilized to develop accurate models in this study, and this overcomes the limitations posed by need for detailed data required by whole-building software models. The application of model predictive control framework led to identification of further minimization methods for multiple zones in a building, based

on individual cooling needs and thermal interactions with other zones (Section 5.1 to 5.5). Results showed that the simultaneous application of a generic optimization methodology to all the zones in a building may not be effective, due to uncontrollable inter-zone thermal interactions (Section 5.5.1). The summary contributions of this dissertation are as follows:

- **Understanding of multi-zone thermal interactions in buildings** (Section 5.5 and 7.5): This research has led to the understanding that zone temperatures in different thermal zones in a multi-zone building can be treated differently. This is because certain zones have more favorable thermal characteristics, which enables them to serve as critical zones, absorbing excess heat from surrounding zones. Such zones play a crucial role in the overall electricity demand and cost for a multi-zone building. This understanding has led to acceptance of the research hypotheses H1 (Section 1.3) that *Zone temperatures for individual zones in a multi-zone building can be treated differently, instead of equally as in traditional building operations*. This has helped to answer the research question *RQ1* by showing that multi-zone thermal interactions can be observed through the use of representative physics-based models of building load and cooling coil when the dynamics of the different thermal zones and the HVAC equipment are integrated into controller design.
- **Understanding of stability issues involved in thermal modeling of building load and cooling coil** (Section 3.5, Section 7.1): The thermal network model of building load has been widely used for load and temperature forecast, but the stability has never been investigated. The stability is critical to understand

feasible parameter domains for which the thermal network model will remain asymptotically stable, in order to physically represent actual building phenomenon. This research has led to understanding of conditions under which the thermal network model of building load will be asymptotically stable (Section 3.5). As a direct consequence of the stability analysis, it is seen that flow-variable R-C model for cooling coil will always be asymptotically stable. The conditions are valid for every finite R-C combination.

- **Understanding of thermal characteristics of building construction** (Section 7.2 and Ogunsola and Song 2014): This research has led to understanding of the temperature floats and thermal response of different construction materials in different climates. The understanding of these behaviors is important for climate-responsive building envelope design which is essential to appropriately size HVAC equipment, minimize buildings cooling or heating needs, and select appropriate construction material for different climate classifications.
- **Understanding of passive thermal storage capabilities of building construction for appropriate sizing of HVAC equipment** (Section 7.3 and Ogunsola et. al 2016): This research has led to identification of downsizing potentials and opportunities for heating system size reduction across different climates in the United States, based on passive thermal storage capability of building construction. The findings show that current heating device standard results in significantly oversized heating system for hot-humid and hot-dry regions of the U.S. Consideration of building dynamics and passive thermal

storage capabilities of building construction in heating system sizing have potential to save between 14% and 54% in heating system size.

- **Extension of the R-C thermal network approach to transient modeling of cooling coils** (Section 3.3, 4.6 and 7.4): This research extended the application of the thermal network model to the transient modeling of cooling coil, through the use of flow-variable resistances and capacitances. The approach was illustrated for both temperature and enthalpy-based approaches. The representation enables us to identify coil parameter from limited data, understand the timescales of the cooling coil, and integrate the cooling coil model to the building load model. This integration enabled the optimization of model predictive approach for the simultaneously optimization of building demand and cooling coil operation despite their different their time scales.
- **Identification of new methods for minimizing buildings electricity demand and cost** (Section 5.5 and 7.7): This research has led to the identification of new methods for minimizing electricity demand and cost in a multi-zone building. The identified methods have not been depicted in literature, and they do not follow conventional curtailment strategies. For example, one of the thermal zones requires continuous cooling and maintenance of zone temperature at the lower limit during peak hours. This is contrary to existing methods in literature, but the adoption of the method led to overall minimized electricity demand and cost for the entire multi-zone building. This also supports the research hypotheses H2 (Section 1.3) that *Individual zones in a multi-zone building*

require different strategies for electricity minimization rather than one strategy applying to all zones as in demand response (DR) literature

- **A demonstration of the electricity cost savings capabilities in air handling units operations:** This was demonstrated through the use of Model predictive control (MPC) strategies, integrated with the thermal network models of building load and cooling coil model (Section 5.5 and 7.7): This research has led to understanding of methods for minimizing electricity demand and cost in a multi-zone building. Results show that different thermal zone may require different minimization approach in order to minimize the overall electricity demand and cost among all thermal zones. This has led to acceptance of the research hypotheses H2 (Section 1.3) that *Individual zones in a multi-zone building require different strategies for electricity minimization rather than one strategy applying to all zones as in demand response (DR) literature*

8.1 Broader Impact

While the methods developed in this dissertation have been validated using typical air handling unit in a multi-zone building, the optimization approach could be generalized and extended to multiple air handling units, in a multi-zone building. Accuracies of building load modeling have been demonstrated at both single zone and multi-zone level. Additional thermal model capabilities that have been explored in this study include investigation of multiple HVAC scenarios, simulation of temperature fluctuations, simulation of both heating and cooling, and flexibility in the choice of thermal model parameters for estimation. These capabilities present cost-effective

solutions and opportunities for fault detection and diagnosis, control, and cost savings in buildings systems operation. The approaches developed in this dissertation could also be extended to other HVAC systems components such as pumps (chilled water pump, condenser water pump) and cooling tower fans for the optimization of water side equipment and operation. The thermal network approach of building load could be applied to any type of building, though the network connections get complicated with building complexity. The understanding of multi-zone interactions may be extended to study of supply-demand, producer-consumer systems or any other types of systems where subsystems compete for resources with other subsystems, but retain their individual characteristics e.g. that shown in Figure 8.1.

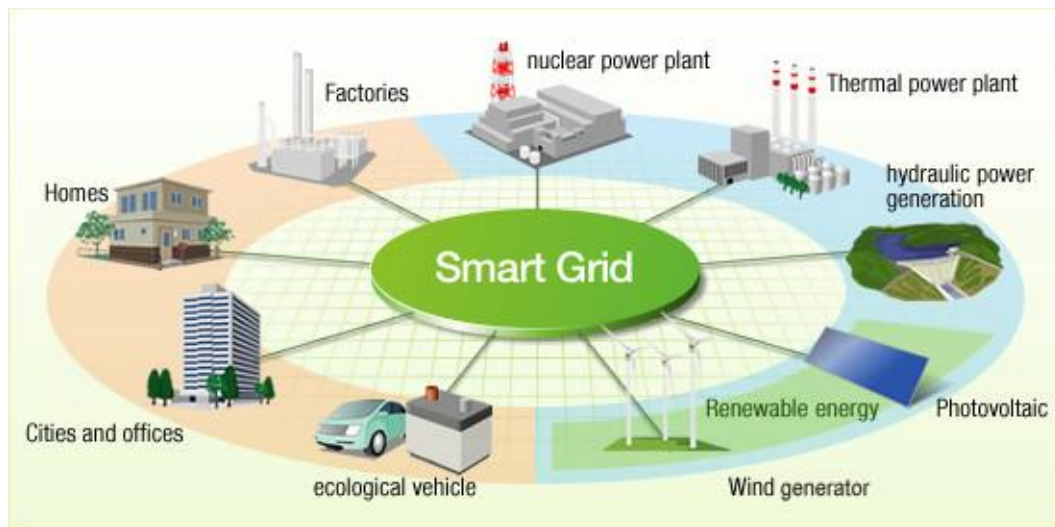


Figure 8.1: Smart Grid Integration

(Source: <http://www.examiner.com/article/smart-grid-initiatives-future-of-power-grid-superhighway>)

This is very useful for smart-grid architecture and integration, which is currently one of the emerging technologies. The new knowledge from this study, extended to

multiple buildings, could assist in demand management and generation of grid-commands, for smart and intelligent operation of grid networks

8.2 Limitations

Some of the limitations in this study include the practicability and real-time deployment of the developed methods, given the current computational limitations in buildings automation system. Other limitations stem from the assumption of static occupancy and internal load profiles for the simulated thermal zones. This study also did not consider the associated controls for valves and dampers, which are necessary for the system to successfully implement the suggested control actions and sequences. However, the opportunity to study multi-zone thermal interactions and the requirement of limited measurement data to accurately capture building systems dynamics make the developed methods in this dissertation promising for existing and future building automation system.

8.3 Future work

How to design critical thermal zones in any multi-zone building?

This research determined two zones in a multi-zone building to be critical zones. The zones were maintained at upper and lower comfort limits of temperature during peak periods. These zones were deemed instrumental to overall minimization of electricity demand and cost for the multi-zone building. Further studies are needed to identify and describe these critical zones for any given multi-zone building.

Water side equipment modeling and optimization

The approach in this dissertation was demonstrated for air handling units' components, using assumed chiller efficiency. Integration of water side equipment (chillers, and cooling towers) into the dynamic modeling and optimization is essential for minimization of electricity demand and cost in a central plant.

Optimization of lighting operation

Inefficient operation of the lighting subsystem is one of the reasons for unnecessary electricity use in buildings. This study only considered air handling unit components. Research into lighting system operation may uncover further methods and opportunities for minimizing electricity cost in a multi-zone building.

Effects of noise and uncertainty

Further studies should consider noise and uncertainty in the observation and dynamics. The basic time-invariant stochastic control problem with linear dynamics has state dynamics given by:

$$x(t + 1) = Ax(t) + Bu(t) + D_1w(t), \quad t = 0, 1, \dots \quad (8.1)$$

$$Y(t) = Cx(t) + D_2v(t) \quad (8.2)$$

Where $w(t)$ is the disturbance and $v(t)$, the measurement noise. For the R-C thermal network, $w(t)$ may also represent the exogenous (uncontrollable) inputs acting on the envelope (solar radiation, internal gains, etc.), or process noise. The MPC framework used in this study may be extended to optimize the stochastic control problem, i.e. to find a control policy that satisfies the state and control constraints, to minimize a certain objective. The stochastic process may be written as $x(t + 1) = Ax(t) + [B \ D_1] \begin{bmatrix} u(t) \\ w(t) \end{bmatrix}$

such that some of the solution methods described in this study may be used. The prediction model for the system will be:

$$x(k + t + 1|k) = Ax(k + t|k) + [B \ D_1] \begin{bmatrix} u(k + t|k) \\ w(k + t|k) \end{bmatrix}, \quad t = 0, 1, \dots \quad (8.3)$$

The prediction horizon should be chosen large enough to capture the periodicity of the exogenous factors, and the state vectors could be estimated using Kalman filters or other methods. Since the R-C network is stable, small perturbations are expected to have marginal impact on the system response.

References

1. “Utility-Scale Smart Meter Deployments, Plans, & Proposals,” **IEE Report**, May 2012, The Edison Foundation, The Institute for Electric Efficiency, www.edisonfoundation.net/iee/Documents/IEE_SmartMeterRollouts_0512.pdf.
2. Afram, A. and Janabi-Sharifi, F., 2014. Theory and applications of HVAC control systems—A review of model predictive control (MPC). *Building and Environment*, 72, pp.343-355.
3. Argyros, I.K. and Szidarovszky, F., 1993. *The theory and applications of iteration methods* (Vol. 4). CRC Press
4. Armstrong, P. R., Leeb, S. B., & Norford, L. K. (2006). Control with building mass-Part II: Simulation. *Transactions-American Society Of Heating Refrigerating And Air Conditioning Engineers*, 112(1), 462.
5. Armstrong, P.R., C. E. Hancock, and J.E. Seem (1992). Commercial Building Temperature Recovery- Part 1: Design procedure based on step response model. *ASHRAE Transactions*, 98(1): 381-396.
6. ASHRAE, *ASHRAE Handbook, Fundamentals Volume*, American Society of Heating, Refrigerating and Air-Conditioning Engineers, Inc., Atlanta, GA, 2005, pp.1989.
7. Bai, J., Wang, S. and Zhang, X., 2008. Development of an adaptive Smith predictor-based self-tuning PI controller for an HVAC system in a test room. *Energy and Buildings*, 40(12), pp.2244-2252.
8. Brakken-Thal, S. (2007). Gershgorin’s theorem for estimating eigenvalues. *Source*: <<http://buzzard.ups.edu/courses/2007spring/projects/brakkenthal-paper.pdf>.
9. Brandemuehl, M.J., S. Gabel and I. Andersen. 1993. A toolkit for secondary HVAC system energy calculation. *American Society of Heating, Refrigerating and Air-Conditioning Engineers*
10. Branesky, Brianna (2012). Masters Thesis. School of Aerospace and Mechanical Engineering, University of Oklahoma.
11. Braun J.E., T.M. Lawrence, C.J. Klaassen, and J.M. House (2002). Demonstration of load shifting and peak load reduction with control of building thermal mass. *Proceedings of the 2002 ACEEE Conference on Energy Efficiency in Buildings*, Monterey, CA.
12. Braun, J. E., and N. Chaturvedi (2002). An inverse grey-box model for transient building load prediction. *Int’l Journal of HVAC&R Research*, 8(1): 73-99
13. Braun, J. E., K.W. Montgomery, and N. Chaturvedi (2001). Evaluating Performance of Building Thermal Mass Control Strategies, *Int’l Journal of HVAC&R Research*, 7(4): 403-428.
14. Braun, J.E. (2003). Load control using building thermal mass. *Journal of Solar Energy Engineering* 125(3):292-301. New York: American Society of Mechanical Engineers.
15. Bueno, B., Norford, L., Pigeon, G., and Britter, R. (2012). A resistance-capacitance network model for the analysis of the interactions between the energy performance of buildings and the urban climate. *Building and Environment*, 54, 116-125.

16. Building and Construction Authority of Singapore (2010). Green Building Planning and Massing, available at <http://www.bca.gov.sg/GreenMark/others/bldgplanningmassing.pdf>, accessed June 25, 2014.
17. C. Lombard, E.H. Mathews. Efficient, steady state solution of a time variable RC network, for building thermal analysis, *Building and Environment*, 27.3 (1992), pp. 279–287
18. Candanedo JA, Athienitis AK. Predictive control of radiant floor heating and solar-source heat pump operation in a solar house. *HVAC R Res* 2011;17: 235e56.
19. Clark, D.R., 1985. HVACSIM+ building systems and equipment simulation program: Reference manual. NBSIR 84-2996, U.S. Department of Commerce, Washington D.C.
20. Cvetković, L., & Nedović, M. (2009). Special H-matrices and their Schur and diagonal-Schur complements. *Applied Mathematics and Computation*, 208(1), 225-230
21. D. Daum, N. Morel (2010). Assessing the total energy impact of manual and optimized blind control in combination with different lighting schedules in a buildingsimulation environment, *J. Build. Perform. Simul.* 3 (1) (2010) 1–16.
22. D. T. Delaney, G. O’Hare, M. P. Gregory, and A. G. Ruzzelli. Evaluation of energy-efficiency in lighting systems using sensor networks, *ACM BuildSys*, 2009.
23. Dobbs, J.R., and Hency, B. M. (2012). Automatic Model Reduction In Architecture: A Window into Building Thermal Structure, Fifth National Conference of IBPSA-USA Madison, Wisconsin August 1-3, 2012.
24. DoE (2010). www.doe2.com/equest/, accessed April 12, 2012
25. DOE, 1980. DOE 2 reference manual, Part 1, Version 2.1. Lawrence Berkeley National, Department of Energy.
26. DOE, EnergyPlus Version 7.0, United States Department of Energy, 2010, www.apps1.eere.energy.gov/buildings/energyplus/ (accessed 17.01.12).
27. DoE, M&V Guidelines: Measurement and Verification for Federal EnergyProjects, Version 3.0, 2008, Available at: http://www1.eere.energy.gov/femp/pdfs/mv_guidelines.pdf (accessed November 2014).
28. Elliott MS. Decentralized model predictive control of a multiple evaporator HVAC system [MSc thesis]. College Station, Texas, United States: Texas A&M University; 2008.
29. F. Causone, S.P. Corgnati, M. Filippi, B.W. Olesen, Solar radiation and coolingload calculation for radiant systems: definition and evaluation of the direct solar load, *Energy Build.* 42 (3) (2010) 305–314.
30. G. Fraisse, B. Souyri, S. Pinard, C. Menezo, Identification of equivalent thermal RC network models based on step response and genetic algorithms, in: *Proceedings of Building Simulation 2011: 12th Conference of International Building Performance Simulation Association*, Sydney, 14–16 November, 2011.

31. Ginestet, S. and Marchio, D., 2010. Control tuning of a simplified VAV system: Methodology and impact on energy consumption and IAQ. *Energy and Buildings*, 42(8), pp.1205-1214.
32. Goldman, C. M., Kintner-Meyer, and G. Heffner (2002). Do 'enabling technologies' affect customer performance in price-responsive load programs?, LBNL- 50328, Lawrence Berkeley National Laboratory, Berkeley, CA.
33. Goyal, S., Liao, C., Barooah, P. (2011). Identification of multi-zone building thermal interaction model from data, 2011 50th IEEE Conference on Decision and Control and European Control Conference (CDC-ECC) Orlando, FL, USA, December 12-15, 2011
34. Haves, P., and L, Gu (2001). Guideline for the operation of demand response HVAC systems, LBNL Report, Lawrence Berkeley National Laboratory, Berkeley, CA.
35. He, M., Cai, W. J., & Li, S. Y. (2005). Multiple fuzzy model-based temperature predictive control for HVAC systems. *Information sciences*, 169(1), 155-174.
36. Henze, G. P., Kalz, D. E., Liu, S., and Felsmann, C. (2005). Experimental analysis of model-based predictive optimal control for active and passive building thermal storage inventory. *HVAC&R Research*, 11 (2), 189-213.
37. Homod, R.Z., 2013. Review on the HVAC system modeling types and the shortcomings of their application. *Journal of Energy*, 2013.
38. Horn, R. A. and Johnson, C. R., *Matrix Analysis*, Cambridge Univ. Press, 1999
39. Horn, R. A. and Johnson, C. R., *Matrix Analysis*, Cambridge University Press, 1985.
40. https://bizenergyadvisor.com/BEA1/PA/PA_Cooling/PA-14
41. Huang G. Model predictive control of VAV zone thermal systems concerning bi-linearity and gain nonlinearity. *Control Eng Pract* 2011;19:700e10.
42. Huang, G. and Jordán, F., 2012. Model-based robust temperature control for VAV air-conditioning system. *HVAC&R Research*, 18(3), pp.432-445.
43. International Renewable Energy Agency (2013). Thermal Energy Storage, Technology Brief, available at www.irena.org/Publications, accessed September 2013
44. J. Hu, Li. Song, R.A. McPherson, M. Zhu, Y. Hong, S. Chen, Developing Standard Procedures for Filling Climatic Data Gaps for Use in Building Performance Monitoring and Analysis, ASHRAE Research Project 1413-RP, 2013.
45. J.D. Feng, S. Schiavon, F. Bauman, Cooling load differences between radiant and air systems, *Energy Build.* 65 (2013) 310–321.
46. J.E. Seem, S.A. Klein, *et al.* Transfer functions for efficient calculation of multidimensional transient heat transfer, *Journal of Heat Transfer*, 111 (1989), pp. 5–12
47. J.R. Dobbs, B.M. Hency, Automatic model reduction in architecture: a window into building thermal structure, in: Fifth National Conference of IBPSA-USAMadison, Wisconsin, August 1–3, 2012.
48. J.R. Dobbs, Brandon Hency: A Comparison of Thermal Zone Aggregation Methods, CDC, 2012, pp. 6938–6944.
49. Jacobon, David. 1986. Bibliography of BLAST Related Articles. BLAST Support Office, University of Illinois at Urbana-Champaign.

50. Javed, F., Arshad, N., Wallin, F., Vassileva, L., Dahlquist, E. (2012). Forecasting for demand response in smart grids: An analysis on use of anthropologic and structural data and short term multiple loads forecasting. *Applied Energy*, Volume 96, issue (August, 2012)
51. Jin, G. Y., Cai, W. J., Wang, Y. W., & Yao, Y. (2006). A simple dynamic model of cooling coil unit. *Energy Conversion and Management*, 47(15), 2659-2672.
52. K. Spees and L. Lave. Ceic-07-02: Impacts of responsive load in pjm: Load shifting and real time pricing
53. Kalogirou, S. A. (1999). Applications of artificial neural networks in energy systems. *Energy Conversion and Management*, 40(10), 1073-1087.
54. Kalogirou, S. A. (2000). Applications of artificial neural-networks for energy systems. *Applied Energy*, 67(1), 17-35.
55. Karlsson H, Hagentoft C-E. Application of model based predictive control for water-based floor heating in low energy residential buildings. *Build Environ* 2011;46:556e69.
56. Keeney, K. R. and J. E. Braun (1997). Application of Building Precooling to Reduce Peak Cooling Requirements, *ASHRAE Transactions*, 103 (1): 463-469.
57. Kintner-Meyer, M., C. Goldman, O. Sezgen, and D. Pratt (2003). Dividends with demand response, *ASHRAE Journal* 45(10): 37-43
58. Kulkarni, M.R. and Hong, F., 2004. Energy optimal control of a residential space-conditioning system based on sensible heat transfer modeling. *Building and Environment*, 39(1), pp.31-38.
59. L. Duanmu, Z. Wang, Z.J. Zhai, X. Li, A simplified method to predict hourly building cooling load for urban energy planning, *Energy Build.* 58 (2013) 281–291.
60. L. Xuemei, D. Lixing, L. Yan, X. Gang, L. Jibin, Hybrid genetic algorithm and support vector regression in cooling load prediction, in: *Third International Conference on Knowledge Discovery and Data Mining, 2010 (WKDD'10)*, IEEE, 2010, January, pp. 527–531.
61. L.C. Braga, A.R. Braga, C.M.P. Braga, On the characterization and monitoring of building energy demand using statistical process control methodologies, *Energy Build.* (2013).
62. Li, C. and Wang, R. Z. (2012). Building Integrated Energy Storage Opportunities in China, *Renewable and Sustainable Energy Reviews*, 16, 6191–6211
63. Li, N., Li, S. Y., & Xi, Y. G. (2004). Multi-model predictive control based on the Takagi–Sugeno fuzzy models: a case study. *Information Sciences*, 165(3), 247-263
64. Lombard, C., and Mathews, E. H. (1992). Efficient, steady state solution of a time variable RC network, for building thermal analysis. *Building and Environment*, 27(3), 279-287.
65. Lombard, C., and Mathews, E. H. (1999). A two-port envelope model for building heat transfer. *Building and environment*, 34(1), 19-30.
66. Lü H, Jia L, Kong S, Zhang Z. Predictive functional control based on fuzzy T-S model for HVAC systems temperature control. *J of Control Theory Appl* 2007;5:94e8.

67. Lu, J., Sookoor, T., Srinivasan, V., Gao, G., Holben, B., Stankovic, J., Field, E. and Whitehouse, K., 2010, November. The smart thermostat: using occupancy sensors to save energy in homes. In *Proceedings of the 8th ACM Conference on Embedded Networked Sensor Systems* (pp. 211-224). ACM.
68. Lu, L., Cai, W., Chai, Y. S., & Xie, L. (2005). Global optimization for overall HVAC systems—Part I problem formulation and analysis. *Energy conversion and management*, 46(7), 999-1014.
69. M. Sourbron, B. Martine, H. Lieve, Thermal response of thermally activated building systems (TABS) in office buildings [C], in: Proceedings of EFFSTOCK, Stockholm, Sweden, 2009, pp. 57–64.
70. Ma J, Qin J, Salsbury T, Xu P. Demand reduction in building energy systems based on economic model predictive control. *Chem Eng Sci* 2011;67:92e100.
71. Mackiw, G., Note on the Equality of the Column and Row Rank of a Matrix, *Mathematics Magazine* 68 (1995), no. 4, 285-286.
72. Maile T., Fischer, M., and Bazjanac, V. (2007). Building Energy Performance Simulation Tools-Life-cycle and Interoperable Perspective, Center for Integrated Facility Engineering, Stanford University.
73. Mao, C., Haberl, J. S., & Baltazar, J. C. (2013). Peak heating/cooling load design methods: how we got to where we are today in the US. In Proceedings of 13th International Conference of the IBPSA, France, pp. 143 – 151.
74. McKenzie, L. W. (1960), Matrices with dominant diagonals and economic theory; in K. J. Arrow, S. Karlin and P. Suppes (Eds.), *Mathematical Methods in the Social Sciences*, Stanford Univ. Press, Stanford, 1960, 47-62
75. Mesonet (2014). http://www.mesonet.org/index.php/weather/mesonet_datafiles (accessed March 2014, February 2016).
76. Moradi, H., Bakhtiari-Nejad, F. and Saffar-Avval, M., 2012. Multivariable robust control of an air-handling unit: A comparison between pole-placement and H_∞ controllers. *Energy Conversion and Management*, 55, pp.136-148.
77. Morgan, S. and Krarti, M. (2010). Field Testing of Optimal Controls of Passive and Active Thermal Storage ASHRAE Transactions 2010, Vol. 116, Part 1.
78. Morosan P-D, Bourdais R, Dumur D, Buisson J. Building temperature regulation using a distributed model predictive control. *Energy Build* 2010;42: 1445e52.
79. Nassif, N., S. Moujaes and M. Zaheeruddin, 2008. Self-tuning dynamic models of HVAC system components. *Energy Build.*, 40: 1709-1720. DOI: 10.1016/j.enbuild.2008.02.026
80. O.T. Ogunsola, L. Song, Performance analysis of a simplified model of cooling load for a typical office building, in: ASME 2013 International Mechanical Engineering Congress and Exposition, American Society of Mechanical Engineers, 2013, V011T06A025–V011T06A025.
81. Ogunsola, O. and Song, L., 2014, November. Investigation of Building Passive Thermal Storage for Optimal Heating System Design. In *ASME 2014 International Mechanical Engineering Congress and Exposition* (pp. V08AT10A040-V08AT10A040). American Society of Mechanical Engineers.
82. Ogunsola, O. T., & Song, L. (2012, November). Review and Evaluation of Using RC Thermal Modeling of Cooling Load Prediction for HVAC System

- Control Purpose. In *ASME 2012 International Mechanical Engineering Congress and Exposition* (pp. 735-743). American Society of Mechanical Engineers.
83. Ogunsola, O., Song, L. and Wang, Y., 2015. Analysis of passive thermal storage opportunities for heating system design. *Science and Technology for the Built Environment*, (just-accepted), pp.00-00.
 84. Ogunsola, O.T. , Song, L. , and Wang, G. (2014). Development and validation of a time-series model for real-time thermal load estimation, *Energy Build.* 76 (2014) 440–449.
 85. Ogunsola, O.T. and Song, L., 2015. Application of a simplified thermal network model for real-time thermal load estimation. *Energy and Buildings*,96, pp.309-318.
 86. Ogunsola, O. T., and Song, L. (2014). Restoration of long-term missing gaps in solar radiation. *Energy and Buildings*, 82, 580-591.
 87. Oldewurtel, F., Parisio, A., Jones, C. N., Morari, M., Gyalistras, D., Gwerder, M., Stauch, V., et al. (2010). Energy efficient building climate control using stochastic model predictive control and weather predictions. *American Control Conference (ACC)*, 2010 (pp. 5100–5105).
 88. Oldewurtel, F., Parisio, A., Jones, C., Morari, M., Gyalistras, D., Gwerder, M., ... & Wirth, K. (2010). Energy efficient building climate control using stochastic model predictive control and weather predictions. In *Proceedings of the 2010 American control conference* (No. EPFL-CONF-169733, pp. 5100-5105). Ieee Service Center, 445 Hoes Lane, Po Box 1331, Piscataway, Nj 08855-1331 Usa.
 89. Parisio, A., Fabietti, L., Molinari, M., Varagnolo, D. and Johansson, K.H., 2014, December. Control of HVAC systems via scenario-based explicit MPC. In *Decision and Control (CDC), 2014 IEEE 53rd Annual Conference on*(pp. 5201-5207). IEEE.
 90. Poole, D., 2014. *Linear algebra: A modern introduction*. Cengage Learning.
 91. Privara S, Siroky J, Ferkl L, Cigler J. Model predictive control of a building heating system: the first experience. *Energy Build* 2011;43:564e72.
 92. Putta, V., Zhu, G., Kim, D., Hu, J., & Braun, J. (2013). Comparative evaluation of model predictive control strategies for a building HVAC system. *American Control Conference (ACC)*, 2013 (pp. 3455–3460). IEEE.
 93. Putta, V.K., Kim, D., Cai, J., Hu, J. and Braun, J.E., 2014. Distributed Model Predictive Control for building HVAC systems: A Case Study.
 94. Qi, Q. and Deng, S., 2009. Multivariable control of indoor air temperature and humidity in a direct expansion (DX) air conditioning (A/C) system. *Building and Environment*, 44(8), pp.1659-1667.
 95. R. Ramanathan, *Introductory Econometrics with Applications*, 3rd ed., HarcourtBrace College Publishers, Fort Worth, 1995, pp. 800.
 96. Radecki, P. and Brandon H. (2012). Online building thermal parameter estimation via Unscented Kalman Filtering, *American Control Conference (ACC)*, 2012. IEEE, 2012.
 97. Rehr J, Horn M. Temperature control for HVAC systems based on exact linearization and model predictive control. In: *Int Conf Control Appl (CCA)*. Denver, Colorado, USA: IEEE; 2011. pp. 1119e24.

98. Ruud, M. D., J. W. Mitchell, and S. A. Klein (1990). Use of Building Thermal Mass to Offset Cooling Loads. *ASHRAE Transactions*, 96(2): 439-446.
99. S. Schiavon, K.H. Lee, F. Bauman, T. Webster, Simplified calculation method for design cooling loads in underfloor air distribution (UFAD) systems, *EnergyBuild*. 43 (2) (2011) 517–528.
100. S.W. Wang, X.H. Xu, Parameter estimation of internal thermal mass of building dynamic models using genetic algorithm, *Energy Convers. Manage.* 47 (2006)13–14.
101. Sadineni, S. B., Madala, S. and Boehm, R. F. (2011). Passive building energy savings: A review of building envelope components, *Renewable and Sustainable Energy Reviews* 15 (2011) 3617–3631
102. Schmidt D., and Johannesson, G. (2004). Optimised RC Networks Incorporated within Macro-Elements for Modelling Thermally Activated Building Constructions, *Nordic Journal of Building Physics*, Vol. 3, 2004.
103. Schnieders, J., and Hermelink, A. (2006). CEPHEUS results: measurements and occupants' satisfaction provide evidence for Passive Houses being an option for sustainable building. *Energy Policy*, 34(2), 151-171.
104. Seem, J.E., P.R. Armstrong, and C.E. Hancock (1989). Algorithms for predicting recovery time from night setback, *ASHRAE Transactions*, 95(2): 439-446.
105. Sherwin, Elton B. 2010. *Addiction to Energy: A Venture Capitalist's Perspective on How to Save Our Economy and Our Climate*. Knoxville, TN: Energy House Publishing.
106. Siroky J, Oldewurtel F, Cigler J, Privara S. Experimental analysis of model predictive control for an energy efficient building heating system. *Appl Energy* 2011;88:3079e87.
107. Snyder, M., and Newell, T. (1990). "Cooling Cost Minimization Using Building Mass for Thermal Storage," *ASHRAE Trans.*, **96_2_**, pp. 830–838.
108. Song, L., Joo, I.S. and Gunawan, S. (2012). Next-day daily energy consumption forecast model development and model implementation. *Journal of Solar Energy Engineering*, 134(3), p.031002.
109. Sourbron, Maarten, Martine Baelmans, and Lieve Helsen (2009). "Thermal response of thermally activated building systems (TABS) in office buildings [C]." *Proceedings of EFFSTOCK*. Stockholm, Sweden (2009): 57-64.
110. Stein, J. and M. Hydeman, 2004. Development and testing of the characteristic curve fan model. *ASHRAE Trans.*, 110: 347-356.
111. T. Chai, R.R. Draxler, Root mean square error (RMSE) or mean absolute error(MAE)? *Geosci. Model Dev. Discuss.* 7 (1) (2014) 1525–1534.
112. T. McKinley, A. Alleyne, Identification of Building Model Parameters and Loads using On-Site Data Logs, *SimBuild 2008*, Berkeley, CA, 2008.
113. United States Green Building Council (2011) <http://www.usgbc.org/>, accessed Jan. 20, 2012.
114. V. L. Erickson, Y. Lin, A. Kamthe, R. Brahme, A. Surana, A. E. Cerpa, M. D. Sohn, and S. Narayanan (2009). Energy Efficient Building Environment Control Strategies using Real-Time Occupancy Measurements, *ACM BuildSys*, 2009.

115. V.L. Chen, M.A. Delmas, W.J. Kaiser, Real-time, appliance-level electricity use feedback system: how to engage users? *Energy Build.* 70 (2014) 455–462.
116. Varga, R. S., & Gillis, J. (1963). Matrix iterative analysis. *Physics Today*, 16, 52 and Varga, R. S. (2009). *Matrix iterative analysis* (Vol. 27). Springer Science & Business Media.
117. Wallace, M., McBride, R., Aumi, S., Mhaskar, P., House, J. and Salsbury, T., 2012. Energy efficient model predictive building temperature control. *Chemical engineering science*, 69(1), pp.45-58.
118. Wang S.W., and Xu, X.H.(2006) Parameter estimation of internal thermal mass of building dynamic models using genetic algorithm, *Energy Conversion and Management* 47 (13–14)
119. Wang, S., & Jin, X. (2000). Model-based optimal control of VAV air-conditioning system using genetic algorithm. *Building and Environment*,35(6), 471-487.
120. Westphalen, D., & Koszalinski, S. (1999). Energy Consumption Characteristics of Commercial Building HVAC Systems. Volume II: Thermal Distribution, Auxiliary Equipment, and Ventilation. *Arthur D. Little Inc (ADLI)*, 20, 33745-00.
121. Westphalen, D., & Koszalinski, S. (1999). Energy Consumption Characteristics of Commercial Building HVAC Systems. Volume II: Thermal Distribution, Auxiliary Equipment, and Ventilation. Arthur D. Little Inc (ADLI), 20, 33745-00.
122. Wetter, M. (2006) Multizone Building Model for Thermal Building Simulation in Modelica, The Modelica Association, Modelica 2006, September 4th – 5th.
123. Wu, Z., Melnik, R.V. and Borup, F., 2007. Model-based analysis and simulation of airflow control systems of ventilation units in building environments. *Building and Environment*, 42(1), pp.203-217.
124. X. Pang, M. Wetter, P. Bhattacharya, P. Haves, A framework for simulation based real-time whole building assessment, *Build. Environ.* 54 (2012) 100–108.
125. X. Xu, Model Based Building Evaluation and Diagnosis (PhD Dissertation), Department of Building Services Engineering, The Hong Kong Polytechnic University, 2005.
126. Xi X-C, Poo A-N, Chou S-K. Support vector regression model predictive control on a HVAC plant. *Control Eng Pract* 2007;15:897e908.
127. Xing, H. Y. (2004). Building load control and optimization, PhD Thesis, Massachusetts Institute of Technology, Cambridge,, MA.
128. Xu M, Li S. Practical generalized predictive control with decentralized identification approach to HVAC systems. *Energy Convers Manag* 2007;48:292e9.
129. Xu, X. (2005). Model Based Building Evaluation and Diagnosis, PhD Dissertation, Department of Building Services Engineering, The Hong Kong Polytechnic University
130. Y. Agarwal, B. Balaji, S. Dutta, R. K. Gupta, and T. Weng. Duty- Cycling Buildings Aggressively: The Next Frontier in HVAC Control. In *IPSN*, 2011.
131. Y. Knyazikhin, J. Glassy, J.L. Privette, Y. Tian, A. Lotsch, Y. Zhang, Y. Wang, J.T. Morissette, P. Votava, R.B. Myneni, R.R. Nemani, S.W. Running. MODIS

- Leaf Area Index (LAI) and Fraction of Photosynthetically Active Radiation Absorbed by Vegetation (FPAR) Product (MOD15) Algorithm Theoretical Basis Document, <http://eosps0.gsfc.nasa.gov/atbd/modistables.html>
132. Yang L, and Li Y (2008). Cooling load reduction by using thermal mass and night ventilation. *Energy and Buildings*, 40 (11):2052–8.
 133. Yao, Y., Huang, M., Mo, J., & Dai, S. (2013). State-space model for transient behavior of water-to-air surface heat exchanger. *International Journal of Heat and Mass Transfer*, 64, 173-192.
 134. Yao, Y., Lian, Z., & Hou, Z. (2004). Thermal analysis of cooling coils based on a dynamic model. *Applied thermal engineering*, 24(7), 1037-1050.
 135. Yuan S, Perez R. Multiple-zone ventilation and temperature control of a single-duct VAV system using model predictive strategy. *Energy Build* 2006;38:1248e61.
 136. Yuan, S. and Perez, R., 2006. Multiple-zone ventilation and temperature control of a single-duct VAV system using model predictive strategy. *Energy and Buildings*, 38(10), pp.1248-1261.
 137. Yuan, S. and Perez, R., 2006. Multiple-zone ventilation and temperature control of a single-duct VAV system using model predictive strategy. *Energy and Buildings*, 38(10), pp.1248-1261.
 138. Zaheer-Uddin, M. and Zheng, G.R., 2000. Optimal control of time-scheduled heating, ventilating and air conditioning processes in buildings. *Energy Conversion and Management*, 41(1), pp.49-60.
 139. Zheng, G.R., 1997. *Dynamic modeling and global optimal operation of multizone variable air volume HVAC systems* (Doctoral dissertation, Concordia University).
 140. Zhou, X., & Braun, J. E. (2007). A simplified dynamic model for chilled-water cooling and dehumidifying coils—Part 1: Development (RP-1194). *HVAC&R Research*, 13(5), 785-804.

Appendix A: Fan Dynamic Model

Considering the dynamic performance of fan-motor will enhance opportunities to identify and save electricity cost, particularly where there are demand charges on electricity. The fan-motor model equations in this section were modified from ASHRAE Research Project RP- 738 which provides reference guide for dynamic models of HVAC Equipment. The dynamics of the electric motor could be represented using Equations (A.1) and (A.2)

$$\frac{dN_{motor}}{d\tau} = \frac{K_i I}{2\pi J_{eq}} - \frac{B_{eq} N_{motor}}{J_{eq}} - \frac{\dot{V}_{fan}(\Delta P_{fan})_{tot}}{(2\pi)^2 J_{eq} N_{motor} \eta_{fan}} \quad (A.1)$$

$$\frac{dI}{d\tau} = \frac{e_a}{L_a} - \frac{R_a I}{L_a} - \frac{2\pi K_b N_{motor}}{L_a} \quad (A.2)$$

As may be seen, the differential equation is nonlinear in the motor speed. The torque applied to the fan shaft is provided by the armature current. It overcomes the inertia and friction forces. The first fan law is used to algebraically model the fan, as shown in Equation (A.3) below:

$$(\Delta P_{fan})_{tot} = C_h \rho_a D_{fan}^2 N_{fan}^2 \quad (A.3)$$

This equation relates the changes in fan speed with the total fan pressure rise,

where: $N_{fan} = \frac{n_m}{n_f} N_{motor}$

There are 2 state variables, N_{mf} and I_{mf} . By linearizing about some operating

conditions N_{mfs} , U_s , and I_{mfs} . Such that the operating point $h_s = \begin{bmatrix} N_{mfs} \\ I_{mfs} \end{bmatrix}$, the state

variable, and inputs become:

$$x = \begin{bmatrix} N_{mf1} \\ I_{mf1} \end{bmatrix} = \begin{bmatrix} N_{mf} - N_{mfs} \\ I_{mf} - I_{mfs} \end{bmatrix} \quad (A.4)$$

$$U = \frac{e_{af}}{L_{af}} U_{fan} - U_s = U_{mf1} - U_s \quad (A.5)$$

The system could now be represented in state space as Equation (A.6):

$$\begin{bmatrix} \dot{N}_{mf} \\ \dot{I}_{mf} \end{bmatrix} = \begin{bmatrix} \dot{N}_{mf1} \\ \dot{I}_{mf1} \end{bmatrix} = \begin{bmatrix} \frac{\partial F_1}{\partial N_{mf1}} & \frac{\partial F_1}{\partial I_{mf1}} \\ \frac{\partial F_2}{\partial N_{mf1}} & \frac{\partial F_2}{\partial I_{mf1}} \end{bmatrix} \begin{bmatrix} N_{mf1} - N_{mfs} \\ I_{mf1} - I_{mfs} \end{bmatrix} + \begin{bmatrix} \frac{\partial F_1}{\partial U_{mf1}} \\ \frac{\partial F_2}{\partial U_{mf1}} \end{bmatrix} [U_{mf1} - U_s] \quad (A.6)$$

Jacobian linearization of the nonlinear ODE yields Equations (A.7) to (A.12)

$$\frac{\partial F_1}{\partial N_{mf1}} = -\frac{B_{eqf}}{J_{eqf}} + \frac{ma \frac{\Delta P_f}{(2\pi)^2 \rho J_{eqf} \eta_f}}{N_{mfs}^2} \quad (A.7)$$

$$\frac{\partial F_1}{\partial I_{mf1}} = \frac{K_i}{2\pi J_{eqf}} \quad (A.8)$$

$$\frac{\partial F_2}{\partial N_{mf1}} = -\frac{2\pi K_{bf}}{L_{af}} \quad (A.9)$$

$$\frac{\partial F_2}{\partial I_{mf1}} = -\frac{R_{af}}{L_{af}} \quad (A.10)$$

$$\frac{\partial F_1}{\partial U_{mf1}} = 0 \quad (A.11)$$

$$\frac{\partial F_2}{\partial U_{mf1}} = 1 \quad (A.12)$$

$$\text{where } F1 = \frac{K_i I}{2\pi J_{eq}} - \frac{B_{eq} N_{motor}}{J_{eq}} - \frac{\dot{V}_{fan} (\Delta P_{fan})_{tot}}{(2\pi)^2 J_{eq} N_{motor} \eta_{fan}} \quad (A.13)$$

$$\text{and } F2 = \frac{e_a}{L_a} - \frac{R_a I}{L_a} - \frac{2\pi K_b N_{motor}}{L_a} \quad (A.14)$$

For simplicity, let $A = \frac{K_i}{2\pi J_{eqf}}$, $B = \frac{B_{eqf}}{J_{eqf}}$, $C = ma \frac{\Delta P_f}{(2\pi)^2 \rho J_{eqf} \eta_f}$, $D = \frac{e_{af}}{L_{af}} U_{fan}$, $E = \frac{R_{af}}{L_{af}}$,

and $F = \frac{2\pi K_{bf}}{L_{af}}$, such that $\frac{\partial F_1}{\partial N_{mf1}} = -B + \frac{C}{N_{mfs}^2}$, $\frac{\partial F_1}{\partial I_{mf1}} = A$, $\frac{\partial F_2}{\partial N_{mf1}} = -F$, and $\frac{\partial F_2}{\partial I_{mf1}} =$

– E , the linearized system could be transformed to state space representation, and solved using the analytical solution method described for the building load in previous section. Figure A.1 and A.2 compares the transient performance of the nonlinear system (solved numerically) with that of the linearized system (solved using state space methods). As could be seen, the linearized systems behavior is very similar to the nonlinear system.

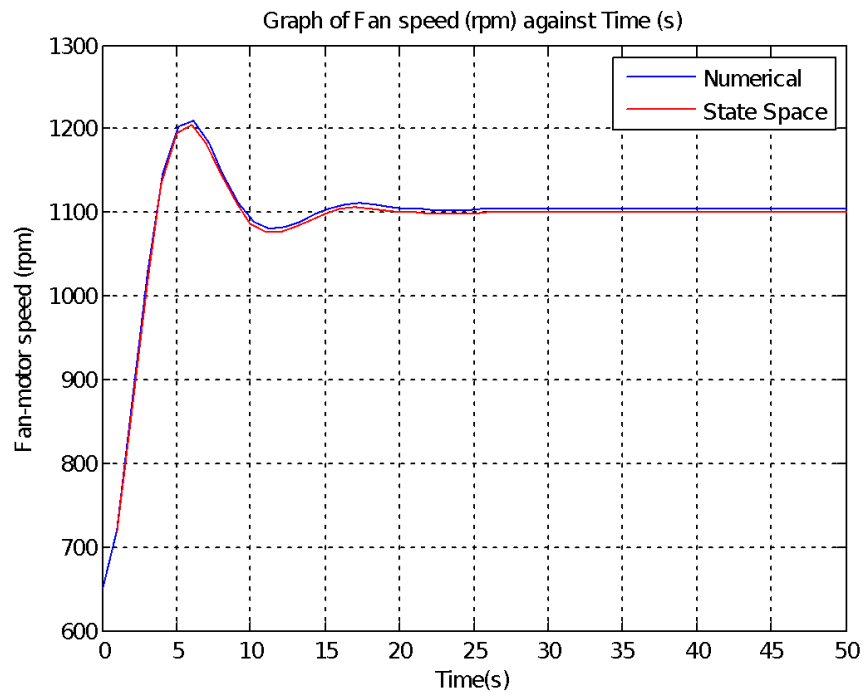


Figure A.1: Transient fan motor speed

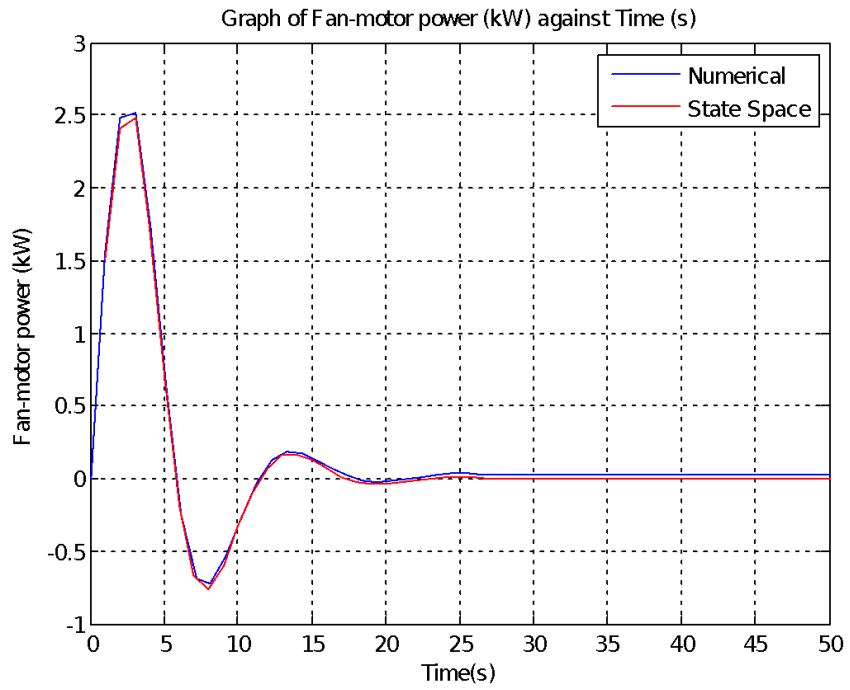


Figure A.2: Transient fan-motor power

The above system can be translated to a thermal network model, where the nodes are the motor speed, and armature currents respectively.

Appendix B: Fan Static Pressure Reset

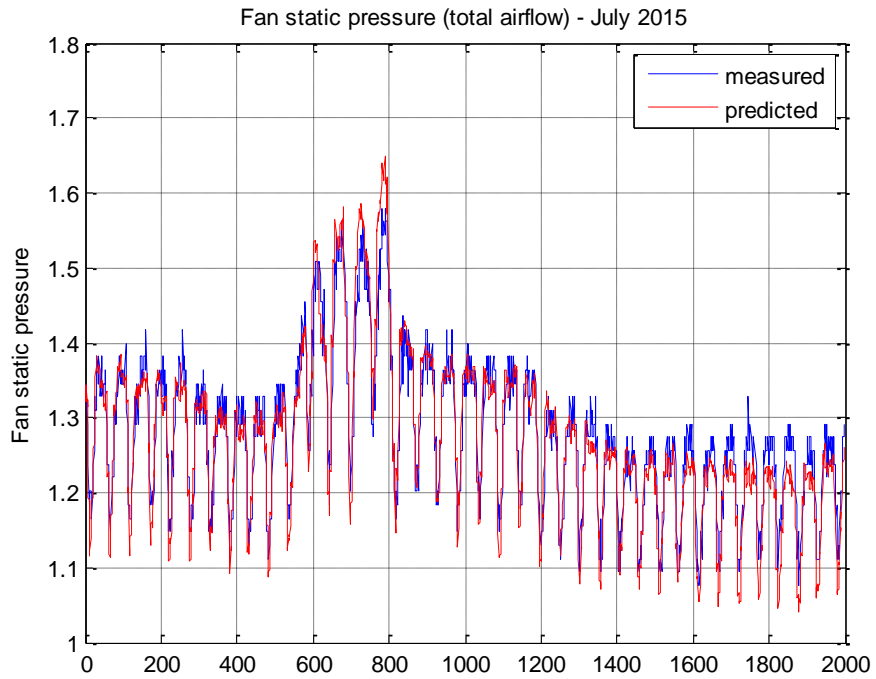


Figure B.1: Fan Static Pressure Reset – July 2015

(ME = -0.0078in; MAE = 0.0266in; MBE_pct = -0.6083%; CVRMSE = 2.6401%)

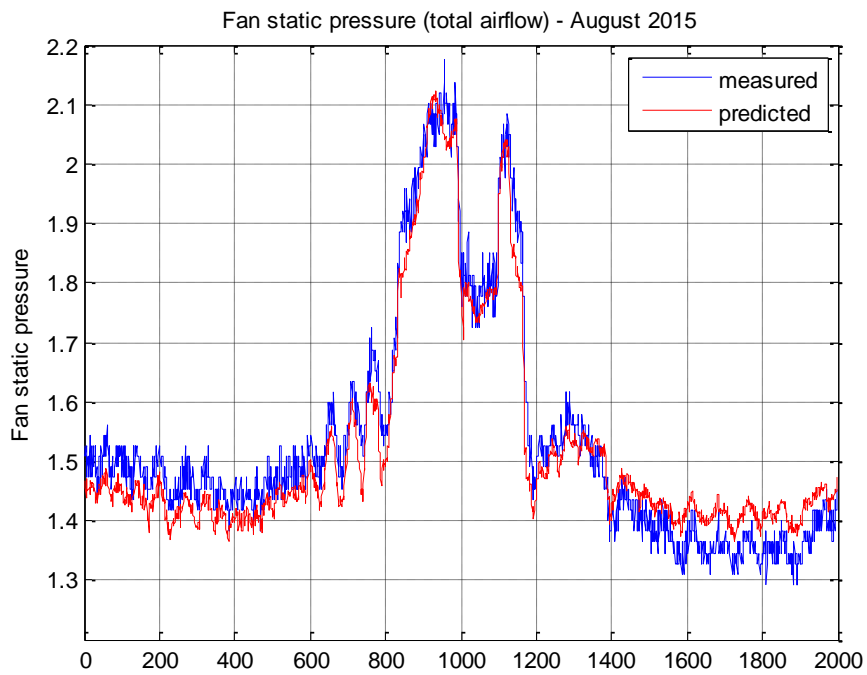


Figure B.2: Fan Static Pressure Reset – August 2015

(ME = 2.1081e-05; MAE = 0.0454; MBE = 0.0014%; CVRMSE = 3.3887%)

Appendix C: Results of Time-Series Solution Method

The baseline comparisons were carried out on a thermal zone in an office building, which is usually conditioned by an AHU. One thermal zone was chosen to capture the dynamics and variations at the zone level. If needed, reasonably high model accuracy at the zone level could easily be extended to multi-zone buildings, but the computation time would be increased.

The input matrix (U) includes ambient air temperature, sol-air temperature, and radiative and convective parts of the internal heat gain. For simplicity, only the surface facing west is exposed to ambient and solar radiation while other surfaces are treated as interior adiabatic surfaces, with no exposure to sun or wind. Other than the weather data used to calculate ambient and sol-air temperatures, the internal load from equipment, people and lights are also needed. In addition, the convective-radiative split is needed to determine the amount of internal heat gain that becomes cooling load instantaneously. Therefore, the following simulation conditions are defined as baseline conditions in order to obtain the inputs needed for Matrix U:

- Ambient and solar radiation values from TMY2 data of Oklahoma City in EnergyPlus. The run period is chosen to be representative of one month of cooling season.
- Use of 50% of nameplate rating for the plug loads. Most office equipment includes a nameplate rating showing the total power consumption. For most common equipment such as printers and computers, the actual power consumption ranges from 14% to 36% of the nameplate ratings [20]. In this study, we chose 50% as a worst case scenario.
- Internal load (equipment and people) density of $2.67\text{W}/\text{ft}^2$ for occupied hours (9am-5pm). This is within the recommended range by ASHRAE/IES 90.1-2010 standards ($1.5\text{-}3.0\text{W}/\text{ft}^2$) for office and some institutional buildings. An internal load density of $0.5\text{W}/\text{ft}^2$ was used for unoccupied hours.

- 30%-70% Convective-Radiative Split for internal load. This implies that 30% of internal heat gain is convection and 70% is thermal radiation. The higher the convection portion of a heat gain, the faster the heat gain can be converted into a cooling load. The original recommendation by ASHRAE was a 30%-70% convective-radiative split. Updated experimental results for equipment and other internal heat gain recommend 20%-80% for radiative fraction and 80%-20% for the convective fraction of equipment [21-22]. A 30%-70% split is more appropriate for lighting and occupant load [23], and it is chosen in this study.

The window-to-wall ratio (WWR) on the exposed surface is approximately 37% because ASHRAE 90.1-2010 standard allows up to 40% WWR. For ease of comparing the nodal temperatures T1 and T2 with outside and inside surface temperature in EnergyPlus, the 3R2C parameters of building envelope are calculated from the wall construction as:

$$R1 = \frac{1}{h_o A}; R3 = \sum_{i=1}^j \frac{l_j}{\lambda_j A}; R5 = \frac{1}{h_i A}; C2 = C4 =$$

$$\frac{1}{2} \sum_{i=1}^j l_i \rho_i c_{pi} A \quad \text{where } l_i, \lambda_i, \rho_i, \text{ and } c_{pi} \text{ are the thickness, conductivity,}$$

density, and specific heat of the i th wall layer. h_o and h_i are the convective heat transfer coefficient on the outside and inside surface, respectively. j is the total number of wall layers.

Using training data of one month in EnergyPlus, the 2R2C parameters of internal mass are found using the genetic algorithm [24] by minimizing the errors between the cooling load predicted by the RC model and EnergyPlus. Table 1 shows the R-C values for obtained for light, medium, and heavy wall construction used in this study.

Table C.1: RC parameters for light, medium, and heavy Walls.

Parameter	Light Wall	Medium Wall	Heavy Wall
R1 (m ² K/W)	0.012	0.012	0.012
C2 (J/(m ² K))	1504.5	16294.4	58701.3
R3 (m ² K/W)	0.370	0.430	0.451
C4 (J/(m ² K))	1504.5	16294.4	58701.3
R5 (m ² K/W)	0.025	0.025	0.025
R6 (m ² K/W)	0.026	0.012	0.033
C7 (J/(m ² K))	275568.3	937302.1	603839.5
R8 (m ² K/W)	0.050	0.085	0.507
C9 (J/(m ² K))	261992.6	250971.0	456829.6
Rwin (m ² K/W)	0.149	0.149	0.149

Results

The figures below show the cooling load comparisons between the simplified time-series model and EnergyPlus for light, medium, and heavy construction under the baseline conditions. The mean absolute percentage error (MAPE) is a reliable measure of accuracy for constructing fitted time series values as applied to trend estimation.

In comparison with EnergyPlus, MAPE values of 6.70%, 5.54%, and 6.31% were obtained for light, medium, and heavy wall construction, respectively.

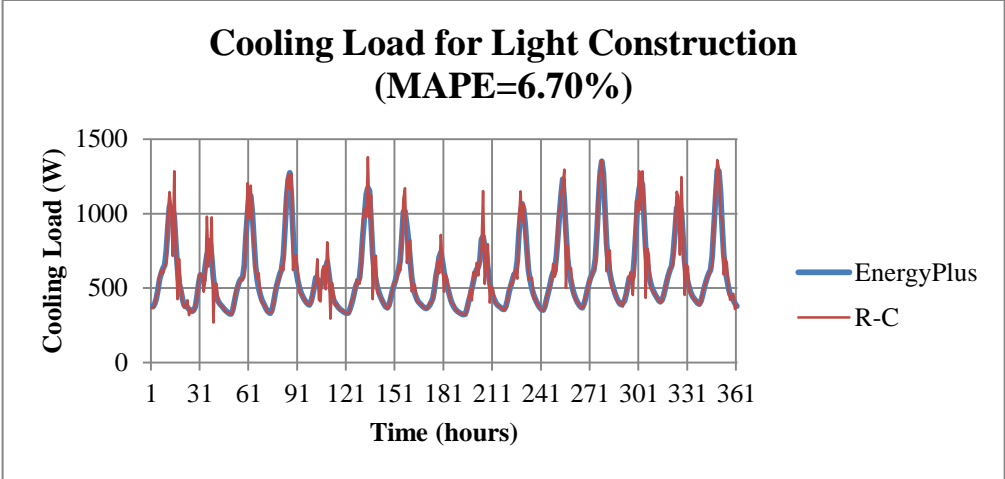


Figure C.1: Cooling load for light construction.

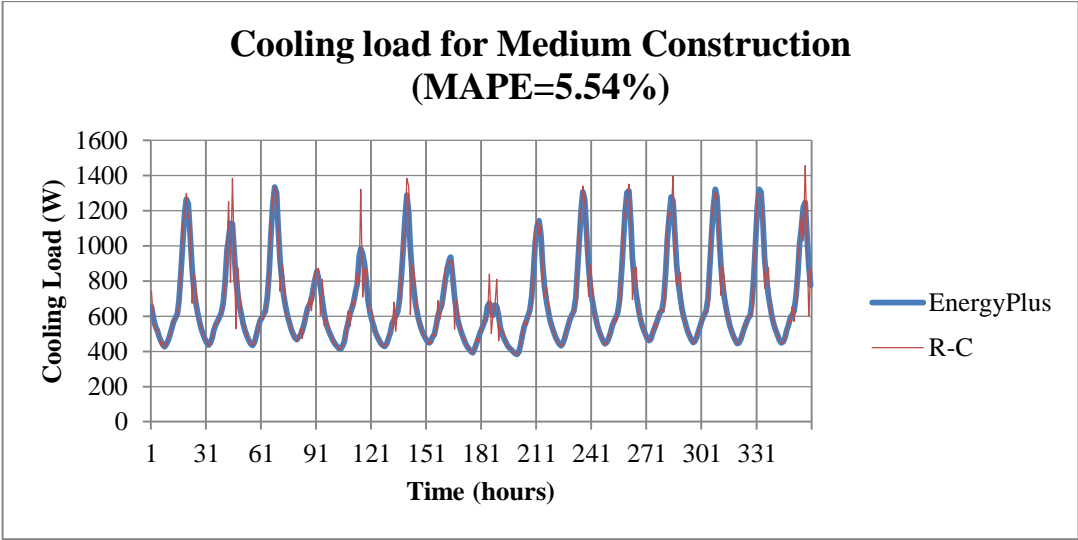


Figure C.2: Cooling load for medium construction.

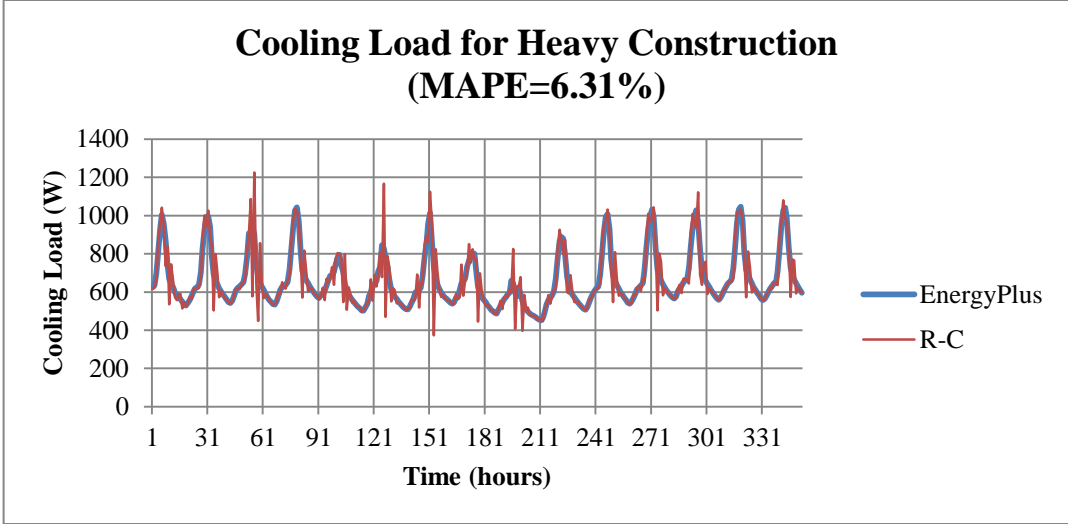


Figure C.3: Cooling load for heavy construction

Appendix D: Alternative MPC Performance Cost

$$\min_{\Delta u(k|k), \dots, \Delta u(m-1+k|k), \varepsilon} \left\{ \sum_{i=0}^{p-1} \left(\sum_{j=1}^{n_y} |w_{i+1,j}^y (y_j(k+i+1|k) - r_j(k+i+1))|^2 + \sum_{j=1}^{n_u} |w_{i,j}^{\Delta u} \Delta u_j(k+i|k)|^2 + \sum_{j=1}^{n_u} |w_{i,j}^u (u_j(k+i|k) - u_{j,\text{target}}(k+i))|^2 \right) + \rho \varepsilon^2 \right\}$$

Subject to:

$$\begin{aligned} u_{j\min}(i) - \varepsilon V_{j\min}^u(i) &\leq u_j(k+i|k) \leq u_{j\max}(i) + \varepsilon V_{j\max}^u(i) \\ \Delta u_{j\min}(i) - \varepsilon V_{j\min}^{\Delta u}(i) &\leq \Delta u_j(k+i|k) \leq \Delta u_{j\max}(i) + \varepsilon V_{j\max}^{\Delta u}(i) \\ y_{j\min}(i) - \varepsilon V_{j\min}^y(i) &\leq y_j(k+i+1|k) \leq y_{j\max}(i) + \varepsilon V_{j\max}^y(i) \\ \Delta u(k+h|k) &= 0 \\ \varepsilon &\geq 0 \end{aligned}$$

where

$$i = 0, \dots, p-1$$

$$h = m, \dots, p-1$$

with respect to the sequence of input increments $\{\Delta u(k|k), \dots, \Delta u(m-1+k|k)\}$ and to the slack variable ε .

The control action sent to the plant is $u(k) = u(k-1) + \Delta u(k|k)^*$. In this case, $\Delta u(k|k)^*$ is the first element of the optimal sequence.

Appendix E: Selected Publications

ANALYSIS OF PASSIVE THERMAL STORAGE OPPORTUNITIES FOR OPTIMAL HEATING SYSTEM DESIGN

Ogunsola, O., Song, L., & Wang, Y. (2015). Analysis of passive thermal storage opportunities for heating system design. *Science and Technology for the Built Environment*, (just-accepted), 00-00.

ABSTRACT

Heating and cooling load calculations are critical to size Heating, Ventilation and Air conditioning (HVAC) systems and determine energy use of their operations. The ASHRAE recommended heating load calculation model is most commonly used for heating load calculations. It adopts a simplified approach by considering only steady-state conductive heat transfer. However, due to thermal storage effect, heat generated in daytime may still be stored in buildings and released at a later time. Such assumption leads to significantly over-sized heating systems which are usually accompanied by high initial cost and higher cost of energy use. This study therefore examines the thermal response and passive storage characteristic of heavy construction for typical office building in continental US states. By allowing space air to drift to reasonably lower values, buildings need to be warmed up before being occupied in the morning. The worst case conditions might happen during warm-up or beginning of occupied hours. This paper evaluates the optimal size of heating system which satisfies thermal comfort while taking advantage of passive thermal storage. Results show varying downsizing opportunities ranging from 14% to 54% across the US. These results have the potential of establishing new heating device design standards for certain climate classifications.

1 INTRODUCTION

The primary aim of building energy system is to satisfy thermal comfort requirements. However, recent studies revealed that about 30% of energy consumed in buildings is used inefficiently or unnecessarily (Energy Star, 2008). This is because excessive energy is consumed when HVAC systems fail to operate as intended, often due to several factors such as inappropriate monitoring and control strategy, lack of understanding of the dynamics of thermal loads, and system complexity. For efficient operation, the heating and cooling equipment should be properly sized, suitable for the particular location and application, and accessible for easy maintenance. Meanwhile, the complex dynamics of temperature and weather fluctuation, thermal characteristics of building construction, internal heat gains, and major changes in occupancy schedules continue to provide challenge for HVAC systems design and control.

Building peak load calculations are necessary for the determination of appropriate size of HVAC equipment which will provide adequate heating and cooling under extreme weather conditions. Prior to 1945, there were few peak load calculation methods. In the U.S., most of the methods used today were implemented after 1946, for example sol-air temperatures, decrement factors and the use of a thermal RC network (Mao et. al 2013). The first edition of ASHRAE Handbook appeared in 1967, and it adopted the existing peak load calculation methods. Since 1970, there have been major advances in peak cooling load calculations but peak heat load methods have not quite changed. Today, the widely adopted ASHRAE Model (ASHRAE, 2009) for heating system design uses a simplified approach to estimate the heating requirement for typical buildings, based on the following assumptions:

- Heat losses are considered to be instantaneous, and essentially conductive, therefore thermal storage effects of building structure or content is ignored
- Construction material is thermally homogeneous
- No solar effect (at night or on cloudy, winter days)
- Lights, and appliances have no offsetting effect
- The system is sized for design conditions, which represents the worst case scenario (ASHRAE, 2009)

The above simplified approach has been justified because it evaluates worst case conditions that can reasonably occur during a heating season, when diurnal temperature variations are considered small enough to ignore. However, the assumptions often lead to over-sizing of the heating system because it

ignores the thermal storage capabilities of building construction. Due to thermal and internal mass effects, heat gains in buildings during daytime may still be stored in the walls and radiation absorbing surfaces within the building. Heat absorbed by the thermal mass during occupied hours could be released during unoccupied hours. The heat released by the thermal mass may partially (or totally) compensate for the space heating needs during unoccupied periods without temperature dropping below the set minimum. To save running costs, the temperature may be allowed to drift to a reasonably low value during unoccupied periods (often called night setback). The building would then need to be warmed up before the start of occupied period. Due to weather phenomenon, the peak demand (which determines the heating system size) is usually recorded between midnight and the start of occupied period. Both passive thermal storage and amount of heating depend strongly on the characteristics of the building construction. To harness the passive thermal storage and simultaneously determine the right amount of heating needed to warm up the building requires an optimization process. This subject area was studied by Ogunsola and Song (2014) for two climate regions in the US but is now being investigated for all climate classifications in U.S continental states.

Therefore, the aim of this paper is to apply the thermal network model for a building with heavy wall construction, in order to optimize the size of the heating system, for all climate zones in continental U.S. states. By investigating the influence of the building construction on heating system capacity and operation, the possibility of harnessing building passive thermal storage for optimal sizing of heating system is investigated and discussed. Typical thermal zones in an office building with heavy construction of the building envelope are used to illustrate the concept.

2 LITERATURE REVIEW

The building envelope is the interface between the indoor and outdoor environment. It determines and controls the fluctuations in the indoor environment, based on its thermal characteristics, and the transient outdoor conditions. Components such as windows, walls, roofs, thermal insulation, external shading devices, and other fenestration components make up the building envelope. On the other hand, thermal mass are the high capacity materials which are capable of absorbing and releasing heat at a later time. By absorbing and progressively releasing heat, thermal mass helps in the regulation of indoor temperature.

According to Li and Wang (2012), thermal storage is one of the most promising and sustainable ways for improving energy storage in buildings. Passive strategies involve improvements to the building envelope while active strategies are those seeking improvements to the HVAC systems.

According to Henze *et. al* (2005), there has been little improvement in thermal storage and peak load reduction potential compared to energy conversion. In their study, the focus was on nighttime pre-cooling. By utilizing both active and passive building thermal storage, under constraints of thermal comfort, and optimal HVAC system operation, the study minimized building operating costs. Braun *et al* (2002) optimized cost of heating by control of passive thermal storage and applied the concept to the Energy Resource Station (ERS), Iowa Energy Center, United States. The temperature was allowed to float between 15°C (59F) and 30°C (86F) during unoccupied periods. The zone temperature was fixed at 22°C (71.6F) during occupied periods. The passive thermal storage capability of the ERS was simulated and solved using quasi-Newton method. The study demonstrated capability of thermal mass for load shifting, with the potential greatest for interior zones. However, as a lightweight structure with significant coupling to ambient and exterior, the ERS was deemed an unsuitable building to fully explore building thermal mass capability. Snyder and Newell (1990) developed a lumped capacitance model to determine least cost cooling strategies using effective building characteristics derived from a medium-sized building. Cooling cost savings of 18% were realized. From their analysis, thermal characteristics of building construction can have a significant impact on the load profile and energy use. Yang and Li (2008) mathematically modeled the effects of thermal mass and night ventilation on cooling load. The simulation model considered the thermal resistance and capacitance of the building construction and room air. Brown (1990) studied different office building thermal designs and two different insulation levels (R10 and R20) and analyzed their energy performance using DOE 2.1C (Department of Energy 2.1C) energy simulation code. It was concluded that additional thermal mass led to energy savings of 18-

20% over the base case of R10 light construction. Through these reductions, the HVAC system could be downsized, thereby offsetting the initial investment on the additional thermal mass.

In a previous study, a time series model was deduced from the R-C model and used to estimate thermal load of a building in real-time (Ogunsola et. al, 2014). Multiple scenarios of building construction, HVAC system operation and strategies have been simulated using the R-C model. Ogunsola and Song (2014), Ogunsola et. al (2014), and Ogunsola and Song (2015) introduced numerical and analytical solution of the RC thermal model and demonstrated opportunities for downsizing heating system capacity based on passive thermal storage. The RC model was determined to be an appropriate model for this study based on the following criteria:

- (i) Capability to represent physical properties of building construction in order to investigate the thermal characteristics of different construction.
- (ii) Capability to simulate internal loads and different HVAC system schedules.
- (iii) Simulation based, in order to investigate multiple scenario of operation across different climates.
- (iv) Ability to determine the system stability from thermal model parameters.
- (v) Capability to optimize heating system output in response to ambient temperature and solar radiation.
- (vi) Capability to simulate internal mass, thereby harnessing the thermal storage effort to the fullest.
- (vii) Capability to simulate floats in space air temperature.

Using case study of two (2) US climates, heavy construction was found to have the largest savings in heating system size, based on its better passive thermal storage capability and moderating effects on temperature swings. The objective of this paper is to extend the method developed by Ogunsola and Song (2014, 2015) to cover all continental US states with the overall goal of identifying further downsizing opportunities and investigating situations under which the ASHRAE approximation is most suitable for heating system design.

3 METHODOLOGY

The R-C thermal model with envelope and internal mass components for a single exterior wall is shown in Figure. 1. The variables are as defined in the nomenclature. The solar air temperature concept was used.

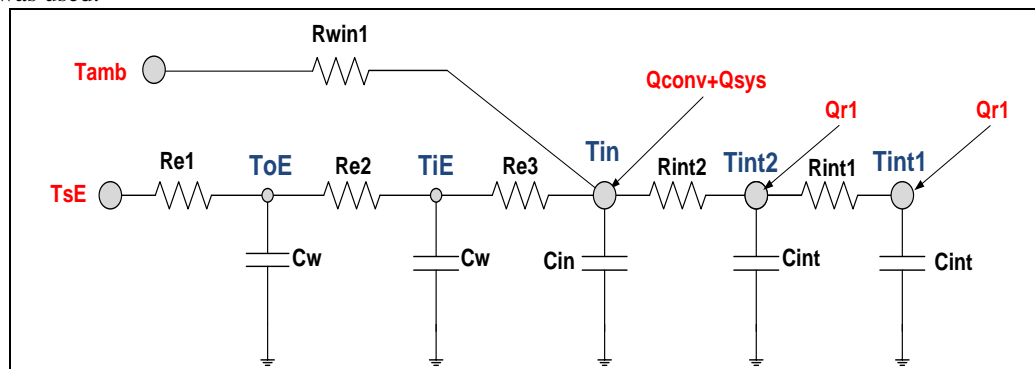


Fig. 1:

R-C Thermal model, showing sol-air temperature and HVAC system input.

To derive a sensible heat balance equation for the R-C model, the following simplifying assumptions are made:

- The zone air is well mixed; therefore the whole indoor circulated air volume is at a uniform temperature.
- The effect of varying wind velocity on external wall convection coefficients is not considered. Hence, a constant heat transfer coefficient is assumed in this study.

- The space is pressurized so infiltration does not create additional heating load in the conditioned space.
- The floor surface is considered adiabatic.
- The long wave radiation exchanges between internal surfaces and multiple reflections are described by the lumped internal thermal R-C model.

The above assumptions are commonly made to simplify the R-C model [Ogunsola and Song (2014); Lombard and Mathews (1992); Ogunsola et. al (2014); Ogunsola and Song (2015)]. The governing equations found by heat balance at each node are given in Equation (1):

$$\frac{dT_n}{dt} = -\frac{1}{C_n} \left(\sum_{i=1}^j \frac{1}{R_i} \right) T_n + \frac{1}{C_n} \left(\sum_{i=1}^j \frac{1}{R_i} T_i \right) + \frac{1}{C_n} \sum_{i=1}^p Q_i \quad (1)$$

where

T_n = temperature of the n th node.

C_n = thermal capacitance of node n .

j = total number of temperature branches (e.g., ambient, sol-air temperature, and neighbor nodal temperatures) connected to node n .

T_i = temperature of the i th branch, connected to node n .

p = total number of heat flux branches (such as convection, radiation, and system input) connected to node n .

Q_i = heat flux of the i th branch connected to node n . This term is made up of internal heat gains such as Q_r and Q_{conv} which are impressed on internal mass and zone temperature nodes respectively. It also includes the heating or cooling supplied by a device (Q_{sys}), which applies only to zone temperature nodes, as shown in Figure 1.

R_i = resistance of the branch between T_n and T_i .

Equation (1) represents an inhomogeneous system of ordinary differential equations. In state space representation, it can be re-written as:

$$\dot{T} = AT + BU \quad (2)$$

where A is the state (or system) matrix and B is the input matrix of dimensions $n \times n$ and $n \times q$, respectively, as shown in Equation (3).

$$A = \begin{pmatrix} a_{11} & \cdots & a_{1n} \\ \vdots & \ddots & \vdots \\ a_{n1} & \cdots & a_{nn} \end{pmatrix} \text{ and } B = \begin{pmatrix} b_{11} & \cdots & b_{1q} \\ \vdots & \ddots & \vdots \\ b_{n1} & \cdots & b_{nq} \end{pmatrix} \quad (3)$$

The matrices A and B are time-invariant matrices whose entries are functions of the R-C parameters. $T = [T_1 \ T_2 \ \dots \ T_n]'$ are the nodal temperatures, and $U = [U_1 \ U_2 \ \dots \ U_q]'$ is the input matrix, which includes heat gains, ambient temperatures, and sol-air temperatures on opaque surfaces. The stability of the system depends on the eigenvalue characteristics of the system matrix, A . In general, $q \geq p$, that is, the input matrix must include not only the heat flux sources but also ambient and sol-temperature inputs. Equation (2) is a system of first order differential equations with constant coefficients, and the solution is given by:

$$T_{t+\delta} = e^{A\delta} T_t + \int_t^{t+\delta} e^{A(t+\delta-\tau)} BU(\tau) d\tau \quad (4)$$

where the exponential matrix of A is defined by the power series

$$e^{A\delta} = I + A\delta + \frac{A^2\delta^2}{2!} + \frac{A^3\delta^3}{3!} + \cdots + \frac{A^n\delta^n}{n!} + \cdots \quad (5)$$

I is the identity matrix of the same dimensions as A , and δ is the time step. As developed by Seem et al. (1989), inputs between time t and $t + \delta$ can be modeled by a continuous, piecewise linear function as:

$$\mathbf{U}(t) = \mathbf{U}_t + \frac{(\tau - t)}{\delta} (\mathbf{U}_{t+\delta} - \mathbf{U}_t) \quad (6)$$

Meanwhile, the input between time t and $t + \delta$ could easily be modeled using other functions (such as sine or cosine for ambient or solar radiation) if they are deemed more appropriate or when longer time steps are used. Substituting Equation (6) into Equation (4) gives

$$T_{t+\delta} = e^{A\delta} T_t + \int_t^{t+\delta} e^{A(t+\delta-\tau)} B \left[\mathbf{U}_t + \frac{(\tau - t)}{\delta} (\mathbf{U}_{t+\delta} - \mathbf{U}_t) \right] d\tau \quad (7)$$

If conditions are known at time, $t=0$, then the solution becomes

$$T_\delta = e^{A\delta} T_o + \int_0^\delta e^{A(\delta-\tau)} B \left[\mathbf{U}_o + \frac{(\tau)}{\delta} (\mathbf{U}_\delta - \mathbf{U}_o) \right] d\tau \quad (8)$$

To obtain the analytical solution, the exponential matrix $e^{A\delta}$ and the convolution integral $\int_0^\delta e^{A(\delta-\tau)} B \left[\mathbf{U}_o + \frac{(\tau)}{\delta} (\mathbf{U}_\delta - \mathbf{U}_o) \right] d\tau$ need to be evaluated. There are several approaches used to evaluate the matrix exponential. These include polynomial methods, Taylor series, inverse Laplace, matrix decomposition, and the ordinary differential equation method (Cleve and Loan, 2003). In this study, the matrix decomposition method is adapted because it is based on similarity transformation of the form:

$$A = CDC^{-1} \quad (9)$$

such that the power series definition of e^{At} becomes

$$e^{At} = Ce^{Dt}C^{-1} \quad (10)$$

The usual approach is to take C as the matrix whose columns are the eigenvectors of A , i.e.,

$$C = V = [v_1 | \dots | v_n] \text{ and } Av_j = \lambda_j v_j, \quad j = 1, \dots, n \quad (11)$$

$$e^{Dt} = \text{diagonal matrix}(e^{\lambda_1 t}, \dots, e^{\lambda_n t}) \quad (12)$$

As long as V is nonsingular, the matrix exponential of At is expressed as

$$e^{At} = V(\text{diag}(e^{\lambda_1 t}, \dots, e^{\lambda_n t}))V^{-1} \quad (13)$$

The analytical solution was applied in Ogunsola and Song (2014, 2015) where it was used for the optimal sizing of the heating system for certain U.S. locations and for building load prediction of actual building. The symbolic solution to nodal temperatures from Equations (8) through (13) requires the heat extraction rate of a heating device, among other inputs. From the analytical solution, the heat extraction rate may be represented as a function of desired temperature and heat gains/loss within the building. In this study, the objective is to minimize the heating system size (i.e. minimize peak heating required) for two typical thermal zones.

The optimization problem is defined as:

Minimize:

$$J = \text{Max} \left((Q_{sys,1} + Q_{sys,2})_{h=1}^L \right) = f(T_{in,i}(h), Q_{sys,i}(h), W(h)) \quad (14)$$

With respect to: $T_{in,i}(h)$ and $Q_{sys,i}(h)$ ($h = 1, \dots, L$) ($i = 1, 2$),

subject to: $T_{in,min}(h) \leq T_{in,i}(h) \leq T_{in,max}(h)$; $Q_{sys,i}(h) \geq 0$;

Optimization variables: $T_{in,i}(h)$ and $Q_{sys,i}(h)$ ($h = 1, \dots, L$) ($i = 1, 2$)

Where $Q_{sys,i}(h)$ is the heating supplied by the heating device to zone i at hour h . The constraint on Q_{sys} implies that only heating mode is considered.

h = hour of the day;

L = Period of optimization (in hours). In this study, L is chosen to be 48 hours.

$T_{in,i}(h)$ = Room temperature of zone i at hour h .

$T_{in,min}(h)$ = minimum allowable zone temperature at hour h . It is specified as 15°C (59°F) for unoccupied hours and \cong 22.2°C (72°F) for occupied hours (9am – 5pm).

$T_{in,max}(h)$ = maximum allowable zone temperature at hour h . It is specified as 22.2°C(72F) when heating system is in operation, otherwise as 24°C(75.2F). This is throttling allowance due to contributions from thermal mass, solar radiation, ambient temperature, or internal heat gains.

$W(h)$ = vector of uncontrolled variables that affect the peak heating required at hour h . They include weather and internal heat gains. Braun (1990) worked on a very similar optimization problem involving the optimal control of building thermal storage for reducing peak electricity demand and energy costs. $Q_{sys,i}$ (and hence, the objective function, J) is not explicit in the zone temperature, weather, and internal heat gains, as explained in Equations (2) to (4). Therefore, the optimal heating system size was estimated using Genetic Algorithm (Mitchell 1997). Since $T_{in,i}(h)$ and $Q_{sys,i}(h)$ are the optimization variables, the Genetic algorithm modifies their values iteratively to achieve the minimum value of J that satisfies the constraints. Genetic Algorithm differs from classical, derivative-based optimization algorithm because it generates a population of points at each iteration. It selects the next population by computation using a random number generator (MathWorks 2015).

4 HEATING OUTDOOR DESIGN DAY TEMPERATURE PROFILE

ASHRAE heating design outdoor air temperature represents a one-time worst case condition which can reasonably occur during winter season. In order to understand and investigate the opportunities for downsizing the heating system through transient heat transfer analysis, it is necessary to perform simulation for a period of time. The current ASHRAE heating design outdoor air temperature (at 99% or 99.6% annual cumulative occurrence frequency) represents a single measurement and it is not sufficient information to derive the temperature profile. For example, there is no information about the hour of the day at which the lowest temperature is recorded. There is also no information about the peak temperature recorded during the design day. Therefore, further information is required to generate temperature profile for the design day. This section discusses the needed inputs, assumptions, and data sources used to generate temperature profile for the heating design day in this study.

The design temperature used in this study is the lower of the 99.6% dry bulb temperature from TMY3 and ASHRAE design condition. The peak temperature for the design day and hour at which the design temperature occurs was determined using a similar approach used for ASHRAE cooling load calculations. For cooling load calculations, the outdoor temperature was assumed to vary in an approximately sinusoidal fashion according to Equation (15)

$$t_o = t_d - DR(X_c) \quad (15)$$

Where:

t_d = cooling design dry bulb temperature, F or °C

DR = daily range, F or °C

X_c = fraction of daily range.

In this study, the hourly outdoor temperature was assumed to also vary in an approximately sinusoidal fashion, with the outdoor temperature given by Equation (16):

$$t_o = t_{d,h} + DR_h(X_h) \quad (16)$$

Where:

$t_{d,h}$ = heating design dry bulb temperature, F or °C

DR_h = daily range for heating design day, F or °C

$X_h = 1 - X_c$ = fraction of daily range for heating design day.

The assumptions and methods used for some of the input in this study are shown in Table 1.

Table 1: Inputs, assumptions, and data source

Inputs	Method or assumption	Data Source or further information
Heating Design Temperature ($T_{d,h}$)	The smaller of 99.6% ASHRAE design and 99.6% TMY3 data	ASHRAE and TMY3
Daily Range (DR_h)	Average daily range for the design month, deduced from TMY3 data	TMY3
fraction of daily range (X_h)	Sinusoidal waveform fraction, generated as $X_h = 1 - X_c$ such that	ASHRAE

	the minimum temperature occurs at night, and maximum occurs during daytime.	
Time of occurrence of maximum temperature (t_{max})	The most frequent hour at which maximum temperature is recorded for the design month, deduced from TMY3 data. If more than one hour fulfills this, the average is taken.	TMY3
Design day temperature profile	Generated as sinusoidal waveform with peak temperature and minimum temperature occurring during daytime and night, based on the daily range fraction, X_h . Table 2 shows the values of X_h used in this study	$t_o = t_{d,h} + DR_h(X_h)$

Table 2: Fraction of the Daily Range, X_h . (Deduced from McQuiston and Spitler, 1992)

Time, hr	Fraction	Time, hr	Fraction	Time, hr	Fraction	Time, hr	Fraction
1	0.13	7	0.07	13	0.89	19	0.66
2	0.08	8	0.16	14	0.97	20	0.53
3	0.04	9	0.29	15	1.00	21	0.42
4	0.01	10	0.34	16	0.97	22	0.32
5	0.00	11	0.61	17	0.90	23	0.24
6	0.02	12	0.77	18	0.79	24	0.18

Thus, the heating design day temperature profile was generated as sinusoidal waveform. In addition, for transient heat transfer calculation, the previous day temperature has remaining thermal impacts and thus we assume two consecutive days (up to 48 hours) have the same winter design day profile, similar to ASHRAE cooling load calculation procedure.

5 CASE STUDY

The study focused on most climatic zones in the U.S. The locations are chosen randomly, to represent all climate classifications according to ASHRAE, Building America Climate (DoE, 2014) and International Energy Conservation Code (ICC, 2012). The studied locations, climate types, and design temperature values are shown in Figure 2 and Appendix. Table 3 shows the conversion between the various classifications.



Fig. 2: Map of USA showing studied locations

The thermal dynamics of the building are modeled using Resistance-Capacitance (R-C) model, which has proved to be a simplified, yet robust model for estimation and analysis of heating and cooling loads in buildings [Ogunsola et. al (2014), Lombard and Mathews (1992), Ogunbiyi et. al 2013, Ogunsola and Song (2015), and Ogunbiyi (2014)].

Table 3: Relationship between Building America and IECC climate classifications

Building America	ASHRAE and IECC
Subarctic	Zone 8 (only found in Alaska)
Very Cold	Zone 7
Cold	Zones 5 and 6
Mixed-Humid	4A and 3A counties above warm-humid line
Mixed-Dry	Zone 4B
Hot-Humid	2A and 3A counties below warm-humid line
Hot-Dry	Zone 3B
Marine	All counties with a “C” moisture regime

Two typical thermal zones (shown in Figure 3) were modeled in this study; Thermal zone 1 is a corner location with 2 windows (one facing north, and the other facing east). Thermal zone 2 has only one window, facing north. The window-to-wall ratio (WWR) on those surfaces is 30%. ASHRAE 90.1-2010 standard allows up to 40% WWR (ASHRAE 2010). Both thermal zones 1 and 2 represent typical orientations in office building. The floors are assumed to be adiabatic for both zones. The composition of the heavy construction was taken from ASHRAE Handbook of Fundamentals (ASHRAE 2009). Hourly temperature and solar radiation values were obtained from Typical Meteorological Year, Version 3 (TMY3) weather data (DoE 2013) and ASHRAE Clear Sky Model (ASHRAE 2009) respectively. The ASHRAE Clear Sky model was used to decompose incident solar radiation from TMY3 data into direct, diffuse, and reflected components for the different wall orientations. Table 4 shows the composition of the heavy wall construction used in this study. The heavy wall construction was taken from Table 21 of ASHRAE Handbook of Fundamentals 2009, which shows some representative constructions for light, medium, and heavy exterior wall. The additional thermal mass within the building, such as the floor/ceiling (see construction materials in Appendix), furniture, carpets etc. is considered by lumping them into the 2R2C model, with the capacitances (C_{int} 's) and resistances (R_{int} 's) trained and determined using physical characteristic of the construction (See Ogunsola and Song 2012, Wang and Xu 2006).

Separately, the partition is represented by 3R2C. The composition of floor and partitions are shown in Appendix.

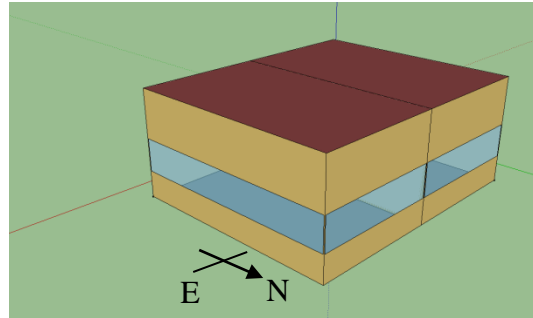


Fig. 3: The Modeled Office Building

Table 4: Heavy Wall Construction

	L (mm) (in)	$k(W/mK)$ (Btu/hftF)	$\rho (kg/m^3)$ (lb/ft ³)	$C_p (J/KgK)$ (Btu/lbF)	Resistance (m ² k/W) (ft ² Fh/Btu)
M01 brick	101.6 (4)	0.89 (0.51)	1920 (119.86)	790 (0.189)	0.15 (0.852)
M15 concrete	203.2 (8)	1.95 (1.13)	2240 (139.84)	900 (0.215)	
I02 insulation	50.8 (2)	0.03 (0.017)	43 (2.68)	1210 (0.287)	
F04 air resistance	-	-	-	-	
G01a gypsum	19 (0.75)	0.16 (0.092)	800 (49.94)	43 (0.01)	

The RC model representation of the building is shown in Figure 4. The inputs to the model include both envelope and internal load components. T_{int} denotes virtual temperature of internal mass nodes. T_{in1} and T_{in2} are room temperature of Zone 1 and 2 respectively. T_{p1} and T_{p2} are temperature of internal partition separating the two zones. C_p = Thermal capacitance of internal partition. Q_{sys} is system output (+ve for heating, and -ve for cooling). It is treated as 100% convective in this study. R_p is resistance of internal partition. Q_r is average of the sum of transmitted solar radiation from windows, and radiative part of internal load for the particular zone. Q_{conv} is convective part of internal load. In this study, the assumed split is 50% convection and 50% radiation. This implies that 50% of internal heat gains is added to the air stream instantaneously, while the remaining 50% is radiated. Note that only 2 external walls are shown in Figure 4. There are additional walls on south and north respectively, but these are not shown in the schematic representation due to space limitations.

The R-C model provides useful and quality information about the system dynamics and thermal characteristic of building construction because it represents the system physically. By analyzing the R-C model and investigating the thermal response of the heavy construction, the influence of thermal characteristics of the building construction on the heating system design and operation are discussed.

The simulation was carried out under two scenarios:

1. Without HVAC system operation: This enabled the study of temperature floats, and comparison of heating needs among different climates. The floating mode is essential for the identification of climates with least heating needs, or potential for heating device to be eliminated. If thermal comfort requirements are nearly met during floating mode for a certain location, then such locations offer very high potential for heating needs to be met through smarter energy use, rather than by use of heating device.
2. With HVAC system operation: This involves the simulation of heating needs, based on comfort conditions, defined as:

a) $15^{\circ}\text{C} (59\text{F}) \leq T_{in} \leq 24^{\circ}\text{C} (75.2\text{F})$, (Temperature limits for the thermal zone during unoccupied periods). The lowest temperature allowable was specified as $15^{\circ}\text{C} (59\text{F})$. This is within ASHRAE 90.1 recommended heating night setback temperature of $12.78^{\circ}\text{C} (55\text{F})$ for residential and non-residential conditioned spaces. The highest temperature allowable during unoccupied periods is specified as $24^{\circ}\text{C} (75.2\text{F})$.

b) $22.2^{\circ}\text{C} (72\text{F}) \leq T_{in} \leq 24^{\circ}\text{C} (75.2\text{F})$ from 9am to 5pm (Temperature maintained around $23^{\circ}\text{C} (73.2\text{F})$ for occupied hours). Therefore, the highest temperature allowable during occupied periods was also specified as $24^{\circ}\text{C} (75.2\text{F})$.

The peak heating load determines the heating system size. In this study, the optimal heating system was estimated using Genetic Algorithm (Mitchell 1997), with the objective to minimize the heating system size, subject to comfort conditions (a) and (b).

The study concludes by presenting the results of the optimal size of the heating system for all the locations. The determined equipment size is compared with ASHRAE method. In this study, the heating system output was moderated to satisfy the constraints on temperature. The heating system was sized based on the largest heating output predicted during the heating season. The downsizing opportunity was expressed as percent savings over the ASHRAE method, as shown in Equation (17).

$$\text{Downsizing} = \frac{\text{ASHRAE}_{\text{predicted}} - \text{RC}_{\text{predicted}}}{\text{ASHRAE}_{\text{predicted}}} \times 100\% \quad (17)$$

6 RESULTS

6.1 Temperature Floats

Results of temperature floats for the two thermal zones are shown in Figures 5 and 6. For the temperature float study, the heating system was turned off at 5PM (which marks the start of the plot in Figures 5 and 6) and remained off the entire time. The purpose was to investigate how long it takes for the temperature to reach the setback temperature of 55F. Additionally, the prolonged hour was used to check if the heat gains of the following day will be sufficient to take the temperature within comfort limits during occupied hours.

Temperature floats was studied after the heating system was shut down, and with minimum effects from lighting and appliances. The temperature trajectory is then mostly influenced by the envelope thermal mass, internal mass, and the incident outdoor conditions. As shown in Figure 5, there are varying behaviors across different climate. For the thermal zone 1, very cold regions will achieve the night setback temperature within 5 hours after the heating system was turned off. Meanwhile, hot-dry climates and marine regions will not reach the setback temperature before the heat gains of the next day kicks in.

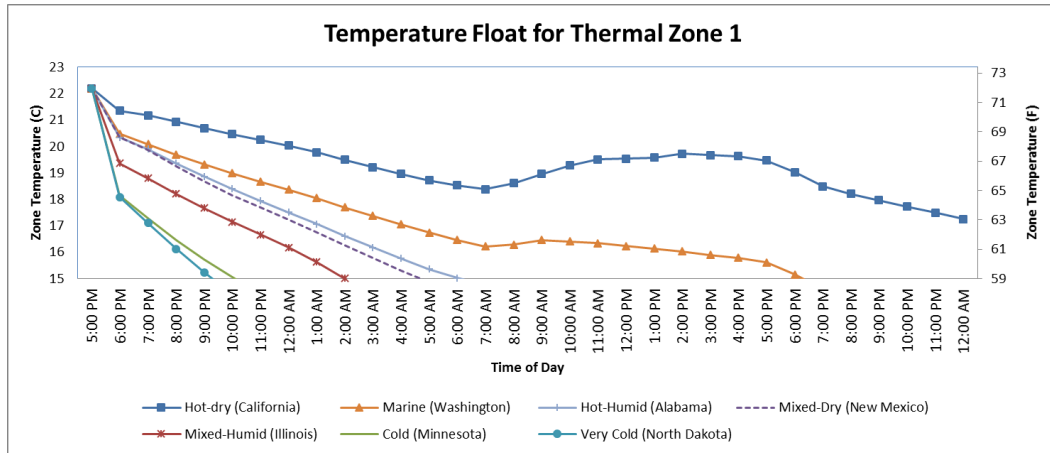


Fig. 5: Temperature Float for Thermal Zone 1

By the start of occupancy period of the following day, typical office buildings in hot-dry climates have only experienced about $3.5C(6.3F)$ drop in zone temperature. The heat gains of the following day are sufficient to take the temperature to within $2.5C(4.5F)$ of desired conditions for comfort.

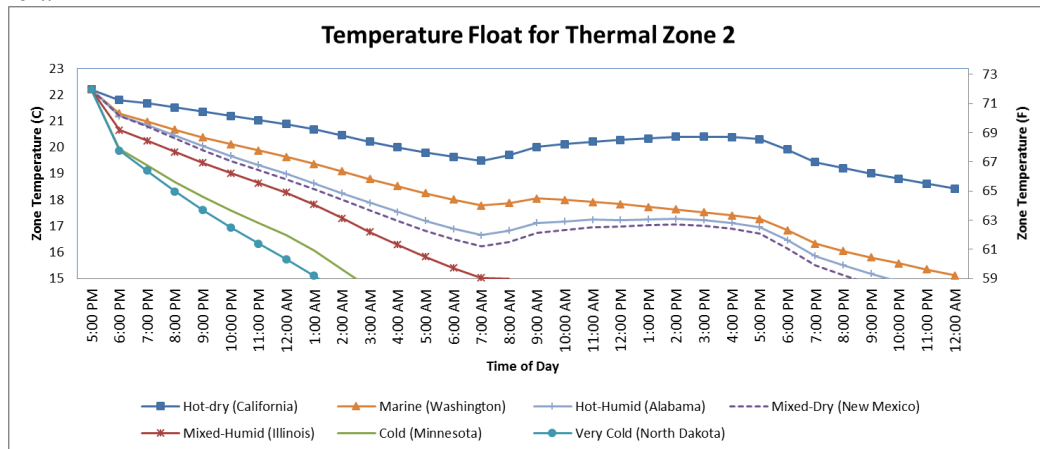


Fig. 6: Temperature Float for Thermal Zone 2

As shown in Figure 6, the temperature floats of thermal zone 2 are very similar to that of zone 1. However, it takes a much longer time for the temperature to reach the night setback setpoint of $15C(59F)$. Very cold regions will not reach the setback temperature until 2am, which is twice as long as the time it takes for zone 1. For thermal zone 2, four (4) climates will not reach the setback temperature before heat gain of the next day kicks in, as shown by increase in zone temperature between 7am and 5pm of the second (2nd) day. Generally, the temperature drops observed for zone 2 are much smaller than those of zone 1. Only $2C(3.6F)$ drop was observed for typical building in hot-dry climate. The heat gains of the next day takes the zone temperature to within $1.5C(2.7F)$ of desired comfort conditions for occupied periods. Note that thermal zone 2 is more representative of typical office buildings, with approximately 30% WWR on one exposed surface.

6.2 Heating System Down-Sizing

Figures 7 to 10 shows sample 2-days ambient and temperature profiles for four climate classifications (very cold, mixed-humid, mixed-dry, and marine) as well as the required heating to achieve the desired temperature. The plots cover days before and on the design day. (Note that, the design day profile was assumed for both days). As shown in Figures 7 to 10, all climate regions offer opportunity for floats in temperature, which may translate to huge energy savings during unoccupied hours. Due to very low temperature in very cold regions (Figure 7), zone temperature quickly reaches the specified

lower limit, therefore requiring that the heating system be turned on, to prevent temperature from dropping any further. On the other hand, though marine regions are much suitable candidate for temperature recovery, as shown in Figure 10, in order to optimize the heating system sizing, which allows the required room air temperature at the room occupied hour, the heating system is on at the same time as in the very cold regions. The mixed-humid and mixed-dry regions (Figures 8 and 9) have moderate temperature response and floats, which follows similar pattern but the heat capacity needed is observed between very cold region and marine region.

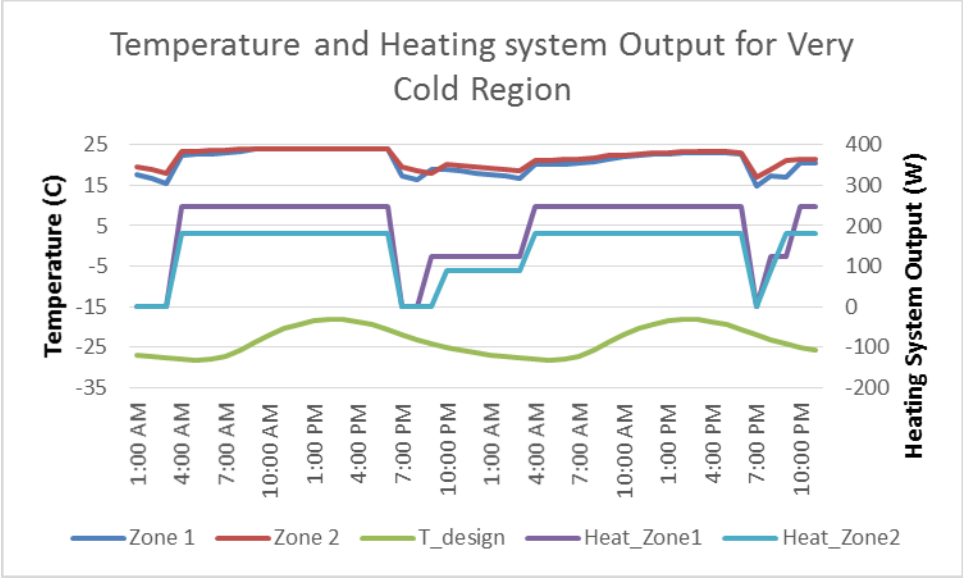


Fig. 7: Temperature Profile for Very Cold Region

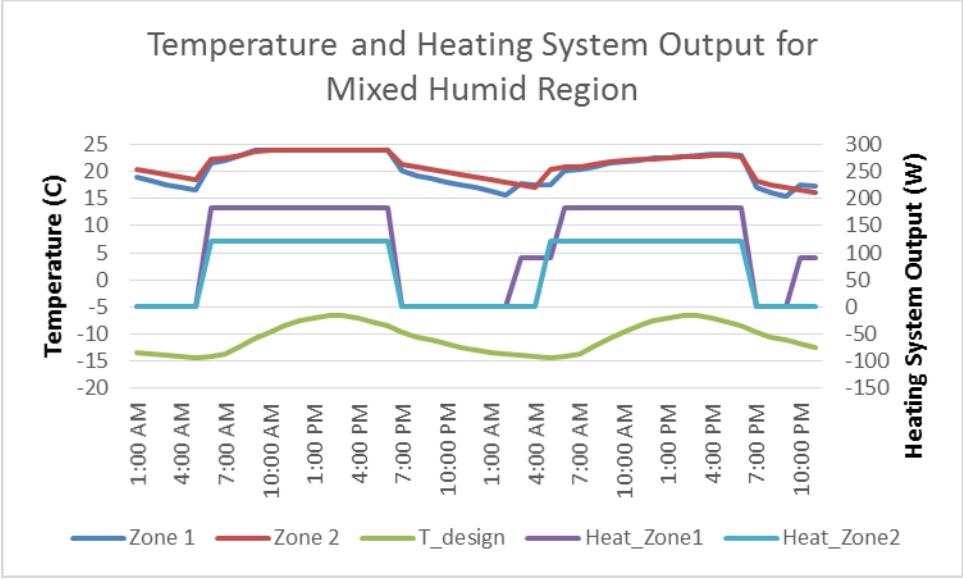


Fig. 8: Temperature Profile for Mixed Humid Region

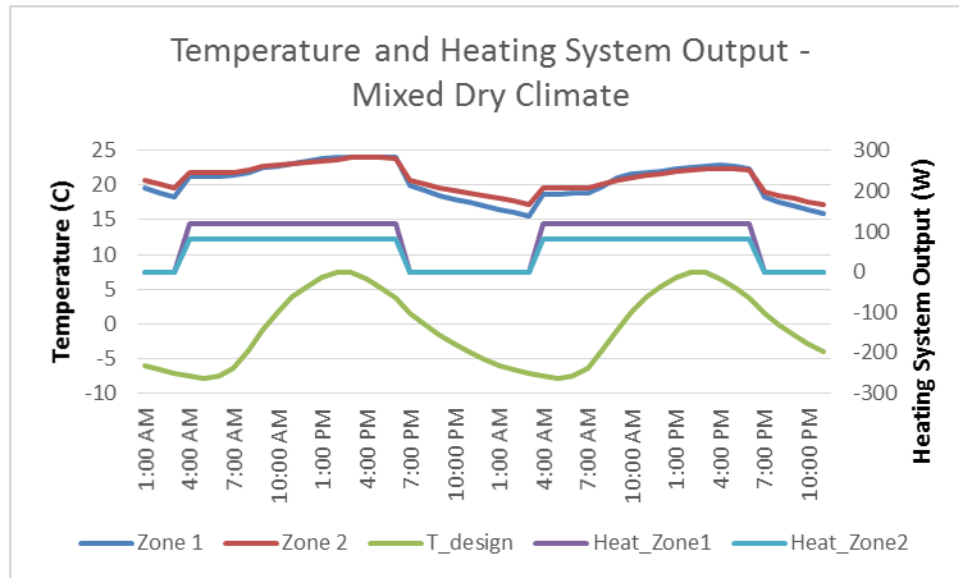


Fig. 9: Temperature Profile for Mixed Dry Region

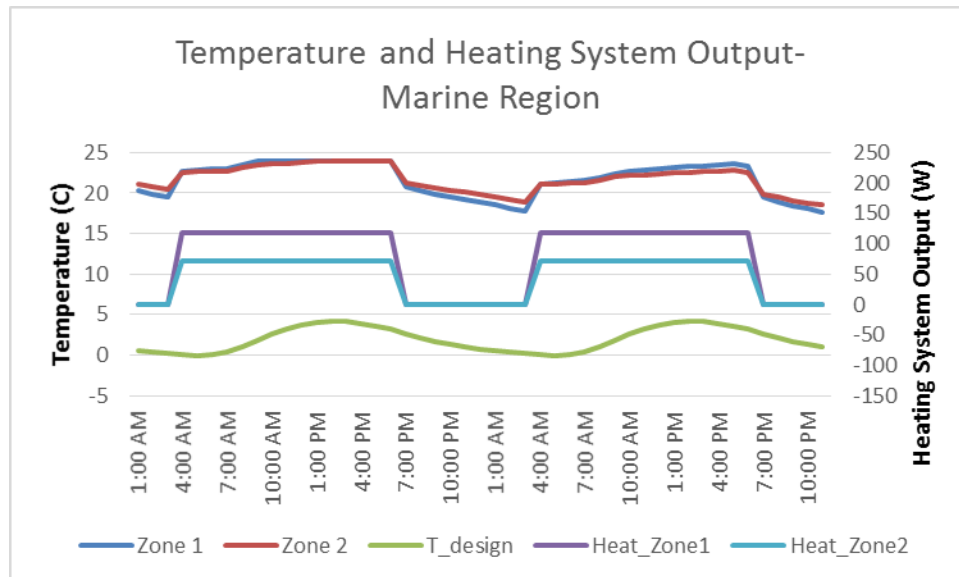


Fig. 10: Temperature Profile for Marine Region

For all cases considered, thermal zone 1 is seen to have lower temperatures as compared with thermal zone 2, since it loses heat to ambient through two windows as opposed to thermal zone 2 which has only one window. Heating results show that the heating system must be operating at full load shortly before and at the time of occurrence of minimum daily temperature for all the cases considered. As expected, zone 1 has higher heating needs than zone 2.

Figures 11 and 12 show the downsizing opportunities for thermal zones 1 and 2 respectively. As could be deduced from Figures 11 and 12, downsizing opportunities vary widely across the U.S. but generally seem to decrease from southern states to northern states. North-eastern states of the U.S. have the least savings. The largest savings is noted in California (54%), and the least was observed for Maine (14%). Overall, hotter regions are seen to have larger downsizing opportunities, as compared with colder regions. This is expected, due to the favorable temperature and solar radiation profile for very hot regions. This implies that using the ASHRAE method for hot regions such as Florida and California may lead to significantly oversized system with the margin greater than 40%. The ASHRAE approximation is thus seen to be more suitable for colder regions, where the percentage of oversize is often less than 20%.

the savings on heating system size is highest for California, which is classified as a hot-dry region and least for Maine, which is a cold region according to ASHRAE classifications. For all the locations studied, there are savings on heating system size by considering passive thermal storage. This study also offers insight into climate regions for which the ASHRAE approximation is most suitable. Results of this study suggests that the current heating device standard results in significantly oversized system for hot humid and hot dry regions of the U.S. These results are significant; with the potential of establishing a new heating device design standard for certain climate classifications.

NOMENCLATURE

α :	Solar radiation absorptivity (dimensionless)
C_{in} :	Thermal capacitance of room air (J/K) (Btu/F)
C_{int} :	Thermal capacitance of internal mass (J/K) (Btu/F)
C_p :	Thermal capacitance of internal wall or partition (J/K) (Btu/F)
Cp :	Specific heat (J/KgK) ($Btu/lbhF$)
Cw :	Thermal capacitance of exterior wall (J/K) (Btu/F)
h :	hour of day
I :	Global solar irradiance (W/m^2) ($Btu/h - ft^2$)
J :	Peak heating rate for the building (W) (Btu/h)
k :	Thermal conductivity (W/mK) ($Btu/hftF$)
L :	Period of optimization (hrs)
Q_{sys} :	System extraction or heating rate (W) (Btu/h)
Q_{conv} :	Convective part of internal load (W) (Btu/h)
Q_r :	Half of the sum of radiative components from internal load and windows (W) (Btu/h)
W :	Vector of uncontrollable variables (weather, internal heat gains, etc)
R_e :	Thermal Resistance of external wall (m^2K/W) ($ft^2F - h/Btu$)
R_{int} :	Thermal Resistance of internal mass (m^2K/W) ($ft^2F - h/Btu$)
R_p :	Thermal Resistance of internal partition (m^2K/W) ($ft^2F - h/Btu$)
R_r :	Thermal Resistance of roof (m^2K/W) ($ft^2F - h/Btu$)
R_{win} :	Windows resistance (m^2K/W) ($ft^2F - h/Btu$)
T_{amb} :	Ambient temperature ($^{\circ}C$) (F)
T_{iE} :	Inside surface temperature of east wall ($^{\circ}C$) (F)
T_{iR} :	Inside surface temperature of roof ($^{\circ}C$) (F)
T_{iW} :	Inside surface temperature of west wall ($^{\circ}C$) (F)
T_{in} :	Room temperature ($^{\circ}C$) (F)
T_{int} :	Internal mass temperature ($^{\circ}C$) (F)
T_{oE} :	Outside surface temperature of east wall ($^{\circ}C$) (F)
T_{oR} :	Outside surface temperature of roof ($^{\circ}C$) (F)

T_{ow} :	Outside surface temperature of west wall ($^{\circ}\text{C}$) (F)
T_p :	Temperature of partition ($^{\circ}\text{C}$) (F)
T_{sE} :	Sol-air temperature of East facing wall ($^{\circ}\text{C}$) (F)
T_{sR} :	Sol-air temperature of roof ($^{\circ}\text{C}$) (F)
T_{sW} :	Sol-air temperature of West facing wall ($^{\circ}\text{C}$) (F)
ΔQ_{ir} :	Extra infrared radiation due to difference between the external air and apparent sky temperature

REFERENCES

- ASHRAE (2009). 2009 ASHRAE Handbook – Fundamentals. Atlanta: American Society of Heating, Refrigerating and Air-Conditioning Engineers, Inc.
- ASHRAE (2010). ASHRAE 90.1-2010, Energy Standard for Buildings Except Low-Rise Residential Buildings
- Braun J.E., T.M. Lawrence, C.J. Klaassen, and J.M. House (2002). Demonstration of load shifting and peak load reduction with control of building thermal mass. *Proceedings of the 2002 ACEEE Conference on Energy Efficiency in Buildings, Monterey, CA.*
- Braun, J. E. (1990). Reducing energy costs and peak electrical demand through optimal control of building thermal storage. *ASHRAE transactions*, 96(2), 876-888.
- Brown, M. Judson. "Optimization of thermal mass in commercial building applications." *Journal of solar energy engineering* 112.4 (1990): 273-279.
- Bueno, B., Norford, L., Pigeon, G., and Britter, R. (2012). A resistance-capacitance network model for the analysis of the interactions between the energy performance of buildings and the urban climate. *Building and Environment*, 54, 116-125.
- Cleve, M. and Loan, C. V. (2003). Nineteen Dubious Ways to Compute the Exponential of a Matrix, Twenty-Five Years Later, *SIAM Review*, Vol. 45, No. 1, pp. 3-000
- DoE (2014). Building America Climate-Specific Guidance, Available at: <http://energy.gov/eere/buildings/building-america-climate-specific-guidance>, accessed November 5, 2014
- Energy Star (2008). Fast Fact on Energy Use. http://www.energystar.gov/ia/business/challenge/learn_more/FastFacts.pdf, Accessed July 2012
- Henze, G. P., Kalz, D. E., Liu, S., and Felsmann, C. (2005). Experimental analysis of model based predictive optimal control for active and passive building thermal storage inventory. *HVAC&R Research*, 11 (2), 189-213.
- Hosni, M.H., and Beck, B.,T. (2010). Updated experimental results for heat gain from office equipment in buildings. ASHRAE Final Report on RP-1482. Atlanta: American Society of Heating, Refrigerating and Air-Conditioning Engineers.
- International Code Council (2012). International Energy Conservation Code, <http://www.iccsafe.org/iccforums/Pages/default.aspx?action=ViewTopics&fid=32&usertoken={token}&Site=icc>, accessed November 7, 2014
- Li, C. and Wang, R. Z. (2012). Building Integrated Energy Storage Opportunities in China, *Renewable and Sustainable Energy Reviews*, 16, 6191–6211
- Lombard, C., and Mathews, E. H. (1992). Efficient, steady state solution of a time variable RC network, for building thermal analysis. *Building and Environment*, 27(3), 279-287.
- Mao, C., Haberl, J. S., & Baltazar, J. C. (2013). Peak heating/cooling load design methods: how we got to where we are today in the US. In *Proceedings of 13th International Conference of the IBPSA, France*, pp. 143 – 151.

- MathWorks (2015). Genetic Algorithm, available at: <http://www.mathworks.com/discovery/genetic-algorithm.html>, accessed August 17, 2015
- McQuiston, F. C., & Spitler, J. D. (1992). *Cooling and heating load calculation manual*. American Society of Heating, Refrigerating and Air-Conditioning Engineers.
- McQuiston, F.C., Parker, J.D., and Spitler, J.D. (2000). *Heating, Ventilating, and Airconditioning Analysis and Design*, 5th ed., ISBN 0-471-35098-2, John Wiley and Sons Inc Publisher.
- Mitchell M. (1997). *An introduction to genetic algorithm*. The MIT Press; 1997.
- Ogunbiyi, O. E. (2014). *Implementation of the lean approach in sustainable construction: a conceptual framework* (Doctoral dissertation, University of Central Lancashire).
- Ogunbiyi, O., Oladapo, A., & Goulding, J. (2013). An empirical study of the impact of lean construction techniques on sustainable construction in the UK. *Construction innovation*, 14(1), 88-107.
- Ogunsola, O. T., & Song, L. (2013). Performance Analysis of a Simplified Model of Cooling Load for a Typical Office Building. In *ASME 2013 International Mechanical Engineering Congress and Exposition* (pp. V011T06A025-V011T06A025). American Society of Mechanical Engineers.
- Ogunsola, O. T., and Song, L. (2012). Review and Evaluation of Using RC Thermal Modeling of Cooling Load Prediction for HVAC System Control Purpose. In *ASME 2012 International Mechanical Engineering Congress and Exposition* (pp. 735-743). American Society of Mechanical Engineers.
- Ogunsola, O. T., Song, L. (2015). Application of a simplified thermal network model for real-time thermal load estimation. *Energy and Buildings*, 96, 309-318.
- Ogunsola, O. T., Song, L., and Wang, G. (2014). Development and validation of a time-series model for real-time thermal load estimation. *Energy and Buildings*, 76, 440-449.
- Ogunsola, O.T. and Song, L. (2014) Investigation of Building Passive Thermal Storage for Optimal Heating System Design, In *ASME 2014 International Mechanical Engineering Congress and Exposition*, Montreal, Canada
- Radecki, P. and Brandon H. (2012). Online building thermal parameter estimation via Unscented Kalman Filtering, *American Control Conference (ACC)*, 2012. IEEE, 2012.
- Schmidt D., and Johannesson, G. (2004). Optimised RC Networks Incorporated within Macro-Elements for Modelling Thermally Activated Building Constructions, *Nordic Journal of Building Physics*, Vol. 3, 2004.
- Seem J.E., Klein S.A. et al. (1989). Transfer functions for efficient calculation of multidimensional transient heat transfer. *Journal of Heat Transfer*, Vol.111:5-12.
- Snyder, M., and Newell, T. (1990). "Cooling Cost Minimization Using Building Mass for Thermal Storage," *ASHRAE Trans.*, 96_2_, pp. 830-838.
- Sourbron, Maarten, Martine Baelmans, and Lieve Helsen (2009). "Thermal response of thermally activated building systems (TABS) in office buildings [C]." *Proceedings of EFFSTOCK. Stockholm, Sweden* (2009): 57-64.
- United States DoE (2013). *EnergyPlus Energy Simulation Software*, available at http://apps1.eere.energy.gov/buildings/energyplus/weatherdata_about.cfm Accessed October 2013
- Wang, S., and Xu, X. (2006). Parameter estimation of internal thermal mass of building dynamic models using genetic algorithm. *Energy Conversion and Management*, 47(13), 1927-1941.
- Yang L, and Li Y (2008). Cooling load reduction by using thermal mass and night ventilation. *Energy and Buildings*, 40 (11):2052-8.

Appendix 1: Studied Locations and Climate Classification

S/N	Station ID	Location	City Name	Climate Type	ASHRAE
1	722230	Alabama	Mobile Regional AP	Hot-Humid	2A

2	722740	Arizona	Tucson International AP	Hot-dry	2B
3	723418	Arkansas	Texarkana Webb Field	Hot-Humid	2A
4	722950	California	Los Angeles Intl Arpt	Hot-dry	2B
5	724769	Colorado	Fort Collins (AWOS)	Cold	5B
6	725040	Connecticut	Bridgeport Sikorsky Memorial	Cold	5A
7	724088	Delaware	Dover AFB	Mixed-Humid	4A
8	722030	Florida	West Palm Beach Intl Arpt	Hot-Humid	2A
9	747810	Georgia	Moody AFB/Valdosta	Hot-Humid	2A
10	726813	Idaho	Caldwell (AWOS)	Cold	
11	725314	Illinois	Cahokia/St. Louis	Mixed-Humid	4A
12	724320	Indiana	Evansville Regional AP	Mixed-Humid	4A
13	725460	Iowa	Des Moines Intl AP	Cold	5A
14	724504	Kansas	Wichita/Col. Jabara	Mixed-Humid	4A
15	724354	Kentucky	Somerset (AWOS)	Mixed-Humid	4A
16	722405	Louisiana	Lafayette Regional AP	Hot-Humid	2A
17	726060	Maine	Portland Intl Jetport	Cold	6A
18	745940	Maryland	Andrews AFB	Mixed-Humid	4A
19	725067	Massachusetts	Barnstable Muni Boa	Cold	5A
20	725375	Michigan	Detroit City Airport	Cold	5A
21	726575	Minnesota	Minneapolis/Crystal	Cold	6A
22	747686	Mississippi	Keesler AFB	Mixed-Humid	4A
23	723489	Missouri	Cape Girardeau Municipal AP	Mixed-Humid	4A
24	727730	Montana	Missoula International AP	Cold	6B
25	725540	Nebraska	Bellevue Offutt AFB	Cold	5A
26	723860	Nevada	Las Vegas McCarran Intl AP	Hot-Dry	2B
27	726055	New Hampshire	Pease Intl Tradepor	Cold	5A
28	725020	New Jersey	Newark International Arpt	Mixed-Humid	4A
29	723650	New Mexico	Albuquerque Intl Arpt	Mixed-Dry	4B
30	744860	New York	New York J F Kennedy Int'l Ar	Mixed-Humid	4A
31	723013	North Carolina	Wilmington International Arpt	Hot-Humid	2A

32	727676	North Dakota	Minot Faa AP	Very Cold	7
33	724288	Ohio	Ohio State University	Cold	5A
34	723575	Oklahoma	Lawton Municipal	Mixed-Humid	4A
35	726959	Oregon	Aurora State	Marine	5A
36	724080	Pennsylvania	Philadelphia International AP	Mixed-Humid	4A
37	725070	Rhode Island	Providence T F Green State Ar	Cold	5A
38	722080	South Carolina	Charleston Intl Arpt	Hot-Humid	2A
39	726625	South Dakota	Ellsworth AFB	Cold	5A
40	723340	Tennessee	Memphis International AP	Mixed-Humid	4A
41	722598	Texas	Dallas/Addison Arpt	Hot-Humid	2A
42	724754	Utah	Saint George (AWOS)	Hot-Dry	2B
43	726170	Vermont	Burlington International AP	Cold	6A
44	724050	Virginia	Washington Dc Reagan AP	Mixed-Humid	4A
45	727938	Washington	Tacoma Narrows	Marine	4C
46	724140	West Virginia	Charleston Yeager Arpt	Mixed-Humid	4A
47	726400	Wisconsin	Milwaukee Mitchell Intl AP	Cold	6A
48	725640	Wyoming	Cheyenne Municipal Arpt	Cold	6B

Reference: DoE (2010). Guide to determining climate regions by county. Available at: http://apps1.eere.energy.gov/buildings/publications/pdfs/building_america/ba_climateguide_7_1.pdf

Appendix 2: Heating Design Temperatures (ASHRAE vs TMY3)

Station ID	Location	City Name	ASHRAE 99.6% design temperature	TMY3 99.6% design temperature	Value Used
722230	Alabama	Mobile Regional AP	-2.8	-5.6	TMY3
722740	Arizona	Tucson International AP	-0.2	-2.2	TMY3
723418	Arkansas	Texarkana Webb Field	-5.8	-6.6	TMY3
722950	California	Los Angeles Intl Arpt	6.9	6.1	TMY3
724769	Colorado	Fort Collins (AWOS)	-17.7	-26.6	TMY3
725040	Connecticut	Bridgeport Sikorsky Memorial	-11.8	-18.3	TMY3
724088	Delaware	Dover AFB	-10.1	-14	TMY3
722030	Florida	West Palm Beach Intl Arpt	6.8	5.4	TMY3
747810	Georgia	Moody AFB/Valdosta	-1.2	-8	TMY3
726813	Idaho	Caldwell (AWOS)	-11.3	-7	ASHRAE

725314	Illinois	Cahokia/St. Louis	-12.5	-14.4	TMY3
724320	Indiana	Evansville Regional AP	-14.7	-13.3	ASHR AE
725460	Iowa	Des Moines Intl AP	-21.6	-21.1	ASHR AE
724504	Kansas	Wichita/Col. Jabara	-14	-11	ASHR AE
724354	Kentucky	Somerset (AWOS)	-10.2	-14.3	TMY3
722405	Louisiana	Lafayette Regional AP	-1.9	-1.1	ASHR AE
726060	Maine	Portland Intl Jetport	-18	-23.3	TMY3
745940	Maryland	Andrews AFB	-10.1	-12	TMY3
725067	Massachusetts	Barnstable Muni Boa	-12.5	-8	ASHR AE
725375	Michigan	Detroit City Airport	-15.5	-16.7	TMY3
726575	Minnesota	Minneapolis/Crystal	-22.6	-27	TMY3
747686	Mississippi	Keesler AFB	-0.9	-4	TMY3
723489	Missouri	Cape Girardeau Municipal AP	-13.7	-19	TMY3
727730	Montana	Missoula International AP	-21.1	-15	ASHR AE
725540	Nebraska	Bellevue Offutt AFB	-19.6	-23	TMY3
723860	Nevada	Las Vegas McCarran Intl AP	-0.8	1.1	ASHR AE
726055	New Hampshire	Pease Intl Tradepor	-16.3	-15.6	ASHR AE
725020	New Jersey	Newark International Arpt	-11.6	-17.8	TMY3
723650	New Mexico	Albuquerque, new mexico	-7.9	-7.8	ASHR AE
744860	New York	New York J F Kennedy Int'l Ar	-10.7	-11.7	TMY3
723013	North Carolina	Wilmington International Arpt	-4.5	-3.9	ASHR AE
727676	North Dakota	Minot Faa AP	-28.8	-28.2	ASHR AE
724288	Ohio	Ohio State Universi	-14	-21	TMY3
723575	Oklahoma	Lawton Municipal	-7.8	-8	TMY3
726959	Oregon	Aurora State	-2.5	-3	TMY3
724080	Pennsylvania	Philadelphia International AP	-10.8	-13.3	TMY3
725070	Rhode Island	Providence T F Green State Ar	-13.8	-14.4	TMY3
722080	South Carolina	Charleston Intl Arpt	-2.8	-4.4	TMY3
726625	South Dakota	Ellsworth AFB	-22.9	-26	TMY3
723340	Tennessee	Memphis International AP	-8.3	-11.7	TMY3
722598	Texas	Dallas/Addison Arpt*	-5.8	-8	TMY3
724754	Utah	Saint George (AWOS)	-2.9	-3	TMY3

726170	Vermont	Burlington International AP	-22.4	-26.7	TMY3
724050	Virginia	Washington Dc Reagan AP	-8.7	-11.3	TMY3
727938	Washington	Tacoma Narrows	-1.4	0	ASHR AE
724140	West Virginia	Charleston Yeager Arpt	-13	-23.9	TMY3
726400	Wisconsin	Milwaukee Mitchell Intl AP	-20	-23.9	TMY3
725640	Wyoming	Cheyenne Municipal Arpt	-21.3	-22.2	TMY3

Appendix 3: Floor composition

	L (mm) (in)	k (W/mK) (Btu/hftF)	ρ (kg/m ³) (lb/ft ³)	C_p (J/KgK) (Btu/lbF)	Resistance (m ² k/W) (ft ² Fh/Btu)
M11 100mm lightweight concrete	101.6 (4)	0.53 (0.304)	1280 (79.91)	840 (0.201)	
F05 Ceiling air space	-	-	-	-	0.18 (1.022)
F16 Acoustic tile	19.1 (0.75)	0.06 (0.034)	368 (22.97)	590 (0.141)	

Appendix 4: Composition of Partitions

	L (mm) (in)	k (W/mK) (Btu/hftF)	ρ (kg/m ³) (lb/ft ³)	C_p (J/KgK) (Btu/lbF)	Resistance (m ² k/W) (ft ² Fh/Btu)
G01a 19mm gypsum	19 (0.75)	0.16 (0.092)	800 (49.94)	43 (0.01)	
F04 Wall air space resistance	-	-	-	-	0.15 (0.852)
G01a 19mm gypsum	19 (0.75)	0.16 (0.092)	800 (49.94)	43 (0.01)	

APPLICATION OF A SIMPLIFIED THERMAL NETWORK MODEL FOR REAL-TIME THERMAL LOAD ESTIMATION

Ogunsola, O.T. and Song, L., 2015. Application of a simplified thermal network model for real-time thermal load estimation. *Energy and Buildings*, 96, pp.309-318.

Abstract

Heating and cooling loads are the major reasons for energy use in buildings. Buildings are usually subject to schedules and set-points which are not optimized in response to the dynamic weather conditions, internal loads, and occupancy patterns. The thermal network model has been widely applied for real-time building load estimation, which is crucial for optimizing the operation of the HVAC system. However, there has been limited exploration of the capabilities of the thermal network model due to constraints imposed by the solution method adopted. In this paper, the exponential matrix method was adopted to simplify the state space equations and solve the thermal network model analytically. This enhances the applications of a simplified thermal network model for investigation of multiple scenarios of HVAC system operations and equipment sizing, and for more accurate estimation of heating and cooling loads. This study also proves that the analytical solution method is asymptotically stable regardless of time step. A typical office was used as a case study and the predicted building loads are compared with measured data and numerical results from EnergyPlus. For the case study, the model demonstrated better accuracy and is seen to be robust for thermal load estimation for cooling season.

Keywords: Cooling Load; RC model; Building Envelope; Internal Mass; EnergyPlus;

1 Introduction

The overall function of an HVAC (Heating, Ventilation and Air Conditioning) system is to compensate for building load in order to provide thermal comfort. The building load is the rate at which heat must be extracted from (or delivered to) the building to maintain the desired set-point, i.e., the rate at which heat is convected from (or to) the zone air. According to a study by Daum and Morel [1], buildings consumed 40% of total primary energy in the USA in 2008, with commercial buildings holding a share of 18.4%. Globally, around 40% of primary energy consumed in buildings is used for HVAC. It is not surprising that regulations and national policies are being developed and implemented to encourage or mandate reduced building energy consumption or prescribe increases in efficiency for relevant building components, such as building envelope elements, HVAC systems and equipment, and lightning equipment.

Buildings are usually subject to absorption and delayed release of radiation, thermal mass effects, infiltration, dynamic internal schedules and other phenomena which are either difficult to model or not accounted for by most models. Likewise, plant and building set-points often follow prescribed schedules which are not optimized in response to dynamic conditions, weather, internal loads, occupancy patterns, and so on. These conditions make building load calculations and optimization challenging. Since buildings account for significant portions of global electricity and energy use, real-time control and forecasts of the building load are important to minimize building electricity use and energy consumption. Oldewurtel *et Al.* [2] predict a 5% delivered energy consumption increase in the building sector by 2035 if building technology from 2009 is used. Therefore, research in energy conservation in the building sector is highly important and accurate forecasting of dynamic building load is essential from a control, environment, and energy standpoint.

There have been several studies on building performance and load calculations. Pang *et al.* [3] developed a simulation-based framework for real-time building performance assessment. The framework allowed for a comparison of a building's actual performance and expected performance in real-time. However, several factors and variables such as HVAC operational schedules, control set-points, and weather data, e.g., solar radiation, relative humidity, wind speed, and direction, have to be updated at each time step.

Causone et al. [4] developed a calculation procedure for cooling loads using the Heat Balance method and the Radiant Time Series (RTS) method, which are well described in the ASHRAE Handbook of Fundamentals [5]. These models need calibration to accurately reflect system performance. Braga et al. [6] developed a statistical process to model and estimate the energy consumption profile of a building during a cycle, e.g., one week. The statistical model was used to monitor and control energy consumption patterns. Using EnergyPlus, Feng et al. [7] compared the cooling load differences between radiant and air systems under the influence of factors such as level of insulation, thermal mass effects, internal heat gains, and solar exposure of floors and ceilings. Chen et al. [8] also assessed the effects of appliance level on real-time and historical energy use in buildings by separate measurements of the appliance plug loads, heating and cooling loads, and lighting loads through the use of energy meters and proxy sensors. Xuemei et al. [9] developed an algorithm for forecasting the cooling load, using a support vector machine (SVM) model, a machine learning technique whose parameters are determined from measured data. Duanmu et al. [10] developed the Hourly Cooling Load Factor Method (HCLFM) for cooling load prediction. The method assumes certain linear relationships between the cooling load components and variables such as temperature and enthalpy differences between indoor and outdoor air. Schiavon et al. [11] developed a calculation method for cooling loads in underfloor air distribution (UFAD) systems. Using EnergyPlus simulations, regression methods were developed to transform cooling loads from traditional overhead mixing systems to UFAD systems. However, the method is only suitable for design cooling load estimation.

The thermal network model of Resistances and Capacitances (RC) model is commonly used to describe the thermal delays caused by a building envelope and internal thermal mass effects, and provides robust and accurate estimates of the cooling load based on measured data. Although there have been many improvements in the RC model over the years, the three resistances and two capacitances (3R2C) arrangement is widely used for modeling transient heat transfer in building envelopes [12,13]. More recent versions of the RC models are 3R4C and 4R5C by Fraisse [14]. The RC model has also been used to investigate thermal coupling among building elements, estimate the cooling load for thermally activated building construction, and compare thermal zone aggregated methods [15-17].

The RC model represents the building envelope and internal mass using lumped capacitors and resistors, as developed by Xu [18]. The envelope RC parameters are usually found using theoretical properties of the building construction in frequency domain, or from construction materials. The internal mass RC parameters are determined by minimizing the differences between the building loads calculated using the model and the actual building loads. This avoids the lengthy calibration process which is necessary in other models, and compensates for errors in the input parameters of the model. The RC parameters have been traditionally estimated using a genetic algorithm and by solving the integrated RC model numerically using Runge-Kutta methods or other classical methods [18, 19]. In a recent study [20], a time series model was deduced from the simplified RC model. Compared with pure statistical models, such as autoregressive models, the time series was deemed superior because it has less sensitivity to outliers and the ability to track sudden input changes such as abrupt air temperature drop or sudden changes in control strategy. However, current solution methods such as the time series and numerical solutions permit limited exploration of the capabilities of the thermal network model. For example, numerical solutions suffer from stability and convergence issues, which are often caused by the need to consider different time steps. For the time series, the previous four (or more) time intervals are needed as inputs. The needed measurements are sometimes unavailable or unreliable due to sensor malfunction or data quality assurance issues. Similarly, in previous RC model studies, there are no documented methods on the search space for the best fit of the internal mass parameters, particularly when the envelope and internal mass components are decoupled. Unreasonable initial guesses and/or bounds could lead to slow convergence. There have also been noticeable spikes in the cooling load prediction by the time series [20]. The identified issues with the current solution methods limit the general applicability of the thermal network model.

Therefore, the aim of this study is to solve the simplified RC thermal model using an analytical solution method and to apply the model to a typical office building. This model requires fewer inputs, depends only on initial (or any previous) time step data and current conditions, is capable of simulating floats in temperature for investigating thermal storage opportunities or for simply comparing several HVAC

systems operation modes, and is consistent. This study also aims to investigate and ascertain the unconditional and asymptotic stability of the thermal network model for all feasible values of envelope and internal mass parameters by applying stability criteria to its resulting state space model. Latent load prediction is not included since latent heat gain instantaneously converts to latent cooling without a time delay.

The paper begins with a general description of the analytical solution to the simplified RC model, after which the stability of the thermal network model is investigated. The stability analysis is crucial and needed because of concerns about the feasible search region of the envelope and internal mass parameters that cause the model to become unstable. Satisfaction of asymptotic stability is highly important for the thermal model to correctly depict the physical and thermal behavior of the building system, since temperatures and heat fluxes are expected to remain bounded at all times. The RC model is then tested on a case study of an office, and compared with field measurements and simulation results from EnergyPlus. Various scenarios of parameter estimation are investigated, with the goal of choosing the most accurate and representative parameter set for forecasting the building load. Finally, the RC thermal model is validated for both the heating and cooling season in order to demonstrate the robustness and suitability of the model for different building system operation modes and scenarios. The paper concludes with a comparison of the RC model with EnergyPlus and actual building load measurements in terms of error indices such as the mean error, mean absolute error, and root mean square error.

2 Analytical Solution of the RC Model

In previous studies, the RC model was solved numerically, using time-series, unscented Kalman filtering, or other advanced methods [12, 18, 19, 21]. In this study, in order to eliminate the numerical calculation for solving the integrated RC model and to reduce the inputs needed for the time-series solution, the RC model is solved analytically using state space methods. The analytical solution gives the exact solution to the governing differential equations for the lumped model.

The RC thermal model with envelope and internal mass components is shown in Fig. 1. The variables are as defined in the nomenclature. The solar air temperature, $T_{sol-air}$ is the combined effect of solar radiation and ambient temperature on the outside surface of the wall [22]. This concept is only suitable for opaque surfaces such as walls and roofs. Therefore, it is only applied to the outside wall and roof. $T_{sol-air}$ is defined in Eq. (1):

$$T_{sol-air} = T_{amb} + \frac{\alpha I - \Delta Q_{ir}}{h_o} \quad (1)$$

where the variables α , I , and ΔQ_{ir} are as defined in the nomenclature. The thermal radiation correction term, $\Delta Q_{ir}/h_o$, is usually approximated as being 4.4°C for horizontal surfaces and 0°C for vertical surfaces [22].

The sol-air temperature varies for different wall orientations due to variations in the incident solar radiation. To derive a sensible heat balance equation for the RC model, the following simplifying assumptions are made:

- The zone air is well mixed; therefore the whole indoor circulated air volume is at a uniform temperature.
- The effect of varying wind velocity on external wall convection coefficients is not considered. Hence, a constant heat transfer coefficient is assumed in this study.
- The space is pressurized so infiltration does not create additional heating load in the conditioned space.
- The floor surface is considered adiabatic.

- The long wave radiation exchanges between internal surfaces and multiple reflections are described by the lumped internal thermal RC model.
- Heat is transferred between ambient and the thermal zone only through the exposed west wall. All other surfaces are treated as adiabatic.

The above assumptions are commonly made to simplify the RC model [12, 18]. The governing equations found by heat balance at each node are given in Eq. (2):

$$\frac{dT_n}{dt} = -\frac{1}{C_n} \left(\sum_{i=1}^j \frac{1}{R_i} \right) T_n + \frac{1}{C_n} \left(\sum_{i=1}^j \frac{1}{R_i} T_i \right) + \frac{1}{C_n} \sum_{i=1}^p Q_i \quad (2)$$

where

T_n = temperature of the n th node.

C_n = thermal capacitance of node n

j = total number of temperature branches (e.g., ambient, sol-air temperature, and neighbor nodal temperatures) connected to node n

T_i = temperature of the i th branch, connected to node n .

p = total number of heat flux branches (such as convection, radiation, and system input) connected to node n .

Q_i = heat flux of the i th branch connected to node n .

R_i = resistance of the branch between T_n and T_i .

Eq. (2) represents an inhomogeneous system of ordinary differential equations. In state space representation, it can be re-written as:

$$\dot{T} = AT + BU \quad (3)$$

where A is the state (or system) matrix and B is the input matrix of dimensions $n \times n$ and $n \times q$, respectively, as shown in Eq. (4).

$$A = \begin{pmatrix} a_{11} & \cdots & a_{1n} \\ \vdots & \ddots & \vdots \\ a_{n1} & \cdots & a_{nn} \end{pmatrix} \text{ and } B = \begin{pmatrix} b_{11} & \cdots & b_{1q} \\ \vdots & \ddots & \vdots \\ b_{n1} & \cdots & b_{nq} \end{pmatrix} \quad (4)$$

The matrices A and B are time-invariant matrices whose entries are functions of the RC parameters.

$T = [T_1 \ T_2 \ T_n]'$ are the nodal temperatures, and $U = [U_1 \ U_2 \ \dots \ U_q]'$ is the input matrix, which includes heat gains, ambient temperatures, and sol-air temperatures on opaque surfaces. The stability of the system depends on the eigenvalue characteristics of the system matrix, A . In general, $q \geq p$, that is, the input matrix must include not only the heat flux sources but also ambient and sol-temperature inputs. Eq. (3) is a system of first order differential equations with constant coefficients, and the solution is given by:

$$T_{t+\delta} = e^{A\delta} T_t + \int_t^{t+\delta} e^{A(t+\delta-\tau)} BU(\tau) d\tau \quad (5)$$

where the exponential matrix of A is defined by the power series

$$e^{A\delta} = I + A\delta + \frac{A^2\delta^2}{2!} + \frac{A^3\delta^3}{3!} + \dots + \frac{A^n\delta^n}{n!} + \dots \quad (6)$$

I is the identity matrix of the same dimensions as A , and δ is the time step. As developed by Seem et al. [23], inputs between time t and $t + \delta$ can be modeled by a continuous, piecewise linear function as:

$$\mathbf{U}(t) = \mathbf{U}_t + \frac{(\tau - t)}{\delta} (\mathbf{U}_{t+\delta} - \mathbf{U}_t) \quad (7)$$

A function or curve is piecewise continuous if it is continuous on all points except for a few discontinuities which are finite. In previous studies [23], the concept of piece-wise continuity was applied only to the building envelope. In this paper, the concept is extended to include solar radiation and the convection term in order to take the 2R2C into account. The concept of piecewise continuity was similarly used for solar radiation absorbed by vegetation [24]. The convection term in the input is predominately from plug loads, which are mostly step functions in reality. For a uniform expression, a piecewise continuous assumption is also made for the convection term. As a result, the assumption substitutes a step input in the time intervals when the step change occurs with a ramp input, and could cause the output of the time series to deviate from reality. However, the deviation is considered to have a small impact on the model accuracy because it only occurs in the time interval when the plug load is enabled, and the convection term takes a smaller percentage of the total plug load compared with the radiation term. Meanwhile, the input between time t and $t + \delta$ could easily be modeled using other functions (such as sine or cosine for ambient or solar radiation) if they are deemed more appropriate or when longer time steps are used. Substituting Eq. (7) into Eq. (5) gives

$$T_{t+\delta} = e^{A\delta}T_t + \int_t^{t+\delta} e^{A(t+\delta-\tau)}B \left[\mathbf{U}_t + \frac{(\tau - t)}{\delta} (\mathbf{U}_{t+\delta} - \mathbf{U}_t) \right] d\tau \quad (8)$$

If conditions are known at time, $t=0$, then the solution becomes

$$T_\delta = e^{A\delta}T_o + \int_0^\delta e^{A(\delta-\tau)}B \left[\mathbf{U}_o + \frac{(\tau)}{\delta} (\mathbf{U}_\delta - \mathbf{U}_o) \right] d\tau \quad (9)$$

To obtain the analytical solution, the exponential matrix $e^{A\delta}$ and the convolution integral $\int_0^\delta e^{A(\delta-\tau)}B \left[\mathbf{U}_o + \frac{(\tau)}{\delta} (\mathbf{U}_\delta - \mathbf{U}_o) \right] d\tau$ need to be evaluated. There are several approaches used to evaluate the matrix exponential. These include polynomial methods, Taylor series, inverse Laplace, matrix decomposition, and the ordinary differential equation method [25]. In this study, the matrix decomposition method is adapted because it is based on similarity transformation of the form:

$$A = CDC^{-1} \quad (10)$$

such that the power series definition of e^{At} becomes

$$e^{At} = Ce^{Dt}C^{-1} \quad (11)$$

The usual approach is to take C as the matrix whose columns are the eigenvectors of A , i.e.,

$$C = V = [v_1 | \dots | v_n] \text{ and } Av_j = \lambda_j v_j, \quad j = 1, \dots, n \quad (12)$$

$$e^{Dt} = \text{diagonal matrix}(e^{\lambda_1 t}, \dots, e^{\lambda_n t}) \quad (13)$$

As long as V is nonsingular, the matrix exponential of At is expressed as

$$e^{At} = V(\text{diag}(e^{\lambda_1 t}, \dots, e^{\lambda_n t}))V^{-1} \quad (14)$$

The analytical solution was tested in [26] where it was used for the optimal sizing of the heating system through investigation of building passive thermal storage. The conditions for non-singularity of V are discussed in the next section.

3 Feasibility analysis of the analytical solution method

Accuracy of the RC thermal model depends strongly on accurate estimation of the model parameters, which are broadly classified as envelope and internal mass components. These parameters have been estimated in several ways. The internal mass parameters are more challenging to estimate, since the physical properties of components such as furniture, carpets, and other surfaces that are capable of absorbing radiation within the indoor environment are not readily available. When information on building construction is available, the most common methods to evaluate the envelope parameters are direct calculation from construction material, use of average values of the RC, and optimization techniques. These methods are described in more detail by Ogunsola and Song [27]. In previous studies, the internal mass parameters were found using a genetic algorithm, by minimizing the differences between the cooling loads estimated using the model and the measured cooling loads. A genetic algorithm has been mostly used because it doesn't require an initial guess. However, there have been concerns about the identification of a feasible search region that assures asymptotic stability of the thermal model for every time-step, particularly when using numerical solutions or the time-series model. Therefore, the stability analysis is critical for the analytical solution which is dependent on the non-singularity of the eigenvector as well as the nature of the eigenvalues. In this section, it is desired to prove that based on some observed properties of the state matrix, the eigenvector, V , is always non-singular.

Analysis of Eq. (2) reveals important properties of the system matrix A : It is a square matrix with sum of each row ≤ 0 , and with at least one row satisfying the inequality. We proceed to prove that the following conditions hold about the stability of any square matrix:

“A square matrix is asymptotically stable if its principal diagonal entries are < 0 and sum of each row ≤ 0 (or sum of each columns ≤ 0), with at least one row or column satisfying the inequality. It can be inferred that such a matrix is non-singular, that is, the determinant is not equal to zero”.

To illustrate, consider a $n \times n$ matrix, $A = \begin{bmatrix} a_{1,1} & a_{1,2} & \cdots & a_{1,n} \\ a_{2,1} & a_{2,2} & \cdots & a_{2,n} \\ \vdots & \vdots & \cdots & \vdots \\ a_{n,1} & a_{n,2} & \cdots & a_{n,n} \end{bmatrix}$. Applying the criteria defined above implies that the matrix A is asymptotically stable when

- (iii) Every entry on the principal diagonal is less than zero, i.e., $a_{1,1} < 0, a_{2,2} < 0, \dots, a_{n,n} < 0$. All other entries are real and positive.
- (iv) $a_{1,1} + a_{1,2} + \dots + a_{1,n} \leq 0, a_{2,1} + a_{2,2} + \dots + a_{2,n} \leq 0, \dots, a_{n,1} + a_{n,2} + \dots + a_{n,n} \leq 0$.
- (v) At least one of the expressions in (2) satisfies the inequality (< 0).

To illustrate this for the thermal network model, consider a three-node model shown in Fig. 2.

The resulting state matrix is $A = \begin{bmatrix} -\frac{1}{C2R1} - \frac{1}{C2R3} & \frac{1}{C2R3} & 0 \\ \frac{1}{C2R3} & -\frac{1}{C2R3} - \frac{1}{C2R5} & \frac{1}{C2R5} \\ 0 & \frac{1}{CinR5} & -\frac{1}{CinR5} \end{bmatrix}$, which can be written as

$$A = \begin{bmatrix} a & b & 0 \\ b & c & d \\ 0 & -e & e \end{bmatrix}, \text{ where } a = -\frac{1}{C2R1} - \frac{1}{C2R3} < 0, c = -\frac{1}{C2R3} - \frac{1}{C2R5} < 0, \text{ and } e = -\frac{1}{CinR5} < 0. \text{ Also note}$$

that sum of each row is equal to zero, except for the first row where $a + b = -\frac{1}{C2R1} < 0$. Since $a + b < 0$ and $c + b + d = 0$, we can write $a = -b - g1$; and $c = -b - d$ where $g1 > 0$. The characteristics equation becomes as shown in Eq. (15):

$$\lambda^3 + \lambda^2(2b + d + g1 + e) + \lambda(bd + g1b + g1d + 2eb + eg1) + eg1b=0 \quad (15)$$

Note that all coefficients are positive, which is a necessary condition for the eigenvalues to be negative. The constant term ($eg1b$) is the determinant, which implies that the matrix becomes singular only if $g1 = 0$. However, $g1 > 0$ as defined, so the three-node model is non-singular. When the characteristics equation is solved symbolically in MATLAB, it shows that the eigenvalues are negative. Larger matrices which satisfy the conditions in (1) to (3) have been tested, too, and the same conclusions are made about the non-singularity and stability of the matrices. As the matrix becomes larger, the symbolic computation becomes overwhelming. However, the symbolic solution can be avoided by assuming random values for the entries of the matrix, provided the diagonal entries, rows, and columns satisfy the conditions stated in (1) to (3). This was done for matrices of different sizes, and the results confirmed the asymptotic stability and invertibility properties.

An important observation is that the state space representation of the governing equations permits the investigation of the stability without necessarily solving the governing differential equations. The analytical solution relies on evaluation of the inverse, eigenvector, and exponential of the state space matrix. Asymptotic stability implies that all eigenvalues of the state matrix must lie in the open left hand plane for the system to be eventually driven by the forcing inputs, rather than by initial conditions. This also implies observability and controllability of the system, and the existence of unique eigenvectors and inverse. Therefore, establishing the asymptotic stability of the thermal network model is sufficient to prove the non-singularity of the eigenvector, as well as the fact that the devised analytical solution method will be suitable for all scenarios and time steps. From assumption of piecewise continuity (Eq. 7) and the evaluation of the matrix exponential (Eq. 9), an analytical solution of all temperature and heat flux is obtainable. Using the state transition matrix and the input matrix, the solution at a current (or future) time step is dependent on the value from a previous time step, inputs from the previous and current steps, and the elapsed time between the two time steps. The building load is expressed as the HVAC system output required to achieve the measured temperature for the period of investigation.

4 Case Study

The procedures described in the preceding section are tested and validated using a case study of a typical office. The selected room is a thermal zone in an office building situated at the University of Oklahoma. One thermal zone was chosen to capture the dynamics and variations at the zone level. Reasonably high model accuracy at the zone level could easily be extended to multi-zone buildings. The needed input includes ambient air temperature, internal heat gains, and solar radiation. The studied building is shown in Fig. 3. The focus in this study is the middle (highlighted) thermal zone, which has adjacent zones on both sides and exposure to ambient temperature on the westside. The selected zone is a good candidate because it has its own thermostat and sensors, which can measure all the variables needed for building load estimation. The needed measurements are obtained from the BAS and the sensors are deemed to be functioning properly and reasonably accurate enough to prevent any data integrity issues. As shown in Fig. 3, the simulated zone is part of a larger building. However, in this study, we assume that the adjacent spaces are similarly conditioned and therefore the studied zone is treated as a single, stand-alone room, with negligible thermal influence from the adjacent zones. This assumption is expected to have minimal influence on the prediction, since all neighboring zones have similar occupancy schedules and set points. The RC model representation of the building is shown in Fig. 4.

The windows are treated as single thermal resistance (without thermal mass), through which the solar radiation directly reaches two virtual internal nodes. The inputs to the model include envelope and internal load components, which have significant influence on the temperature and load profile of the building. The RC parameters are denoted using the resistor and capacitor symbols in the thermal network, and include parameters such as the windows resistance (R_{win}), the envelope parameters (e.g., $Re2$ and Cw), and the internal mass parameters (such as the R_{int1} and C_{int}). The unknown nodal temperatures are T_{oE} , T_{iE} , T_{int1} , T_{int1} , and T_{in} . The input to the model include T_{sW} , T_{amb} , Q_{conv} , Q_{sys1} , Q_{r1} , and Q_{r2} . A brief description of key variables is given below:

T_{oE} and T_{iE} : Temperature of building envelope (outside surface, and inside surface)

T_{int1} and T_{int2} :	Virtual temperatures of internal mass nodes
T_{in} :	Zone Temperature
T_{sw} :	Solar-air temperature on west-facing wall
T_{amb} :	Ambient temperature
Q_{sys1} :	System input (+ve for heating, and –ve for cooling). It is 100% convective.
$Q_{r1} = Q_{r2} = Q_r$:	Average of the sum of transmitted solar radiation from windows, and radiative part of the internal load for the particular zone.
Q_{conv} :	Convective part of the internal load. In this study, the assumed split is 50% convection and 50% radiation. This implies that 50% of the internal heat gain is added to the air stream instantaneously, while the remaining 50% is radiated.

Internal load (equipment and people) density of 25 W/m² for occupied hours (9 am–5 pm). This is within the recommended range by ASHRAE/IES 90.1-2010 standards (16.15–32.3 W/m²) for office and some institutional buildings. An internal load density of 5 W/m² was used for unoccupied hours.

As shown in Fig. 1, there are 6 resistances and 5 capacitances. Training data are needed to determine the RC parameters that optimally represent the building physically and also match the temperature and building load. The indoor capacitance, C_{in} is derived from the air mass within the occupied space, and hence is a known parameter. The window resistance and building envelope are assumed to be from a typical office (as shown in Tables 1 and 2) due to limited information about the building construction. For readability, the assumed composition of partitions, roof/ceiling, and floor are shown in Appendix. The RC properties of other supporting structural components are assumed to be lumped into the estimated RC parameters. The capacitances C_{int1} and C_{int2} are generally assumed to be equal [12, 18]. The above assumptions reduce the unknown parameters to 5 resistances (R_{e1} , R_{e2} , R_{e3} , R_{int1} , and R_{int2}) and 2 capacitances (C_w and $C_{int1}=C_{int2}$). For this situation, there are several possible implementations. The scenarios investigated in this study are shown in Table 3. The first scenario involves estimation of all 7 parameters. The other scenarios involve fixing certain known parameter(s), e.g., by assuming values for the outside and inside convection resistances through construction documents for the building envelope or by selecting typical medium construction for this case due to the lack of design documents. Typical medium wall construction was chosen because of limited and unavailability of building construction information for the studied zone. This is one of the limitations of whole simulation software like EnergyPlus, when the construction information is not available. Using the RC thermal model, feasible building parameters can be deduced from limited information and measured data. The likely known parameters are mostly the thermal resistances of the building envelope (R_{e1} , R_{e2} , and R_{e3}). The different scenarios investigated are summarized in Table 3.

The optimal RC parameters are usually estimated by matching the building load and temperature predicted by the RC model to the measured data. In this study, 3 days of training data (summer: July 1-3, 2013 and winter: January 1-3, 2013) are used to determine the RC parameters and 10 days of data (summer: July 22-31, 2013 and winter: January 21-30, 2013) are used for validation. Two solution options are proposed. The first method involved estimation of the RC parameters of each scenario in Table 3 using the cooling season, after which time the model is validated for both the heating and cooling season. Under the second option, the RC parameters of each scenario will be estimated from actual data recorded during heating season, and validated by comparing the predicted temperature and building load results with measured values for both the heating and cooling seasons. This is to ensure selection of the most accurate, robust, and representative values of the RC parameters for the building under consideration. Estimation periods are selected based on typical building occupancy and operation in cooling and heating seasons, respectively. The RC combination that offers the best fit with measured data, based on R^2 value and error indices such as the mean error (ME), mean bias error (MBE) and coefficient of variation of root mean square error (CVRMSE), will be chosen.

Applying Eq. (2) to the five-node model in Fig. 4 yields the following equations:

$$\frac{dT_{oE}}{dt} = -\frac{1}{C_w} \left(\frac{1}{R_{e1}} + \frac{1}{R_{e2}} \right) T_{oE} + \frac{1}{C_w} \left(\frac{1}{R_{e1}} T_{sw} + \frac{1}{R_{e2}} T_{iE} \right) \quad (16)$$

$$\frac{dT_{iE}}{dt} = -\frac{1}{C_w} \left(\frac{1}{R_{e2}} + \frac{1}{R_{e3}} \right) T_{iE} + \frac{1}{C_w} \left(\frac{1}{R_{e2}} T_{oE} + \frac{1}{R_{e3}} T_{in} \right) \quad (17)$$

$$\begin{aligned} \frac{dT_{in}}{dt} = & -\frac{1}{C_{in}} \left(\frac{1}{R_{e3}} + \frac{1}{R_{int1}} + \frac{1}{R_{win1}} + \frac{1}{R_{win2}} \right) T_{in} + \\ & \frac{1}{C_{in}} \left(\frac{1}{R_{e1}} T_{iE} + \frac{1}{R_{int1}} T_{int1} + \frac{1}{R_{win1}} T_{amb} + \frac{1}{R_{win2}} T_{amb} + Q_{conv} + Q_{sys1} \right) \end{aligned} \quad (18)$$

$$\frac{dT_{int1}}{dt} = -\frac{1}{C_{int1}} \left(\frac{1}{R_{int1}} + \frac{1}{R_{int2}} \right) T_{int1} + \frac{1}{C_{int1}} \left(\frac{1}{R_{int1}} T_{in} + \frac{1}{R_{int2}} T_{int2} + Q_{r1} \right) \quad (19)$$

$$\frac{dT_{int2}}{dt} = -\frac{1}{C_{int2}} \left(\frac{1}{R_{int2}} \right) T_{int2} + \frac{1}{C_{int2}} \left(\frac{1}{R_{int2}} T_{int1} + Q_{r2} \right) \quad (20)$$

For the selected thermal zone, there are 2 wall temperatures, 2 virtual temperatures to account for internal mass, and 1 room temperature. In total, there are 5 differential equations. The inputs are 1 ambient, 1 solar-air temperature, 1 convection, 1 radiation, and 1 system input (which could be heating or cooling). The sets of differential equations can be expressed in state space where A is a 5×5 matrix of constant coefficients. T is a matrix of dimension 5×1 , since there are 5 temperature nodes. B is of dimension 5×5 , and U is a 5×1 matrix, since there are 5 inputs. A summary of the nodal and adjacent temperatures is presented in Table 4.

From the measured data for the cooling season, it was observed that the temperature of the studied building was kept nearly constant at 22.2°C, which allows EnergyPlus simulation with assumption of an ideal HVAC system and typical office schedule internal load profile. EnergyPlus is a whole-building simulation software [28]. The temperature set-point was specified as 22.2°C, and through model calibration process, the TMY3 weather file [29] was modified by replacing the ambient, solar radiation, and wind speeds with the actual measured data obtained from Mesonet [30]. The material of building construction is a required input in EnergyPlus. A medium construction, according to ASHRAE classification, was assumed for the office building. The RC model was also simulated for the building, with the same inputs as those used for EnergyPlus, except that the RC model required significantly fewer variables. While the relatively constant zone temperature for cooling season permits the comparison of EnergyPlus and RC model results, the zone temperature recorded for the heating season fluctuated a lot for both test and validation periods. Because of difficulty in tuning the EnergyPlus model to follow the complex temperature trajectory, only the heating season results of the RC model are compared with the actual measured values.

4.1 Evaluation Indices

To evaluate the accuracy of the methods in accurately estimating the building load, the ME, MBE, and CVRMSE are used. MBE and RMSE are most commonly used to validate forecast models [31]. Any single error indices provide only one projection of the model errors, and therefore only emphasize a certain aspect of the accuracy. For reliability of performance, it is necessary to have a combination of error indices including, but not limited to, the RMSE and MBE [32]. Therefore, we also consider the use of the Mean Error, which is the difference between the mean of the actual and predicted data set. The formulas for the different errors are given in Eqs. (21) to (23):

$$ME = \frac{\sum_{i=1}^n (y_i^{est} - y_i)}{n} \quad (21)$$

$$CVRMSE = \sqrt{\frac{\sum_{i=1}^n (y_i^{est} - y_i)^2}{n}} \frac{1}{(\sum_{i=1}^n y_i)/n} \times 100 \quad (22)$$

$$MBE (\%) = \frac{\sum_{i=1}^n (y_i^{est} - y_i)}{\sum_{i=1}^n y_i} \times 100 \quad (23)$$

where y_i^{est} is the estimated building load, y_i is the measured building load, and n is the number of data points. Typical acceptable calibration tolerances for hourly simulations are MBE values of $\leq 10\%$ and CVRMSE values of $\leq 30\%$ [33]

4.2 Compare accuracies for different scenarios

This section presents the temperature and building load results of the RC model as compared with the measured data. The periods for testing and validation are deliberately selected to be disjointed. Tables 5 and 6 show the error indices for the different scenarios investigated. These are:

- (v) RC parameters estimated using heating season training data and validated for another period in the heating season.
- (vi) RC parameters estimated using heating season training data and validated for the cooling season.
- (vii) RC parameters estimated using cooling season training data and validated for the heating season.
- (viii) RC parameters estimated using cooling season training data and validated for another period in the cooling season.

The values highlighted in Tables 5 and 6 are those with least error and highest correlation to the measured cooling load. Tables 5 and 6 compare the accuracy of the RC scenarios and EnergyPlus with well-established error indices such as the CVRMSE. Table 5 compares how both cooling season trained and heating season trained RC values perform for a cooling season validation period. Table 6 compares how these trained RC values perform for heating season validation period. The results aid in selection of most appropriate RC scenario for year-round prediction of building load, based on acceptable calibration tolerances. As shown in Table 5, using cooling season training data generally yields better accuracies in predicting the building load. This could be due partly to the near-constant zone temperatures recorded in the cooling season, which is favorable for simulation and parameter estimation purposes. The 2R2C parameters estimated using cooling season data perform superior to the other scenarios for both the cooling and heating seasons. This superiority is also reflected in the R^2 values, which are much higher when cooling season estimated parameters are used. From the error indices and tabulated R^2 values in Table 5, it can be inferred that cooling season estimated RC parameters are more accurate for the validation period, irrespective of the season. More importantly, the 2R2C is superior to the other scenarios for virtually the entire validation period. Further studies are needed to fully understand why this is the case. As shown in Table 6, the error indices are higher for validation in heating season. Only the 2R2C scenario has $MBE < 10\%$ but the $CVRMSE$ is greater than the recommended threshold of 30%. All RC scenarios and EnergyPlus performed worse for heating season, but the 2R2C demonstrated better accuracy. Using cooling season training data generally yields better accuracies in predicting the building load.

Overall, most of the RC parameters scenario demonstrated better accuracy as compared with EnergyPlus. EnergyPlus has been validated for different scenarios [28], and it is not our intention to re-validate the software. However, as could be seen in Tables 5 and 6, due to lack of parameter estimation methods, EnergyPlus results may be unreliable when building construction information is limited or not available. The 2R2C scenario is seen to pass both validation criteria of $MBE < 10\%$ and $CVRMSE < 30\%$ for the cooling season. However, all of the other RC scenarios and EnergyPlus did not meet this criteria. This implies that the RC model is more suitable for cooling season than the heating season, for the case study. Overall, the 2R2C was selected as the appropriate RC scenario to represent the studied thermal zone.

4.3 Overall comparison of RC model, EnergyPlus and measured data

The 2R2C scenario was then used to test the overall effectiveness through comparison with EnergyPlus and measured data from the 2012 summer season and the 2014 winter season. The periods of testing are deliberately selected to be disjointed in order to ascertain the robustness of the 2R2C. Figures 5 to 7 show results of the building loads and zone temperatures simulated using the 2R2C as they compare with measurements and EnergyPlus.

As shown in Fig. 5, both the EnergyPlus and 2R2C models are observed to trend the cooling load, but there are occasional under-predictions. Meanwhile, the 2R2C captured many fluctuations in the cooling load which were not captured by EnergyPlus. With only 3 days training data, an accurate building load forecast was made for 10 days in the cooling season. The temperature trajectory for both 2R2C and EnergyPlus shows satisfaction of zone temperature within errors of less than ± 0.05 °C and is therefore not presented here. The analytical solution has eliminated the issues of noticeable and unwanted spikes that were observed after using the time series [19]. The RC model is also seen to consistently track the cooling load for both occupied and unoccupied hours. Comparison of the building load for the heating season is shown in Fig. 6. The validation period covers simultaneous heating (-ve values) and cooling (+ve values), as indicated by the positive and negative values on the building load axis.

The RC model is seen to generally track the building load patterns even where there is switch from heating to cooling, and vice versa. With only 3 days of training data, reasonably accurate building load estimation was made for up to 10 days in this heating season. Occasional spikes are noted in the 2R2C model predictions as noted in Fig. 6, but they die out gradually. EnergyPlus simulation of the building load is also shown in Fig. 6. Fig. 7 shows the measured room temperature, RC predicted zone temperature, EnergyPlus predicted zone temperature, and ambient temperature. Fig. 7 explains the reason for the switch from heating to cooling, which is consistent with the ambient temperature crossing below and above the room temperature, respectively. It also shows how the RC and EnergyPlus predicted temperature trends well with the measured room temperature. The computational expense of the RC model is mainly due to the parameter estimation, which is done using Genetic Algorithm and pattern search. On a desktop computer with core i3, 1.7 GHz processor, 4 GB RAM, and 500 GB hard disk drive, the parameter estimation takes between 45 minutes and 1hr. Once the RC parameters are estimated, the simulation requires little computational efforts. Simulation of building load for a 1-week period takes approximately 1 minute to complete on a desktop computer with above configuration. This is quite large when compared with EnergyPlus (which uses 0.9s). However, the RC computation time for each time-step is within reasonable range of value that is appropriate for control purposes.

5 Conclusion and Recommendation

This study introduces the formulation, analytical solution, and validation of the simplified RC model using a case study of a thermal zone in a typical office building. It has been proved that the analytical solution is asymptotically stable for all time steps, and therefore, there are no constraints on the feasible search region of the RC parameters. This eliminates the concerns about invertibility or stability of the thermal model, which is a necessary condition for all nodal temperatures to remain bounded. The RC parameters were estimated from training data in the heating and cooling seasons under different scenarios. The estimated parameters from the cooling season generated more accurate results for the validation period. The selected RC parameters may be deemed indicative and representative of building

thermal characteristics since they are deduced from actual building load measurements. Despite its requirement of significantly fewer variables and inputs, the RC model is observed to be superior to EnergyPlus for the cooling season due to the estimation of the RC parameters from actual building measurements. The RC model is also seen to be sufficiently accurate in predicting building loads and zone temperatures for both summer and winter season. The thermal model capabilities explored in this study include investigation of multiple HVAC scenarios, simulation of temperature fluctuations, simulation of both heating and cooling, and flexibility in the choice of RC parameters for estimation. These capabilities present cost-effective solutions and opportunities for fault detection and diagnosis, optimized control, and energy savings. The accuracy of this model will be increased further where there are equipment usage data and occupancy sensors to generate the actual internal load profile for both the training and validation periods. Since some accuracy is lost when the model is used for predicting building load in heating season, the model needs to be refined further to enhance its application and suitability for year-round prediction of building load. Inherent sensor uncertainties also account for some of the observed deviations between the measured values and the simulation results. This model is proposed as a simplified but robust model which is embeddable in existing and future BAS without the need to install additional sensors.

NOMENCLATURE

ρ =density

λ = thermal conductivity, eigenvalue

t =time

sa =supply air

l =length

in = indoor

i, j, k = counter

h_i =inside convective heat transfer coefficient

h_o =outside convective heat transfer coefficient

amb =ambient

U =input

TMY =typical meteorological year

T = temperature

RC =resistance-capacitance

R_{win} =window resistance

C_{in} =indoor air capacitance

A_s, B_s, C, D =state space matrix

a_{ij} =ith row and jth column entry of matrix A

b_{ij} =ith row and jth column entry of matrix B

Q_r = half of total radiation from windows and radiative part of internal load

Q_o = incident solar on outside surface

Q_{conv} = convective part of internal load

C_p = specific heat

α = solar radiation absorptivity

I = global solar irradiance

ΔQ_{ir} = extra infrared radiation due to difference between the external air and apparent sky temperature

h_o = convection coefficient on the external surface.

APPENDIX

Table A1: Assumed Composition of Building Construction

Exterior Wall	Partitions	Roof/Ceiling	Floor	Windows
M01 100mm brick	G01a 19mm gypsum	M11 100mm lightweight concrete	HF-C5	Clear 3mm
I02 50mm insulation	F04 Wall air space resistance	F05 Ceiling air space resistance		Air 13mm
F04 Wall air space resistance	G01a 19mm gypsum	F16 Acoustic Tile		Clear 3mm
G01a 19mm gypsum				

REFERENCES

- [1] Daum D., Morel. N. (2010). Assessing the total energy impact of manual and optimized blind control in combination with different lighting schedules in a building simulation environment. *Journal of Building Performance Simulation*, 3(1), p. 1-16.
- [2] Oldewurtel F., Parisio A., Jones C., Morari M., D. Gyalistras D. (2010). Energy Efficient Building Climate Control using Stochastic Model Predictive Control and Weather Predictions. In: *Proceedings of the American Control Conference*, Baltimore, MD.
- [3] Pang, X., Wetter, M., Bhattacharya, P., and Haves, P. (2012). A framework for simulation based real-time whole building assessment, *Building and Environment* 54.
- [4] Causone, F., Corngati, S. P., Filippi, M., & Olesen, B. W. (2010). Solar radiation and cooling load calculation for radiant systems: Definition and evaluation of the Direct Solar Load. *Energy and Buildings*, 42(3), 305-314.

- [5] ASHRAE (2005). *ASHRAE Handbook, Fundamentals Volume*, American Society of Heating, Refrigerating and Air-Conditioning Engineers, Inc. Atlanta, GA, 1989
- [6] Braga, L. C., Braga, A. R., & Braga, C. M. P. (2013). On the Characterization and Monitoring of Building Energy Demand Using Statistical Process Control Methodologies. *Energy and Buildings*.
- [7] Feng, J. D., Schiavon, S., & Bauman, F. (2013). Cooling load differences between radiant and air systems. *Energy and Buildings*.
- [8] Chen, V. L., Delmas, M. A., & Kaiser, W. J. (2014). Real-time, appliance-level electricity use feedback system: How to engage users?. *Energy and Buildings*,70, 455-462.
- [9] Xuemei, L., Lixing, D., Yan, L., Gang, X., & Jibin, L. (2010, January). Hybrid genetic algorithm and support vector regression in cooling load prediction. In: *Knowledge Discovery and Data Mining, 2010. WKDD'10. Third International Conference on* (pp. 527-531). IEEE.
- [10] Duanmu, L., Wang, Z., Zhai, Z. J., & Li, X. (2013). A simplified method to predict hourly building cooling load for urban energy planning. *Energy and Buildings*, 58, 281-291.
- [11] Schiavon, S., Lee, K. H., Bauman, F., & Webster, T. (2011). Simplified calculation method for design cooling loads in underfloor air distribution (UFAD) systems. *Energy and Buildings*, 43(2), 517-528.
- [12] Wang S.W., and Xu, X.H.(2006). Parameter estimation of internal thermal mass of building dynamic models using genetic algorithm, *Energy Conversion and Management* 47 (13–14)
- [13] McKinley, T. and Alleyne, A. (2008). "Identification of Building Model Parameters and Loads using On-Site Data Logs," SimBuild 2008, Berkeley, CA, July 2008.
- [14] Fraisse, G., Souyri, B., Pinard, S., and Menezo, C. (2011). Identification of Equivalent Thermal RC Network Models Based on Step Response and Genetic Algorithms, *Proceedings of Building Simulation 2011: 12th Conference of International Building Performance Simulation Association, Sydney, 14-16 November*.
- [15] Dobbs, J.R., and Hency, B. M. (2012). Automatic model reduction in architecture: a window into building thermal structure, Fifth National Conference of IBPSA-USA Madison, Wisconsin August 1-3, 2012.
- [16] Justin R. Dobbs, Brandon Hency: A comparison of thermal zone aggregation methods. CDC 2012: 6938-6944
- [17] Sourbron, Maarten, Martine Baelmans, and Lieve Helsen (2009). "Thermal response of thermally activated building systems (TABS) in office buildings [C]." *Proceedings of EFFSTOCK. Stockholm, Sweden* (2009): 57-64.
- [18] Xu, X. (2005). Model Based Building Evaluation and Diagnosis, PhD Dissertation, Department of Building Services Engineering, The Hong Kong Polytechnic University.
- [19] Ogunsola, O. T., & Song, L. (2013). Performance Analysis of a Simplified Model of Cooling Load for a Typical Office Building. In *ASME 2013 International Mechanical Engineering Congress and Exposition* (pp. V011T06A025-V011T06A025). American Society of Mechanical Engineers.
- [20] Ogunsola, O. T., Song, L., & Wang, G. (2014). Development and validation of a time-series model for real-time thermal load estimation. *Energy and Buildings*,76, 440-449.
- [21] Radecki, Peter, and Brandon Hency. "Online building thermal parameter estimation via Unscented Kalman Filtering." *American Control Conference (ACC), 2012*. IEEE, 2012.

- [22] McQuiston, F.C., Parker, J.D., and Spitler, J.D. (2000). Heating, Ventilating, and Air-conditioning Analysis and Design, 5th ed., ISBN 0-471-35098-2, John Wiley and Sons, Inc. Publisher.
- [23] Seem J.E., Klein S.A. et al. (1989). Transfer functions for efficient calculation of multidimensional transient heat transfer. *Journal of Heat Transfer*, Vol.111:5-12.
- [24] Y. Knyazikhin, J. Glassy, J. L. Privette, Y. Tian, A. Lotsch, Y. Zhang, Y. Wang, J. T. Morisette, P. Votava, R.B. Myneni, R. R. Nemani, S. W. Running (1999). MODIS Leaf Area Index (LAI) and Fraction of Photosynthetically Active Radiation Absorbed by Vegetation (FPAR) Product (MOD15) Algorithm Theoretical Basis Document, <http://eosps0.gsfc.nasa.gov/atbd/modistables.html>, 1999.
- [25] M. Cleve, and Loan, C. V. (2003). Nineteen Dubious Ways to Compute the Exponential of a Matrix, Twenty-Five Years Later, *SIAM Review*, Vol. 45, No. 1, pp. 3-49.
- [26] Ogunsola, O.T. and Song, L. (2014) Investigation of Building Passive Thermal Storage for Optimal Heating System Design, In *ASME 2014 International Mechanical Engineering Congress and Exposition*, Montreal, Canada.
- [27] Ogunsola, O. T., and Song, L. (2012). Review and Evaluation of Using RC Thermal Modeling of Cooling Load Prediction for HVAC System Control Purpose. In *ASME 2012 International Mechanical Engineering Congress and Exposition* (pp. 735-743). American Society of Mechanical Engineers.
- [28] DOE. (2010). EnergyPlus version 7.0. United States Department of Energy, www.apps1.eere.energy.gov/buildings/energyplus/, accessed Jan. 17, 2012
- [29] NREL (2014). 1991-2005 Update: Typical Meteorological Year 3, available at: http://rredc.nrel.gov/solar/old_data/nsrdb/1991-2005/tmy3/, accessed January 2014.
- [30] Mesonet (2014). http://www.mesonet.org/index.php/weather/mesonet_data_files, accessed March 2014.
- [31] Ramanathan, R., 1995. *Introductory Econometrics with Applications* (3rd edition), Harcourt Brace College Publishers, Fort Worth, 800 p.
- [32] Chai, T., and Draxler, R. R. (2014). Root mean square error (RMSE) or mean absolute error (MAE)? *Geoscientific Model Development Discussions*, 7(1), 1525-1534.
- [33] DoE (2008). M&V Guidelines: Measurement and Verification for Federal Energy Projects, Version 3.0, available at: http://www1.eere.energy.gov/femp/pdfs/mv_guidelines.pdf, accessed November 2014.

List of Figures

Fig. 1: RC Thermal model, showing sol-air temperature and AHU input.

Fig. 2: A three-node thermal network model.

Fig. 3: Modeled thermal zone.

Fig. 4: RC Model representation for the building.

Fig. 5: Comparison of building load for the cooling season.

Fig. 6: Comparison of building load for heating season.

Fig. 7: Comparison of zone and ambient temperatures for the heating season.

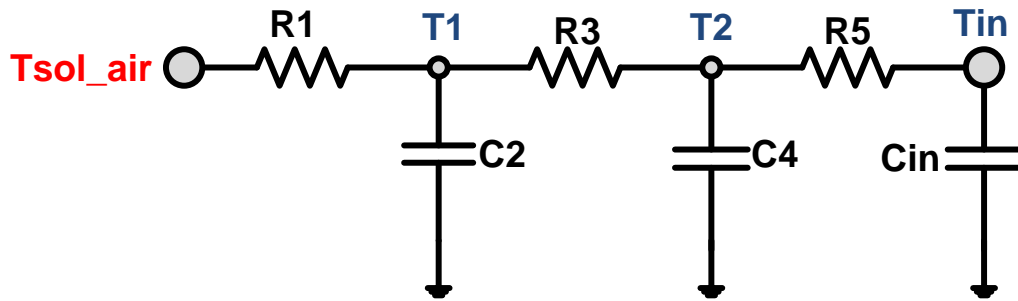
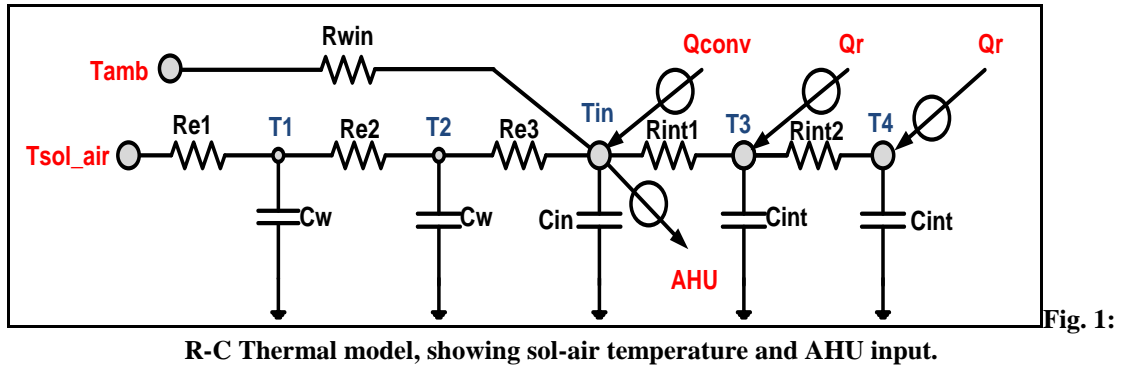


Fig. 2: A three-node thermal network model.

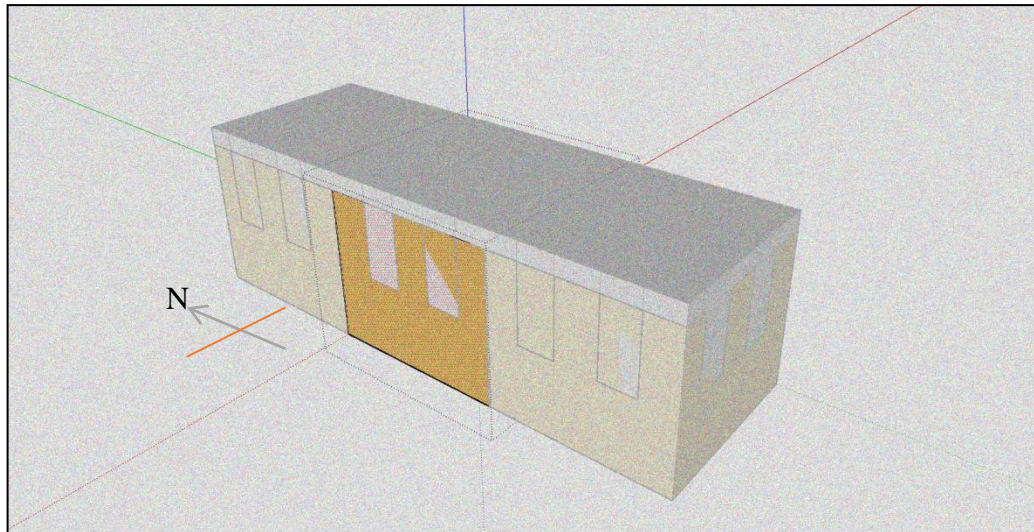
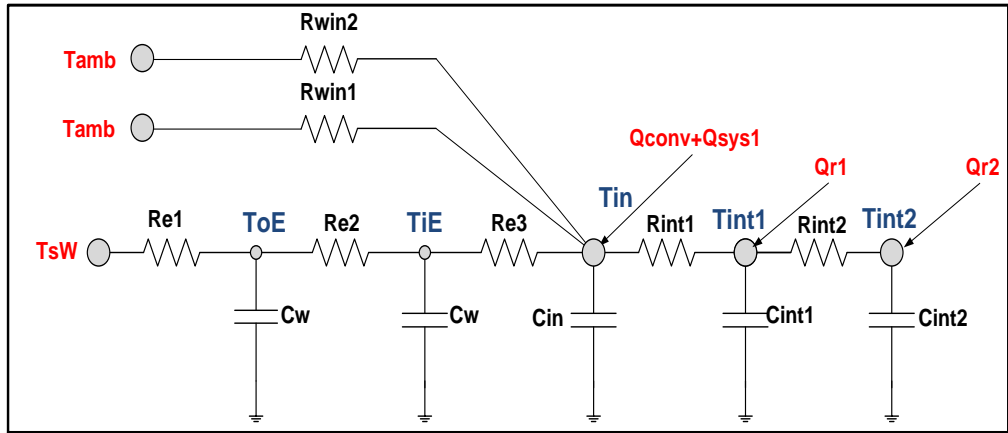


Fig. 3: Modeled thermal zone.



R-C Model representation for the building.

Fig. 4:

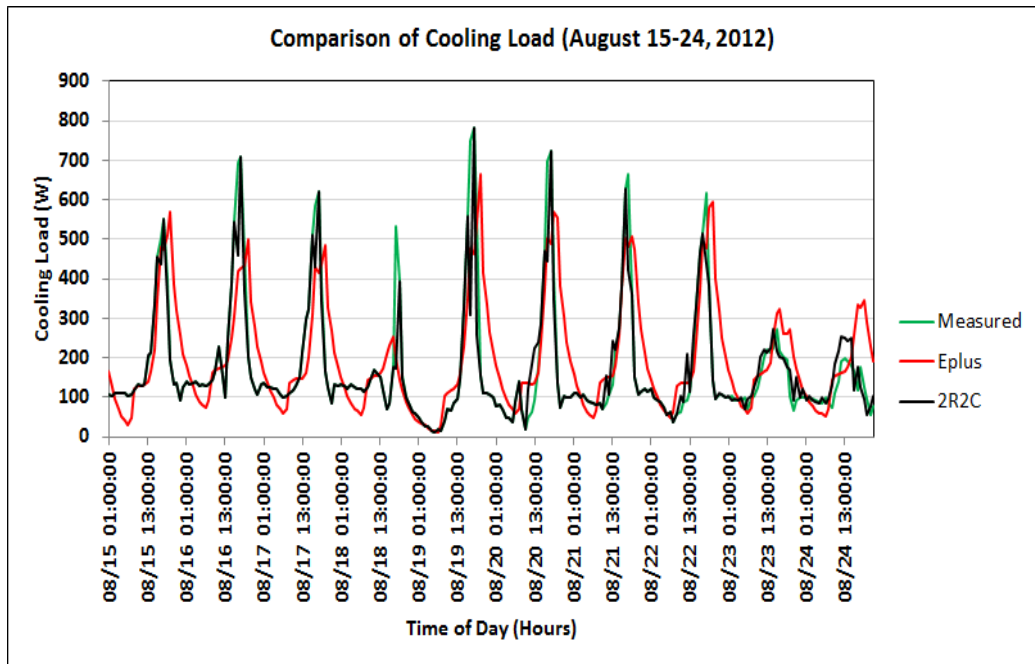


Fig. 5: Comparison of building load for the cooling season.

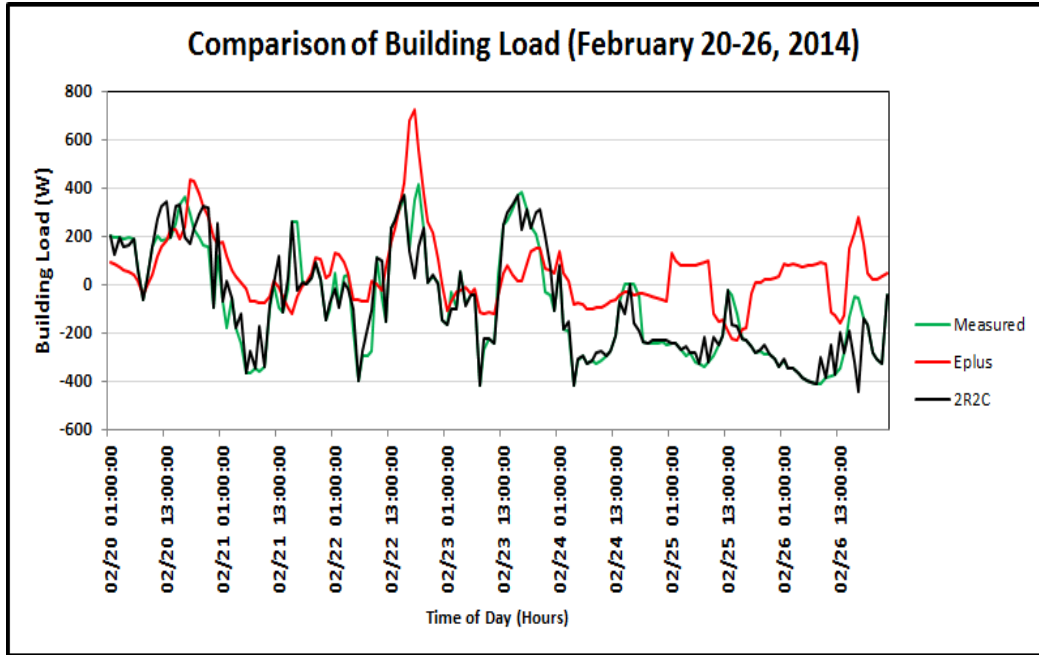


Fig. 6: Comparison of building load for heating season.

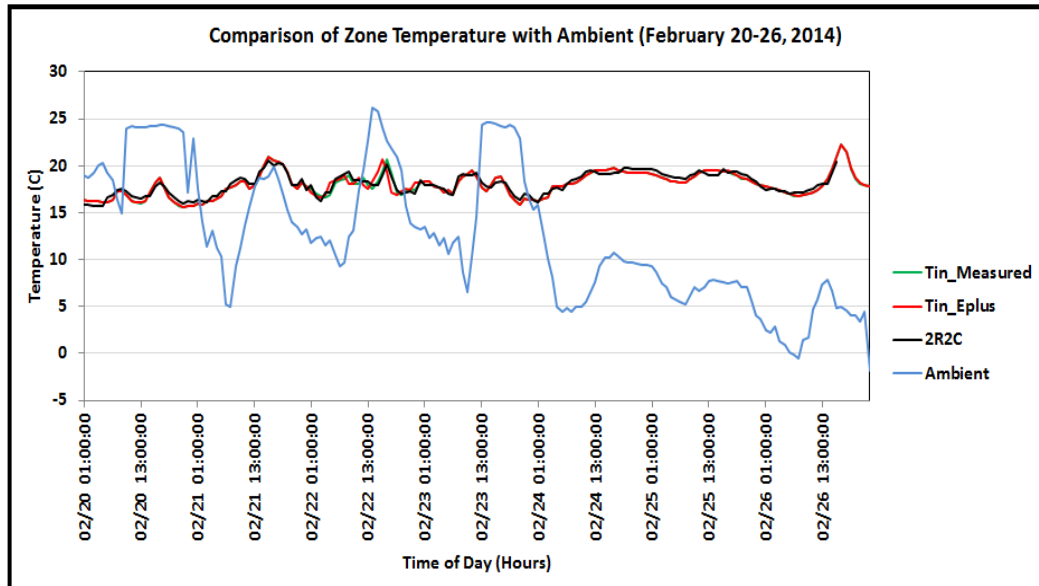


Fig. 7: Comparison of zone and ambient temperatures for the heating season

Table 1: Medium Wall Composition

Thickness and thermal properties				
	L(m)	λ (W/mK)	ρ (kg/m ³)	Cp(J/KgK)
M01 100mm brick	0.102	0.89	1920	790
I02 50mm insulation	0.051	0.03	43	1210
F04 Wall air space resistance				
G01a 19mm gypsum	0.019	0.16	800	43

Table 2: Window Composition

	L(m)	λ (W/mK)	ρ (kg/m ³)	Cp(J/KgK)	R(m ² K/W)
Clear 3mm	-	-	-	-	0.003
Air 13mm	-	-	-	-	0.003
Clear 3mm	-	-	-	-	0.003

Table 3: Different scenarios for the R-C parameters.

Scenario	Parameters Fixed	Parameters estimated	Assumed Values
5R2C	None	($R_{e1}, R_{e2}, R_{e3}, R_{int1}, R_{int2}, C_w$ and C_{int})	-
4R2C	R_{e3}	($R_{e1}, R_{e2}, R_{int1}, R_{int2}, C_w$ and C_{int})	outside air convection coefficient
3R2C	R_{e1} and R_{e3}	($R_{e2}, R_{int1}, R_{int2}, C_w$ and C_{int})	outside and inside convection coefficient
2R2C	R_{e1}, R_{e3} , and R_{e2}	(R_{int1}, R_{int2}, C_w and C_{int})	outside and inside convection coefficient, and medium construction

Table 4: Summary of the nodal and adjacent temperature branches.

Type	Nodal Temperature	Adjacent Temperature Branches	Thermal Capacitance	Heat Flux Branches
Room Temperature	T_{in}	T_{iE}, T_{int1} , and T_{amb}	C_{in}	Q_{conv}, Q_{sys}
External Wall	T_{oE}	T_{sW}, T_{iE}	C_w	
	T_{iE}	T_{oE}, T_{in}		
Internal Mass	T_{int1}	T_{int2}, T_{in}	C_{int1}	Q_{r1}
	T_{int2}	T_{int1}	C_{int2}	Q_{r2}

Table 5: Comparison of error indices for Cooling Season Validation

		Case	RC Predicted vs Measured				EnergyPlus vs Measured			
			ME (W)	MBE (%)	CV RMSE (%)	R^2	ME (W)	MBE (%)	CV RMSE (%)	R^2
Training Season	Cooling	5R2C	6.02	4.984	36.331	0.7	23.73	-0.86	58.36	0.67
		4R2C	4.54	4.854	36.936	0.7				
		3R2C	3.79	3.447	28.947	0.74				
		2R2C	-3.33	4.137	17.271	0.87				
	Heating	5R2C	6.5	6.752	41.619	0.66				
		4R2C	11.08	8.501	47.995	0.52				
		3R2C	37.08	1.469	43.988	0.56				
		2R2C	16.06	4.023	43.893	0.61				

Table 6: Comparison of error indices for Heating Season Validation

		Case	RC Predicted vs Measured				EnergyPlus vs Measured			
			ME (W)	MBE (%)	CV RMSE (%)	R^2	ME (W)	MBE (%)	CV RMSE (%)	R^2
Training Season	Cooling	5R2C	65.57	73.676	-149.27	0.74	97.9	111.5	-232.17	0.37
		4R2C	67.51	75.039	-155.38	0.73				
		3R2C	35.63	38.456	-115.96	0.83				
		2R2C	8.17	6.6761	-95.88	0.88				
	Heating	5R2C	29.37	-33.288	322.73	0.66				
		4R2C	40.75	-70.631	345.13	0.52				
		3R2C	66.05	-145.10	346.16	0.56				
		2R2C	8.86	-40.970	313.64	0.61				

DEVELOPMENT AND VALIDATION OF A TIME-SERIES MODEL FOR REAL-TIME THERMAL LOAD ESTIMATION

Ogunsola, O.T., Song, L. and Wang, G., 2014. Development and validation of a time-series model for real-time thermal load estimation. *Energy and Buildings*, 76, pp.440-449.

ABSTRACT

Dynamic cooling load changes caused by weather, occupants and equipment use are prevailing challenges for heating, ventilating and air conditioning (HVAC) system design, operation and controls. The thermal capacity of a building envelope delays conduction heat gains while the thermal capacity of the whole structure delays radiative cooling loads. These delays make cooling load calculations inherently complicated. It has been challenging to accurately estimate cooling load in a building in real-time. In this paper, a time-series cooling load model is deduced from a simplified Resistance-Capacitance (RC) model to provide an efficient solution with manageable computational requirements. In addition, the time-series model is also tested on a thermal zone in an office building, defined in EnergyPlus as a single zone with an ideal HVAC system. RC parameters of building envelope and internal mass are obtained using theoretical characteristics of the building construction in frequency domain and EnergyPlus data, respectively. These are used in formulation of a time-series representation of the cooling load for three scenarios of light, medium, and heavy construction of a thermal zone in an office building. For all scenarios, cooling load with the simplified time series model is estimated within 7% mean absolute percentage error relative to EnergyPlus.

Keywords: Cooling Load; Time Series; RC model; Building Envelope; Internal Mass; EnergyPlus; Robustness/Uncertainty Analysis

1 Introduction and Review of R-C Models

According to the United States Green Building Council [1], buildings are responsible for at least 40% of energy use in most countries of the world, and for up to 21% of greenhouse gas emissions globally. The amount of energy in buildings that is used inefficiently or unnecessarily is 30 percent [2]. Deficiencies in building operation are caused by faulty equipment and inappropriate operation challenged by dynamic load changes in large commercial buildings. Dynamic load changes also make the fault detections of heating, ventilating and air-conditioning (HVAC) systems difficult, because the fault-free energy baseline of an HVAC system is a variable unlike lights or other plugged electronic devices in buildings. Pang et al [3] developed a framework for simulation based real-time whole building performance assessment that allows a comparison of building actual performance and expected performance in real-time. The building control virtual test bed (BCVTB) developed by Haves and Xu [4] was used to link EnergyPlus [5] with building control system for real-time data communication. The middleware allowed synchronization of simulation time and real time, data exchange between the simulated and actual building, and storage of building time series data. The method was tested on a two-storied building with floor area of approximately 70,000ft². Using 5 days of validated data, the simulation results of the building total electric power agree to each other, which further demonstrate the usefulness of a dynamic simulation using instantaneous measured weather data. However, using this method, several factors and variables such as HVAC operational schedules, control setpoints, and weather data such as solar radiation, relative humidity, wind speed, and direction have to be updated at each time step. Additionally, the use of middleware and supplementary interfaces introduce additional complexity for a building automation system (BAS), which is usually built on proprietary communication protocols or with only minimum compatibility through an open protocol such as BACnet [6]. In addition, the current BAS technology only allows limited computational capacity in a BAS supervisory controller. A revolutionary advancement in BAS is needed for the adoption of such a method.

Attempts of other load estimation methods were also exercised. Causone et al [7] developed a calculation procedure for cooling loads using the Heat balance method and the radiant time series method, with consideration of solar gains and solar radiation effects. The procedure considered the thermal mass of the building layers and defined two components of the cooling load as room load, and direct solar load. Braga et al [8] developed a statistical process to model and estimate the energy consumption profile of a building during a cycle, for example, a week. The statistical model was deemed suitable for monitoring and control of energy consumption patterns. Feng et al [9] compared cooling load differences between radiant and air systems with consideration given to level of insulation, thermal mass effects, internal heat gains, and solar exposure of floors and ceilings. There have been a number of studies on the development of time series for variables affecting building load. For example, Zhanga et al [10] developed a time series for estimation and prediction of ambient temperature using information on past or forecast solar radiation. The prediction model requires the solar radiation profile of the past 12 hours and the time delay of radiative heat gains was modeled as a parameterized Box Lucas function. Hokoi and Matsumoto [11] developed a statistical time series for ambient temperature and solar radiation, which are critical for cooling load calculations and to HVAC system operation. The stochastic time series was modeled using Kalman filters. Chen et al [12] also accessed the effect of appliance level on real-time and historical energy use in buildings by separate measurements of appliance plug load, heating and cooling loads, and lighting load through the use of energy meters and proxy sensors.

In order to enable energy-use reduction through BAS embedded intelligence, in this paper, we propose a near-term solution using a simplified time-series model to predict expected building performance in real time with less computational and fewer inputs requirements for the determination of sensible cooling load. Latent load prediction is not included since latent heat gain instantaneously converts to latent cooling without a time delay. The time-series model is constructed based on a physical resistance-capacitance (R-C) model, which is used effectively to describe the thermal delays caused by a building envelope and internal thermal mass effects. R-C models have been used to describe the thermal delays caused by the envelope and internal mass effects. They have proved to provide robust and accurate estimates of the cooling load based on measured data [13], and have been used for a wide number of cases and scenarios.

In 1985, Hassid [14] used two resistances (R_o and R_i) and one capacitor (C) or 2R1C as the electrical equivalent of a multi-layer wall (see Figure 1). The internal capacitor, C_{in} , shown in Figure 1, is a measure of indoor air thermal mass, and is equal to the product of air mass and specific heat. In 1989, Seem et al. [15] used two node models for representation of plane walls, with three resistances (R_1 , R_3 and R_5) and two capacitors (C_2 and C_4) or 3R2C as shown in Figure 2. When R_3 is chosen to be equal to the wall resistance, T_1 and T_2 represent outside and inside surface temperature of the wall, respectively, and R_1 and R_5 represent outside and inside surface heat transfer resistances. Over time, improvements of the R-C method have taken place, with the 3R2C arrangement now widely used for modeling of transient heat transfer in building envelopes [16, 17]. More recent versions of the R-C models are 3R4C and 4R5C by Fraisse [18].

R-C model has been widely applied in various research and studies as well. Goyal et al [19] applied the RC model for identification of multi-zone building thermal interaction model. The RC parameters of the convection edges were estimated through an exhaustive search to minimize a prediction error cost. Dobbs and Hency [20] used the RC model to investigate thermal coupling among building elements, which provides insights to adjust building layout or control system design in early phase. Schmidt and Johannesson [21] investigated the use of optimized RC networks within macro-element modeling for thermally activated building construction. Dobbs and Hency [22] applied the RC model for comparison of thermal zone aggregated methods. Sourbron et al [23] also demonstrated the use of RC model for thermally activated building systems in office buildings. The study shows the choice of model parameters has a large impact on the amplitude of the model output. Radecki and Hency [24] estimated building thermal parameter of a multi-zone network using unscented Kalman filter and compared the results with EnergyPlus simulation data. The 1R2C network and 3R3C loop were used in the study. Using less than 2 weeks training data, reliable 48 hour predictions of zone temperatures were made on a passive 5-room

model. Bueno et. al [25] developed a RC model for analysis of the interaction between the energy performance of buildings and the urban climate. Lombard and Mathews [26] implemented steady state solution of a time variable RC networking for building thermal analysis. Lombard and Mathews [27] also applied the RC model in a 2-port envelope model for building heat transfer. The building zone was represented with a single heat storage capacitance. The method was tested on a one storey commercial building and the results of the total sensible cooling load, and instantaneous sensible heat gain were compared with the commercial building example in ASHRAE Fundamentals.

A significant progress in R-C models is the representation of building internal mass using lumped capacitors, as developed by Xu [28]. The physical properties of components such as furniture, carpets, and other surfaces that are capable of absorbing and releasing radiation within the indoor environment, are not readily available. All these components were lumped together and represented by a 2R2C network with two resistances (R_6 and R_8) and two capacitors (C_7 and C_9) for internal mass. As seen in Figure 3, two nodal temperatures, T_3 and T_4 are introduced by this arrangement. They are virtual temperature nodes used to capture internal mass effects, and thermal delay of thermal radiation of internal heat gains and solar radiation through windows.

The combined 3R2C model for building envelope and the 2R2C model for building internal mass was developed and tested by Wang and Xu [16,28]. Figure 4 shows the combined R-C thermal network with 3R2C for the envelope and 2R2C for the internal mass. R_1 , R_3 , R_5 , C_2 , and C_4 are the 3R2C parameters of the building envelope. R_6 , R_8 , C_7 , and C_9 are the 2R2C parameters of the internal mass. R_{win} is the window's resistance. Xu (2005) obtained the R-C parameters using a genetic algorithm and solved the integrated R-C model numerically using Runge Kutta classical methods [28]. The 3R2C parameter was found using theoretical characteristics of the building in frequency domain. The 2R2C parameter was found using the genetic algorithm by minimizing the difference between the cooling loads estimated using the model and the actual cooling load. The nodal temperature and cooling load have to be solved numerically at each time step.

In this paper, in order to eliminate the numerical calculation for solving the integrated 3R2C and 2R2C model and thus realize a BAS embedded cooling load prediction, an explicit representation of relationship between inputs and outputs, a time-series model is formed based on the integrated 3R2C and 2R2C, which requires only three input variables, solar, ambient temperature and an occupancy sensor to indicate internal loads. Despite of lumping intriguingly complex heat transfer effects into time-series coefficients, a similar expression to auto-regressive models proposed by Javed et al. [29] and Song et al. [30], the time-series model is constructed based on a physical R-C model. Consequently, a time-series model is superior to those auto-regressive models because the auto-regressive models are very sensitive to outliers and less reliable due to inability to track sudden input changes such as an abrupt ambient air temperature drop or sudden changes in control strategy.

The paper is laid out by formulating a simplified R-C model for a studied thermal zone first after which a time-series model is deduced based on the R-C model. The time-series cooling load model is expressed by an explicit equation using past cooling load, as well as current and past values of independent input variables such as ambient temperature, solar radiation, and internal loads. The time-series model is then tested on a baseline case and compared with simulated cooling loads from EnergyPlus. Finally, in order to understand the robustness of the time-series model, up to 10% random normal uncertainties in the input variables are introduced to understand the effects of such uncertainty on the accuracy of cooling load predictions.

2 R-C Model Formulation for a Studied Thermal Zone

In this section, a simplified R-C model shown in Figure 5 is formed. It is a special case of a thermal zone with only one wall surface exposed to ambient temperature and solar radiation as well as one window surface with single thermal resistance (without thermal mass), through which the solar radiation directly reaches two virtual internal nodes. All other surfaces are interior.

The effects of solar radiation and ambient temperature on the outside surface of the wall have been combined into one, using the concept of sol-air temperature, $T_{sol-air}$ [31]. This concept is only suitable for opaque surfaces, such as walls. Thus, it was only applied to the wall outside surface in this study. $T_{sol-air}$ is defined in Equation (1) :

$$T_{sol-air} = T_o + \frac{\alpha I - \Delta Q_{ir}}{h_o} \quad (1)$$

where the variables α , I , and $-\Delta Q_{ir}$ are as defined in the nomenclature.

The thermal radiation correction term is usually approximated as being 7°F for horizontal surfaces and 0°F for vertical surfaces [31]. To write the sensible heat balance equation for the R-C model, the following simplifying assumptions are made:

- The zone air is well mixed, so the whole indoor circulated air volume is at a uniform temperature.
- The effect of varying wind velocity on external wall convection coefficients is not considered. Hence, a constant heat transfer coefficient was assumed in this study.
- The space is pressurized so infiltration does not create a cooling load in spaces.
- The ceiling, floor, and interior surfaces are considered adiabatic.
- The long wave radiation exchanges between internal surfaces and multiple reflections are described by the lumped internal thermal R-C model.

The above assumptions have been commonly made to simplify the R-C model [13,16,28]. The governing equations found by heat balance at each node are:

$$C_2 \frac{dT_1}{dt} = \frac{T_{sol-air} - T_1}{R_1} + \frac{T_2 - T_1}{R_3} \quad (2)$$

$$C_4 \frac{dT_2}{dt} = \frac{T_1 - T_2}{R_3} + \frac{T_{in} - T_2}{R_5} \quad (3)$$

$$C_7 \frac{dT_3}{dt} = \frac{T_{in} - T_3}{R_6} + \frac{T_4 - T_3}{R_8} + Q_r \quad (4)$$

$$C_9 \frac{dT_4}{dt} = \frac{T_3 - T_4}{R_8} + Q_r \quad (5)$$

With a given space temperature, the heat extracted from the space becomes a cooling load. The heat balance equation to calculate the sensible cooling load is:

$$Q_{cool} = \left(\frac{T_2 - T_{in}}{R_5} \right) + \left(\frac{T_3 - T_{in}}{R_6} \right) + \left(\frac{T_{amb} - T_{in}}{R_{win}} \right) + (Q_{conv}) \quad (6)$$

The first two terms on the right hand side of Equation (6) are heat transfer from the envelope (i.e., the outer shell of the zone). In this instance, the envelope is the exterior surface that is exposed to ambient and solar radiation. The second term is the heat transfer by virtue of the window's temperature difference. In Figure 5, Q_r is half of the total radiation, including the solar radiation transmitted and inwardly absorbed through the window, as well as the radiative part of internal heat gains. Internal heat gains are from people, lights, and equipment in the zone. Due to internal mass effects, radiative heat gain is first absorbed by walls and other surfaces within the zone, and gradually released into the room air by convection at a later time. Capacitors C_7 and C_9 are introduced to capture and represent this delay due to internal mass. Q_{conv} is the convective part of internal heat gain. This is the portion of heat gain that becomes the cooling load instantaneously. An AHU is in operation to accommodate the cooling load. The amount of AHU output is defined as the heat extraction rate.

Since the heat extracted by an AHU is not always equivalent to the cooling load, space temperature fluctuates around the set point. Dynamic space temperature can be determined by node heat balance

equations, Equations (2) to (5), as well as the space heat balance, Equation (7), with a given heat extraction rate.

$$C_{in} \frac{dT_{in}}{dt} = \left(\frac{T_2 - T_{in}}{R_5} \right) + \left(\frac{T_{amb} - T_{in}}{R_{win}} \right) + \left(\frac{T_3 - T_{in}}{R_6} \right) + (Q_{conv}) + Q_{ext} \quad (7)$$

The simplified R-C model, as a lumped physical model, provides a means for real-time HVAC controls and performance monitoring. For example, the efficient cooling load prediction given in Equation (6) sets a baseline to control chilled water charging or discharging to a thermal storage system, which is critical to maximize the operation efficiency; the room air variations under a given AHU extraction rate shown in Equation (7) can be used to predict the floats of the room air temperature when the AHU operation is constrained. For example, under a grid integrated demand control, smart decisions on AHU operation can be made to minimize thermal comfort impact. On the other hand, if the room air temperature is measureable, the AHU heat extraction rate can be calculated by Equation (7) as a reference to compare with the measured AHU heat extraction rate, which serves as an effective AHU fault detection index. Despite a variety of applications of the R-C model, instantaneous cooling load calculation is the focus in this paper.

3 Time Series Model Formulation for Cooling Load Calculation

In order to calculate instantaneous cooling load, for the R-C model formed in Section 2, the room air temperature node will not be included since an ideal HVAC system (a system of sufficient capacity to meet its heating or cooling loads) is assumed. Thus, only four nodal temperatures are needed.

Equations (2) to (5) are an inhomogeneous system of differential equations. In state space representation, Equations (2) to (5) can be re-written as:

$$\dot{T} = A_s T + B_s U \quad (8)$$

From equation (6),

$$Q_{cool} = CT + DU \quad (9)$$

where A_s , B_s , C , and D are matrices of constant coefficients whose entries are functions of the R-C parameters.

$$A_s = \begin{pmatrix} a_{11} & \cdots & a_{14} \\ \vdots & \ddots & \vdots \\ a_{41} & \cdots & a_{44} \end{pmatrix}; B_s = \begin{pmatrix} b_{11} & \cdots & b_{14} \\ \vdots & \ddots & \vdots \\ b_{41} & \cdots & b_{44} \end{pmatrix}; C = [c_{11} \ c_{12} \ c_{13} \ c_{14}]; D = [d_{11} \ d_{12} \ d_{13} \ d_{14}]; \quad (10)$$

$$T = [T_1; T_2; T_3; T_4]; \quad (11)$$

$$U = [T_{amb}; T_{sol-air}; Q_r; Q_{conv}]; \quad (12)$$

The above is a system of first order differential equations with constant coefficients, and the solution is given by:

$$T_{t+\delta} = e^{A_s \delta} T_t + \int_t^{t+\delta} e^{A_s(t+\delta-\tau)} B_s U(\tau) d\tau \quad (13)$$

where the exponential matrix is defined by the power series

$$e^{A_s \delta} = I + A_s \delta + \frac{A_s^2 \delta^2}{2!} + \frac{A_s^3 \delta^3}{3!} + \cdots + \frac{A_s^n \delta^n}{n!} + \cdots \quad (14)$$

where I is the identity matrix of same dimensions as A_s . As developed by Seem et al. [9], inputs between time t and $t + \delta$ can be modeled by a continuous, piecewise linear function as

$$U(t) = U_t + \frac{(\tau - t)}{\delta} (U_{t+\delta} - U_t) \quad (15)$$

A function or curve is piecewise continuous if it is continuous on all points except for few discontinuities which are finite. In previous studies [15], the concept of piece-wise continuity was applied only to the building envelope. In this paper, the concept is extended to include solar radiation and the convection term in order to take the 2R2C into account. The concept of piecewise continuity was similarly used for solar radiation absorbed by vegetation [32]. Convection term in the input is majorly from plug loads, which are mostly step functions in reality. For a uniform expression, a piecewise

continuous assumption is also made for the convection term. As a result, the assumption substitutes a step input in the time intervals when the step change occurs with a ramp input and could cause the output of the time series to deviate from reality. However, the deviation is considered to have a small impact on the model accuracy because it only occurs in the time interval when the plug load is enabled, and the convection term takes a smaller percentage of the total plug load compared with the radiation term. Substituting Equation (15) into Equation (13) gives

$$T_{t+\delta} = e^{A_s\delta}T_t + \int_t^{t+\delta} e^{A_s(t+\delta-\tau)}B_s \left[\mathbf{U}_t + \frac{(\tau-t)}{\delta}(\mathbf{U}_{t+\delta} - \mathbf{U}_t) \right] d\tau \quad (16)$$

By changing variable $\alpha = \tau - t$, the equation can be rewritten as

$$T_{t+\delta} = e^{A_s\delta}T_t + \left[\int_0^\delta e^{A_s(\delta-\alpha)} d\alpha \right] B_s \mathbf{U}_t + \left[\int_0^\delta \alpha e^{A_s(\delta-\alpha)} d\alpha \right] \left[\frac{B}{\delta}(\mathbf{U}_{t+\delta} - \mathbf{U}_t) \right] \quad (17)$$

Seem et al. [9] described the steps for integrating the two integrals. The solution to the first integral is

$$\left[\int_0^\delta e^{A_s(\delta-\alpha)} d\alpha \right] = A_s^{-1}(e^{A_s\delta} - I) \quad (18)$$

and the solution to the second integral is

$$\left[\int_0^\delta \alpha e^{A_s(\delta-\alpha)} d\alpha \right] = A_s^{-1}A_s^{-1}(e^{A_s\delta} - I) - A_s^{-1}\delta \quad (19)$$

Substituting these into Equation (17) yields

$$T_{t+\delta} = \varphi T_t + (\Gamma_1 - \Gamma_2)\mathbf{U}_t + \Gamma_2\mathbf{U}_{t+\delta} \quad (20)$$

where

$$\varphi = e^{A_s\delta}; \quad \Gamma_1 = A_s^{-1}(e^{A_s\delta} - I)B = A_s^{-1}(\varphi - I)B; \quad \Gamma_2 = A_s^{-1}\left(\frac{\Gamma_1}{\delta} - B\right)$$

Equation (20) relates the state at time $t + \delta$ to the state at time t , and the inputs at the times t , and $t + \delta$. Using the forward shift operator, defined by $FT_t = T_{t+\delta}$ to relate the states to previous input, Equation (20) can be written as

$$(FI - \varphi)T_t = (F\Gamma_2 + \Gamma_1 - \Gamma_2)\mathbf{U}_t \quad (21)$$

$$T_t = (FI - \varphi)^{-1}(F\Gamma_2 + \Gamma_1 - \Gamma_2)\mathbf{U}_t \quad (22)$$

Substituting Equation (22) into Equation (9) yields

$$Q_{cool,t} = [C(FI - \varphi)^{-1}(F\Gamma_2 + \Gamma_1 - \Gamma_2)\mathbf{U}_t + D\mathbf{U}_t] \quad (23)$$

Equation (23) relates the output from the system to the input, and the intermediate nodal temperatures do not factor into the formulation. Since the inverse of a matrix is equal to the adjunct divided by the determinant, the $(FI - \varphi)^{-1}$ matrix can be rewritten as:

$$(FI - \varphi)^{-1} = \frac{R_0F^{n-1} + R_1F^{n-2} + \dots + R_{n-2}F + R_{n-1}}{F^n + e_1F^{n-1} + \dots + e_{n-1}F + e_n} \quad (24)$$

By further manipulation, the equation above reduces to:

$$Q_{cool,t} = \sum_{j=0}^n (S_j\mathbf{U}_{t-j\delta}) - \sum_{j=1}^n (e_j y_{t-j\delta}) \quad (25)$$

where

$$S_o = CR_oT_2 + D; S_j = C[R_{j-1}(T_1 - T_2) + R_jT_2] + e_jD \text{ for } 1 \leq j \leq n - 1; S_n = CR_{n-1}(T_1 - T_2) + e_nD$$

Equation (25) relates current outputs to time series of current and past inputs and time series of past outputs. The value of n depends on the dimension of the Matrix A_s . For the R-C model used in this study, $n=4$ since there are 4 nodal temperatures. Therefore, the current cooling load can be calculated using current inputs, the inputs in the previous four time intervals and the cooling load in the previous four time intervals.

4 Model Comparisons Using Baseline Conditions

In this section, the accuracy of the time-series model is investigated by comparisons with the results from EnergyPlus when the same baseline conditions are used as inputs to both models.

4.1 Baseline condition definitions

The baseline comparisons were carried out on a thermal zone in an office building, which is usually conditioned by an AHU. One thermal zone was chosen to capture the dynamics and variations at the zone level. If needed, reasonably high model accuracy at the zone level could easily be extended to multi-zone buildings, but the computation time would be increased.

According to Equation (22), in the simulation, the input matrix (U) in Equation (12) and state-space matrixes (A_s, B_s, C, D) in Equation (10) need to be defined.

The input matrix (U) includes ambient air temperature, sol-air temperature, and radiative and convective parts of the internal heat gain. For simplicity, only the surface facing west is exposed to ambient and solar radiation while other surfaces are treated as interior adiabatic surfaces, with no exposure to sun or wind. Other than the weather data used to calculate ambient and sol-air temperatures, the internal load from equipment, people and lights are also needed. In addition, the convective-radiative split is needed to determine the amount of internal heat gain that becomes cooling load instantaneously. Therefore, the following simulation conditions are defined as baseline conditions in order to obtain the inputs needed for Matrix U:

- Ambient and solar radiation values from TMY2 data of Oklahoma City in EnergyPlus. The run period is chosen to be representative of one month of cooling season.
- Use of 50% of nameplate rating for the plug loads. Most office equipment includes a nameplate rating showing the total power consumption. For most common equipment such as printers and computers, the actual power consumption ranges from 14% to 36% of the nameplate ratings [33]. In this study, we chose 50% as a worst case scenario.
- Internal load (equipment and people) density of 28.74W/m² for occupied hours (9am-5pm). This is within the recommended range by ASHRAE/IES 90.1-2010 standards (16.15-32.3W/m²) for office and some institutional buildings. An internal load density of 5.38W/m² was used for unoccupied hours.
- 30%-70% Convective-Radiative Split for internal load. This implies that 30% of internal heat gain is convection and 70% is thermal radiation. The higher the convection portion of a heat gain, the faster the heat gain can be converted into a cooling load. The original recommendation by ASHRAE was a 30%-70% convective-radiative split. Updated experimental results for equipment and other internal heat gain recommend 20%-80% for radiative fraction and 80%-20% for the convective fraction of equipment [33,34]. A 30%-70% split is more appropriate for lighting and occupant load [35], and it is chosen in this study.

State-space matrixes are defined by the R's and C's of the building construction materials and the amount of internal mass. In the baseline comparisons, three different scenarios of light, medium, and heavy wall constructions of the building envelope are assumed according to ASHRAE classifications. The wall compositions are shown in the Appendix. The window-to-wall ratio (WWR) on the exposed surface is approximately 37% because ASHRAE 90.1-2010 standard allows up to 40% WWR. For ease of comparing the nodal temperatures T1 and T2 with outside and inside surface temperature in EnergyPlus, the 3R2C parameters of building envelope are calculated from the wall construction as:

$$R1 = \frac{1}{h_o A}; R3 = \sum_{i=1}^j \frac{l_j}{\lambda_j A}; R5 = \frac{1}{h_i A}; C2 = C4 = \frac{1}{2} \sum_{i=1}^j l_i \rho_i c_{pi} A \quad (26)$$

where l_i , λ_i , ρ_i , and c_{pi} are the thickness, conductivity, density, and specific heat of the i th wall layer. h_o and h_i are the convective heat transfer coefficient on the outside and inside surface, respectively. j is the total number of wall layers. Using training data of one month in EnergyPlus, the 2R2C parameters of internal mass are found using the genetic algorithm [36] by minimizing the errors between the cooling load predicted by the RC model and EnergyPlus. Table 1 shows the R-C values for obtained for light, medium, and heavy wall construction used in this study.

4.2 Results

Figures 6, 7, and 8 show the cooling load comparisons between the simplified time-series model and EnergyPlus for light, medium, and heavy construction under the baseline conditions. The mean absolute percentage error (MAPE) is a reliable measure of accuracy for constructing fitted time series values as applied to trend estimation. In this paper, MAPE is defined by Equation (27).

$$MAPE = \frac{100\%}{n} \sum_{i=1}^n \left| \frac{Q_{act} - Q_{pred}}{Q_{act}} \right| \quad (27)$$

where Q_{act} is the actual value, Q_{pred} is the forecast value, and n is the number of fitted points.

In comparison with EnergyPlus, MAPE values of 6.70%, 5.54%, and 6.31% were obtained for light, medium, and heavy wall construction, respectively.

5 Robustness/Uncertainty Analysis

In this section, the robustness of the time-series model in the presence of uncertainties in the input matrix is investigated. The ambient temperature, solar radiation, internal load, nameplate rating, and convective-radiative split are selected for the investigation since they are used to directly determine the input matrix (U).

To introduce uncertainty in the variables mentioned, a perturbation of up to 10% Gaussian distribution is first introduced into the variables one at a time (OAT). Since a Gaussian normal distribution theoretically spreads to infinity on both tails, the empirical rule is applied to ensure that at least 99.7% of the values are within 10% of the mean. According to the empirical rule, a bell-shaped distribution has approximately 68% of the values within 1 standard deviation (1σ), 95% within 2 standard deviations, and 99.7% within 3 standard deviations of the mean. So, a Gaussian normal distribution with mean of 1 and $3\sigma=0.1$ ensures 99.7% of the values within $\pm 10\%$ of the mean. This distribution was generated using the randn function in Matlab. Coincidentally, 100% of the values lie within 3 standard deviations of the mean as can be seen in Figure 9.

With the uncertainties in each variable, the time-series model is then re-applied for cooling load estimation. The variation in the cooling load introduced by variations from each input variable is

investigated, and then the effect of simultaneously varying all the variables on the cooling load is investigated. The purpose is to investigate the sacrifice in model accuracy due to uncertainty in the input variables, which comes mostly from sensor or human errors. For fair and absolute comparison, the mean absolute percentage error was chosen as a measure of accuracy.

5.1.1 Uncertainty in Nameplate Rating

For the baseline case, 50% of nameplate rating was used in the simulation. A 10% Gaussian uncertainty means a spread of normal distribution between 45% of nameplate rating and 55% of nameplate rating, with a mean of 50%. Significant difference in the cooling load predictions was observed by the time-series model when compared with the results of the baseline simulation using EnergyPlus (Table 2). The MAPE increased from 6.70% to 11.0% for light construction, from 5.54% to 9.91% for medium construction, and from 6.31% to 10.0% for heavy construction.

5.1.2 Uncertainty in Convective-Radiative Split

For the baseline case, 30%-70% was used as the convective-radiative split. A 10% Gaussian uncertainty in the radiative fraction means a spread of normal distribution between 23%-77% convective-radiative split and 37%-63% convective radiative split, with a mean split of 30%-70%. Similarly, significant differences are observed. As shown in Table 3, the MAPE increased significantly from 6.7% to 18.2% for light construction, from 5.54% to 17.4% for medium construction, and from 6.31% to 16.5% for heavy construction.

5.1.3 Uncertainty in Ambient Temperature

A 10% Gaussian uncertainty was introduced for each hourly temperature data in the run period. The perturbed values were then used as input into the RC model. In reality, uncertainties in ambient temperature come mostly from sensor errors. With 10% random normal uncertainty in ambient temperature, the MAPE increased significantly for all 3 cases of light, medium, and heavy construction as shown in Table 4. The MAPE significantly increased from 6.70% to 14.8% for light construction, from 5.54% to 12.9% for medium construction, and from 6.31% to 13.3% for heavy construction. This shows that up to 10% uncertainty in the ambient temperature can double the MAPE error in the cooling load predicted by the time-series model.

5.1.4 Uncertainty in Internal Load Profile

Internal loads such as loads from people, lights and equipment in a space depend greatly on the actual usage of the space and the behavior of the occupants. Typically, internal loads are represented by schedules in energy simulation models; the actual usage of the building, however, changes on a daily basis. The use of occupancy sensors to track internal load changes is becoming popular. However, the use of static schedules in energy performance simulation is expected to continue for a while. With a 10% uncertainty in the internal load profile, the MAPE significantly increased from 6.70% to 11.9% for light construction, from 5.54% to 10.3% for medium construction, and from 6.31% to 10.5% for heavy construction (Table 5). This shows that up to 10% uncertainty in the internal load can lead to MAPE of above 10% in all cases. However, the increase is slightly less than that introduced by uncertainty in the ambient temperature.

5.1.5 Uncertainty in Solar Radiation

In most cases, solar radiation cannot be measured directly at the site. Instead, horizontal global radiation data from available weather stations is used, and decomposed into direct normal and diffuse solar radiation. Since the concept of sol-air temperature was used in the RC model, the effect of varying the solar radiation will translate to the model through the sol-air temperature. As shown in Table 6, a 10% Gaussian uncertainty in solar radiation values has no significant effect on the MAPE for the three cases of light, medium, and heavy construction.

5.1.6 *Uncertainty in the Factors Combined*

The uncertainties in cooling load contributed by the combined effects of multiple operation parameters are investigated. The combined effect of a 10% Gaussian uncertainty in solar radiation, ambient temperature, internal load, convective-radiative split, and nameplate rating as propagated to the cooling load is not additive. With the uncertainty in all factors combined, the MAPE of light construction increased from 6.70% to 27.1%, the MAPE of medium construction increased from 5.54% to 25.2%, and the MAPE of heavy construction increased from 6.31% to 25.1% for heavy construction (see Table 7). The range of uncertainties for each category is summarized in Figures 10 to 12.

6 **Conclusion and Recommendations**

This study introduces the formulation and robustness tests of the time series cooling load model deduced from the simplified R-C model. The R-C parameters of the building envelope were determined from the building construction while the R-C parameters of internal mass were found using the genetic algorithm. Three cases of building construction (light, medium, and heavy) of a thermal zone in a medium-sized office were simulated in EnergyPlus. The variable of interest in this study is the cooling load, but the model could also be used to solve for the nodal temperature and heat fluxes. With the time series formulation, the current and future cooling loads were estimated from the past cooling load and past and current values of independent variables such as ambient and room temperature, internal load, and solar radiation. A reasonably high degree of accuracy was obtained for the three cases considered in this paper. Relative to EnergyPlus, mean absolute percentage errors of 6.7%, 5.5%, and 6.4% were obtained for prediction of the cooling load for light, medium, and heavy construction, respectively.

This study also contributes to the understanding of the impacts of key operation parameters and variables on cooling load and accuracy of the time-series model. This was achieved by introducing 10% random normal uncertainty in key variables such as solar radiation, ambient temperature, internal load, convection-radiation split, and nameplate rating. Among all factors considered, the uncertainty in ambient temperature and convective-radiative split were found to be the most influential on the cooling load. The combined effects of the uncertainties were less than the addition of individual uncertainties. Since the introduced uncertainty followed a Gaussian distribution, the uncertainty in cooling load prediction can be determined for any given confidence level, and the accuracy of the RC model investigated for different scenarios. The uncertainty in room temperature set point was not investigated in this study because the Ideal HVAC System was assumed in EnergyPlus.

A future direction of research is to test the time series formulation on real buildings with multiple zones and a real HVAC system. This is currently a work in progress. There is also a need for model improvement, since there are occasional spikes in the cooling load predicted by the time-series.

APPENDIX A

NOMENCLATURE

ρ =density

λ = thermal conductivity

t =time

sa =supply air

l =length

in = indoor

i, j, k = counter

h_i =inside convective heat transfer coefficient

h_o =outside convective heat transfer coefficient

amb =ambient

U =input

$TMY2$ =typical meteorological year, version 2

T = temperature

RC =resistance-capacitance

R_{win} =window resistance

C_{in} =indoor air capacitance

A =area

A_s, B_s, C, D =state space matrix

a_{ij} =ith row and jth column entry of matrix A

b_{ij} =ith row and jth column entry of matrix B

Q_r = half of total radiation from windows and radiative part of internal load

Q_o =incident solar on outside surface

Q_{conv} =convective part of internal load

C_p =specific heat

\dot{m}_a =mass flow rate

α = solar radiation absorptivity

I = global solar irradiance

ΔQ_{ir} = extra infrared radiation due to difference between the external air and apparent sky temperature

h_o = convection coefficient on the external surface.

**APPENDIX B
WALL COMPOSITION**

Light Wall Composition

Thickness and thermal properties				
	L(mm)	λ (W/mK)	ρ (kg/m ³)	Cp(J/KgK)
Wood Siding-1	9	0.14	530	900
Fiberglass quilt	66	0.04	12	840
Plasterboard-1	12	0.16	950	840

Table 2: Medium Wall Composition

Thickness and thermal properties				
	L(mm)	λ (W/mK)	ρ (kg/m ³)	Cp(J/KgK)
M01 100mm brick	101.6	0.89	1920	790
I02 50mm insulation	50.8	0.03	43	1210
F04 Wall air space resistance				
G01a 19mm gypsum	19	0.16	800	43

Table 3: Heavy Wall Composition

Thickness and thermal properties				
	L(mm)	λ (W/mK)	ρ (kg/m ³)	Cp(J/KgK)
M01 100mm brick	101.6	0.89	1920	790
M15 200mm heavyweight concrete	203.2	1.95	2240	900
I02 50mm insulation	50.8	0.03	43	1210
F04 Wall air space resistance				
G01a 19mm gypsum	19	0.16	800	43

Table 4: Window Composition

Thickness and thermal properties	
R(m ² k/W)	
Outside surface film	0.059
Clear 6mm	0.006
Air 3mm	0.0032
Clear 6mm	0.006
Inside surface film	0.121

REFERENCES

- [1] United States Green Building Council (2011) <http://www.usgbc.org/>, accessed Jan. 20, 2012.
- [2] Energy Star (2008). Fast Fact on Energy Use. http://www.energystar.gov/ia/business/challenge/learn_more/FastFacts.pdf

- [3] Pang, X., Wetter, M., Bhattacharya, P., and Haves, P. (2012). A framework for simulation based real-time whole building assessment, *Building and Environment* 54 (2012).
- [4] Haves P. and Xu P. (2007). The building controls virtual test Bed e a simulation environment for developing and testing control Algorithms, strategies and systems, *Proceedings of Building simulation 2007*. Beijing, China.
- [5] DOE. (2010). EnergyPlus version 7.0. United States Department of Energy, www.apps1.eere.energy.gov/buildings/energyplus/, accessed Jan. 17, 2012
- [6] BACnet (2013). ASHRAE SSPC 135, <http://www.bacnet.org/Overview/index.html>, accessed June 2013.
- [7] Causone, F., Corgnati, S. P., Filippi, M., & Olesen, B. W. (2010). Solar radiation and cooling load calculation for radiant systems: Definition and evaluation of the Direct Solar Load. *Energy and Buildings*, 42(3), 305-314.
- [8] Braga, L. C., Braga, A. R., & Braga, C. M. P. (2013). On the Characterization and Monitoring of Building Energy Demand Using Statistical Process Control Methodologies. *Energy and Buildings*.
- [9] Feng, J. D., Schiavon, S., & Bauman, F. (2013). Cooling load differences between radiant and air systems. *Energy and Buildings*.
- [10] Zhang, X., Tan, S. C., & Li, G. (2014). Development of an Ambient Air Temperature Prediction Model. *Energy and Buildings*.
- [11] Hokoi, S., Matsumoto, M., & Ihara, T. (1991). Statistical time series models of solar radiation and outdoor temperature—identification of seasonal models by Kalman filter. *Energy and Buildings*, 15(3), 373-383.
- [12] Chen, V. L., Delmas, M. A., & Kaiser, W. J. (2014). Real-time, appliance-level electricity use feedback system: How to engage users?. *Energy and Buildings*, 70, 455-462.
- [13] Zheng O'Neill, Satish Narayanan, and Rohini Brahme (2010), Model-Based Thermal Load Estimation In Buildings, Fourth National Conference of IBPSA-USA New York City, New York August 11 – 13, 2010
- [14] Hassid S. (1985). A linear model for passive solar calculations: Evaluation of Performance, *Building and Environment*: 20 (1), pp 53-59.
- [15] Seem J.E., Klein S.A. et al. (1989). Transfer functions for efficient calculation of multidimensional transient heat transfer. *Journal of heat transfer*, Vol.111:5-12.
- [16] Wang S.W., and Xu, X.H.(2006) Parameter estimation of internal thermal mass of building dynamic models using genetic algorithm, *Energy Conversion and Management* 47 (13–14)
- [17] McKinley, T. and Alleyne, A. (2008) “Identification of Building Model Parameters and Loads using On-Site Data Logs,” *SimBuild 2008*, Berkeley, CA, July 2008.
- [18] Fraisse, G., Souyri, B., Pinard, S., and Menezo, C. (2011). Identification of Equivalent Thermal Rc Network Models Based on Step Response and Genetic Algorithms, *Proceedings of Building Simulation 2011: 12th Conference of International Building Performance Simulation Association, Sydney, 14-16 November*
- [19] Goyal, S., Liao, C., Barooah, P. (2011). Identification of multi-zone building thermal interaction model from data, 2011 50th IEEE Conference on Decision and Control and European Control Conference (CDC-ECC) Orlando, FL, USA, December 12-15, 2011
- [20] Dobbs, J.R., and Hency, B. M. (2012). AUTOMATIC MODEL REDUCTION IN ARCHITECTURE: A WINDOW INTO BUILDING THERMAL STRUCTURE, Fifth National Conference of IBPSA-USA Madison, Wisconsin August 1-3, 2012.

- [21] Schmidt D., and Johannesson, G. (2004). Optimised RC Networks Incorporated within Macro-Elements for Modelling Thermally Activated Building Constructions, *Nordic Journal of Building Physics*, Vol. 3, 2004.
- [22] Justin R. Dobbs, Brandon Hency: A comparison of thermal zone aggregation methods. *CDC 2012*: 6938-6944
- [23] Sourbron, Maarten, Martine Baelmans, and Lieve Helsen (2009). "Thermal response of thermally activated building systems (TABS) in office buildings [C]." *Proceedings of EFFSTOCK. Stockholm, Sweden* (2009): 57-64.
- [24] Radecki, Peter, and Brandon Hency. "Online building thermal parameter estimation via Unscented Kalman Filtering." *American Control Conference (ACC), 2012*. IEEE, 2012.
- [25] Bueno, B., Norford, L., Pigeon, G., and Britter, R. (2012). "A resistance-capacitance network model for the analysis of the interactions between the energy performance of buildings and the urban climate." *Building and Environment* 54 (2012): 116-125.
- [26] Lombard, C., and E. H. Mathews. "Efficient, steady state solution of a time variable RC network, for building thermal analysis." *Building and Environment* 27.3 (1992): 279-287.
- [27] Lombard, C., and E. H. Mathews. "A two-port envelope model for building heat transfer." *Building and environment* 34.1 (1999): 19-30.
- [28] Xu, X. (2005). Model Based Building Evaluation and Diagnosis, PhD Dissertation, Department of Building Services Engineering, The Hong Kong Polytechnic University.
- [29] Javed, F., Arshad, N., Wallin, F., Vassileva, L., Dahlquist, E. (2012). Forecasting for demand response in smart grids: An analysis on use of anthropologic and structural data and short term multiple loads forecasting. *Applied Energy*, Volume 96, issue (August, 2012)
- [30] Song, L. , Joo, I., and Gunawan, S. Next-Day Daily Energy Consumption Forecast Model Development and Model Implementation, *Journal of Solar Energy Engineering*, 2012.
- [31] McQuiston, F.C., Parker, J.D., and Spitler, J.D. (2000). Heating, Ventilating, and Airconditioning Analysis and Design, 5th ed., ISBN 0-471-35098-2, John Wiley and Sons Inc Publisher.
- [32] Y. Knyazikhin, J. Glassy, J. L. Privette, Y. Tian, A. Lotsch, Y. Zhang, Y. Wang, J. T. Morisette, P. Votava, R.B. Myneni, R. R. Nemani, S. W. Running (1999). MODIS Leaf Area Index (LAI) and Fraction of Photosynthetically Active Radiation Absorbed by Vegetation (FPAR) Product (MOD15) Algorithm Theoretical Basis Document, <http://eosps0.gsfc.nasa.gov/atbd/modistables.html>, 1999.
- [33] Hosni, M.H., and Beck, B.,T. (2010). Updated experimental results for heat gain from office equipment in buildings. ASHRAE Final Report on RP-1482. Atlanta: American Society of Heating, Refrigerating and Air-Conditioning Engineers.
- [34] Spitler, J.D., Fisher, D.E., and Pedersen, C.,O. (1997). The Radiant Time Series Cooling Load Calculation Procedure. ASHRAE Transactions 1997, Vol. 103, Part 2.
- [35] Zhong, Z., and Braun, E. J. (2008). Combined Heat and Moisture Transport Modeling for residential buildings, Sponsored by U.S. National Institute of Standards and Technology HL 2008-3, Project Award No: 60NANB4D1091.
- [36] Mitchell M. An introduction to genetic algorithm. The MIT Press; 1997.

FIGURE CAPTIONS

Figure 1: 2R1C model of a multilayer wall.

Figure 2: 3R2C model.

Figure 3: 2R2C model for internal mass.

Figure 4: 3R2C Building envelope and 2R2C internal mass.

Figure 5: Simplified RC model.

Figure 6: Cooling load for light construction.

Figure 7: Cooling load for medium construction.

Figure 8: Cooling load for heavy construction

Figure 9: Gaussian distribution with mean=1 and $\sigma=0.1/3$.

Figure 10: Effect on MAPE for light construction

Figure 11: Effect on MAPE for medium construction

Figure 12: Effect on MAPE for heavy construction

INVESTIGATION OF BUILDING PASSIVE THERMAL STORAGE FOR OPTIMAL HEATING SYSTEM DESIGN

Ogunsola, O. and Song, L., 2014, November. Investigation of Building Passive Thermal Storage for Optimal Heating System Design. In *ASME 2014 International Mechanical Engineering Congress and Exposition* (pp. V08AT10A040-V08AT10A040). American Society of Mechanical Engineers.

ABSTRACT

Heating and cooling load calculations are critical to size Heating, Ventilation and Air conditioning (HVAC) systems and determine energy use of their operations. The ASHRAE (2009) model, which is most commonly used for heating load calculations, adopts a simplified approach by considering only steady-state instantaneous conductive heat transfer and ignoring internal heat gains and thermal storage effects. Those assumptions evaluate the worst case conditions which can reasonably occur at nights when the outdoor air temperature is lowest and with no inputs from solar, occupants, lights, or any electronic devices. However, due to thermal storage effect, heat generated in daytime can be still stored in buildings. Such ignorance leads to significantly over-sized heating system, consequently resulting in high initial cost and a higher cost of energy uses. On the other hand, though heating load might not exist at nights, by considering passive thermal storage of buildings and allowing space air to drift to reasonably lower values, buildings need to be warmed up in the morning before being occupied. The worst case conditions might happen in the morning warm-up period, when heating is needed. This study therefore examines the thermal response of different constructions (heavy, medium, and light) of the building envelope and investigates the effect of their passive thermal storage on the size of the heating system. Results show tremendous opportunities for downsizing of the heating system while still maintaining thermal comfort requirements. As such, this paper is a fundamental study of building thermal characteristics in order to investigate the potentials of establishing a new heating device design standard.

INTRODUCTION

According to the United States Green Building Council [1], buildings account for 36% of total energy use, 65% of electricity consumption, 30% of raw materials use, and 12% of portable water consumption in the United States. Buildings are responsible for at least 40% of energy use in most countries of the world, and for up to 21% of greenhouse gas emissions globally. In the United States, 14% of total energy used in commercial buildings is attributed to heating (United States Department of Energy 2008 [2]). This is usually compensated by Heating, Ventilating, and Air-conditioning (HVAC) Systems.

The primary aim of building energy system is to satisfy thermal comfort requirements. However, recent studies revealed that about 30% of energy consumed in buildings is used inefficiently or unnecessarily [3]. This is because excessive energy is consumed when HVAC systems fail to operate as intended, often due to several factors such as inappropriate monitoring and control strategy, lack of understanding of the dynamics of thermal loads, system complexity, and wrong sizing of heating and cooling system. For efficient operation, the heating and cooling equipment should be suitable for the particular location and application, properly sized, accessible for easy maintenance, and have a simple arrangement, since ductwork and piping make up a significant part of the HVAC system. Meanwhile, the complex dynamics of temperature and weather fluctuation, thermal characteristics of building construction, internal heat gains, and major changes in occupancy schedules continue to provide challenge for HVAC systems design and control.

The ASHRAE Model [5] is currently adopted for heating system design. It uses a simplified approach to estimate the heating requirement for typical buildings, based on the following assumptions:

- Heat losses are considered to be instantaneous, and essentially conductive
- Thermal storage effects of building structure or content is ignored
- Thermal bridging effects on wall and roof conduction are greater
- No solar effect (at night or on cloudy, winter days)
- Heat flow is assumed to be one-dimensional and parallel.
- Construction material is thermally homogeneous

- Presence of people, lights, and appliances has no offsetting effect
- Design interior and exterior conditions [5]

The above simplified approach has been justified because it evaluates worst case conditions that can reasonably occur during a heating season. However, the assumptions often lead to over-sizing of the heating system because it ignores the thermal storage capabilities of building construction. Due to thermal and internal mass effects, heat gains in buildings during daytime may still be stored in the walls and radiation absorbing surfaces within the building. As such, heat absorbed by the thermal mass during occupied hours could be released during unoccupied hours, where the temperature may be allowed to drift to a reasonably low value. The heat released by the thermal mass may partially (or totally) compensate for the space heating needs during unoccupied periods without sacrifice of thermal comfort. The building would often need to be warmed up before the start of occupied period. Meanwhile, the highest heating demand (which determines the heating system size) is recorded between midnight and 9am. Both passive thermal storage and amount of heating depend strongly on the characteristics of the building construction. To simultaneously harness the passive thermal storage and determine the right amount of heating needed to warm up the building require an optimization process. This subject area has not been investigated.

Therefore, the aim of this study is to carry out a fundamental study of building thermal characteristics, in order to optimize the size of the heating system. By investigating the influence of the building construction on heating system capacity and operation, the possibility of harnessing building passive thermal storage for optimal sizing of heating system is discussed. A typical office building with 3 scenarios of light, medium, and heavy construction of the building envelope is used to illustrate the concept. The study focused on 2 different geographic locations namely Minneapolis- MN, and Miami-FL. These are two different regions according to ASHRAE climate classification: Minneapolis MN: Climate zone 6A (Cold-Humid) and Miami-FL: Climate Zone 1A (Very Hot – Humid). The heat and temperature dynamics of the building are modeled using Resistance-Capacitance (R-C) model, which has proved to be a simplified, yet robust model for estimation and analysis of heating and cooling loads [6]. The R-C model provides useful and quality information about the system dynamics and thermal characteristic of building construction because it represents the system physically [7]. By analyzing the R-C model, and investigating the thermal response of the light, medium, and heavy construction, the influence of thermal characteristics of the building construction on the heating system design and operation are discussed. The study concludes by presenting the results of the optimal size of the heating system for the 2 locations. The determined equipment size is compared with ASHRAE method and recommendations are made for future research.

NOMENCLATURE

T_{int} :	Internal mass temperature
T_{amb} :	Ambient temperature
R_{int} :	Thermal Resistance of internal mass
Q_{conv} :	Convective part of internal load
Q_{sys} :	System extraction or heating rate
C_{in} :	Thermal capacitance of room air
C_w :	Thermal capacitance of exterior wall
C_p :	Thermal capacitance of internal wall or partition
C_{int} :	Thermal capacitance of internal mass
R_{win} :	Windows resistance
Q_r :	Half of the sum of radiative components from internal load and windows
R_p :	Thermal Resistance of internal partition
T_{sR} :	Sol-air temperature of roof
T_{sE} :	Sol-air temperature of East facing wall
T_{sW} :	Sol-air temperature of West facing wall
α :	Solar radiation absorptivity (dimensionless)
I :	Global solar irradiance (W/m^2)
ΔQ_{ir} :	Extra infrared radiation due to difference between the external air and apparent sky temperature

k : Thermal conductivity
 C_p : Specific heat
MNPLS: Minneapolis

LITERATURE REVIEW

According to Li and Wang [8], thermal storage is one of the most promising and sustainable ways for improving energy storage in buildings. Thermal energy storage can help balance daily, weekly, and seasonal energy demands and supply [9]. Also, there are other claims that passive thermal storage can compensate for the extra investment on insulation in buildings [10]. Passive strategies involve improvements to the building envelope while active strategies are those seeking improvements to the HVAC systems. The building envelope is the interface between the indoor and outdoor environment. It determines and controls the fluctuations in the indoor environment, based on its thermal characteristics, and the transient outdoor conditions. Components such as windows, walls, roofs, thermal insulation, external shading devices, and other fenestration components make up the building envelope. On the other hand, thermal mass are the high capacity materials which are capable of absorbing and releasing heat at a later time. By absorbing and progressively releasing heat, thermal mass helps in the regulation of indoor temperature. This is reflected in the shift of peak indoor load [11]. For effective thermal mass optimization, the diurnal variations in ambient temperature should exceed 10K (18F) [12].

Morgan and Krarti [13] developed a simulation environment to implement various control strategies such as predictive optimal control. By allowing the zone temperature to drift during unoccupied periods, the energy use profile of the HVAC system was modeled and compared with actual data. According to Henze *et. al* [11], there has been little improvement in thermal storage and peak load reduction potential compared to energy conversion. In their study, the focus was on nighttime pre-cooling. By utilizing both active and passive building thermal storage, under constraints of thermal comfort, and optimal HVAC system operation, the study minimized building operating costs. Braun [14] identified potentials for reducing building operating costs as including demand reduction, ventilation with cool nighttime air, pre-cooling, and improved mechanical efficiency. Braun et al [15] optimized cost of heating by control of passive thermal storage and applied the concept to the Energy Resource Station (ERS), Iowa Energy Center, United States. The temperature was allowed to float between 15°C (59F) and 30°C (86F) during unoccupied periods. The zone temperature was fixed at 22°C (71.6F) during occupied periods. The passive thermal storage capability of the ERS was simulated and solved using quasi-Newton method. The zone sensible cooling requirement was estimated from on-site measurements. The study demonstrated capability of thermal mass for load shifting, with the potential greatest for interior zones. However, as a lightweight structure with significant coupling to ambient and exterior, the ERS was deemed an unsuitable building to fully explore building thermal mass capability. Snyder and Newell [16] developed a lumped capacitance model to determine least cost cooling strategies using effective building characteristics derived from a medium-sized building. Cooling cost savings of 18% were realized. From their analysis, thermal characteristics of building construction can have a significant impact on the load profile and energy use. Yang and Li [17] mathematically modeled the effects of thermal mass and night ventilation on cooling load. The simulation model considered the thermal resistance and capacitance of the building construction and room air. In [18], additional thermal mass led to energy savings of 18-20% over the base case. Through these reductions, the HVAC system could be downsized, thereby offsetting the initial investment on the additional insulation.

Snyder and Newell [16] and Yang and Li [17] utilized the resistance and thermal capacitance of building construction in their studies. Their models fall under the general class of Resistance-Capacitance (R-C) model, which has been widely used for building performance simulation [18-26]. The R-C model utilizes physical and thermal characteristics of building construction to generate the heat balance equation in the presence (and absence of disturbance). The R-C model is translatable to state space methods, where the stability can be investigated from the Eigenvalues of the state space matrix. It could also be solved using auto-regressive, time-series, numerical, or analytical methods. In a previous study, a time series model was deduced from the R-C model and used to estimate thermal load of a building in real-time [27]. Multiple scenarios of building construction, HVAC system operation and strategies have been simulated

using the R-C model. The RC model was determined to be the appropriate model for this study based on the following criteria:

- (i) Capability to represent physical properties of building construction in order to investigate the thermal characteristics of light, medium, and heavy construction
- (ii) Capability to simulate internal loads and different HVAC system schedules
- (iii) Simulation based, in order to investigate multiple scenarios of operation across different climates
- (iv) Ability to determine the system stability from model parameters
- (v) Capability to optimize heating system output in response to ambient temperature, solar
- (vi) Capability to simulate internal mass, thereby harnessing the thermal storage effort to the fullest.
- (vii) Capability to simulate floats in space air temperature.

Case Study

A typical office building (shown in Figure 1) having multiple zones was modeled in this study. A rectangular shaped building was deemed appropriate for a study of this nature. The rectangular shape used is for near accurate determination of the solar distribution on the different surfaces, based on their orientation. Three (3) scenarios of building envelope with light, medium, and heavy construction were considered. The composition of the light, medium, and heavy construction were taken from ASHRAE Handbook [28]. Hourly temperature and solar radiation values were obtained from Typical Meteorological Year, Version 3 (TMY3) weather data [29]. Occupancy schedules and internal loads corresponding to typical office were applied, based on ASHRAE recommendations.

The design temperature used in this study is the 99.6% dry bulb temperature for the studied locations. The peak temperature and hour at which the design temperature occurs was determined from statistical analysis of the TMY3 data for the design month. Design temperature profile was then generated as sinusoidal waveform. The optimal heating system was estimated using Genetic Algorithm [30]. As shown in Figure 1, the modeled office building has two thermal zones. Thermal zone 1 has 2 windows (one facing north, and the other facing east). Thermal zone 2 has only one window, facing north. The window-to-wall ratio (WWR) on the exposed surface is 30%. ASHRAE 90.1-2010 standard allows up to 40% WWR [31]. Tables 1 to 3 show the composition of light, medium, and heavy wall construction used in this study.

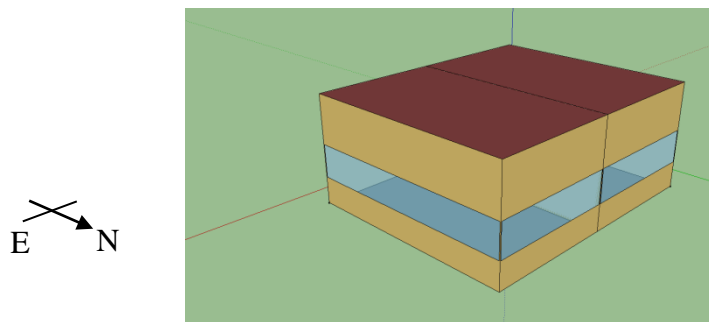


Figure 1: The Modeled Office Building

Table 1: Heavy Wall Construction

	$L(\text{mm})$	$k(\text{W/mK})$	ρ (kg/m^3)	C_p (J/KgK)
M01 brick	101.6	0.89	1920	790
M15 concrete	203.2	1.95	2240	900
I02 insulation	50.8	0.03	43	1210
F04 air resistance	-	-	-	-
G01a gypsum	19	0.16	800	43

Table 2: Medium Wall Construction

	$L(\text{mm})$	$k(\text{W/mK})$	ρ (kg/m^3)	C_p (J/KgK)
M01 brick	101.6	0.89	1920	790
I02 insulation	50.8	0.03	43	1210
F04 air resistance	-	-	-	-
G01a gypsum	19	0.16	800	43

Table 3 Light Wall Construction

	L (mm)	k (W/mK)	ρ (kg/m^3)	C_p (J/KgK)
Wood Siding-1	9	0.14	530	900
Fiberglass quilt	66	0.04	12	840
Plasterboard-1	12	0.16	950	840

As shown in Figure 2, the **red** colored variables are input to the model. They include both envelope and internal load components and have significant influence on the temperature and load profile of the building. The **black** colored are the R-C parameters. The **blue** colored are the unknown nodal temperatures. T_{int} denotes virtual temperature of internal mass nodes. T_{in1} and T_{in2} are room temperature of Zone 1 and 2 respectively. T_{p1} and T_{p2} are temperature of internal partition separating the two zones. C_p = Thermal capacitance of internal partition. Q_{sys} is system output (+ve for heating, and -ve for cooling). It is treated as 100% convective in this study. R_p is resistance of internal partition. Q_r is average of the sum of transmitted solar radiation from windows, and radiative part of internal load for the particular zone. Q_{conv} is convective part of internal load. In this study, the assumed split is 50% convection-50% radiation. This implies that 50% of internal heat gains is added to the air stream instantaneously, while the remaining 50% is radiated. Note that only 2 external walls are shown in Figure 2. There are additional walls on facing south and north respectively, but they are not shown due to space limitations.

The effects of solar radiation and ambient temperature on the outside surface of the wall have been combined into one, using the concept of sol-air temperature, T_s [4]. This concept is only suitable for

opaque surfaces, such as walls and roofs. Therefore, it was only applied to the outside wall and roof. $T_{sol-air}$ is defined in Equation (4.1):

$$T_s = T_{amb} + \frac{\alpha I - \Delta Q_{ir}}{h_o} \quad (1)$$

where the variables α , I , and ΔQ_{ir} are as defined in the nomenclature. The thermal radiation correction term, $\Delta Q_{ir}/h_o$, is usually approximated as being 3.89°C (7F) for horizontal surfaces and 0°C (0F) for vertical surfaces [4]. The sol-air temperature varies for different wall orientation due to variations in the incident solar radiation. Therefore, the sol-air temperature on different orientations are distinguished in this study. For example, T_{sE} is sol-air temperature on east facing wall while T_{sW} is the sol-air temperature on west facing wall.

To write the sensible heat balance equation for the R-C model, the following simplifying assumptions are made:

- The zone air is well mixed; therefore the whole indoor circulated air volume is at a uniform temperature.
- The effect of varying wind velocity on external wall convection coefficients is not considered. Hence, a constant heat transfer coefficient was assumed in this study.
- The space is pressurized so infiltration does not create additional heating load in the conditioned space.
- The floor surface is considered adiabatic
- The long wave radiation exchanges between internal surfaces and multiple reflections are described by the lumped internal thermal R-C model.

The above assumptions have been commonly made to simplify the R-C model [6,7,18,26]. The governing equations found by heat balance at each node are given in Equation (2):

$$\frac{dT_n}{dt} = -\frac{1}{C_n} \left(\sum_{i=1}^j \frac{1}{R_i} \right) T_n + \frac{1}{C} \left(\sum_{i=1}^j \frac{1}{R_i} T_i \right) + \frac{1}{C} \sum_{m=1}^p Q_m \quad (2)$$

Where

T_n = temperature of n th node. j =total number of temperature branches connected to node n . T_i = temperature of i th branch, connected to node n ; p =total number of heat flux branches (such as convection, radiation, and system input) connected to node n . Q_m = heat flux of m th branch connected to node n ; C_n = capacitance of node n ; R_i = resistance of branch between T_n and T_i .

For the selected office building, there are 4 roof temperatures, 12 exterior wall temperatures (2 temperature nodes for each exterior wall), 2 internal wall temperatures, and 4 virtual temperatures to account for internal mass, and 2 room temperatures. In total, there are 24 differential equations. The inputs are ambient, 5 sol-air temperature (one for horizontal surface, and 4 for the different orientation of vertical surface), 1 convection input (assumed same for both thermal zones), 2 radiation input (different for the thermal zones due to additional window in zone 1), and 2 system output (since the demand of each zone is different). The sets of differential equation can be expressed in state space as:

$$\dot{T} = AT + BU \quad (3)$$

Where A is a 24×24 matrix of constant coefficients. T is a matrix of dimension 24×1 , since there are 24 temperature nodes. B is of dimension 24×10 , and U is a 10×1 matrix, since there are 10 inputs. The coefficients of the state matrices A and B are defined by the R's and C's of the building construction materials and the amount of internal mass. Components such as furniture, carpets and other surfaces that are capable of absorbing and releasing thermal radiation within the indoor environment constitute the internal mass. Since their physical properties are not readily available, these components are lumped together and represented by two internal resistances and two internal capacitances (2R2C). The internal mass R-C parameters were estimated using Genetic Algorithm by matching the predicted building load with EnergyPlus simulation under the assumption of ideal load system.

Simulation conditions of the R-C model

The following simulation conditions are defined as baseline conditions in order to obtain the inputs needed for Matrix U:

- Ambient and solar radiation values from TMY3 data of Minneapolis- MN, and Miami- FL. The run period is chosen to be the whole of January, which is the design month for both locations.
- Use of 35% of nameplate rating for the plug loads. Most office equipment includes a nameplate rating showing the total power consumption. For most common equipment such as printers and computers, the actual power consumption ranges from 14% to 36% of the nameplate ratings [36].
- Internal load (equipment and people) density of $26.9W/m^2$ for occupied hours (9am-5pm). This is within the recommended range by ASHRAE/IES 90.1-2010 standards ($16.1W/m^2$ - $32.2W/m^2$,) for office and some institutional buildings. An internal load density of $5.4W/m^2$ was used for unoccupied hours. 50%-50% Convective-Radiative Split for internal load. This implies that 50% of internal heat gain is convection and 50% is thermal radiation. The higher the convection portion of a heat gain, the faster the heat gain can be converted into a cooling load. The original recommendation by ASHRAE was a 30%-70% convective-radiative split. Updated experimental results for equipment and other internal heat gain recommend 20%-80% for radiative fraction and 80%-20% for the convective fraction of equipment [32,33]. A moderate split of 50% convective and 50% radiative fraction is chosen in this study.

The differential equations for the temperature nodes (Equation 4.6) are inhomogeneous, with the following matrices

$$A = \begin{pmatrix} a_{1,1} & \cdots & a_{1,24} \\ \vdots & \ddots & \vdots \\ a_{24,1} & \cdots & a_{24,24} \end{pmatrix}; \mathbf{T} = [T_{1,1} \ T_{2,1} \ \dots \ T_{24,1}]'$$

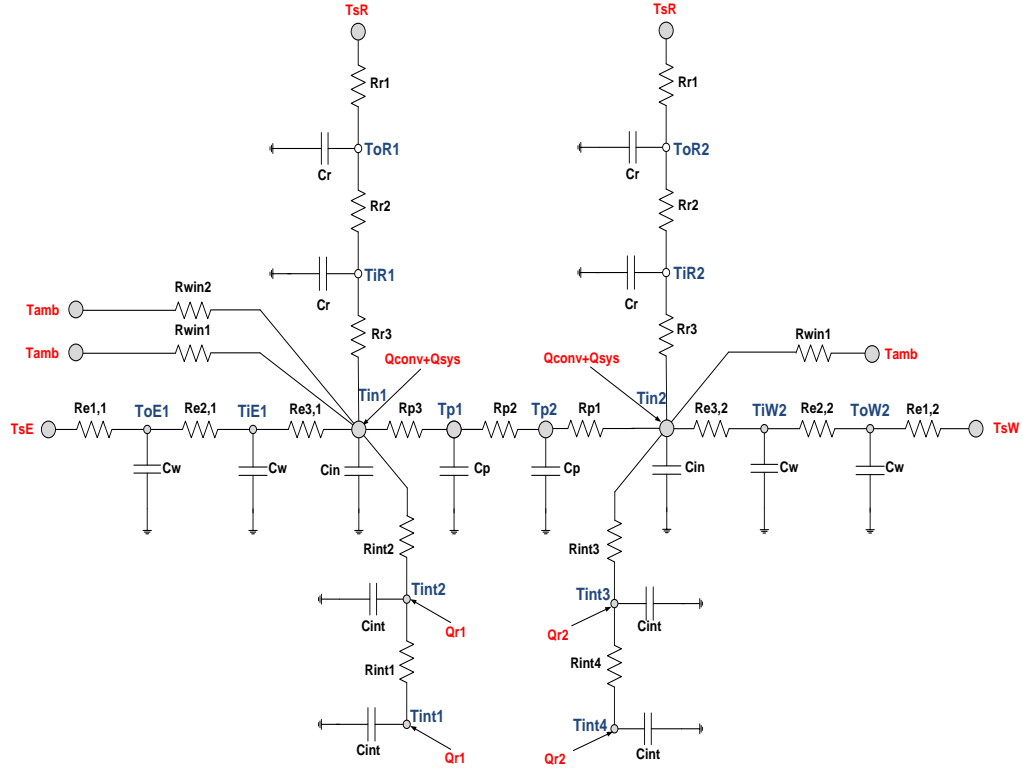


Figure 2: R-C Model Representation for the Building

$$B = \begin{pmatrix} b_{1,1} & \cdots & b_{1,10} \\ \vdots & \ddots & \vdots \\ b_{24,1} & \cdots & b_{24,10} \end{pmatrix}; \quad \mathbf{U} = [U_{1,1} \ U_{2,1} \ \dots \ U_{10,1}]'; \quad (4)$$

Where ' denotes transpose. Equation (4) is a system of first order differential equations with constant coefficients, and the solution is given by:

$$T_{t+\delta} = e^{A\delta} T_t + \int_t^{t+\delta} e^{A(t+\delta-\tau)} B U(\tau) d\tau \quad (5)$$

where the exponential matrix of A is defined by the power series

$$e^{A\delta} = I + A\delta + \frac{A^2\delta^2}{2!} + \frac{A^3\delta^3}{3!} + \dots + \frac{A^n\delta^n}{n!} + \dots \quad (6)$$

where I is the identity matrix of same dimensions as A and δ is the time step. As developed by Seem et al. [34], inputs between time t and $t + \delta$ can be modeled by a continuous, piecewise linear function as

$$\mathbf{U}(t) = \mathbf{U}_t + \frac{(\tau - t)}{\delta} (\mathbf{U}_{t+\delta} - \mathbf{U}_t) \quad (7)$$

A function or curve is piecewise continuous if it is continuous on all points except for few discontinuities which are finite. In previous studies [34], the concept of piece-wise continuity was applied only to the building envelope. The concept of piecewise continuity was similarly used for solar radiation absorbed by vegetation [35]. In this paper, the concept is extended to include solar radiation and the convection term in order to take the 2R2C of internal mass into account. Convection term in the input is majorly from plug loads, which are mostly step functions in reality. For a uniform expression, a piecewise continuous assumption is also made for the convection term. As a result, the assumption substitutes a step input in the time intervals when the step change occurs with a ramp input and could cause the output of the time series to deviate from reality. However, the deviation is considered to have a small impact on the model accuracy because it only occurs in the time interval when the plug load is enabled, and the

convection term takes a smaller percentage of the total plug load compared with the radiation term. Substituting Equation (7) into Equation (5) gives

$$T_{t+\delta} = e^{A\delta}T_t + \int_t^{t+\delta} e^{A(t+\delta-\tau)}B \left[\mathbf{U}_t + \frac{(\tau-t)}{\delta}(\mathbf{U}_{t+\delta} - \mathbf{U}_t) \right] d\tau \quad (8)$$

If conditions are known at time, $t=0$, then the solution becomes

$$T_\delta = e^{A\delta}T_o + \int_0^\delta e^{A(\delta-\tau)}B \left[\mathbf{U}_o + \frac{(\tau)}{\delta}(\mathbf{U}_\delta - \mathbf{U}_o) \right] d\tau \quad (9)$$

To obtain the analytical solution, the exponential matrix $e^{A\delta}$ and the convolution integral $\int_0^\delta e^{A(\delta-\tau)}B \left[\mathbf{U}_o + \frac{(\tau)}{\delta}(\mathbf{U}_\delta - \mathbf{U}_o) \right] d\tau$ need to be evaluated. There are several approaches used to evaluate the matrix exponential such as polynomial methods, Taylor series, inverse Laplace, and ordinary differential equation method [36]. In this study, the Matrix Decomposition Method is used. It is based on similarity transformation of the form

$$A = CDC^{-1} \quad (10)$$

Such that the power series definition of e^{At} becomes

$$e^{At} = Ce^{Dt}C^{-1} \quad (11)$$

The usual approach is to take C as the matrix whose columns are the eigenvectors of A , i.e.

$$C = V = [v_1 | \dots | v_n] \text{ and } Av_j = \lambda_j v_j, \quad j = 1, \dots, n \quad (12)$$

$$e^{Dt} = \text{diag}(e^{\lambda_1 t}, \dots, e^{\lambda_n t}) \quad (13)$$

Since V is nonsingular, the matrix exponential of At is expressed as

$$e^{At} = V(\text{diag}(e^{\lambda_1 t}, \dots, e^{\lambda_n t}))V^{-1} \quad (14)$$

The difficulty with using this approach is when the matrix does not have a complete set of orthogonal eigenvectors. In such situations, the matrix V is not invertible and the algorithm breaks down. The eigenvectors of the light, medium, and heavy construction used in this study were checked for this requirement. The eigenvalues of the state matrix A are also checked for asymptotic stability. From assumption of piecewise continuity and the evaluation of the matrix exponential, an analytical solution of the temperature is obtainable. The solution was symbolically evaluated in Matlab, for each time step. Using the state transition matrix and the input matrix, the solution at a current (or future) time step is dependent on the value from a previous time step, inputs from previous and current step, and the elapsed time between the two time steps.

To generate the heating design day temperature profile, the time of occurrence of minimum temperature and the peak temperature need to be known. The minimum temperature is the 99.6% dry bulb temperature, which is given in ASHRAE Handbook [28]. In this study, the peak temperature is assumed to be equal to the smallest peak temperature for January, as obtained from the TMY3 data for the different locations.

With information about the daily minimum, daily maximum, and the time of occurrence of the minimum temperature, the design day temperature profile was generated for the three different locations, as shown in Table 4

The objective is to minimize the heating system size, subject to:

a) $15 \leq T_{in1} \leq 22.2$, (Temperature limits for Zone 1, °C)

b) $15 \leq T_{in2} \leq 22.2$, (Temperature limits for Zone 2, °C)

c) $T_{in1} \cong 22.2$ from 9am to 5pm (Zone 1 occupied hours)

d) $T_{in2} \cong 22.2$ from 9am to 5pm (Zone 2 occupied hours)

where T_{in1} is the room temperature of thermal zone 1, and T_{in2} is the room temperature of thermal zone 2.

Table 4: Temperature Profile for Design Day

Location	Time of Min.	Temperature Function (°C)
Miami	7am	$T = 12.7 - 4\sin((t - 1)\pi/12)$
MNPLS	5am	$T = -23.7 - 1.5 \sin\left((t + 1)\frac{\pi}{12}\right)$

RESULTS

In this study, the heating system output was moderated to satisfy the constraints on temperature. The heating system was sized based on the largest heating output recorded during the heating season. Due to space limitations however, only the heating system size and few days temperature results are presented here.

As shown in Figures 3 to 6, the thermal responses of light, medium, and heavy construction are different for the studied locations. The design days are the sinusoidal part of the Figures 3 to 6 as indicated. The temperature responses depicted in the three figures offer insightful information to the behavior of the different construction.

For Miami, temperature drift was witnessed for a couple of days, during unoccupied periods. This means that the HVAC system could be turned off for several hours, without the temperature dropping too sharply. As seen in Figures 3 and 4, the heavy construction has very strong moderating effect, with capability to keep the temperature around the setpoint of 22.2°C, even after the HVAC system is turned off. For the light construction, the temperature drops sharply (with approximately the same slope as the ambient) when the heating system is turned off. The setback to this is that larger amounts of heating are then required to bring the temperature back to the required value at the start of occupied period. The behavior of the medium construction is between the two extremes. The implication is that the light construction experiences larger heating loads, due to lower capability to store thermal energy. The heavy construction on the other hand, has capability to offset the heating requirement by gradual release of the stored thermal energy.

For Minneapolis, temperature drift was witnessed for very few hours during unoccupied periods, which are mostly for the design day (see Figures 5 and 6). This means that the HVAC system could not be turned off for more than two hours without the temperature dropping below the lower limit. This situation is necessary because the ambient temperature is sub-zero for all the days during the simulation period. This unfavorable temperature causes the heating system to be operational for longer hours than what was observed for Miami. However, the behavior of heavy and medium construction is similar for both Miami and Minneapolis. Both have very good moderating effects on temperature swings. The implication is that the light construction experiences larger heating loads, due to lower capability to store thermal energy. The heavy construction on the other hand, has capability to offset the heating requirement by gradual release of the stored thermal energy.

Results show that the heating system must be operating at full load shortly before and at the time of occurrence of minimum daily temperature.

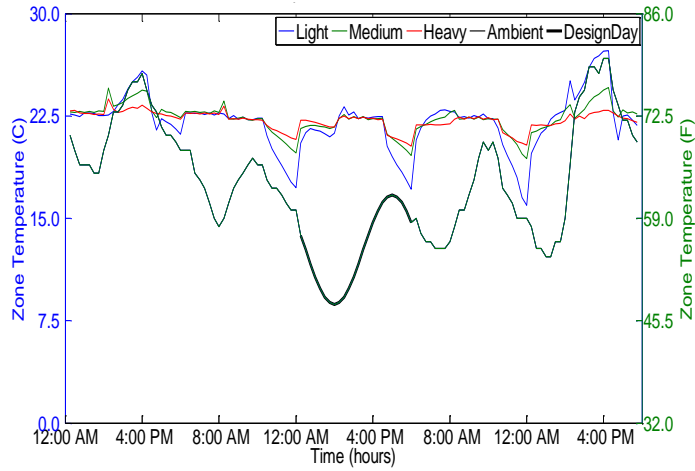


Figure 3: Thermal Response of Miami- Zone 1

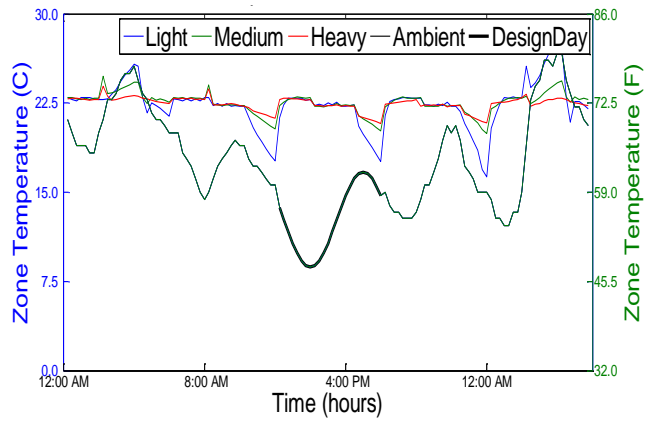


Figure 4: Thermal Response of Miami- Zone 2

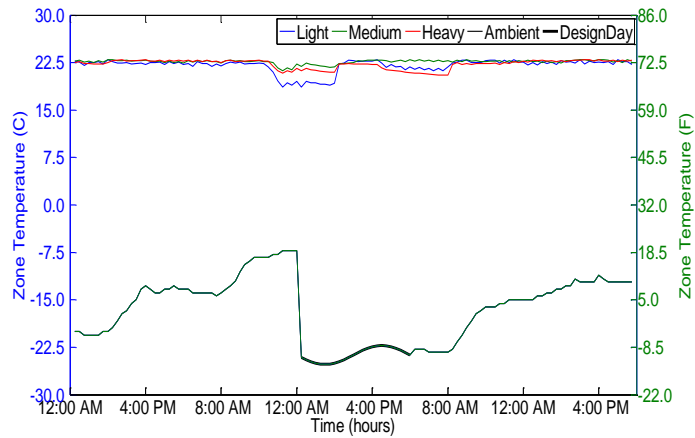


Figure 5: Thermal Response of Minneapolis- Zone 1

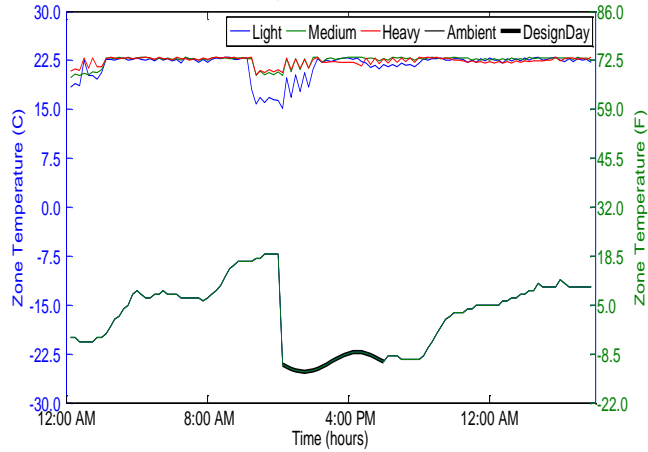


Figure 6: Thermal Response of Minneapolis- Zone 2

The resulting heating system sizes are presented and compared with the ASHRAE method, as shown in Figures 7 and 8. It is seen that the heavy construction has the least heating system size while light construction has the largest heating system size. By factoring the passive thermal storage of building construction into the design of heating system, the heating system could be downsized by up to 33% for heavy construction, 23% for medium construction, and 22% for light construction in Miami. In Minneapolis, savings of up to 18%, 12%, and 9% are possible for heavy, medium, and light construction respectively. The savings on equipment size are largest for Miami due to the favorable temperature pattern and design conditions.

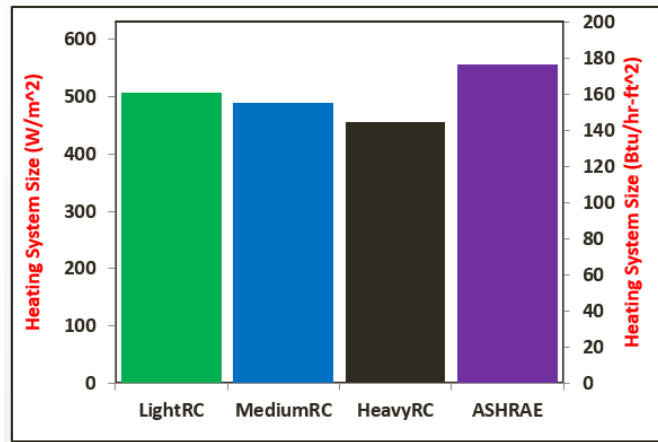


Figure 7: Heating System Size (Minneapolis)

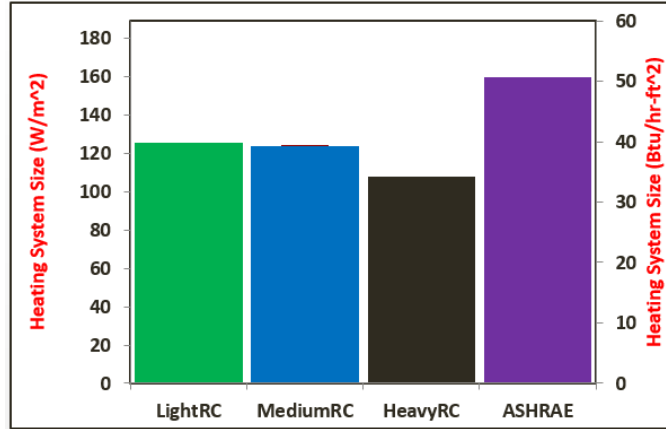


Figure 8: Heating System Size (Miami)

CONCLUSIONS

A typical office building with two thermal zones was considered in this study. The thermal characteristics of building constructions have significant influence on heating system operation and size for the different locations considered in this study. By analyzing the thermal response of the different constructions for the heating season, the results show that heating is not necessary to maintain thermal comfort on a typical day in Miami where there are no strict temperature requirements. From the thermal response to design day conditions however, heating is required for the design day in Miami. In Minneapolis, heating is always required to maintain thermal comfort for both typical day and design conditions, because the ambient temperature is sub-zero during winter. Miami which requires a smaller heating system has the largest savings while Minneapolis has the smallest reduction in the size of the heating system.

Passive thermal storage also offers opportunities for energy savings during heating system operation. Once the desired temperature is reached, the heating system could be turned off in a typical building with heavy construction. The heavy constructions save more energy during floating and hold periods than during the warm up period, by moderating swings in temperature. Light and medium constructions save more energy during warm up periods.

Overall, the savings on heating system size is highest for Miami, which is classified as a very hot-humid region and least for Minneapolis which is a cold-humid region according to ASHRAE classifications. For all the locations studied, there are savings on heating system size for all types of construction. Based on the analysis in this study, the following conclusions could be drawn:

- There are tremendous opportunities for downsizing the heating system by considering passive thermal storage of building construction
- The savings on heating system size is highest for heavy construction due to better thermal storage and moderating effects on temperature
- The savings is higher for Miami due to favorable temperature profile for heating season.
- A smaller sized system is also expected to generate additional savings in HVAC systems operating cost where efficient control strategy is adopted.

REFERENCES

- [1] United States Green Building Council (2011) <http://www.usgbc.org/>, accessed Jan. 20, 2012.
- [2] United States Department of Energy (2008). Energy Efficiency Trends in Residential and Commercial Buildings,

- http://apps1.eere.energy.gov/buildings/publications/pdfs/corporate/bt_stateindustry.pdf
Accessed October, 2013
- [3] Energy Star (2008). Fast Fact on Energy Use.
http://www.energystar.gov/ia/business/challenge/learn_more/FastFacts.pdf,
Accessed July 2012
- [4] McQuiston, F.C., Parker, J.D., and Spitler, J.D. (2000). Heating, Ventilating, and Airconditioning Analysis and Design, 5th ed., ISBN 0-471-35098-2, John Wiley and Sons Inc Publisher.
- [5] ASHRAE. 2009. 2009 ASHRAE Handbook – Fundamentals. Atlanta: American Society of Heating, Refrigerating and Air-Conditioning Engineers, Inc.
- [6] Zheng O'Neill, Satish Narayanan, and Rohini Brahme (2010), Model-Based Thermal Load Estimation In Buildings, Fourth National Conference of IBPSA-USA New York City, New York August 11 – 13, 2010
- [7] Wang S.W., and Xu, X.H.(2006) Parameter estimation of internal thermal mass of building dynamic models using genetic algorithm, *Energy Conversion and Management* 47 (13–14)
- [8] Li, C. and Wang, R. Z. (2012). Building Integrated Energy Storage Opportunities in China, *Renewable and Sustainable Energy Reviews* 16 (2012) 6191–6211
- [9] International Renewable Energy Agency (2013). Thermal Energy Storage, Technology Brief, available at www.irena.org/Publications, Accessed September 2013
- [10] Schnieders, J., Hermelink, A., 2006. CEPHEUS results: measurements and occupants satisfactory provide evidence for passive house being an option for sustainable building. *Energy Policy* 34, 151–171.
- [11] Henze, G. P., Kalz, D. E., Liu, S., & Felsmann, C. (2005). Experimental analysis of model-based predictive optimal control for active and passive building thermal storage inventory. *HVAC&R Research*, 11 (2), 189-213.
- [12] Sadineni, S. B., Madala, S. and Boehm, R. F. (2011). Passive building energy savings: A review of building envelope components, *Renewable and Sustainable Energy Reviews* 15 (2011) 3617–3631
- [13] Morgan, S. and Krarti, M. (2010). Field Testing of Optimal Controls of Passive and Active Thermal Storage ASHRAE Transactions 2010, Vol. 116, Part 1.
- [14] Braun, J.E. 2003. Load control using building thermal mass. *Journal of Solar Energy Engineering* 125(3):292-301. New York: American Society of Mechanical Engineers.
- [15] Braun J.E., T.M. Lawrence, C.J. Klaassen, and J.M. House. 2002. Demonstration of load shifting and peak load reduction with control of building thermal mass. *Proceedings of the 2002 ACEEE Conference on Energy Efficiency in Buildings, Monterey, CA*.
- [16] Snyder, M., and Newell, T., 1990, "Cooling Cost Minimization Using Building Mass for Thermal Storage," ASHRAE Trans., **96_2_**, pp. 830–838.
- [17] Yang L, Li Y. Cooling load reduction by using thermal mass and night ventilation. *Energy and Buildings* 2008; 40 (11):2052–8.
- [18] Goyal, S., Liao, C., Barooah, P. (2011). Identification of multi-zone building thermal interaction model from data, 2011 50th IEEE Conference on Decision and Control and European Control Conference (CDC-ECC) Orlando, FL, USA, December 12-15, 2011
- [19] Dobbs, J.R., and Hency, B. M. (2012). AUTOMATIC MODEL REDUCTION IN ARCHITECTURE: A WINDOW INTO BUILDING THERMAL STRUCTURE, Fifth National Conference of IBPSA-USA Madison, Wisconsin August 1-3, 2012.
- [20] Schmidt D., and Johannesson, G. (2004). Optimised RC Networks Incorporated within Macro-Elements for Modelling Thermally Activated Building Constructions, *Nordic Journal of Building Physics*, Vol. 3, 2004.
- [21] Sourbron, Maarten, Martine Baelmans, and Lieve Helsen (2009). "Thermal response of thermally activated building systems (TABS) in office buildings [C]." *Proceedings of EFFSTOCK. Stockholm, Sweden* (2009): 57-64.
- [22] Radecki, Peter, and Brandon Hency. "Online building thermal parameter estimation via Unscented Kalman Filtering." *American Control Conference (ACC), 2012*. IEEE, 2012.

- [23] Bueno, B., Norford, L., Pigeon, G., and Britter, R. (2012). "A resistance-capacitance network model for the analysis of the interactions between the energy performance of buildings and the urban climate." *Building and Environment* 54 (2012): 116-125.
- [24] Lombard, C., and E. H. Mathews. "Efficient, steady state solution of a time variable RC network, for building thermal analysis." *Building and Environment* 27.3 (1992): 279-287.
- [25] Lombard, C., and E. H. Mathews. "A two-port envelope model for building heat transfer." *Building and environment* 34.1 (1999): 19-30.
- [26] Xu, X. (2005). Model Based Building Evaluation and Diagnosis, PhD Dissertation, Department of Building Services Engineering, The Hong Kong Polytechnic University.
- [27] Ogunsola, O. T., Song, L., & Wang, G. (2014). Development and Validation of a Time-series Model for Real-time Thermal Load Estimation. *Energy and Buildings*.
- [28] ASHRAE. (2005). ASHRAE Handbook, Fundamentals Volume. Atlanta: American Society of Heating, Refrigerating and Air-Conditioning Engineers, Inc.
- [29] United States DoE (2013). [EnergyPlus Energy Simulation Software](http://apps1.eere.energy.gov/buildings/energyplus/weatherdata_about.cfm), available at http://apps1.eere.energy.gov/buildings/energyplus/weatherdata_about.cfm Accessed October 2013
- [30] Mitchell M. An introduction to genetic algorithm. The MIT Press; 1997.
- [31] ASHRAE (2010). ASHRAE 90.1-2010, Energy Standard for Buildings Except Low-Rise Residential Buildings
- [32] Hosni, M.H., and Beck, B.,T. (2010). Updated experimental results for heat gain from office equipment in buildings. ASHRAE Final Report on RP-1482. Atlanta: American Society of Heating, Refrigerating and Air-Conditioning Engineers.
- [33] Spitler, J.D., Fisher, D.E., and Pedersen, C.,O. (1997). The Radiant Time Series Cooling Load Calculation Procedure. ASHRAE Transactions 1997, Vol. 103, Part 2.
- [34] Seem J.E., Klein S.A. et al. (1989). Transfer functions for efficient calculation of multidimensional transient heat transfer. *Journal of heat transfer*, Vol.111:5-12.
- [35] Y. Knyazikhin, J. Glassy, J. L. Privette, Y. Tian, A. Lotsch, Y. Zhang, Y. Wang, J. T. Morisette, P.Votava, R.B. Myneni, R. R. Nemani, S. W. Running (1999). MODIS Leaf Area Index (LAI) and Fraction of Photosynthetically Active Radiation Absorbed by Vegetation (FPAR) Product (MOD15) Algorithm Theoretical Basis Document, <http://eosps0.gsfc.nasa.gov/atbd/modistables.html>, 1999.
- [36] M. Cleve, and Loan, C. V. (2003). Nineteen Dubious Ways to Compute the Exponential of a Matrix, Twenty-Five Years Later, *SIAM Review*, Vol. 45, No. 1, pp. 3-000



Restoration of long-term missing gaps in solar radiation



Oluwaseyi T. Ogunisola, Li Song^{*}

University of Oklahoma, Norman, OK, United States

ARTICLE INFO

Article history:

Received 19 January 2014

Received in revised form 28 July 2014

Accepted 30 July 2014

Keywords:

Solar radiation

Weather data

Singular spectrum analysis

Missing data restoration

Clear sky model

Temperature-based approach

ABSTRACT

Solar radiation is an important climatic variable and widely used in building performance monitoring and analysis. However, due to sensor malfunction, data transmission problems, and quality assurance issues, there are often short-term or long-term missing data on solar radiation. These gaps are challenging for engineers involved in building performance monitoring and control. This paper examines and compares three different approaches, namely, singular spectrum analysis (SSA), statistically adjusted solar radiation (SASR), and the temperature-based approach (TBA), for restoring missing solar data. The TBA, SASR, and SSA are applied to fill artificial gaps which are generated continuously as representative of up to 25 days missing data in actual hourly solar radiation data of Oklahoma City North (OKCN) for 2012 and Albuquerque for 2005. Results show that SSA outperforms the other methods for filling solar radiation gaps of up to 5 days. For gaps up to 20 days, the SSA and TBA have similar performance. For gaps larger than 20 days, the TBA is more suitable. The SASR performs similarly to the TBA for dry and sunny Albuquerque climates, but worse in OKCN. Accuracy of the SSA decreases with increasing gap lengths. The study concludes by recommending appropriate methods for different gap lengths.

© 2014 Published by Elsevier B.V.

1. Introduction

Solar radiation is an important variable in building performance simulation, monitoring and analysis. Measured data, such as solar radiation, has shown to be useful in improving the accuracy and reliability of building energy simulations especially for commercial buildings due to the existence of large glazed area [1,2]. Solar radiation is made up of several broad classes of electromagnetic radiation. It is one of the climatic variables recorded by most weather stations. Solar radiation data can have significant impact on energy use, as well as building performance, control, monitoring, and analysis. It is a very important variable in the design and operation of heating, ventilation and air-conditioning (HVAC) systems. The availability of reliable solar radiation data is very critical for the selection of appropriate control measures or for maximization of energy savings opportunities. Although solar radiation data is recorded by weather stations all over the world, a certain level of measured data is often not available. Data from nearby stations may not be a true representation of the solar radiation at neighboring locations. Also, the available data may contain missing data for several days. This might be caused by sensor error and damage, time and cost limitations, data transmission problems, or data quality

assurance methods. Therefore, there are often short or long-term missing solar radiation data. These issues present challenges for building designers, modelers, operators, and other users of solar radiation data, since the missing gaps have to be filled before the data can be utilized. Unreasonable interpolation of missing solar radiation data can lead to costly errors, particularly when applied to design, or assessment of control efforts in building systems operations.

Many methods have been investigated for filling gaps in time-series data, and these methods are not necessarily limited to solar data restoration. Chen and Claridge [3] evaluated Single Variable Regression, Polynomial models, Lagrange Interpolation, and Linear Interpolation models to estimate values for 1–6 h gaps in weather, heating, and cooling measurements for commercial buildings. Hu et al. [4,5] also utilized Lagrange Interpolation, Linear Interpolation, and Spatial-temporal Interpolation to fill short- and long-term missing gaps in climate variables such as solar radiation, temperature, and wind speed. Hocke and Kämpfer [6] filled data gaps using the Lomb-Scargle periodogram, which is well-known for estimation of the power spectral density of sampled data. The Lomb-Scargle periodogram provides least squares spectrum in case of uneven data, but reduces to the Fourier transform when there are evenly sampled data. In the Lomb-Scargle method, the time series is usually modified in a frequency domain by imposing a confidence limit on the amplitude or by considering only those spectral components within a specified frequency domain. The time series data

^{*} Corresponding author. Tel.: +1 405 325 1714.
E-mail address: lsong@ou.edu (L. Song).

Restoration of 1–24 hour dry-bulb temperature gaps for use in building performance monitoring and analysis—Part I

JUNJUN HU^{1,2}, OLUWASEYI T. OGUNSOLA³, LI SONG^{3*}, RENEE A. McPHERSON⁴, MEIJUN ZHU⁵, YANG HONG^{2,6,7}, and SHENG CHEN^{2,6,7}

¹*School of Computer Science, University of Oklahoma, Norman, OK 73019, USA*

²*School of Civil Engineering and Environmental Science, University of Oklahoma, Norman, OK 73019, USA*

³*School of Aerospace and Mechanical Engineering, University of Oklahoma, Engineering Laboratory 112, 865 Asp. Ave., Norman, OK 73019, USA*

⁴*Oklahoma Climatological Survey, Norman, OK 73072, USA*

⁵*Department of Mathematics, University of Oklahoma, Norman, OK 73019, USA*

⁶*Hydrometeorology and Remote Sensing Laboratory, University of Oklahoma, Norman, OK 73072, USA*

⁷*Advanced Radar Research Center, University of Oklahoma, Norman, OK 73072, USA*

Building energy system retrofit and retro-commissioning projects present tremendous opportunities to save energy. Energy consumption in buildings, especially HVAC systems, is significantly impacted by weather conditions. However, short- or long-term climatic data are frequently missing because of data transmission problems, data quality assurance methods, sensor malfunction, or a host of other reasons. These gaps in climatic data continue to provide challenges for HVAC engineers in monitoring and verifying building energy performance. This article examines eight classical approaches that use Linear interpolation, Lagrange interpolation, and Cubic Spline interpolation techniques, and eleven approaches that use two newly developed methods, i.e., Angle-based interpolation and Corr-based interpolation, to restore up to 24 h of missing dry-bulb temperature data in a time series for use in building performance monitoring and analysis. Eleven one-year hourly data sets are used to evaluate the performance of these 19 different methods. Each method is applied to deal with artificial gaps that are generated randomly. In terms of the difference between estimated values and measured values, two types of comparisons are carried out. The first comparison is conducted with three evaluation indices: MAE, RMSE, and STDBIAS. The second comparison is based on the percentage of the total data that can be estimated by an approach within specific error thresholds, including 1°F (0.56°C), 2°F (1.11°C), 3°F (1.67°C), and 5°F (2.78°C), from measured values. The comparison results show that Linear interpolation performs best when filling 1–2 h gaps, Lagrange interpolation (Lag2L2R) outperforms other methods when gaps are 3–8 h long, and the Corr-based interpolation method (Corr1L1R24Avg) is a better technique for filling 9–24 h gaps. This article presents the first part of the research results through the ASHRAE 1413 research project. The second part of the results focuses on methods to filling long-term dry-bulb temperature gaps.

Introduction

Tremendous energy savings can be realized through building energy system retrofit and retro-commissioning projects. However, energy consumption in building energy systems, especially HVAC systems, is significantly impacted by cooling/heating loads and HVAC outside air intake. In the past, internal heat gains dominated the cooling/heating loads of

commercial buildings. With the development of new energy codes and standards [i.e., ASHRAE Standard 90.1 (2010)], the proportion of weather-related load has increased. In addition, HVAC cooling coil loads and heating coil loads are significantly influenced by weather, especially in locations where it is hot and humid during the summer and cold during the winter, due to direct outside air intake required for indoor air quality (ASHRAE 2009). Thus, weather data plays an essential role in assessing the potential for energy savings prior to retrofits and retro-commissioning projects, and in validating energy savings after completion of these projects. As clearly stated in ASHRAE's guideline 14 (2002), baseline energy use and demand need to be adjusted to different conditions of weather, occupancy, or other variables, with weather-related adjustment listed as the first priority. The most recent International Performance Measurement and Verification Protocol (IPMVP 2012) also indicates that a complete year of baseline data is typically needed because energy consumption is significantly affected by weather conditions.

Received December 4, 2013; accepted April 8, 2014

Junjun Hu, is a PhD Student. **Oluwaseyi T. Ogunsola**, Student Member ASHRAE, is a Graduate Student. **Li Song, PhD, PE**, Member ASHRAE, is an Assistant Professor. **Renee A. McPherson, PhD**, is a Professor. **Meijun Zhu, PhD**, is a Professor. **Yang Hong, PhD**, is a Professor. **Sheng Chen, PhD**, is a Post Doc.

*Corresponding author e-mail: lsong@ou.edu

Color versions of one or more of the figures in the article can be found online at www.tandfonline.com/uhvc.

IMECE2012-86988

**REVIEW AND EVALUATION OF USING R-C THERMAL MODELING OF COOLING
LOAD PREDICTION FOR HVAC SYSTEM CONTROL PURPOSE**

Oluwaseyi T. Ogunsola
Aerospace and Mechanical Engineering
University of Oklahoma
Oklahoma, United States

Li Song
Aerospace and Mechanical Engineering
University of Oklahoma
Oklahoma, United States

ABSTRACT

Heating and cooling loads which are compensated by heating, ventilation, and air-conditioning (HVAC) systems, are the main reason for energy uses in buildings. Energy utilized by HVAC system accounts for two-thirds of a building's total energy consumption. Excessive energy is consumed when HVAC systems fail to operate as intended. This is often due to several factors such as inappropriate monitoring and control strategy, lack of understanding of the dynamics of thermal loads, and system complexity. Amidst several models, estimation of cooling load using Resistance Capacitance (RC) models have proved to provide more robust and accurate estimates of the building load based on measured data but the use of this method is not without challenges. This study aims to highlight common challenges associated with implementation of the RC method for thermal modeling of cooling load. Past and current research have handled some of the challenges by introducing simplifying assumptions which if not adequately selected can lead to significant deviation between model performance and measured data. Without proper understanding of the challenges, engineers may not be able to place a high degree of confidence in load calculation methods and the computer implementations that they use.

INTRODUCTION

According to the United States Green Building Council [1], buildings account for 36% of total energy use, 65% of electricity consumption, 30% of raw materials use, and 12% of portable water consumption. Buildings are responsible for at least 40% of energy use in most countries of the world, and for up to 21% of greenhouse gas emissions globally. Deficiencies in building operation are not only caused by improper operation and faulty equipment but also by the dynamic load changes in large commercial buildings. To improve performance, system efficiency must be maximized for both design and partial load

conditions. Since thermal models are essential to predict transient cooling or heating requirements for performance monitoring, diagnosis and control strategy analysis, poor control is often attributed to unavailability of reliable and simplified thermal models for estimation of building loads. In the HVAC industry, optimizing operation of building energy systems and assuring reliability of system control is one of the most cost effective engineering practices available. Traditionally, building energy could be measured on site or calculated using black box models, using whole-building simulation programs such as EnergyPlus [2], BLAST [3], and e-Quest [4], or by use of physics-based models [5-6]. Whole building simulation programs are physical models and always require detailed information about the physical features of the building. The accuracy of the simulation results heavily depends on the accuracy of the input information. These details are mostly limited, unavailable, or unreliable (e.g. features of components such as furniture and partitions within the zone) thereby making physical models less accurate and cost ineffective. In addition, the computational time required for detailed physical model simulation prohibits application for real-time control purpose. Black box modeling needs huge amount of training data and accuracy may be lost once the operating conditions are beyond the training data. [7-8].

Simplified RC models have proved to provide more robust and accurate estimates of the building load based on measured data [9]. However, most available models tend to overestimate the cooling load when data for occupied and unoccupied hours are considered. In this paper, the simplified RC model is first introduced and feasibility of using simplified RC model for precisely predicting the building load is also evaluated. Factors affecting the accuracy of RC models in predicting cooling load are discussed, such as uncertainty in input measurements, use of static occupancy and schedules, choice of validation method, and failure to account for factors such as thermal bridges and infiltration. The study concludes with ways to account for the

IMECE2013-64040

PERFORMANCE ANALYSIS OF A SIMPLIFIED MODEL OF COOLING LOAD FOR A TYPICAL OFFICE BUILDING

Oluwaseyi T. Ogunsola
Aerospace and Mechanical Engineering
University of Oklahoma
Norman, Oklahoma, United States

Li Song
Aerospace and Mechanical Engineering
University of Oklahoma
Norman, Oklahoma, United States

ABSTRACT

Buildings are responsible for at least 40% of energy use in most countries of the world, and for up to 21% of greenhouse gas emissions globally. As this trend continues, real-time building load measurements are essential for dynamic load response control, understanding and improvement of load distributions and profiles, and for climate-responsive design, particularly in commercial buildings. The focus in this paper is the cooling load, which is the rate at which heat must be removed from the controlled zone to maintain the desired temperature. Estimation of maximum cooling load is necessary for sizing of cooling equipments. However, details needed for whole-building simulation are often unreliable or unavailable. As such, simplified models with reasonable accuracy and computational requirements are often used. A cyber-physical system, integration of physical sensors and mathematical model, is proposed in this paper for cooling load estimation. The physical sensor measurements are limited to outside air temperature, solar radiation, room air temperature, and building plug load. Meanwhile, resistance-capacitance (RC) concept was adopted to describe the physics and dynamics of the building envelope for its simplicity and reasonable computational requirements. The cyber-physical system was tested using a typical office having two thermal zones and compared with simulation results from EnergyPlus, a whole building simulation program. Phenomenon such as infiltration, inter-zone air mixing, and air moisture control were not taken into account for the model. Results are presented to determine the accuracy of the simplified model for cooling load estimation.

INTRODUCTION

According to the United States Green Building Council [1], buildings account for 36% of total energy use, 65% of

electricity consumption, 30% of raw materials use, and 12% of portable water consumption. Buildings are responsible for at least 40% of energy use in most countries of the world, and for up to 21% of greenhouse gas emissions globally. Deficiencies in building operation are not only caused by improper operation and faulty equipment but also by the dynamic load changes in large commercial buildings.

The overall aim of building energy modeling in using least energy input for the optimal control of Heating, Ventilation, and Air-conditioning (HVAC) System in order to provide the desired indoor comfort and operating conditions. One of the objectives is the prediction of current and future load requirement in order to attain optimal set points and control for temperature and flow values as they affect indoor comfort and energy consumption. An optimal control is the one which minimizes the building operating costs, and effectively uses energy without compromise of thermal comfort. This has been sought after since the beginning of time. However, about 20% of commercial building energy is consumed by cooling consumption [2]. Portion of energy in buildings used inefficiently or unnecessarily is 30 percent [3].

The aim of this study is performance analysis of simplified models of cooling load for a typical office. To achieve this aim, we proceed to develop a cyber-physical system which serves to integrate physical sensor measurements with the mathematical model for real-time load measurement. This is essential for dynamic load response control, understanding load distributions and profiles, and for climate-responsive design, particularly in commercial buildings. Energy performance simulation programs have been used to predict and study energy performance. Numerous of such tools are available today with differences in their underlying equations, applicability, graphical user interface, and thermodynamic model. All internal heat gains transferred from building envelope and

Appendix F: Compositions of Floor and Partitions

Floor composition

	$L(mm)$ (in)	$k(W/mK)$ (Btu/hftF)	$\rho (kg/m^3)$ (lb/ft³)	$C_p (J/KgK)$ (Btu/lbF)	Resistance (m^2k/W) (ft²Fh/Btu)
M11 100mm lightweight concrete	101.6 (4)	0.53 (0.304)	1280 (79.91)	840 (0.201)	
F05 Ceiling air space	-	-	-	-	0.18 (1.022)
F16 Acoustic tile	19.1 (0.75)	0.06 (0.034)	368 (22.97)	590 (0.141)	

Composition of Partitions

	$L(mm)$ (in)	$k(W/mK)$ (Btu/hftF)	$\rho (kg/m^3)$ (lb/ft³)	$C_p (J/KgK)$ (Btu/lbF)	Resistance (m^2k/W) (ft²Fh/Btu)
G01a 19mm gypsum	19 (0.75)	0.16 (0.092)	800 (49.94)	43 (0.01)	
F04 Wall air space resistance	-	-	-	-	0.15 (0.852)
G01a 19mm gypsum	19 (0.75)	0.16 (0.092)	800 (49.94)	43 (0.01)	